NTATION PAGE

Form Approved
OMB No 0704 0188

AD-A243 600

ORT DATE	3. REPORT TYPE AND DATES COVERED
	XXXXXX/DISSERTATION

4. TITLE AND SUBTITLE
The Effect of Physical Aging on the Creep Response of A Thermoplastic Composite.

5. FUNDING NUMBERS

6. AUTHOR(S)
Robert L. Hastie, Jr., Major

7. PERFORMING ORGANIZATION NAME(S) AND ADDRESS(ES)
AFIT Student Attending: Virginia Polytechnic Institute and State University

8. PERFORMING ORGANIZATION REPORT NUMBER
AFIT/CI/CIA- 91-017D

9. SPONSORING / MONITORING AGENCY NAME(S) AND ADDRESS(ES)
AFIT/CI
Wright-Patterson AFB OH 45433-6583

10. SPONSORING / MONITORING AGENCY REPORT NUMBER

11. SUPPLEMENTARY NOTES

12a. DISTRIBUTION / AVAILABILITY STATEMENT
Approved for Public Release IAW 190-1
Distributed Unlimited
ERNEST A. HAYGOOD, Captain, USAF
Executive Officer

12b. DISTRIBUTION CODE

13. ABSTRACT *(Maximum 200 words)*

14. SUBJECT TERMS

15. NUMBER OF PAGES
240

16. PRICE CODE

17. SECURITY CLASSIFICATION OF REPORT	18. SECURITY CLASSIFICATION OF THIS PAGE	19. SECURITY CLASSIFICATION OF ABSTRACT	20. LIMITATION OF ABSTRACT

THE EFFECT OF PHYSICAL AGING ON THE CREEP RESPONSE OF A THERMOPLASTIC COMPOSITE.

Robert L. Hastie Jr., Major, USAF

Doctor of Philosophy, 1991, 240 pages
Department of Engineering Science and Mechanics
Virginia Polytechnic Institute and State University
Blacksburg, Virginia

(ABSTRACT)

The effect of thermoreversible physical aging on the linear viscoelastic creep properties of a thermoplastic composite was investigated. Radel X/IM7, an amorphous composite material considered for use in the next generation high speed transport aircraft, was studied. The operating environment for the aircraft material will be near 188°C (370°F) with a service life in excess of 60,000 hours at temperature. Accurate predictions of the viscoelastic properties of the material are essential to insure that design strength and stiffness requirements are met for the entire service life.

The effect of physical aging on the creep response was studied using momentary tensile creep tests conducted at increasing aging times following a rapid quench from above the glass transition temperature (T_g) to a sub-T_g aging temperature. As the aging time increased, the creep response of the material significantly decreased. The tensile creep compliance data for each aging time were fit to the empirical equation for the creep compliance D(t):

$$D(t) = D_0 e^{\left\{(t/t_0)^m\right\}}$$

where D_o, t_o, and m are fitting parameters determined using a nonlinear fitting program based on the Levenberg-Marquardt finite difference algorithm. The short-term creep compliance curves, obtained at various aging times, were then shifted to form a momentary master compliance curve. The double-logarithmic aging shift rate μ and its dependence on sub-T_g aging temperature were determined. The aging characterization process was conducted on unidirectional specimens with 0, 90, and 45 degree fiber direction orientations. This permitted the calculation of the complete principal compliance matrix for the composite material.

The effect of physical aging becomes more apparent during long-term tests when creep and aging occur simultaneously. This results in a gradual stiffening and decrease in the creep response with increased time. Predictions based solely on the Time-Temperature Superposition Principle would significantly over-predict the creep response if physical aging effects were ignored. Theoretical predictions for long-term creep compliance were made using an effective time theory and compared to long-term experimental data for each fiber orientation. Finally, experimental results of a long-term test of a 30 degree fiber angle orientation specimen were compared to theoretical predictions obtained by transforming the principal compliance matrix to the 30 degree orientation.

THE EFFECT OF PHYSICAL AGING ON THE CREEP RESPONSE OF A THERMOPLASTIC COMPOSITE

by

Robert L. Hastie Jr.

Dissertation submitted to the Faculty of the
Virginia Polytechnic Institute and State University
in partial fulfillment of the requirements for the degree of

DOCTOR OF PHILOSOPHY

in

Engineering Mechanics

APPROVED:

Don H. Morris
D.H. Morris, Chairman

Edmund G. Henneke II
E.G. Henneke II

Dean T. Mook
D.T. Mook

Wayne W. Stinchcomb
W.W. Stinchcomb

E.R. Johnson
E.R. Johnson

26 June 1991
Blacksburg, Virginia

THE EFFECT OF PHYSICAL AGING ON THE CREEP RESPONSE OF A THERMOPLASTIC COMPOSITE.

by

R.L. Hastie Jr.

Committee Chairman: D.H. Morris

Engineering Mechanics

(ABSTRACT)

The effect of thermoreversible physical aging on the linear viscoelastic creep properties of a thermoplastic composite was investigated. Radel X/IM7, an amorphous composite material considered for use in the next generation high speed transport aircraft, was studied. The operating environment for the aircraft material will be near 188°C (370°F) with a service life in excess of 60,000 hours at temperature. Accurate predictions of the viscoelastic properties of the material are essential to insure that design strength and stiffness requirements are met for the entire service life.

The effect of physical aging on the creep response was studied using momentary tensile creep tests conducted at increasing aging times following a rapid quench from above the glass transition temperature (T_g) to a sub-T_g aging temperature. As the aging time increased, the creep response of the material significantly decreased. The tensile creep compliance data for each aging time were fit to the empirical equation for the creep compliance **D(t)**:

$$D(t) = D_0 e^{\{(t/t_0)^m\}}$$

where D_o, t_o, and m are fitting parameters determined using a nonlinear fitting program based on the Levenberg-Marquardt finite difference algorithm. The short-term creep compliance curves, obtained at various aging times, were then shifted to form a momentary master compliance curve. The double-logarithmic aging shift rate μ and its dependence on sub-T_g aging temperature were determined. The aging characterization process was conducted on unidirectional specimens with 0, 90, and 45 degree fiber direction orientations. This permitted the calculation of the complete principal compliance matrix for the composite material. The effect of physical aging becomes more apparent during long-term tests when creep and aging occur simultaneously. This results in a gradual stiffening and decrease in the creep response with increased time. Predictions based solely on the Time-Temperature Superposition Principle would significantly over-predict the creep response if physical aging effects were ignored. Theoretical predictions for long-term creep compliance were made using an effective time theory and compared to long-term experimental data for each fiber orientation. Finally, experimental results of a long-term test of a 30 degree fiber angle orientation specimen were compared to theoretical predictions obtained by transforming the principal compliance matrix to the 30 degree orientation.

ACKNOWLEDGEMENTS

The author gratefully acknowledges the numerous individuals who have made this study possible. Each of you have made your own special contribution to help me over this hurdle in my life.

I especially thank Colonel Cary Fisher, Head of the Department of Engineering Science and Mechanics, USAF Academy, for the opportunity to continue my education and for expressing his confidence in me and my abilities. Your respected voice of encouragement reached a long way to boost my morale.

My deepest thanks go to my Committee chairman Dr. Don Morris for his advice, patience, and never ending enthusiasm. You provided the shining light for all those dark moments that occur during experimental work.

I'd also like to thank Dr. E.G. Henneke II, Dr. D.T. Mook, Dr. W.W. Stinchcomb, and Dr. E.R. Johnson for serving as committee members. It has been a pleasure knowing and working with each of you.

I thank Dr. Charles Harris and Dr. Thomas Gates from NASA Langley Research Center for their patience during the initial stages of the project and for providing the composite material.

A special thanks goes to everyone who has helped me with the details of conducting my experiments. Bob Simmons provided the data acquisition system. Dr. D. Dillard, Yeou Shin Chang,

and Danny Reed gave their advice and shared the Adhesive Science lab equipment. Dr. Hyer donated the NASA oven controller and data acquisition board for use in this study. Rob Swain, Jack Lesko, Greg Carman, and Ahmad Razvan provided friendship and long term use of MRG equipment. George Lough provided the strain gage conditioning amplifiers. Bob Davis, Bill Shaver, and Archie Montgomery squeezed in my no notice machining needs. Randy Waldan did the welding of the numerous thermocouples. Min-Chung Li helped determine the fiber volume fraction of the composite. Paul Vail, from the Chemistry department, conducted the DSC and TGA scans. Pedro Morales shared the office in 309 Femoyer with me. Robert Canfield and Mike Smith provided timely comments on dissertation text.

To my wife, Vicki, and daughter Jessica, your love, understanding, and little hugs gave me the will to continue. I'll always be there for you, as you were here for me. We can make it through anything as long as we have each other.

To my mother, Joan, and my sister Sheryl, thanks for all your love and support during my periods of shaken confidence. It was enjoyable living close enough so we could have weekend visits together.

Finally, I'd like to dedicate this work to my deceased father, Bob Hastie. He sacrificed everything during his life so that my life would be better. No deeds or acts can ever fully express my gratitude...

TABLE OF CONTENTS

TABLE OF TABLES

TABLE OF FIGURES

1 INTRODUCTION

The use of composite materials has dramatically increased during recent years. Today, numerous industries use composite materials to fabricate products. Composite materials are used in products ranging in diversity from aircraft structures, automobile parts, boat hulls, submarines, to artificial hip joints, sporting equipment, and body armor. The potential advantages of composite materials over conventional materials are numerous. Two important advantages, especially in weight sensitive applications, are the improved strength-to-weight and strength-to-stiffness ratios composites materials have over metal alloys. The aerospace industry initially capitalized on these material advantages by building replacement parts for aircraft using composite materials. The replacement parts were lighter in weight and contained fewer pieces than their metal counterparts. More importantly, the aerospace industry gained valuable experience working with composite materials during the design, fabrication, and life validation of the replacement parts. This positive experience with composites helped convince aerospace industry leaders to start utilizing composite materials in new aircraft designs.

Another advantage of composites is the ability to "tailor-design" the directional properties of the material. Single-ply direction laminated fiber reinforced plastic composites are highly orthotropic in stiffness and strength. The properties of a composite material can vary from quasi-isotropic, orthotropic, to anisotropic, depending upon the ply orientations used in the laminate. Conventional metal alloys are usually considered isotropic in both stiffness and strength. The X-29 forward swept wing aircraft is an example of how the orthotropic nature of composites was utilized in the aircraft design to solve an aerodynamic instability problem. The aircraft wing structure was fabricated using a selective layering of graphite-epoxy plies of various thickness and angle orientations. The resulting forward swept wing twists the leading edge down when the wing bends upward. This decreases the angle of attack of the wing and keeps the structure aerodynamically stable.

The military, in its quest for state of the art aerospace equipment, is a primary driver and funding source for composite material research and development. Recent aircraft development programs, like the F-117 stealth fighter and B-2 bomber, extensively utilized composite materials. The advanced tactical fighter (ATF), currently in the demonstrator phase of development, is projected to be constructed using 50% to 70%, by weight, composite materials.

The weight savings and material direction property tailoring advantages must be weighted against the possible disadvantages of composites. A key disadvantage of polymer-based composites is that they exhibit time dependent properties. These time dependent or viscoelastic properties must be fully characterized in order to predict the long-term response of the material. The viscoelastic characterization is complicated by several factors. One factor is the time required to perform arduous long-term characterization tests. Fortunately, the test time has been successfully reduced by applying accelerated testing techniques, like the Time-Temperature Superposition Principle (TTSP) [25,68]. Another complicating factor is the number of material constants required to describe the behavior of orthotropic composite materials. Metal alloys, normally considered isotropic, require only two independent material variables, such as Young's modulus and the shear modulus to characterize the material. Orthotropic composite materials require nine independent material variables [29] for a full three dimensional characterization. Typically, composites are used in the form of thin sheets with the loading applied in-plane. Under these conditions, i.e., a two dimensional state of plane stress, the number of independent material constants is reduced from nine to four. Additional complication

arises from the possible dependence of the four material constants on temperature, moisture, ultraviolet radiation, aging time, aging temperature, and stress level.

This study concentrated on characterizing the effect of thermoreversible physical aging on the viscoelastic creep response of a composite in its glassy state. Specifically, the effects of aging temperature and aging time on the creep response of Radel X/IM7, a thermoplastic composite, were studied. The goal was to predict the long-term creep response of unidirectional off-axis composites as the material experiences simultaneous physical aging and creep deformation associated with an applied load.

While the details are discussed in section 2.2, the concept of thermoreversible physical aging is briefly summarized here. A polymer, quenched from the rubbery state above the glass transition temperature, T_g, to some lower temperature, does not achieve thermodynamic equilibrium [31]. This is due to the rapid increase in viscosity as T_g is approached from above. As the viscosity increases, the motion of polymer chains are impaired and the polymer is unable to reach the equilibrium degree of packing before solidification. A characteristic of a polymer, in the quenched state, is that an excess of trapped free volume exists in the structure. As a result, the polymer exhibits volume relaxation with time as the structure tends toward the equilibrium state. Struik [62] referred to this

slow gradual approach to volume equilibrium as physical aging. During the physical aging process, many of the physical and mechanical properties of the material change [67]. These changes include an increase in density, tensile yield stress, and elastic modulus. Also, a decrease occurs in impact strength, fracture energy, ultimate elongation, and creep rate. This study concentrates specifically on investigating how the creep response of a composite material is affected by physical aging.

1.1 Literature Review

The literature review is divided into two sections. First, a review of the creep characterization work, completed at Virginia Polytechnic Institute and State University (VPI & SU), is presented. This section outlines the results of previous efforts to characterize the creep response of composite materials and illustrates the need for the current research effort. Next, a summary of the effects physical aging has on polymer-based materials is presented. Polymer based composites are expected to show similar aging effects, since the polymer matrix constituent mainly controls the viscoelastic response of the composite.

1.1.1 Creep Characterization at VPI & SU

Over the past ten years, extensive work has been completed at VPI & SU to improve the understanding of the viscoelastic

response of polymer-based composite materials. The focus of this work has been to characterize the creep compliance and the time to rupture of various composite material systems.

Yeow et al [74] initiated the viscoelastic characterization work at VPI & SU with the investigation of the creep response of T300/934 graphite/epoxy composite material. He used the Time-Temperature Superposition Principle (TTSP) to shift the results of short-term (16 minute) creep tests, at various temperatures, to form transverse, S_{22}, and shear, S_{66}, master creep compliance curves. Among his noteworthy findings was the observation that the fiber direction compliance, S_{11}, and fiber/transverse coupling compliance term, S_{12}, were both time-independent. Also, from the results of Yeow's work, Morris et al [47] reported the coupling compliance terms S_{12} and S_{21} were symmetric with only a small difference in magnitude.

Griffith et al [26] continued the viscoelastic characterization of the T300/934 composite material. He generated master compliance curves for the S_{22} and S_{66} directions using both temperature and stress as shifting parameters. The fiber dominated S_{11} compliance term was found to have a slight decrease with temperature, but no stress dependence. The slight temperature dependence was attributed to the viscoelastic nature of the strain gage adhesive. The master compliance curves were used to generate compliance predictions for 30 and 60 degree off-axis lamina specimens. The predictions had fairly

good agreement with the test data up to a test time of about 4 days. After this period, the prediction and test data tended to digress. Griffith also expressed concern about possible effect of physical aging on the T300/934 material. In order to avoid the physical aging, he heated the specimens above T_g and then cooled them at a very slow rate (several °F per hour) to a point reasonably below T_g. Griffith assumed this annealing process would freeze the equilibrium amount of free volume into the specimen and minimize the effects of physical aging.

Dillard et al [13,14] continued working with the T300/934 graphite/epoxy composite material. He used the nonlinear Findley power law to represent the S_{22} and S_{66} creep compliance terms at a constant temperature of 160°C (320°F). The power law compliance representation was then incorporated into an incremental numerical computer program, based on lamination theory, called VISLAP. The program was used to predict the creep compliance and rupture time for general laminates at 160°C (320°F). Predictions for matrix dominated laminates, at several different stress levels, agreed with experimental data. Fiber dominated laminate predictions were erroneously bounded by the lamination theory assumption that no interlaminar deformations exist [13]. The absence of interlaminar deformations fixed the predicted laminate deformation at the value set by the truss network formed by the time-independent fiber ply directions in the laminate.

Caplan et al [7] applied nonlinear viscoelastic models developed by Findley and Schapery to polycarbonate creep and recovery data obtained at various temperatures and stress levels. The creep tests lasted 30 minutes and were followed by a 60 minute recovery period. The Findley power law model parameters were fit to the data using a linear regression technique. The predictions resulting from the model deviated from the experimental data at longer creep times. The Schapery model was then used to fit the data using a graphical technique. A reasonable fit was obtained after a correction for unrecoverable strain effects. No attempt was made during this study to compare the predictive capability of either model beyond the 30 minute short-term tests.

Bertolotti [4] developed a numerical procedure for evaluating the parameters in Schapery's nonlinear viscoelastic model. The procedure was based on the Levenberg-Marquardt algorithm [28]. This algorithm finds the minimum of the sum of the squared error between the data points and a nonlinear function. This numerical fitting procedure provided an easy and repeatable means of fitting the Schapery model parameters to actual test data.

Hiel et al [27] continued work on the viscoelastic characterization of T300/934 graphite/epoxy composite material following Dillard. He used the numerical procedure developed by Bertolotti to fit the Schapery model to experimental data

generated at various temperatures and stress levels. The stress dependence of the Schapery model parameters was determined for the shear compliance S_{66} term. It was also reported that the transverse compliance S_{22} term was independent of stress during the short time creep (1 hour) test conducted during this study. However, when compared to long-term test data previously generated by Griffith et al [26], it was determined that the stress independence of the S_{22} term required further examination. Long-term tests to verify compliance predictions derived using the Schapery model were not conducted during this study.

Yen [73] continued the creep characterization work at VPI & SU but switched from orientated laminated composite materials to a random fiber composite material known as SMC-R50. He developed a numerical procedure, similar to Bertolotti's, to fit the Findley model parameters to creep data. It was found that the time exponent, "n" in the Findley equation, depended on the duration of the creep test, but approached an asymptotic value for long tests. The predictions derived form the Findley equation accurately predicted long-term creep response. In addition, the creep response due to multiple step loadings was predicted using a modified superposition principle with success. Yen noted that the random fiber composite required mechanical conditioning prior to each creep and recovery test

in order to obtain repeatable results. Additionally, Yen found the results from the conditioned specimen tests were within the data scatter band of unconditioned specimens.

Tuttle et al [68] investigated the viscoelastic creep response of T300/5208 graphite epoxy composite laminates. He used a 480/120 minute creep/recovery test cycle on 0, 10, and 90 degree specimens, at various stress levels, with the temperature held constant at 149°C (353°F). The Schapery nonlinear viscoelastic model parameters were successfully fit to the test data using the numerical technique developed by Bertolotti. Tuttle noted that long-term predictions from the Schapery model were most sensitive to errors in the exponent "n". Long-term creep tests of unidirectional laminates, to verify the predictive capability of the Schapery model, were not conducted during this study. Instead, long-term tests, lasting 10^5 minutes, were conducted on two multiangle symmetric laminates. Analytical creep compliance predictions were obtained using the VISLAP program written by Dillard. The program was modified to utilize the Schapery nonlinear viscoelastic model instead of the Findley power law. The long-term testing revealed that the predicted viscoelastic response was significantly less than the measured response. This discrepancy was not definitely explained, but was thought to be due to stress interaction effects within individual plies or due to interlaminar shear deformations effects.

Owens [51] conducted an experimental investigation of the material properties of graphite/polyphenylene sulfide, a thermoplastic composite system. His creep tests, conducted on $(\pm 45_2)_s$ specimens at 177°C (350°F), produced results of particular interest to the present study. The testing consisted of two 72 hour creep tests run sequentially. The first creep test was followed by a recovery period until the strain returned to zero. The second test was then started with the temperature continuing to be held at 177°C (350°F). Owens observed that the stiffness significantly increased between the two creep tests. Unable to explain this phenomenon, the test sequence was repeated with a new specimen. Again, the stiffness was found to increase. It is well known (see Struik [59]) that polymer based materials increase in stiffness as they physically age. Thus, physical aging, occurring simultaneously with the creep deformations during the first test, offers an explanation for the increase in stiffness during the second creep test.

Gramoll et al [25] studied the thermoviscoelastic response of Kevlar 49/Fiberlite 7714A epoxy composite lamina and laminates. Both the matrix and fiber in this material system exhibit viscoelastic behavior. Thus, all four material compliance terms were time dependent. The viscoelastic response was determined using short-term (20 minute) tests at various temperatures and stress levels. Gramoll used TTSP and the Findley power law to model the linear viscoelastic behavior.

Nonlinear effects were modeled with a new quadratic power law developed during the study to facilitate numerical implementation. A new program called VCAP (Viscoelastic Composite Analysis Program) was written to predict the viscoelastic response of composite laminates. The program was based on a nonlinear differential equation formulation using a series of Kelvin elements (i.e. Prony series) to represent the viscoelastic material behavior. Numerical predictions for unidirectional, two direction and three direction laminates agreed very well with the 4 week long test data generated during the study.

1.1.2 Physical Aging Effects

Interest in the effects of physical aging on polymeric material properties dates back to early work by Kovacs [31]. His research showed that the volume of a polyvinylacetate sample, after a quench from far above T_g to a constant temperature below T_g, slowly decreased with time. Struik [59] studied more than 35 amorphous polymers and found that the small-strain mechanical properties changed dramatically during this volume relaxation process. Struik reported the effect of physical aging on both the elastic and viscoelastic material properties. Among his findings were the observations that during physical aging the material increases in stiffness and

becomes more brittle. He was able to characterize the rate at which physical aging occurs and developed a model to predict the long-term viscoelastic response of amorphous polymers.

Fundamental to Struik's model was the observation that momentary creep compliance curves exhibit an universal shape in the temperature range associated with physical aging. Momentary compliance curves are formed using results of creep tests where the test duration remains small compared to the time measured starting after the quench from above T_g and continued till the start of the creep test, referred to as the aging time. Momentary tests are essentially a "snapshot" of the compliance properties taken at a constant aging time. The existence of this universal shape of the momentary creep compliance curves has been reported by other investigators [63]. The universal shape implies that the relaxation spectrum does not change with temperature or aging time [6]. Thus, the relaxation times contained in the relaxation spectrum are all identically shifted by temperature or aging time [70]. The effect of temperature or aging time on short-term momentary creep compliance curves was seen as a horizontal shift of the curve on the log-time scale. The marked curvature of the compliance curves allows the shift factor for each short-term test to be unambiguously determined. A master momentary creep compliance curve was formed by shifting several short-term curves obtained at different temperatures or aging times. The

actual long-term creep response was obtained using an effective time theory developed by Struik with the derivation details found in section 2.2.5.4. The theory is based on the assumption that the relaxation times all have the same aging dependence. The aging dependence is characterized by the aging rate of the material. The theory is applied by replacing the current time t, used in the momentary master creep curve, with an effective time λ. The effective time accounts for the shifting of the relaxation times as the material ages.

Booij et al [6] noted that the physical aging effects are influenced by the rate the material is cooled from above T_g. This influence is due to the free volume dependence on the cooling rate. At faster cooling rates, the difference between the material volume state and the equilibrium volume state is larger than it is at slower cooling rates. The larger volume difference equates to a greater change in the physical properties of the material during the physical aging process.

During physical aging, the enthalpy of the material exhibits the same relaxation phenomena as volume [38]. The enthalpy and heat capacity, i.e., first derivative of enthalpy with respect to temperature, at a constant pressure, are thermodynamic quantities that can be monitored using differential scanning calorimetry (DSC) equipment. The effect of physical aging on these thermodynamic properties has been reported by several investigators [10,49,67]. They noted a correlation

between aging time and the location of the endothermic peak as the temperature was raised during a DSC test. This correlation was used as a method to monitor the extent of physical aging in the material.

The effects of physical aging continue until the material reaches volume equilibrium. The time required to reach volume equilibrium depends on the aging temperature. At aging temperatures less than T_g minus 27°F (15°C), the material will not reach thermodynamic equilibrium in a practical time frame [66]. Therefore, polymer products used in the aging temperature range can be expected to change physical properties during a normal service life of 10 - 50 years [59]. Predicting the physical aging effect on the material properties has prompted considerable research. Several recent papers have reported physical aging effects on neat resin and composite laminate materials.

Vleeshouwers et al [70] recently reported the effects of physical aging on the creep and stress relaxation properties of cured EPON 828/Epoxy in the linear viscoelastic range. They successfully measured the aging rate at several temperatures below T_g. The short-term momentary creep and stress relaxation curves were successfully shifted to form master curves. Long-term test results were not reported to verify the accuracy of the master curves.

Work by Wang and Ogale [71] showed the effect of physical aging on the relaxation and dynamic mechanical moduli properties of neat epoxy and an epoxy/carbon fiber reinforced composite at a constant test temperature. It was reported that both the epoxy and composite had the same aging shift rate. Their conclusion was that the fiber reinforcing did not alter the aging characteristics of the epoxy.

The most recent physical aging study on composites was performed by Sullivan [66]. He worked with neat Dow Derakane 470-36 resin and an unidirectional glass reinforced composite. The thermoset resin and composite were both found to have the same aging shift rate. This observation is consistent with the work of Wang and Ogale [71]. Momentary creep master curves were constructed for the neat resin and the four composite compliance directions. The S_{11} and S_{12} directions were found to be independent of physical aging. Long-term predictions, using Struik's effective time theory, agreed with experimental data up to about 200 hours of creep. After this time period, the predictions followed the same data trend but differed in the magnitude of the creep compliance.

1.2 Overview of Proposed Study

The goal of this study was to determine the effect of physical aging on a thermoplastic composite material. Radel X/IM7 composite material was chosen for evaluation. This material is currently being considered by NASA Langley for use

in the next generation high speed transport aircraft. The operating environment for this aircraft will be near 188°C (370°F) with the service life of 60,000 to 120,000 hours at temperature. Accurate predictions of the viscoelastic properties of the material are essential to insure the material meets the design strength and stiffness requirements for the entire service life.

Three project objectives were defined to meet the goal of this study. The first objective was to develop the experimental procedures required to conduct physical aging creep experiments. Several experimental problems were encountered during preliminary creep testing. In particular problems with strain measurement, data acquisition, oven thermal stability, and specimen quenching procedures were experienced. The experimental procedures developed to solve these problems were documented to ensure future aging experiments are conducted in a repeatable and consistent manner.

The second objective was to apply the developed experimental procedures to characterize the influence of sub T_g physical aging on the creep response of Radel X/IM7 composite material. Short-term creep tests were used to determine the aging rate and its dependence on aging temperature. In addition, various ply angle orientations were tested to determine the effect of the physical aging on each of the four compliance matrix terms (S_{11}, S_{12}, S_{22}, and S_{66}) in the linear viscoelastic range.

The third and final objective was to conduct long-term creep tests to verify the influence of physical aging on the creep response of the Radel X/IM7 composite material. The long-term tests were initially conducted on each of the ply angle orientations tested during determination of the compliance matrix terms. The test results were then compared with theoretical predictions calculated using Struik's effective time theory. Finally, a 30 degree off-axis specimen was tested and compared to the creep compliance prediction obtained by transforming the compliance matrix to the specimen's angle orientation.

2 BACKGROUND INFORMATION

Viscoelasticity, as its name implies, is a combination of the studies of viscous fluids and elasticity. Viscoelastic materials are characterized by having time-dependent mechanical behavior with a memory effect. The discussion herein will describe the terminology and analysis models used to describe viscoelastic material behavior. Also, the effects of physical aging on the viscoelastic response of the material are discussed. Additional information on the subject is located in several reference books [1,11,16,22,23,59].

2.1 Viscoelastic Materials

Viscoelastic materials exhibit time-dependent mechanical behavior with memory effects. This type of material response is demonstrated when a viscoelastic tensile specimen is loaded with a constant force. A viscoelastic material will initially elongate when the load is applied, as in any normal elastic material, but will also continue to elongate with time while the load remains applied. This continuing time-dependent elongation is referred to as creep. During this creep process, the apparent Young's modulus E will steadily decrease as the specimen elongates with time. Upon removal of the load, the viscoelastic material will remember its original configuration and will tend to recover to that configuration with time.

2.1.1 Common Tests

Three types of tests are commonly used to characterize the mechanical response of a viscoelastic material. The tests used are the creep/creep recovery test, the stress relaxation test, and the constant strain rate test. The least complex test to conduct of the three is the two part creep/creep recovery test. The first part, known as the creep portion, is defined by the response up to time t_1. During this time segment, a constant uniaxial step input load is applied to the specimen, as shown in figure 2.1. The viscoelastic material responds with an initial elastic strain ε_e, followed by a continually increasing creep strain ε_c, also shown in figure 2.1. The second part, known as the recovery portion, starts after time t_1, when the input load is removed. During this portion, a reverse elastic strain ε_e is followed by recovery of a portion of the creep strain at a continuously decreasing rate, as shown in the material response illustration in figure 2.1. The viscoelastic material may recover to the entire creep strain if sufficient time is allowed for recovery. This is the simplest test of the three tests to conduct, because the applied force is either a constant or zero. Additionally, the creep compliance D(t) is easily calculated by dividing the strain, measured at the center of the specimen, by the applied constant stress value. Specimens for this test are designed

with adequate length to insure the effect of the end constraint, provided by the gripping fixtures, has a minimal effect on the stress at the center of the specimen.

The next increasingly complex test which can be conducted is the stress relaxation test. This test measures the stress relaxation in the specimen as it is subjected to a constant uniaxial strain input load, shown as ε_o in figure 2.2. The input load produces an initial stress σ_o, which slowly relaxes with increased time, as shown in the material response illustration in figure 2.2. The increased complexity of this test is partly due to the equipment required to hold a constant strain on the test specimen. In order to accomplish this, the testing machine must be able to decrease the load applied to the specimen as time increases. Another complication is the requirement to minimize the effect of end constraint provided by the grips on a anisotropic specimen. The assumption of constant strain for the length of the specimen cannot be satisfied at the specimen attachment points unless proper grip rotation is provided.

The final test discussed herein is the constant strain rate test. This test was suggested by Smith [58] to determine the relaxation modulus E(t) of elastomers. During this test, the viscoelastic material is loaded with an uniaxial strain that is increased as some constant rate R, as shown in figure 2.3. The axial load required to produce the constant strain

rate is monitored during the test and used to calculate the stress response. Viscoelastic materials respond to the loading with a nonlinear increase in stress with increasing time, as shown in the material response illustration of figure 2.3. The relaxation modulus is found by calculating the instantaneous slope of the stress strain curve. This test is also more difficult to conduct in view of the increased complexity of the test machine required to produce a constant strain rate in the specimen.

2.1.2 Linear Viscoelasticity

2.1.2.1 Definition

Viscoelastic materials, like elastic materials, may be classified as either linear or nonlinear. Findley et al [22] and Schapery [57] both define a viscoelastic material as linear when stress is proportional to strain at a given time and when linear superposition holds. Mathematically these requirements are represented by the equations:

$$\varepsilon[c\sigma(t)] = c\varepsilon[\sigma(t)] \tag{2.1}$$

$$\varepsilon[\sigma_1(t) + \sigma_2(t-t_1)] = \varepsilon[\sigma_1(t)] + \varepsilon[\sigma_2(t-t_1)] \tag{2.2}$$

where σ is the input stress, ε is the output strain and c is a constant. The first requirement, equation 2.1, states that the strain response of a scalar times the input stress equals the scalar times the strain response of the original input stress. This is illustrated in figure 2.4 (a). The second requirement, equation 2.2, states that the combined strain response of two different loadings applied at different times is the sum of the strain outputs of each load acting separately and is illustrated in figure 2.4 (b). This second requirement is also commonly referred to as the Boltzmann's Superposition Principle.

2.1.2.2 Boltzmann's Superposition Principle

The concept of summing the effects of various input loads can be extended to arbitrary stress or strain histories. This is accomplished by approximating the arbitrary stress history with a series of steps of stress inputs as shown in figure 2.5. Mathematically this is represented by:

$$\sigma(t) = \Delta\sigma_0 H(t) + \Delta\sigma_1 H(t-\tau_1) + \Delta\sigma_2 H(t-\tau_2) + \cdots + \Delta\sigma_i H(t-\tau_i) \qquad (2.3)$$

where the Heaviside function H(t) is defined as:

$$H(t) = \begin{cases} 0, \text{when } t < 0 \\ 1, \text{when } t \geq 0 \end{cases} \qquad (2.4)$$

with the strain response to this stress input given by:

$$\varepsilon(t) = D(t)\Delta\sigma_0 + D(t-\tau_1)\Delta\sigma_1 + D(t-\tau_2)\Delta\sigma_2 + \cdots + D(t-\tau_i)\Delta\sigma_i \qquad (2.5)$$

where $D(t-\tau_i)$ is the compliance for each time step. If the time intervals between steps shrinks to an infinitesimal amount, an integral expression of the total strain is given by:

$$\varepsilon(t) = \int_0^t D(t-\tau)\, H(t-\tau)\, d[\sigma(\tau)]. \qquad (2.6)$$

Assuming the stress history is differentiable and knowing that the Heaviside function is unity over the range of integration, equation 2.6 reduces to the following form:

$$\varepsilon(t) = \int_0^t D(t-\tau)\frac{\partial\sigma(\tau)}{\partial\tau}\, d\tau. \qquad (2.7)$$

Similarly, an expression for the stress response to an arbitrary strain history is given by:

$$\sigma(t) = \int_0^t E(t-\tau)\frac{\partial\varepsilon(\tau)}{\partial\tau}\, d\tau \qquad (2.8)$$

where $E(t)$ is the relaxation modulus.

2.1.2.3 Mechanical Models

Many types of mechanical analog models can be used to model viscoelastic behavior. Mechanical models are constructed using various combinations of linear spring and linear dashpot elements. The stress and strain in a linear spring are related by the equation:

$$\sigma_{spring} = \sigma_s = E\,\varepsilon \tag{2.9}$$

where **E** is interpreted as a linear spring constant or Young's modulus. The stress in a linear dashpot is related to the strain rate in the dashpot by:

$$\sigma_{dashpot} = \sigma_d = \mu \frac{d\varepsilon}{dt} = \mu\,\dot{\varepsilon} \tag{2.10}$$

where μ is called the coefficient of viscosity. The two simplest mechanical models are derived by combining a single spring and single dashpot element. The Maxwell model connects the two elements in series, whereas the Kelvin model uses a parallel arrangement. Both models are graphically represented in figure 2.6.

The Maxwell model is examined in more detail first. In this model, the total strain and total strain rate are calculated

by summing the component carried by each of the two elements. These relationships and the stress definitions in equations 2.9 and 2.10, are used to derive the following stress-strain equation:

$$\dot{\varepsilon}=\frac{\dot{\sigma}}{E}+\frac{\sigma}{\mu}. \tag{2.11}$$

This differential equation can be solved for various stress or strain inputs. Classical solutions include the strain response to a constant stress input $\sigma=\sigma_0$, applied at $t=0$, given by the following relationship:

$$\varepsilon(t)=\frac{\sigma_0}{E}+\frac{\sigma_0}{\mu}t. \tag{2.12}$$

or the stress response to a constant strain input $\varepsilon=\varepsilon_0$, applied at $t=0$, given by the relationship:

$$\sigma(t)=E\,\varepsilon_0\,e^{-(Et/\mu)}=E\,\varepsilon_0\,e^{-(t/\lambda)} \tag{2.13}$$

where $\lambda=\mu/E$ is called the relaxation time.

The Kelvin model uses a parallel arrangement of the spring and dashpot elements. In this model, the total stress carried

by the model is calculated by summing the amount of stress carried by each of the two elements. This relationship is used with equations 2.9 and 2.10 to derive the following stress-strain equation:

$$\dot{\varepsilon}+\frac{E}{\mu}\varepsilon=\frac{\sigma}{\mu}. \tag{2.14}$$

This differential can be solved for creep loading with $\sigma=\sigma_0$, applied at $t=0$. The resulting strain solution is:

$$\varepsilon(t)=\frac{\sigma_0}{E}(1-e^{-(Et/\mu)})=\frac{\sigma_0}{E}(1-e^{-(t/\lambda)}) \tag{2.15}$$

where $\lambda=\mu/E$ is called the retardation time.

The use of the Maxwell and Kelvin models to accurately represent viscoelastic materials is limited. This is due to the inability of the models to describe the entire actual material response. For example, the Maxwell model does not show time-dependent recovery after a constant stress input load is removed. Additionally, upon loading or unloading, the Kelvin model fails to exhibit time-independent strain that usually occurs with actual materials. More complex mechanical models have been developed by combining Maxwell and Kelvin

models in various combinations. These variations will not be described here, but may be found in a book by Findley et al [22].

One complex model that is widely used for viscoelastic modeling where the stress history has been prescribed is the generalized Kelvin model, illustrated in figure 2.7. This model, sometimes referred to as the Prony series, consists of n Kelvin elements connected in series. The Prony series offers the advantage that each Kelvin element can be solved independently. The total solution is obtained by summing each of the individual Kelvin element solutions. The Prony series solution for creep loading with $\sigma = \sigma_0$, applied at $t = 0$, is written as:

$$\varepsilon(t) = \sigma_0 \sum_{i=1}^{n} \frac{1}{E_i}\left(1 - e^{-(E_i t/\mu_i)}\right) = \sigma_0 \sum_{i=1}^{n} \frac{1}{E_i}\left(1 - e^{-(t/\lambda_i)}\right). \tag{2.16}$$

An initial elastic time-independent strain can be added to the model by placing a single spring element in series with the Kelvin elements. The solution for creep loading becomes:

$$\varepsilon(t) = \frac{\sigma_0}{E_s} + \sigma_0 \sum_{i=1}^{n} \frac{1}{E_i}\left(1 - e^{-(t/\lambda_i)}\right) \tag{2.17}$$

where E_s is the spring constant of the additional single spring element.

The obvious disadvantage to the Prony model is the large number of material constants required to describe the material. The model requires both E and μ for each Kelvin element used in the summation. Gramoll et al [25] used the Prony series in his work and suggests spacing the retardation times $\lambda_i = \mu_i / E_i$ at about one per each decade of time that is modeled. Gramoll solved for the numerous material constants in the Prony series by initially fitting the viscoelastic data with a power law model. Then, he utilized a numerical procedure to fit the Prony series constants to the power law model for each time decade.

2.1.2.4 Power Law Model

Findley et al [17,19,20,22,33,34] observed that the following power function of time empirically fit creep data of many linear rigid plastics over a wide time span:

$$\varepsilon(t) = \varepsilon_0 + m\, t^n \tag{2.18}$$

where ε_0, m, n are material constants of the model. Findley et al [22] have reported that the material constants ε_0 and m are functions of stress and temperature, whereas n is independent

of stress and nearly independent of temperature.

Several investigators at VPI & SU have used the Findley power law model to represent viscoelastic behavior. Notably, Dillard el al [13] found that the coefficients of the power law equation may become singular when fit to creep data using a fitting procedure developed by Boller [5]. Additionally, Dillard noted how small errors in experimental data may result in large errors in the determined power law material constants. Yen [73] found the material constants using a Levenberg-Marquardt algorithm, available on IMSL [28] FORTRAN subroutines, to minimize the sum of the squares of error between the data points and the power law function. This method provided an accurate and consistent method for determining the power law constants.

2.1.2.5 Struik Model

Struik [59], in his studies of physical aging of polymers, experimentally determined that momentary creep curves, in the small strain behavior range of polymeric materials, have the same shape when plotted on double-logarithmic scale. The requirement for momentary creep testing, i.e., when the creep test duration is short compared to the previous aging time, is fully explained in section 2.2. Struik found the shape of the creep compliance curve could be described by the equation:

$$D(t) = D_0 e^{(t/t_0)^m} \tag{2.19}$$

where D_0 represents the compliance immediately after stress application, t_0 is variable proportional to the mechanical relaxation time and m is a material constant. In uniaxial tensile creep tests, the applied stress σ is constant and is related to the compliance and strain by the equation:

$$D(t) = \frac{\varepsilon(t)}{\sigma}. \tag{2.20}$$

Using equation 2.20, equation 2.19 is rewritten in terms of strain response as:

$$\varepsilon(t) = \varepsilon_0 e^{(t/t_0)^m} \tag{2.21}$$

where $\varepsilon_0 = \sigma D_0$. The analytical representation of the compliance response (equation 2.19) is useful for determining logarithmic shift factors used in time-aging shifting and time-temperature superposition.

2.1.2.6 Time-Temperature Superposition Principle

The goal of accelerated characterization of a material is to develop a method that uses short-term testing results for

the prediction of long-term behavior. Time-Temperature Superposition Principle (TTSP), also known as The Method of Reduced Variables, uses temperature as a parameter to accelerate time dependent processes, like creep. Leaderman [35] introduced TTSP in 1943 as an empirical observation about the shape of creep compliance curves at elevated temperatures. He noted that compliance curves at various temperatures are basically the same shape, but displaced along the time axis. The principle is illustrated by shifting several compliance curves, each measured at a different temperature, along the time axis to form the master compliance curve shown in figure 2.8. The amount of horizontal shifting, labeled a_{T_1} and a_{T_2} respectively for each curve in figure 2.8, is a function of the temperature differential between the shifted curve and the curve chosen as the reference.

Two functional forms for the shift factor function are widely used and work for many materials. First, when the temperature is less than the glass transition temperature ($T<T_g$), the Arrhenius equation [16] is usually applicable and is written as:

$$\log a_T = \frac{\Delta H}{2.303\,R}\left(\frac{1}{T}-\frac{1}{T_R}\right) \tag{2.22}$$

where ΔH is the constant activation energy (per mole), R = 1.987 (cal/mole K) is the universal gas constant, and both the temperature T and reference temperature T_R are in degrees Kelvin.

The second equation, called the Williams-Landel-Ferry (WLF) equation [72], normally applies when the temperature is greater than the glass transition temperature ($T > T_g$). The WLF equation is given as:

$$\log a_T = \frac{-C_1(T - T_R)}{(C_2 + T - T_R)} \tag{2.23}$$

where C_1 and C_2 are constants, and the reference temperature T_R is generally equal to the glass transition temperature or higher.

The shift factor a_T relates the master compliance response at the reference temperature to the response at any other temperature using the "reduced time" approach. The compliance at any temperature T follows the relationship:

$$D(T,t) = D(T_R, \zeta) \tag{2.24}$$

where t is the actual time measured from the start of load application, T_R is the reference temperature and ζ is the

"reduced time". During transient temperature conditions i.e., when $a_T\{T(\tau)\}$ is a function of temperature and time, the reduced time is related to the actual time by:

$$\zeta(t) = \int_0^t \frac{d\tau}{a_T\{T(\tau)\}} \tag{2.25}$$

where τ is an arbitrary time variable prior to t. This relationship is simplified for constant temperature testing to:

$$\zeta = \frac{t}{a_T} \tag{2.26}$$

where a_T does not change with time. The relationship between the reference creep curve and a different temperature creep curve becomes more obvious when the log of equation 2.26 is taken.

$$\log\zeta = \log t - \log a_T \tag{2.27}$$

It is easily noted that the new temperature creep curve is a shift of the reference curve in log time by an amount of $\log a_T$.

The class of material where the viscoelastic response at various temperatures can be manipulated with translation or horizontal shifting to form smooth master curve is referred to as a "Thermorheologically Simple Material" (TSM). Often, simple horizontal shifts fail to produce a smooth master curve. In these cases, additional vertical shifts of the data may be required to obtain a smooth master curve. When this additional shifting is required, due to moisture, stress or other influences, the material is referred to as a "Thermorheologically Complex Material" (TCM). Griffith et al [26] reviews the shifting procedures for TCM. He reported that the graphical normalization procedure provided the best average material properties.

2.1.3 Nonlinear Viscoelasticity

Materials that fail to meet the linearity requirements stated by equations 2.1 and 2.2 are called nonlinear. The demarcation between linear and nonlinear is somewhat arbitrary depending on the accuracy required in the analysis. Testing variables, i.e., stress level, temperature, moisture and aging time, can each influence the nonlinear viscoelastic response of a material. The Findley and Schapery models have gained popularity for modeling nonlinear effects and are discussed in further detail.

2.1.3.1 Findley Model

Findley et al [18,21] proposed modifying the simple power law function for strain response given as:

$$\varepsilon(t) = \varepsilon_0 + m\, t^n \tag{2.18}$$

where ε_0, m and n are material constants, to include nonlinear stress effects by making ε_0 and m functions of stress. The function chosen was in the form of a hyperbolic sine such that:

$$\varepsilon_0 = \varepsilon'_0 \sinh\left(\frac{\sigma}{\sigma_\varepsilon}\right) \tag{2.28a}$$

$$m = m' \sinh\left(\frac{\sigma}{\sigma_m}\right) \tag{2.28b}$$

$$n = \text{constant (independent of stress level)} \tag{2.28c}$$

where ε'_0, m', σ_ε and σ_m are material constants and may be functions of the testing variables. Substitution of equations 2.28 a, b, and c into equation 2.18 yield the Findley nonlinear model written as:

$$\varepsilon(t) = \varepsilon'_0 \sinh\left(\frac{\sigma}{\sigma_\varepsilon}\right) + m' \sinh\left(\frac{\sigma}{\sigma_m}\right) t^n. \tag{2.29}$$

Findley et al [18,21] and others [14,73] have used this empirical fitting approach to successfully model various material systems. An advantage of the Findley model is that the five material constants ($\varepsilon'_0, m', \sigma_\varepsilon, \sigma_m, n$) can be solved for using creep test strain measurements without the recovery measurements.

Gramoll et al [25] noted a problem with the Findley nonlinear model at high stress levels. The problem involved numerical difficulties when the sinh function rapidly increases for values larger than 1. Gramoll solved the numerical problem by using an alternative model which he referred to as the "Quadratic Power Law". This model replaced the sinh functions with quadratic functions such that:

$$\varepsilon_0 = \varepsilon'_0 \sinh\left(\frac{\sigma}{\sigma_\varepsilon}\right) = \varepsilon'_0(1 + g\sigma^2) \tag{2.30a}$$

$$m = m' \sinh\left(\frac{\sigma}{\sigma_m}\right) = m'(1 + f\sigma^2). \tag{2.30b}$$

The constants g and f are determined by a least-squared fit of ε_0 and m data from a series of creep tests, at various stress levels, to the quadratic function.

2.1.3.2 Schapery Model

Another popular nonlinear viscoelastic model is the Schapery integral model derived from irreversible thermodynamic

theory [54,56]. The Schapery model has been successfully applied to many materials [3,37,45]. Work at VPI & SU has also used the Schapery model. Caplan et al [7] modeled the nonlinear creep response of polycarbonate material. Hiel et al [27] characterized T300/934 graphite-epoxy composites. Tuttle et al [68] studied the nonlinear effects in T300/5208 graphite-epoxy composites.

The Schapery model's popularity is due to its single time-integral form to represent nonlinear constitutive relationships. The constitutive equation for a isotropic material under uniaxial loading with isothermal conditions can be written as:

$$\varepsilon(t) = g_0 D_0 \sigma(t) + g_1 \int_{0^-}^{t} \Delta D(\psi - \psi') \frac{d[g_2 \sigma(t)]}{d\tau} d\tau \tag{2.31}$$

with

$$\psi = \int_{0^-}^{t} \frac{dt'}{a_\sigma[\sigma(t')]} \tag{2.32a}$$

$$\psi' = \psi(\tau) = \int_{0^-}^{\tau} \frac{dt'}{a_\sigma[\sigma(t')]} \tag{2.32b}$$

where D_0 and $\Delta D(\psi)$ are the initial and transient components of compliance, g_0, g_1, g_2 and a_σ are stress dependent material functions.

The strain response for a uniaxial creep/creep recovery test can be derived by integrating equation 2.31. The creep/creep recovery stress input, shown in figure 2.1, can be written as:

$$\sigma_0[H(\tau) - H(\tau - t_1)] \tag{2.33}$$

where $H(\tau)$ is the Heaviside step function. Schapery [55] notes the time dependent creep compliance function can be represented with a power law function as:

$$\Delta D(\psi) = D_1 \psi^n. \tag{2.34}$$

Substituting equations 2.33 and 2.34 into equation 2.31 and noting that $\frac{dH(\tau)}{d\tau}$ is zero, except at $\tau = 0$ and $\tau = t_1$, and $\frac{dH(\tau)}{d\tau} = \delta(\tau)$, yields the creep strain response for $0 < t < t_1$

$$\varepsilon_c(t) = \left[g_0 D_0 + \frac{g_1 g_2 D_1 t^n}{a_\sigma^n} \right] \sigma_0 \tag{2.35}$$

and the creep recovery strain response for $t > t_1$

$$\varepsilon_r(t) = \frac{\Delta \varepsilon_c}{g_1} [(1 + a_\sigma \lambda)^n - (a_\sigma \lambda)^n] \tag{2.36}$$

where

$$\lambda = \frac{(t - t_1)}{t_1} \tag{2.37}$$

$$\Delta\varepsilon_c = \varepsilon_c(t_1) - g_0 D_0 \sigma = \left[\frac{g_1 g_2 D_1 t_1^n}{a_\sigma^n}\right]\sigma_0. \tag{2.38}$$

The strain $\Delta\varepsilon_c$ represents the transient creep component immediately before the stress is removed.

Several methods have been used to solve for the parameters in the Schapery model. Original procedures, developed by Schapery [55] and Lou et al [37], were based on graphical methods requiring horizontal and vertical shifting of linear and nonlinear data to find a best fit of the parameters. Bertolotti [4] developed a computer-based solution using the Levenberg-Marquardt algorithm to find the model parameters. Similarly, Augl et al [2] obtained the parameters using a least-squares fit of experimental data to the nonlinear power law formulation of the Schapery model.

Schapery [55] generalized his nonlinear model (equation 2.35) to the Findley nonlinear model (equation 2.29) by noting the following relationships between constants:

$$g_0 = \frac{\sinh\left(\frac{\sigma}{\sigma_\varepsilon}\right)}{\frac{\sigma}{\sigma_\varepsilon}} \tag{2.39a}$$

$$\frac{g_1 g_2}{a_\sigma^n} = \frac{\sinh\left(\frac{\sigma}{\sigma_m}\right)}{\frac{\sigma}{\sigma_m}} \tag{2.39b}$$

$$\varepsilon'_0 = D_0 \sigma_\varepsilon \tag{2.39c}$$

$$m' = D_1 \sigma_m. \tag{2.39d}$$

Additionally, when the power law compliance function (equation 2.34) is used in the Schapery model and the stresses and strains are in the linear material range, the Schapery constants become $g_0 = g_1 = g_2 = a_\sigma = 1$, with equation 2.35 reducing to:

$$\varepsilon_c(t) = D_0 \sigma_0 + D_1 \sigma_0 t^n \tag{2.40}$$

which is a form of the Findley linear power law.

2.2 Physical Aging Effects

This section describes various subjects regarding physical aging and its effects on the viscoelastic creep response of amorphous polymers. Included are discussions explaining what physical aging is and how it is related to the free volume state in the material. Also, the methods used to characterize the effect of physical aging on creep compliance response of materials are examined.

2.2.1 Basic Polymer Concepts

The free volume concept is frequently used to explain physical aging of polymer materials. This concept is easily understood with the help of a two-dimensional hard-sphere molecule model used by Zallen [75]. The free volume associated with three particular molecules A, B, and C are shown as shaded areas in figure 2.9. The shaded areas define the region accessible to the mass center of the molecule when constrained by the repulsive forces of the neighboring molecules. Molecules B and C cannot move to locations where they can be influenced by different nearest neighbor molecules. They are therefore confined to small oscillations within their free volume regions. The small oscillations are associated with secondary relaxations in the material. Molecule A, with its larger amount of free volume, is capable of changing its nearest neighbors by translating to a new location, labeled A' in figure 2.9. The ability of molecules to translate, commonly referred to as mobility, is controlled by the amount of free volume in the material. A qualitative relationship between mobility and free volume is shown in figure 2.10. Note, that at high values of free volume, the degree of packing of the molecules is small, and the mobility of the molecules is high. The mobility of the molecules effects many of the properties of

the material. As the mobility increases, the material becomes more compliant and ductile. Also, the damping ability and creep rate of the material increase.

Another important concept is the distinction between thermoplastic and thermoset classes of polymer composites. Thermoplastic polymers are characterized by their thermal reversibility. The material will soften upon heating and flow when a stress is applied. When cooled, the material reversibly regains its solid or rubbery form. Quite differently, thermoset materials undergo an irreversible curing reaction upon heating and will not regain their original form upon cooling. During the curing process, the polymer chains cross-link with strong covalent bonds that strengthen the material and increase the stiffness.

A schematic of master creep compliance curves for typical thermoplastic and thermoset polymers are shown in figure 2.11. The basic difference between the two classes of polymers is their behavior above T_g. Thermoplastic materials melt, whereas thermoset materials char above T_g. Master curves are constructed by shifting compliance data, from tests at various temperatures, along the log time axis using TTSP. Test segments are arranged with lower temperature tests on the left side and higher temperature tests shifted towards the right side of the

figure 2.11. In this study the region of particular interest is between the β transition and the α transition temperatures and is referred to as the glassy region.

The β transition defines the highest secondary transition temperature. Below this temperature side groups or parts of chain segments can rotate and vibrate, but the available thermal energy is too small to allow entire chain segment to move. In the region above the β transition temperature and below the α transition temperature, the motion of entire chain segment is possible but is limited by the amount of free volume available for the segments to move into. Above the α transition temperature, commonly referred to as the glass transition temperature (T_g), the free volume is directly related to temperature. The thermal energy available above T_g is large enough to allow the polymer chain segments to move easily. Thus, it is possible to reach the equilibrium free volume state very rapidly at temperatures above T_g.

The matrix material of the composite analyzed during this study is classified as an amorphous thermoplastic polymer. The amorphous type of polymer is characterized by a random non-ordered arrangement of polymer chains. When the polymer chains have a regular ordered chain structure packed into a crystal lattice, somewhere in the material, it is classified as a semicrystalline polymer. The degree of crystallinity is often given as a percentage of amorphous structure that has

formed into the crystal lattice structure. Struik [60.61,64,65], Chai et al [8] and Ogale et al [48] have studied how crystallinity effects physical aging in semicrystalline materials.

2.2.2 Physical Aging Definition

The term aging is used to describe the process that changes the properties of a material with time. Aging processes are generally grouped into either a physical aging or chemical aging category. Physical aging processes are characterized by the thermoreversibility of the change in the material properties. The material can be rejuvenated by heating it above Tg and holding there until a state of equilibrium free volume is reached. Conversely, chemical aging is characterized by the irreversibly of the change in material properties. Chemical aging processes, such as oxidation, curing, and cross-linking, permanently change the material properties.

Early work by Kovacs et al [32] showed that amorphous solids fail to reach their equilibrium free volume state when they are rapidly cooled from above their T_g. The equilibrium free volume state is achieved by cooling the material at an infinitely slow cooling rate. Physical aging is the process, occurring below T_g, where the macromolecules gradually change their packing in order to approach the equilibrium free volume state. The origin of physical aging is illustrated in figure 2.12. As the material is cooled from above T_g, the free volume

linearly decreases with temperature. Also, the polymer chain mobility decreases following its relationship with free volume, shown in figure 2.11. At T_g, the viscosity rapidly increases and the polymer chain motion is impaired. The polymer is unable to reach the equilibrium degree of packing before solidification. Continued cooling creates a free volume differential between the quenched and equilibrium states. As the polymer undergoes isothermal aging, the free volume gradually decreases towards the equilibrium state.

The process controlling the isothermal free volume relaxation is a nonlinear closed-loop scheme symbolically written as:

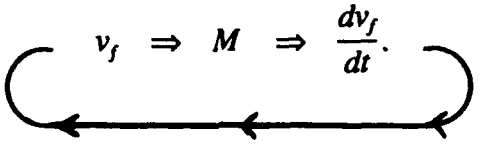

(2.41)

Equation 2.41 implies that the initial free volume (v_f) determines the mobility (M) of the polymer segments. The mobility available to the polymer segments then determines the time rate of change of the free volume. The whole process starts after the quench from above T_g when the initial mobility prompts a change in free volume towards the equilibrium value. The decrease in free volume forces the mobility to also decrease. This is followed by a decrease in the rate that the free volume relaxes from the material. An interesting consequence of

equation 2.41 is that below T_g the mobility can only asymptotically approach zero. This is explained by noting that a decrease in mobility requires a decrease in free volume. In order for the free volume to change, there must be some mobility. Therefore, the mobility cannot disappear over a finite time period but may become very small as the material approaches the equilibrium free volume value. As the free volume and mobility decrease, all the properties of the material that depend on them will also change.

2.2.3 Effect of Physical Aging on Material Properties

Although this study concentrates on the effect of physical aging on the creep properties of a material, many other material properties also depend on mobility or free volume state in the material. An excellent review of the material properties of polymer glasses that are effected by the nonequilibrium volume behavior is presented by Tant and Wilkes [67]. Therefore, only a brief summary is given here. Associated with a decrease in mobility and free volume are increases in density, viscosity, yield stress, and elastic modulus. An initial assessment might suggest that the increases in yield stress and stiffness, due to physical aging, would be beneficial during the life of an aerospace structure. Unfortunately, physical aging also decreases the impact strength and fracture energy of the material. Degradation of these properties must be considered in aerospace applications susceptible to impact type damage.

2.2.4 Effect of Physical Aging on Creep Compliance

The effect of physical aging on creep compliance of a material appears as a horizontal shift of the compliance data on a logarithmic time scale. An illustration of the aging effect on amorphous polymer poly(vinyl chloride) (PVC) obtained from Struik [59], is shown in figure 2.13. The PVC material was quenched from 90°C to 20°C and tested at aging times ranging form 0.03 to 1000 days. The creep compliance data associated with each aging time was horizontally shifted to the 1000 day aging time to form a master compliance curve. The excellent superimposability of the individual creep curves shows that the shape of the curve remains constant during aging. It is also important to note that the individual creep curves, at various aging times, extend over several decades in time. This implies that the creep process requires a wide distribution of relaxation times instead of a single relaxation time. However, since the shape of the creep curve remains constant, all the relaxation times associated with a particular aging time must be shifted by the same factor, usually referred to as a. Note, henceforth the term relaxation time, as adopted by Struik [59], is used generically in the description of the characteristic time associated with either stress relaxation or creep mechanical models.

Also illustrated in figure 2.13 is the thermoreversibility of physical aging. After the 1000 days of aging, the sample was heated back to 90°C for 20 minutes and quenched to the 20°C aging temperature. The creep compliance was measured again after aging one day (data represented by x symbol in figure 2.13) was within 2% of the original measurements made nearly four years earlier. Thus, previous aging can be completely erased by heating the material above T_g for a short period of time.

The horizontal shift, on the logarithmic time scale, between successive creep curves are approximately constant, as shown in figure 2.13. This implies there is a relationship between the amount of horizontal shift ($\log a$) and the log of the aging time ($\log t_e$). Using Struik's [59] sign convention, $\log a$ is a measurement of the horizontal shifting of the referenced compliance curve and is taken positive for a shift to the left. The aging can be characterized by the double-logarithmic shift rate μ, defined as:

$$\mu = -\frac{d(\log a)}{d(\log t_e)} \tag{2.42}$$

where $-\log a$ defines the amount of horizontal shift required to move the individual compliance curve from its original location to the shifted position required to form the master momentary

compliance curve at the referenced aging time. The horizontal shift values used to shift the t_e=1 hour reference aging curve to the aging times shown in figure 2.13 are plotted verses $\log t_e$ in figure 2.14. The slope of this curve is the shift rate μ. It was calculated at about unity for the PVC material.

The effect of temperature on the shift rate, μ, for several polymer materials, is shown in figure 2.15. Each material in the figure shows a rapid increase in μ below T_g to a value near unity. As the temperature continues to decrease, μ reaches a plateau near unity for a range of temperatures and then decreases at a lower temperature which varies with each material. The changes in μ with temperature can be explained using free volume theory. Struik [59] describes the decrease in mobility associated with physical aging as a "self-retarding" process. As the mobility decreases during aging, following the relationship given by equation 2.41, the rate of decrease of mobility will also decrease. Struik [59] suggested that the mobility associated with self-retarding processes is inversely proportional to the aging time:

$$M \sim \frac{k_1}{t_e} \tag{2.43}$$

where k_1 is a constant. Since, the retardation times associated with creep tests are also inversely proportional to mobility,

equation 2.43 indicates that they will also increase proportionally to the aging time. Therefore, an increase in t_e by a factor of ten will also increase the retardation times by a factor of ten. This produces a shift of the creep curve along the logarithmic time axis by one decade. This explains why the shift rate, μ, is nearly constant in the aging temperature range and why it is approximately unity. The shift rate decreases to zero as the equilibrium volume state is approached at temperatures near T_g. At T_g, volume equilibrium is reached and physical aging ceases with $\mu=0$. The aging rate decreases at lower temperatures as the material approaches the highest secondary transition temperature, T_β. Below this temperature, only secondary relaxations exist which do not change the free volume state in the material.

2.2.5 Characterizing and Predicting the Effect of Physical Aging

In this section the methodology used to characterize the effect of physical aging on linear small-strain creep compliance is discussed. Also, a method of predicting long-term creep behavior form short-term aging characterization tests is presented for a single compliance direction. Further explanation of the process required to characterize the compliance response in each of the principal directions of a two dimensional orthotropic composite material is contained in section 2.3.

2.2.5.1 Momentary Compliance Curves

This section describes the differences between short-term (momentary) and long-term creep tests. Momentary tests are essentially a "snapshot" of the material properties taken at a constant aging time. The duration of the momentary test remains small compared to the aging time at the beginning of the test. In this study, the relationship between total test duration (t_t) and aging time (t_e) of $t_t \leq t_e/10$ was used. In contrast, long-term tests have aging occurring simultaneously with the creep. The test duration, therefore, becomes much larger than the aging time at the beginning of the test.

During a short-term test, the retardation times hardly change due to aging and the resulting compliance curve is referred to as a momentary curve. A schematic of a sequence of momentary creep and recovery tests is shown in figure 2.16. After the temperature is quenched from above T_g to a constant aging temperature below T_g, shown as the dashed line in figure 2.16, the aging time starts for the entire aging test sequence. Next, successive creep tests are conducted at various aging times. The recovery strain built up from previous creep tests is extrapolated into the next creep period and subtracted from the total strain response. Thus, the creep strain associated with each aging test can be singled out. The extrapolation is reliable since the creep test duration is less than 20% of the previous recovery period time scale.

The creep test sequencing procedure can only be used with small strain levels in the linear viscoelastic behavior range where Boltzmann's Superposition Principle is valid. The validity of the sequencing procedure can be checked by comparing the compliance results of an intermediate aging time creep test from a sequence test with a second test. The second test measures the creep response at the same intermediate aging time, but eliminates the creep tests conducted prior to the intermediate aging time. A reasonable comparison of the compliance between the two tests verifies the applicability of the sequencing test procedure. Creep tests outside the linear range require a more laborious procedure which requires a new quench before each creep test.

2.2.5.2 Aging Shift Rate Determination

The aging shift rate, μ, was determined from the results of a sequence of aging tests conducted at a constant temperature. Struik [59], states that the amount of horizontal and vertical shifting required to make a master compliance curve can be determined unambiguously, from the marked curvature of the creep curves. In practice, matching the curvatures of the momentary creep curves is a precarious process. Historically, shift factors have been determined by shifting creep curves by hand. This process is a time consuming and tedious job utilizing a trial and error procedure. In this study, a

computer program was written to automate the shifting process. The program is based on a procedure described by Vleeshouwers et al [72] where the Levenberg-Marquardt [28] nonlinear finite difference scheme was used to fit each momentary creep compliance curve to Struik's compliance model given by equation 2.19 as:

$$D(t) = D_0 e^{(t/t_0)^m}. \tag{2.19}$$

The program determines the values of D_0, t_0, and m that best fit the test data. The variables controlling the amount of horizontal and vertical shift, on a logarithmic scale, become apparent after taking the log of both sides of equation 2.19, yielding:

$$\log D(t) = \log D_0 + (t/t_0)^m \log e. \tag{2.44}$$

Clearly, D_0 controls the vertical shift, t_0 controls the horizontal shift, and m defines the shape of the curve on a log compliance vs. log time plot. Both D_0 and t_0 are functions of temperature and aging time, whereas m is a constant that defines the shape of the compliance curve.

The first pass of the computer program determines the values of D_0, t_0, and **m** that best fit the compliance data for each aging time. The **m** values of all the compliance curves from a test sequence are compared, and an average **m** value is calculated. The second pass of the computer recalculates D_0 and t_0 with the **m** value forced to the average value. The amount of horizontal shift , $-\log a$, required to move each compliance curve to the referenced curve is computed using:

$$-\log a = \log\left(\frac{t_0(t_e)}{t_0(t_{e,ref})}\right). \tag{2.45}$$

An illustration of the shifting of momentary creep compliance curves is shown in figure 2.17. The individual compliance curves in figure 2.17 are obtained at different aging times during a sequence of creep tests conducted at a constant temperature and stress level. Note that the last aging time in the test sequence was chosen as the referenced creep curve. The amount of horizontal shift, $-\log a$, required to shift each aging test to the referenced creep curve are also shown on figure 2.17. Finally, the shift rate, μ, was determined using a linear regression routine to determine the slope of a plot of $-\log a$ vs. $\log t_e$, shown inserted in the upper left corner of figure 2.17. The aging rate calculation was found to be insensitive to the average value of **m** used to fit the aging

curves in a test sequence. The sensitivity was checked by varying m average value from .34 to .48 by .02 increments and calculating the aging rate for each value. The resulting aging rates were all within ±0.6% of the mean aging rate calculated for the eight m values.

The small amount of vertical shifting on the logarithmic scale was required to bring the various aging creep compliance curves into alignment with the referenced aging curve. The amount of vertical shift, $\log B$, was computed using:

$$\log B = \log\left(\frac{D_0(t_{e,ref})}{D_0(t_e)}\right). \tag{2.46}$$

The small vertical shift accounts for in increase in initial compliance value as the material physically ages. The small vertical shift factors used in the data reduction procedure are tabulated in chapter 4.0. Additionally, vertical shift factors are used to correct for the change in initial compliance with temperature. Sullivan [66] reported that the vertical shift factors account for the increase in creep compliance found with increasing temperature.

The momentary compliance curve resulting from the shifting procedure is referenced to the test temperature and last aging time in the test sequence. The effect of temperature on the shift rate is determined by repeating the entire creep test

sequence and shifting the resulting momentary creep curves to determine the shift rate at the new temperature. The number of time decades the compliance curve covers is limited to the duration of the longest aging test. In order expand the time range, use of the time-temperature superposition principle is required.

2.2.5.3 TTSP Master Momentary Compliance Curve

TTSP Master momentary compliance curves were formed by shifting momentary compliance curves, obtained at different temperatures with the same aging time, using the time-temperature superposition principle. An illustration of the shifting of momentary compliance curves to form a TTSP master momentary compliance curve is shown in figure 2.8. The master curve in this figure is referenced to the lowest temperature at the referenced aging time $t_{e,ref}$. The amount of horizontal shift, $-\log a_T$, for each compliance curve is a function of both temperature and the referenced aging time.

Two methods were used to determine the shifting factors associated with temperature. The first method used the same computer program and procedures described in the previous section to fit each compliance curve to Struik's equation. This method requires the calculation of an average m value from the short-term momentary compliance curves at various temperatures. The horizontal shift factors were calculated using:

$$-\log a_T = \log\left(\frac{t_0(T, t_{e,ref})}{t_0(T_{ref}, t_{e,ref})}\right). \tag{2.47}$$

The calculated shift factors are referenced to a particular reference temperature T_{ref}, aging time $t_{e,ref}$, and the average m value. Also, using this method, the average m value chosen predetermines the shape of the master compliance curve. The average m value was calculated from compliance data with a limited time range (~ 3 decades) and may or may not be the best representation of the actual shape of the master compliance curve.

The second method utilized a graphical procedure to determine the shift factors. The compliance curves, from various temperatures at a constant aging time, were all plotted using the Freelance graphical package by Lotus [24]. The master curve was generated by matching the slopes of the compliance curves. The ruler option in Freelance was utilized to scale the x and y axis in logarithmic units. The shift factors for each curve were easily determined by subtracting the final curve position from the initial position. The shifted compliance data was then fit to Struik's equation using the nonlinear finite difference program. Comparisons between the two master curve construction methods and their effect on momentary and long-term compliance predictions are discussed in section 4.0 and 5.0 respectively.

2.2.5.4 Effective Time Theory

In this section, the effective time theory developed by Struik [59] is examined. The effective time theory was developed to account for the effect of aging during long-term creep compliance tests. Although time-temperature superposition works well for momentary creep compliance curves at a constant aging state, it overestimates the creep response during long-term tests. Thus, it is necessary to use the effective time theory to account for the gradual stiffening of the material during physical aging.

In order to avoid confusion, a few time variables associated with long-term creep tests will be defined. First, the aging time at the start of the creep test, t_e, is measured starting after the quench from above T_g. The variable, t, is used to define the time after the creep load is applied. Finally, the aging time during the creep test, t'_e, is calculated by adding t to t_e. Each of these time variables is illustrated in figure 2.18.

Development of the effective time theory begins by noting that the shift rate μ remains constant for very long periods of time. Struik [41] suggests that the shift rate, determined from short-term tests, should be close to unity (e.g., $0.7 < \mu < 1.0$) in order to obtain reliable long-term predictions. The shift rate is determined using:

$$\mu = -\frac{d\log a}{d\log t_e} = -\frac{\log a_{t'_e} - \log a_{t_e}}{\log t'_e - \log t_e} \tag{2.48}$$

where a is the acceleration factor. The master momentary creep curve is referenced to the aging time at the start of the long-term test. Thus, the value of $\log a_{t_e}$ term will be zero at t_e. Substituting this relationship into equation 2.48 yields:

$$\mu \log\left(\frac{t_e}{t'_e}\right) = \log a_{t'_e}. \tag{2.49}$$

Raising both sides of equation 2.49 to the tenth power yields:

$$a(t'_e, t_e) = \left(\frac{t_e}{t'_e}\right)^{\mu}. \tag{2.50}$$

Abbreviating the acceleration factor as a(t) and writing it in terms of t and t_e yields:

$$a(t) = \left(\frac{t_e}{t_e + t}\right)^{\mu}. \tag{2.51}$$

At aging times greater than t_e, the effect of physical aging shifts the referenced momentary compliance curve in the negative

(to the right using Struik's sign convention) direction. This has the effect of extending the momentary creep compliance curve along the time axis to form the long-term compliance curve as illustrated in figure 2.18. The momentary compliance, $D_{t_e}(\lambda)$, is related to the long-term compliance, $\overline{D}_{t_e}(t)$, using an effective time λ. The relationship is given by:

$$\overline{D}_{t_e}(t) = D_{t_e}(\lambda). \tag{2.52}$$

Both compliance representations are referenced to the aging time, t_e, at the start of the creep test. As the creep test progresses from time t to $t+dt$, the relaxation processes are all slowed down by the same amount. The time interval dt is related to the effective time interval, $d\lambda$, by:

$$d\lambda = a(t)\, dt. \tag{2.53}$$

Integration of equation 2.53 yields the effective time λ given by:

$$\lambda(t) = \int_0^t a(\xi) d\xi. \tag{2.54}$$

where ξ is a dummy integration variable on the t time scale. An analytical form for λ is obtained by combining equations 2.51 and 2.54 and performing the integration. This yields the effective time expression used by Struik [59] given as:

$$\lambda = t_e \ln\left[1+\frac{t}{t_e}\right] \qquad for \quad \mu = 1$$

$$\lambda = \frac{t_e}{\alpha}\left[\left(1+\frac{t}{t_e}\right)^{\alpha}-1\right] \qquad for \quad \mu < 1 \tag{2.55}$$

where

$$0 < \alpha = 1-\mu < 1$$

The two variables that influence the effective time and therefore the long-term compliance predictions are the aging rate μ, determined from short-term tests, and the aging time t_e, at the start of the long-term test. The long-term compliance predictions, associated with the real time axis, are made by substituting the effective time, computed using equation 2.55, into:

$$\overline{D}(t) = D_0 e^{(\lambda/t_0)^m}. \tag{2.56}$$

In addition to the dependence on effective time, the long-term compliance prediction also depends on how well the variables D_0, t_0, and m define the momentary master compliance curve at t_e. Therefore, obtaining a correct representation of the momentary creep response of the material using TTSP is essential for accurate long-term predictions.

2.3 Composite Material Compliance Relationships

The composite material system of interest in this study consisted of Radel X matrix material surrounding IM7 fibers. The fibers were embedded in the matrix to form a thin lamina sheet approximately 0.005 inch (0.013 cm) thick. The thin unidirectional lamina sheets were stacked, with the fibers all orientated in the same direction, to form a 12-ply unidirectional laminate. After curing, the completed unidirectional laminate panel is classified as an orthotropic material. Therefore, nine independent material properties are required for full characterization. However, since the thickness of the panel is quite small in comparison to the other dimensions it is commonly classified as a two dimensional orthotropic material. Thus, under in-plane loading ($\sigma_{33} = \tau_{23} = \tau_{31} = 0$) only four independent properties are required.

The coordinate system used to define the directionality of the material properties followed a convention used by Jones [29] and is illustrated in figure 2.19. In this system, the loading or global axis is the (X-Y) axis and the material or

local axis is referred to as the (1-2) axis. The angle between the coordinate systems is referred to as θ and is measured in a positive direction from the X axis to the 1 axis. The four material properties associated with creep testing are defined in terms of the compliance matrix in the material principal directions. The elastic constitutive equations relating stress, strain, and compliance for the two dimensional orthotropic unidirectional laminate are:

$$\begin{Bmatrix} \varepsilon_1 \\ \varepsilon_2 \\ \gamma_{12} \end{Bmatrix} = \begin{bmatrix} S_{11} & S_{12} & 0 \\ S_{21} & S_{22} & 0 \\ 0 & 0 & S_{66} \end{bmatrix} \begin{Bmatrix} \sigma_1 \\ \sigma_2 \\ \tau_{12} \end{Bmatrix} \tag{2.57}$$

This matrix equation, written in condensed notation, is given by:

$$\{\varepsilon\}_{12} = [S]_{12}\{\sigma\}_{12} \tag{2.58}$$

where

$\{\varepsilon\}_{12}$ = in-plane local strains

$[S]_{12}$ = principal compliance matrix

$\{\sigma\}_{12}$ = in-plane local stresses.

The compliance terms are related to common engineering properties by the following equations:

$$S_{11} = \frac{1}{E_{11}} \tag{2.59a}$$

$$S_{12} = S_{21} = -\frac{\nu_{12}}{E_{11}} = -\frac{\nu_{21}}{E_{22}} \tag{2.59b}$$

$$S_{22} = \frac{1}{E_{22}} \tag{2.59c}$$

$$S_{66} = \frac{1}{G_{12}} \tag{2.59d}$$

Determination of the principal compliance terms requires testing unidirectional laminates at different angle orientations between the local material axis and the global load axis. It is therefore necessary to relate local and global coordinate systems through transformation equations. The transformations between the local (1-2) axis and global (X-Y) axis for stress and strain are:

$$\{\sigma\}_{12} = [T_1]\{\sigma\}_{xy} \tag{2.60}$$

$$\{\varepsilon\}_{12} = [T_2]\{\varepsilon\}_{xy} \tag{2.61}$$

where the transformation matrices are defined as:

$$[T_1] = \begin{bmatrix} \cos^2\theta & \sin^2\theta & 2\cos\theta\sin\theta \\ \sin^2\theta & \cos^2\theta & -2\cos\theta\sin\theta \\ -\cos\theta\sin\theta & \cos\theta\sin\theta & \cos^2\theta - \sin^2\theta \end{bmatrix} \quad [T_2] = \begin{bmatrix} \cos^2\theta & \sin^2\theta & \cos\theta\sin\theta \\ \sin^2\theta & \cos^2\theta & -\cos\theta\sin\theta \\ -2\cos\theta\sin\theta & 2\cos\theta\sin\theta & \cos^2\theta - \sin^2\theta \end{bmatrix}.$$

Also for completeness, the inverse transformations between the global (X-Y) axis and local (1-2) axis for stress and strain are

$$\{\sigma\}_{xy} = [T_1]^{-1}\{\sigma\}_{12} \tag{2.62}$$

$$\{\varepsilon\}_{xy} = [T_2]^{-1}\{\varepsilon\}_{12} \tag{2.63}$$

where the inverse transformation matrices are defined as:

$$[T_1]^{-1} = \begin{bmatrix} \cos^2\theta & \sin^2\theta & -2\cos\theta\sin\theta \\ \sin^2\theta & \cos^2\theta & 2\cos\theta\sin\theta \\ \cos\theta\sin\theta & -\cos\theta\sin\theta & \cos^2\theta - \sin^2\theta \end{bmatrix} \quad [T_2]^{-1} = \begin{bmatrix} \cos^2\theta & \sin^2\theta & -\cos\theta\sin\theta \\ \sin^2\theta & \cos^2\theta & \cos\theta\sin\theta \\ 2\cos\theta\sin\theta & -2\cos\theta\sin\theta & \cos^2\theta - \sin^2\theta \end{bmatrix}.$$

The compliance matrix in the material principal direction can also be transformed to the global coordinate system. This is accomplished by substituting equations 2.58 into 2.63 yielding:

$$\{\varepsilon\}_{xy} = [T_2]^{-1}[S]_{12}\{\sigma\}_{12} \tag{2.64}$$

which is followed by a substitution of $\{\sigma\}_{12}$ from equation 2.60. The result is:

$$\{\varepsilon\}_{xy} = [T_2]^{-1}[S]_{12}[T_1]\{\sigma\}_{xy} \tag{2.65}$$

or written in condensed notation as:

$$\{\varepsilon\}_{xy} = [\bar{S}]_{12}\{\sigma\}_{xy} \tag{2.66}$$

where

$$[\bar{S}]_{12} = [T_2]^{-1}[S]_{12}[T_1]. \tag{2.67}$$

$[\bar{S}]_{12}$ is referred to as the transformed or rotated compliance matrix. It represents the material compliance in the global coordinate directions. The expanded rotated compliance terms are computed by completing the matrix multiplication in equation 2.67 yielding:

$$\bar{S}_{11} = S_{11}\cos^4\theta + (2S_{12} + S_{66})\sin^2\theta\cos^2\theta + S_{22}\sin^4\theta \tag{2.68a}$$

$$\bar{S}_{12} = S_{12}(\sin^4\theta + \cos^4\theta) + (S_{11} + S_{22} - S_{66})\sin^2\theta\cos^2\theta \tag{2.68b}$$

$$\bar{S}_{22} = S_{11}\sin^4\theta + (2S_{12} + S_{66})\sin^2\theta\cos^2\theta + S_{22}\cos^4\theta \tag{2.68c}$$

$$\bar{S}_{16} = (2S_{11} - 2S_{12} - S_{66})\sin\theta\cos^3\theta - (2S_{22} - 2S_{12} - S_{66})\sin^3\theta\cos\theta \tag{2.68d}$$

$$\bar{S}_{26} = (2S_{11} - 2S_{12} - S_{66})\sin^3\theta\cos\theta - (2S_{22} - 2S_{12} - S_{66})\sin\theta\cos^3\theta \tag{2.68e}$$

$$\bar{S}_{66} = 2(2S_{11} + S_{22} - 4S_{12} - S_{66})\sin^2\theta\cos^2\theta + S_{66}(\sin^4\theta + \cos^4\theta). \tag{2.68f}$$

The four principal compliance terms S_{11}, S_{12}, S_{22}, and S_{66} were determined from the results of creep tests conducted at known aging times. The compliance was calculated by dividing the

known stress level applied to the specimen by the measured strain response. The strain response was determined using foil resistance strain gages mounted on the specimens. Further details on the use the strain gages are contained in section 3.4. Other methods of strain measurement such as extensometers, Moire interferometry, and laser-interferometry are possible, but were not used in this study.

A specific orientation of the unidirectional fibers, with respect to the global axis, was required in order to determine each principal compliance term. The S_{11} compliance term was obtained using a specimen with the fibers aligned along the global X axis. This orientation is referred to as a 0 degree specimen. S_{11} was calculated by substituting the axial strain measured in the specimen into the equation:

$$S_{11} = \frac{\sigma_1}{\varepsilon_1}. \tag{2.69}$$

The S_{22} compliance term was determined using a specimen with the fibers oriented perpendicular to the global X axis. This orientation is referred to as a 90 degree specimen. S_{22} was calculated by substituting the axial strain along the load axis into the equation:

$$S_{22}=\frac{\sigma_2}{\varepsilon_2}. \tag{2.70}$$

The S_{12} compliance term was obtained by using the measured strain in the transverse direction from the 0 degree specimen test. S_{12} was calculated using the equation:

$$S_{12}=\frac{\sigma_1}{\varepsilon_2}. \tag{2.71}$$

The compliance tensor was assumed symmetric such that $S_{12}=S_{21}$. This assumption has been confirmed by other investigators [47,66] for similar two dimensional orthotropic materials under in-plane loading. The symmetric assumption was not verified in this study due to the difficulty of accurately measuring the transverse strain in a 90 degree specimen. The small loads applied to the 90 degree specimen produced very small transverse strains in the 0 degree direction. Thus, it was impractical to accurately determine S_{21}.

The shear compliance term, S_{66}, is not as easily determined as the other compliance terms. Several test methods have been proposed to determine S_{66}. Possible methods include the rail-shear test, picture-frame test, and off-axis tensile specimen test. Among these, the off-axis tensile specimen

test has gained wide acceptance. The 10 degree off-axis test, proposed by Chamis and Sinclair [9], has been used by several investigators at VPI & SU [25,68] to characterize the shear compliance term. A disadvantage of this test is the requirement for a specimen gage-length to gage-width ratio of at least 14. The relatively long and narrow specimen is required to minimize the effect of the end constraint produced by the specimen grips. Unfortunately, the required length for 0.5 inch (1.27 cm) wide specimens, used in this study, was too long to fit in the available ATS oven. The test configuration selected for shear characterization utilized a 45 degree off-axis specimen. Pindera and Herakovich [52] proposed this configuration to minimize the effect of end constraints. They found that, for even highly anisotropic composites, the effect of end constraints becomes negligible for off-axis angles greater than 45 degree. The shear compliance, S_{66}, is determined by measuring the shear strain in the 45 degree specimen during uniaxial tension loading. The shear strain in the principal material axis, γ_{12}, is determined using the strain readings from a three strain gage rosette. The orientation of the strain gage rosette on the 45 degree specimen is shown in figure 2.20. The angle β, is defined as the angle between the X, global load axis, and a line parallel to the gage orientation. The following standard strain transformation equation:

$$\varepsilon_{gage} = \frac{\varepsilon_x + \varepsilon_y}{2} + \frac{\varepsilon_x - \varepsilon_y}{2}\cos 2\beta + \frac{\gamma_{xy}}{2}\sin 2\beta \tag{2.72}$$

can be used to relate the measured gage strain with the global axis strains. These relationships, for the gages shown in figure 2.20 are:

for gage 1 with β_{g1} = +45°

$$\varepsilon_{g1} = \frac{\varepsilon_x + \varepsilon_y}{2} + \frac{\gamma_{xy}}{2} \tag{2.73}$$

for gage 2 with β_{g2} = 0°

$$\varepsilon_{g2} = \varepsilon_x \tag{2.74}$$

and finally for gage 3 with β_{g3} = -45°

$$\varepsilon_{g2} = \frac{\varepsilon_x + \varepsilon_y}{2} - \frac{\gamma_{xy}}{2}. \tag{2.75}$$

Solving for the global strains $\varepsilon_x, \varepsilon_y$, and γ_{xy} in terms of the gage strains, yields the following relationships:

$$\varepsilon_x = \varepsilon_{g2} \tag{2.76a}$$

$$\varepsilon_y = \varepsilon_{g1} - \varepsilon_{g2} + \varepsilon_{g3} \tag{2.76b}$$

$$\gamma_{xy} = \varepsilon_{g1} - \varepsilon_{g3}. \tag{2.76c}$$

Using equation 2.61, the material axis shear strain is related to the global axis strains by:

$$\gamma_{12} = 2\sin\theta\cos\theta(\varepsilon_y - \varepsilon_x) + (\cos^2\theta - \sin^2\theta)\gamma_{xy}. \tag{2.77}$$

This can be simplified using trigonometric double angle relationships to the equation:

$$\gamma_{12} = (\varepsilon_y - \varepsilon_x)\sin 2\theta + \gamma_{xy}\cos 2\theta. \tag{2.78}$$

Upon the substitution of equations 2.76a-c into equation 2.78, the shear strain in the material axis can be written in terms of the measured gage strains as:

$$\gamma_{12} = (\varepsilon_{g1} - 2\varepsilon_{g2} + \varepsilon_{g3})\sin 2\theta + (\varepsilon_{g1} - \varepsilon_{g3})\cos 2\theta. \tag{2.79}$$

Finally, the shear compliance S_{66} can be computed by substituting the stress strain relationship $\gamma_{12} = S_{66}\tau_{12}$ from equation 2.57 and the stress transformation equation $\tau_{12} = -\sin\theta\cos\theta\sigma_x$ from equation

2.60 into equation 2.79, yielding:

$$S_{66} = \frac{(\varepsilon_{g1} - 2\varepsilon_{g2} + \varepsilon_{g3})\sin 2\theta + (\varepsilon_{g1} - \varepsilon_{g3})\cos 2\theta}{-\sin\theta\cos\theta\sigma_x}. \tag{2.80}$$

When a 45 degree specimen, θ = +45°, is used for shear characterization the shear compliance equation reduces to

$$S_{66} = \frac{2(-\varepsilon_{g1} + 2\varepsilon_{g2} - \varepsilon_{g3})}{\sigma_x} \tag{2.81}$$

3 EXPERIMENTAL METHODS

This chapter describes the experimental equipment and methods used during the characterization of the Radel X/IM7 composite material. The accuracy of the long-term creep predictions, with simultaneous physical aging, ultimately depends on the quality of test data used in developing the prediction models. The term "quality data" is used to imply the data was obtained with the best possible accuracy using the available experimental equipment. The experimental methods used were closely scrutinized to insure quality data was collected. Included in this chapter are descriptions of testing equipment, calibration techniques, specimen preparation, strain measurement techniques, data collection, aging creep test procedures and data reduction procedures. Each description is presented to document actual experimental methods used during this study.

3.1 Testing Equipment

Creep testing utilized an Applied Test System (ATS) series 2240 lever arm tester with a 20:1 load ratio and a 8000 lb (35.6 N) maximum load capacity. Mounted on the frame was an ATS 3610 oven used to provide the temperature environment for the tests. The oven temperature was controlled using an ATS 2931 oven controller. The frame, oven, and controller are

shown in figure 3.1. Friction type grips were used to apply load to the specimen. The frictional force was increased by inserting a fine steel mesh between the specimen and the grip face. Additionally, possible slippage of the specimen in the grips was eliminated by placing a 1/8 inch (0.3175 cm) steel pin thru the grips and specimen. The grips were attached to the ATS creep frame using 3/8 inch (0.9525 cm) steep pins in a conventional pin-thru-the-grip arrangement. An illustration of how the specimen was attached to the load frame is shown in figure 3.2.

3.2 Calibration Techniques

3.2.1 Oven Temperature

The temperature distribution in the ATS 3610 oven was checked prior to creep testing. The temperature was measured at 3 locations equally spaced along a 8 inch (20.32 cm) length located in line with the load path. Iron-constantan (ANSI symbol "J") thermocouples were used to measure temperatures. Initial measurements, at oven temperatures up to 450°F (232°C), indicated ≈ 9°F (5°C) maximum temperature variation, from the top to bottom of the 8 inch (20.32 cm) test length. Owens [51] reported a similar temperature variation, ≈ 1°F (0.5°C) per inch of gage length at 400°F (204°C), in the same ATS oven. This initial temperature variation along the specimen seemed high. Sullivan [66] described a similar temperature variation

problem encountered using Satec test chambers. He found that placing an aluminum cylinder around the specimen and running preheated nitrogen through the oven reduced the temperature variation along a 4 inch (10.16 cm) length from about 18°F (10°C) to 5°F (3°C). The improved variation in the Satec oven is close to the initial variation in the ATS oven. Further improvement is the ATS temperature variation was accomplished by using a simple aluminum air duct placed in the bottom the ATS oven. This air duct directed the heated air to the front of the oven and improved the mixing of the air within the oven. A repeated heating test revealed that the temperature variation had decreased to less than 4°F (2°C), over the 8 inch (20.32 cm) length. This small temperature variation was deemed acceptable for the proposed creep testing. Additionally, it is important to note that the temperature variation along the 1/2 inch (1.27 cm) strain gage length was negligible.

Initially, the desired oven temperature was set using an ATS series 3821 oven temperature controller. This controller utilized a rheostat knob and an analog needle gage for setting and monitoring the oven temperature. Unfortunately, the pointing needle in the gage was broken. This made it nearly impossible to repeat the same temperature setting. This problem was alleviated by installing an ATS series 2931 oven controller. This controller utilized digital thumbwheels to set the desired oven temperature and a type E thermocouple to sense the oven

temperature. The controller was calibrated by comparing the digital temperature set on the controller to oven temperature readings from a Fisher Scientific type 14-983-10E precision mercury thermometer and an Omega type J thermocouple thermometer. The thermocouples and the thermometer were placed within a 1/2 inch (1.27 cm) of the location of the strain gages in the test oven. The mercury and E thermocouple thermometer readings were within 1.8°F (1°C) over the calibrated temperature range between 338-446°F (170-230°C). The controller thumbwheel settings required to obtain a desired oven temperature were recorded in 9°F (5°C) increments over the oven temperature operating range. During testing, the mercury thermometer had to be removed from the oven. Long-term temperature monitoring was accomplished by connecting the J thermocouple to a GRAPHTEC strip chart recorder, model DX SR6335, with a J-1 thermocouple module. The strip chart record was used to check for power interruptions and verify that the oven temperature remained constant during long-term tests. The series 2931 controller was found to hold the oven temperature within ≈ 1 °F (.5°C) after stabilizing at the set temperature. The oven temperature was also found to be slightly affected by the ambient room temperature. This affect required an adjustment of the oven controller setting by up to ±2°F (±1°C) to account for seasonal temperature variations and periods when the air conditioner in the lab was not working properly.

3.2.2 Quench Rate Determination

Booij and Palmen [6] reported that the quench rate used to cool a specimen from above T_g to the aging temperature influences the linear viscoelastic properties of the resulting glassy material for a very long time. In order to compare viscoelastic properties at temperatures below T_g, it is essential to know the thermal history of the specimen as it passed through T_g during cooling. Very slow cooling of the specimen produces a smaller specific volume than a fast cooling. Thus, the initial free volume state of the specimen also varies with the quench rate. A fast quench rate produces a larger differential between the trapped free volume state and the equilibrium free volume state than is obtained with a very slow cooling rate. Thus, physical aging effects (i.e. free volume relaxation) are more prevalent in a rapidly quenched material containing a large free volume differential from the equilibrium state.

The method used to quench specimens from above T_g to the aging temperature varies between investigators. Booij and Palmen [6] quenched their samples using liquid nitrogen. Kong [30] quenched his graphite/epoxy laminate specimens in an ice-water bath. A procedure used by Sullivan [66] utilized high pressure air to quench the specimen and was adopted for use in this study. This method provided the only practical means to quench the material when strain gages and wires are

attached to the specimen. The injection of high pressure air into the oven had two effects. First, the air cooled the specimen providing the desired high quench rate. Secondly, the air cooled the test oven to the desired aging temperature. Both of these effects were characterized using a 90 degree specimen instrumented with a J thermocouple embedded in the material. The instrumented specimen, mounted in the test oven, was initially stabilized at a temperature T_g + 18°F (10°C), 441°F (227°C). The quenching procedure was started by first turning off the oven controller. Next, the oven door was opened and the high pressure air was injected into the oven around the specimen. After a set time, the oven door was closed and the specimen temperature monitored to determine the stabilization temperature. This procedure was repeated with the duration of the air quench varied. A plot of the stabilization temperature vs. quench time duration is shown in figure 3.3. This plot was used to determine the quench time required to obtain a desired aging temperature. The specimen temperature was also monitored as a function of time during the air quench using the GRAPHTEC strip recorder. The specimen temperature vs. time data for five different quench cycles was plotted and is shown in figure 3.4. A linear regression fit to the test data yielded a quench rate of 9.5°F/sec (5.3°C/sec).

Another concern resulting from the quenching procedure was the formation of microcracks in the matrix material. This concern was investigated by polishing the edge of a 90 degree specimen and photoreplicating it before and after all heat treatments of the specimen. A few small cracks were found in matrix rich regions of the specimen during the strain gage curing procedure. The maximum length of the cracks was about 4 times the fiber diameter of 0.197 mil (5 microns). The microcracks usually connected two fibers through the matrix rich region. Subsequent repeated quenches and creep tests of the specimen revealed no further increase in crack formation or noticeable growth in the initially formed cracks. Quenching of laminates formed with various ply angle orientations will likely increase the formation of microcracks due to the high thermal expansion mismatch between plies.

3.2.3 Specimen Stress

The uniaxial stress applied to the specimen is calculated by dividing the measured applied load by the specimen cross-sectional area. Accurate measurement of the specimen geometry and applied load are required to determine an accurate applied stress. The specimen geometry was measured using a Starrett No. 722 digital micrometer. The applied load on the specimen was more difficult to accurately obtain and required calibration of the loading mechanism of the creep frame.

The calibration of the loading mechanism was initially attempted using a simple balancing procedure. The first step of this procedure was to balance the loading arm in a horizontal position without any input load applied to the arm. The term "null force" is used to describe the amount of weight required to balance the arm with zero input load applied. The null force is the load on the specimen due to the initial unbalance of the loading mechanism. Next, a small amount of lead weight was measured and added as an input load. Following this step, a balancing load, approximately 20 times the input load, was added to the load train side of the lever arm. This weight was tweaked until the lever arm was balanced in the horizontal position. The actual load ratio was then calculated by dividing the balancing load by the input load. Unfortunately, the load ratio didn't remain constant and depended upon the magnitude of the balancing load. This indicated that the frictional forces induced by the three knife edge contact points on the lever arm must be included in the frame calibration.

The actual calibration procedure used during this study consisted of three steps. The first step was to calibrate a 500 lb (2224 N) capacity Baldwin SR-4 type U-1 load cell. This calibration step was accomplished by connecting the load cell to a Vishay 2120 strain gage conditioner and recording the output voltage as known weights were applied to the cell. The conditioner used an excitation voltage of 1.994 volts and a

calibration voltage of .583 volts per 1000 με units. The load cell was zeroed while loaded by its own weight. This insured that only the applied loads to the cell were measured. The output voltage and applied load data was plotted and fit using a linear regression routine and is shown in figure 3.5. The resulting equation relating the force in the load cell to the output voltage is:

$$force(lb) = 73.97618498*(Voltage) - 0.05480718 \quad . \qquad (3.1)$$

The significant digits displayed in the equation are carried only to insure accurate calculation of the linear regression fit of the data.

The second calibration step consisted of using the calibrated load cell to determine the actual force applied to the specimen. The load cell was carefully installed in the load train path where the specimen would be located. The load cell, loaded by its own weight, was zeroed and the proper excitation and calibration voltages were checked. Next, the support under the lever arm was removed and the null force voltage was measured. Conversion of the null voltage to a force, using equation 3.1, yielded the force on the specimen with zero input load applied to the lever arm. The calibration process continued with gradual increases in the amount of input load as the corresponding output voltages were recorded. A Mettler PJ6000

balance was used to measure the weight of the input load to an accuracy of ±0.1 grams. Using equation 3.1, the output voltage data was converted to pounds force and plotted verses the input load measured in grams. This plot is shown in figure 3.6. The results of a linear regression fit to the data yielded the following relationship between input load and force measured by the load cell:

$$LoadCellForce(lb.) = 0.045616212 * InputLoad(gm.) + 6.594689666 \quad . \quad (3.2)$$

The 6.594689666 constant represents the null force with the load cell attached.

The final calibration step consisted of balancing the lever arm in a way that the specimen would be unloaded when zero input load was applied. This was accomplished by replacing the load cell with the top mounting grip, specimen, and strain gage wires. Next, the lever arm was balanced to a level position by moving a weight attached to the lever arm, as illustrated in the initial balance diagram in figure 3.2. Finally, the lower grip and attachment hardware was attached to the specimen. The weight of this lower assembly rested on the lower frame plate until the load was applied as shown in figure 3.2. Upon load application, the lower assembly travels

slightly upward until the lower nut contacts the lower frame plate to counteract to applied load. The resulting calibration equation after this final balancing step is:

$$SpecimenForce(lb.) = 0.045616212 * InputLoad(gm.). \quad (3.3)$$

An estimate of the error in the specimen load was made by summing the standard error estimate of the two dependent linear regression fits as suggested in [53]. This yielded an applied specimen force with $\pm$0.17 lb (0.75 N) error in the 0 to 150 lb (667 N) calibration range.

3.3 Specimen Preparation

The Radel X/IM7 composite material used in this study was supplied by NASA Langley. A grey scale imaging program was used to estimate the composite fiber volume fraction. The program separately counts the number of pixels contained in the fibers and matrix material from a scanned video image of a micrograph of the edge of a 90 degree specimen. Using a weighted average from three separate scans of the micrograph the fiber volume fraction was estimated at 0.65. The material was received in 11 inch (28 cm) by 11 inch (28 cm) unidirectional panels with a 12 ply thickness. A 50 ton (445 KN) hot press, programmed to follow the consolidation cycle shown in figure 3.7, was used to make the panels. Upon receipt at VPI & SU

the panels were C-scanned to locate any irregularities in the material. Panel regions with suspected irregularities were avoided during the fabrication of specimens. A 0 degree reference axis was produced on the panel by pealing off a thin strip of material along an edge parallel to the fibers. A water-cooled diamond wheel abrasive saw was used to cut the panels into 8 inch (20.32 cm) long by 1/2 inch (1.27 cm) wide off-axis specimens. Standard machining methods were used to cut the specimens at 0, 90, 45, and 30 degree angles from the reference fiber direction.

Since the same specimens would be used to characterize physical aging at various temperatures, a means of rejuvenating the specimen, i.e., erasing the previous physical aging history, was required. Booij and Palmen [6] recommended raising the material to a temperature of T_g + 18°F (10°C) to eliminate the effects of the previous thermal history. They stated that the volume equilibrium state is reached in a few seconds at this temperature. Other investigators have used rejuvenating temperatures ranging from T_g + 12.6°F (7°C) [70] to T_g + 72°F (40°C) [66]. The important point is that the temperature amount above Tg is sufficient to erase the previous thermal history during the time period the material is held at the temperature.

The T_g of the Radel X/IM7 composite was determined using a DuPont 2100 Differential Scanning Calorimetry (DSC) at a 10°C/min. heating rate. Various methods of defining the T_g

from the DSC trace exist [141]. The midpoint of the glass transition region, utilizing a half height calculation method, was used in this study. Using this method, T_g is determined at the heat flow value halfway between the onset and the end of the glass transition region. The DCS trace for the Radel X/IM7 material is shown in figure 3.8. The T_g value calculated was 424°F (217.8°C). Osiroff [50] reported a similar T_g value of 419°F (215°C) for a Radel X/T650-42 composite material. A temperature of 437°F (225°C) was chosen as a rejuvenating temperature for the Radel X/IM7 material. This temperature corresponded to the end of the glass transition region defined by the DSC trace shown in figure 3.8. Preliminary tests verified the material was rejuvenated by holding at this temperature for 15 minutes.

The Radel X/IM7 material was also subjected to a Thermal Gravimetric Analyzer (TGA) test to determine if the material would degrade at the maximum testing temperature. As shown in figure 3.9, no significant weight loss occurred up to temperatures of 788°F (420°C). This temperature was well beyond the 437°F (225°C) temperature used for rejuvenation of the specimens.

3.4 Strain Gage Installation

Creep strain measurement was accomplished using resistance foil strain gages. Strain gages were chosen over extensometers for several reasons. Most notable were the cheaper cost and

availability of strain gages over extensometers. Another reason was the versatility strain gages offer over extensometers in measuring strain in directions other than the normal axial and transverse directions. This versatility was particularly useful for measuring strains in the three directions required to compute the shear compliance term S_{66}.

The strain gages used were from the WK gage series made by Micro-Measurements. The normal operating temperature range of the WK gages is between -452° to 550°F (-269° to 290°C). WK-06-125TM-350 general purpose 2-element 90 degree tee rosette gages were used on the 0 and 90 degree specimens. WK-06-125RA-350 general purpose 3-element 45 degree rectangular rosette gages were used on the 45 and 30 degree specimens. The 350-Ohm resistance gages were chosen over 120-Ohm gages in order to reduce the effect of localized heating of the material under the gages et al [69]. The K-alloy gages were fully encapsulated with high-endurance leadwires pre-attached. The leadwires were attached to bondable terminals placed away from the gages. This isolated any local damage caused by the hot soldering tip away from the gage location. Micro-Measurements 430-FST four conductor cable was used to extend the leadwires to the strain gage signal conditioning amplifier unit. The individual conductor wires in this cable were twisted together and covered with a braided shield and Teflon jacket to minimize line noise. The length of each cable was a constant

six feet to insure each gage experienced the same leadwire resistance. The cable was rated for use up to a temperature of 500°F (260°C).

Strain gages were placed on both sides of each specimen. During testing, both an active and a thermal compensating "dummy" specimen we placed in the oven. The active and dummy specimens were of the same fiber orientation and experienced the same thermal history. The four gages, two each from the active and dummy specimens, were wired in a full bridge Wheatstone circuit [12]. A diagram of the circuit is shown in figure 3.10. Specific placement of the active and dummy gages in the circuit allowed electronic averaging of bending effects and cancelation of thermal effects. Thus, the output signal is entirely due to the applied tension load.

Actual mounting of the strain gages on the specimens was done following the procedures recommended by Micro-Measurements [39]. Both the strain gage and the bondable terminal were glued to the specimen using M-bond 610 high temperature adhesive. An initial problem encountered was that the pre-attached leadwires would bond to the specimen. This provided an electrical conductance path that shorted out the strain gage. This problem was solved by adding a layer of mylar JG high temperature tape between the pre-attached lead wires and the specimen surface before curing. This kept the lead wires from adhering to the specimen. The adhesive was cured at 347°F

(175°C) for 2 hours in a model 838F Fisher Scientific Isotemp programmable oven. The oven temperature was increased and decreased at a rate 9°F (5°C) per minute as illustrated in the strain gage cure cycle shown in figure 3.11. Following this cure cycle, the specimens were removed from the clamping fixtures and the high temperature mylar tape was removed. Next, the specimens were subjected to the two level post cure cycle also shown in figure 3.11. The first level, a 12 hour hold at 212°F (100°C), was required as a drying cycle to remove absorbed moisture from the specimens. Initial specimens were found to form surface blisters when heated directly to the upper post cure temperature. Investigators at NASA Langley had observed the same phenomena and recommended using the drying cycle to avoid the blister formation associated with trapped moisture. The second level, a 8 hour hold at 437°F (225°C), was used as a high temperature post cure cycle to insure the M-bond 610 strain gage adhesive was fully cured.

After the post cure cycle, the specimens were placed inside a desiccator until they were actually wired and used in the aging tests. Monitoring the weight of a sample specimen during this storage period revealed no significant increase or decrease in weight. Desiccant material was also placed inside the ATS oven to minimize any moisture absorption during the testing period.

The final step, in preparation for testing, was to solder the pre-attached lead wires to the bondable terminals and the extension cables. This simple sounding task turned out to be physically quite difficult. The pre-attached leadwires were quite fragile and easily pulled off the strain gage. In addition, the Micro Measurements 570-28R-20 high temperature solder was found to rapidly oxidize the soldering tip making wetting and flowing of the solder difficult. After completion of the soldering process, the resistance of each gage was checked at the end of the extension cables. This provided a good spot check of each gage to insure that the solder joints were satisfactory completed. Next, the gages were wired in the full bridge circuit and connected to the Vishay signal conditioning amplifier unit. The circuit was then checked for proper electrical balance. After passing these screening tests, the solder joints were cleaned with M-Line rosin solvent to remove any residual flux material. Following cleaning, the specimens were ready for mounting in the test oven.

The 8 inch (20.31 cm) long active specimen was mounted with 1.5 inches (3.81 cm) inserted into each grip. This resulted in a test length of 5 inches (12.7 cm) and a 10 to 1 length to width aspect ratio. The grips were placed in a special fixture that eliminated any load transfer to the specimen while the Allen screws were tightened on each grip. After removal from the fixture, a 6 inch (15.2 cm) metal ruler

was placed between the grips to avoid any bending of the specimen during transfer to the test frame. The dummy specimen, used for thermal compensation, was initially supported from the upper 3/8 inch (0.9525 cm) pin in the load train. Later, a method of mounting the specimen from the lower grip was devised in order to eliminate any possible loading of the dummy specimen by the weight of the lead wire extension cables.

Once mounted in the test frame, each strain gage circuit was checked for excessive zero drift (i.e. drift in the bridge output voltage with no load applied). Possible explanations for zero drift include a gradual change in the gage zero resistance, oxidation of the solder joints, temperature changes, moisture changes, or a slight load applied to the specimen. The initial zero drift for the three gages on the 45 degree specimen at 392°F (200°C) is shown in figure 3.12. The zero drift during this 14 hour test seemed excessive for all three gages. The oven was therefore cooled in order to check the solder joints on the strain gages. The pre-attached leadwires seemed loose in several joints, possibility due to oxidation of the solder, and were resoldered. Another zero drift check at 392°F (200°C) revealed a dramatic decrease in voltage drift as shown in figure 3.13. At this point, it was decided to check the effect of mounting the dummy specimen from the bottom grip instead to the top grip. Mounting from the bottom grip would eliminate any loading from the lead wire

extension cables that were attached below the strain gages. The drift measurements, after this remounting, were observed to change direction for gages 1 and 2, as shown in figure 3.14. It was impossible to determine if the changes were due to unloading of the dummy specimen or due to a slight change in the balance of the loading system that would place a small load on the active specimen. The zero drift rate was observed to always decrease with time. Micro Measurements [40] reports the same decrease in drift rate with time for most gage alloys.

3.5 Data Collection

Initial tests using a Vishay 2100 series signal conditioner amplifier were plagued with excessive line noise in the strain gage output voltage. The source of the line noise was traced to the circulating fan within the ATS oven. An oscilloscope was used to determine that the noise was concentrated at 60 Hz with a peak magnitude of about 20 mv. This voltage equated to approximately $\pm$15 micro strain change in the strain readings on a 90° test specimen. The line noise was eliminated by switching to a Vishay 2210 series signal conditioner amplifier. This unit incorporated a noise filtering system that was set to eliminate line noise above 10Hz. A comparison of the strain measurements obtained from the two amplifiers is shown in figure 3.15. The Vishay 2210 amplifier clearly reduced the line noise and was used exclusively thereafter in this study. Additionally, all test equipment, except the test oven, were

plugged into a Trip Lite BC-750a battery backup system to guard against short power interruptions. This unit also protected the equipment against voltage spikes and suppressed line noise from the power distribution system.

All strain gage measurements were taken with the amplifier gage factor set at 2.0. Adjustments for the actual gage factor and temperature induced variations were included during the data reduction process using the procedures recommended by Micro Measurements [42]. The strain gages were calibrated using a shunt calibration procedure [12,44]. The shunt was applied at the connector box where the extension cable was attached to the conditioner unit. The equivalent strain, due to the applied shunt, was calculated using

$$\varepsilon_{SHUNT} = \frac{R_g}{nF(R_g + R_s)} \tag{3.4}$$

where

$$\varepsilon_{SHUNT} = equivalent\ shunt\ strain$$

$$R_g = resistance\ of\ gage$$

$$R_s = resistance\ of\ shunt$$

$$n = number\ of\ active\ gages$$

$$F = assumed\ gage\ factor.$$

Precision 87,150 ohm and 174,650 ohm calibration resistors were used to simulate 1000 and 500 micro strain respectively

in the full bridge circuit. The bridge excitation voltage was determined using procedures recommended by Micro Measurements [41]. The composite material was characterized as a poor heat-sink material. The recommended power density for this type material is about 0.086 watts/in^2 (0.138 KW/m^2) for each gage. The larger grid area WK-06-125TM-350 gages, used on the 0 and 90 degree specimens, were excited with 1.50 volts. The smaller grid area WK-06-125RA-350 gages, used on the 45 and 30 degree specimens, were excited with 0.96 volts. The estimated gain required to obtain the desired bridge output voltage with the shunt applied was calculated using:

$$G = \frac{4E_0}{nF\varepsilon_{SHUNT}V} \tag{3.5}$$

where

$$G = estimated\,gain$$

$$E_o = bridge\,output\,voltage$$

$$n = number\,of\,active\,gages$$

$$F = assumed\,gage\,factor$$

$$\varepsilon_{SHUNT} = equivalent\,shunt\,strain$$

$$V = bridge\,excitation\,voltage.$$

The estimated gain was set on the signal conditioning amplifier and delicately adjusted in order to obtain the proper calibration output voltage for each particular gage.

The actual output voltages from the strain gages were recorded using an IBM PC computer with a Data Translation 2805/5716 digitial/analog (D/A) board. A BASIC program written for data acquisition named AP1 [46] was modified for use during this study. One modification fixed a timing problem that occurred at midnight when the day changed. Another modification incorporated a procedure to take three readings from the D/A board and average them to obtain the reading at the particular time step. The averaging process was installed as a possible method to minimize the line noise while using Vishay 2100 signal conditioning amplifier. Unfortunately, the averaging process had little effect on the line noise concentrated at 60 Hz but was left in the program to smooth the data. The time required to take three data samples for the averaging process was negligible since the DT board has an A/D throughput of 2500 samples per second. The resolution of the 2805/5716 D/A board was 16 bits. This allowed the +10 to -10 voltage range to be divided with a resolution of 0.0003 volts. This voltage resolution equated to strain resolution of less than 0.2 $\mu\varepsilon$ for the strain per volt calibration ranges used in this study.

Ideally, strain data should be taken on a logarithmic time spacing for creep testing. This feature could not be easily added to the AP1 program. Instead, the data was taken at increasing time intervals and later reduced to approximate

logarithmic spacing using a post-processing program. The data was collected at time intervals of 1, 10, 100, and 1000 seconds. The number of points collected at each time interval were 350, 100, 100 and up to 1450 respectively. This data collection scheme allowed choosing the final data set at time intervals approximately equal to 0.1 log time units for a period up to 16.9 days.

3.6 Aging Creep Test Procedures

Both short-term and long-term creep tests were conducted during this study. The results of the short-term (momentary) creep tests were used to characterize the aging rate of the material as described in section 2.2.5.1. The results of the long-term creep tests were used to verify the physical aging models. The procedures used to conduct both test types were identical, except for the duration of the test.

The testing sequence was started by heating the specimens to the rejuvenation temperature of 437°F (225°C) and holding for a minimum of 15 minutes. Initial tests revealed that the 90 degree orientations were particularity susceptible to warping when heated above T_g. The warpage was minimized by placing a six inch metal ruler between the grips before heating above T_g. The ruler provided additional rigidity to the specimen and solved the warpage problem. As a precaution, the ruler was used on all other angle ply orientations to minimize the chance of warping occurring. Before the quench, the oven

controller was set to 90°F to keep the oven from heating during the cooling process. After the desired air quench was conducted, the metal ruler was removed and the oven door was closed. The oven temperature typically overshot the desired aging temperature by about 5°F (3°C) while the oven temperature stabilized. The aging start time and date was consistently started when the desired aging temperature was reached after this slight temperature overshoot. Upon reaching the desired aging temperature, the oven controller was reset to the aging temperature. Next, a sequence of short-term tests were conducted at aging times, t_a, of 1, 3, 9, 27, and 81 hours after the quench. These particular aging times were selected to allow sufficient recovery time between tests and to provide a manageable testing schedule. Before starting the first creep test after the quench, the amp balance, excitation voltage, circuit balance, and shunt calibration voltage for each Wheatstone circuit was checked and properly adjusted.

The AP1 data acquisition program was initiated for each creep and recovery test in order to create a separate data file for each short-term test segment. The first entry in the data file was the time and date the local test segment started. This information was used to relate the local time data, referenced to the start of the local test segment, to the global time scale, referenced to the aging start time and date for the entire isothermal test sequence.

3.7 Data Reduction Procedures

The data reduction process was initiated by calculating the aging time, t_a, for each creep test segment. This was accomplished by subtracting the global aging start time and date from the local segment starting time and date stored in each data file. Next, several adjustments were made to the strain gage data. First, the strain data for each creep test was adjusted by subtracting the extrapolated residual recovery voltages from the previous recovery period as explained in section 2.2.5.1. The extrapolated recovery voltages for each gage were calculated by fitting the last 50% of the recovery data with a linear equation. An example of the linear fit, i.e., the recovery voltages for the 45° specimen at 365°F (185°C), after the t_a=9 hr creep test, is shown in figure 3.16. The global time scale was used in the recovery data so that the extrapolated recovery voltages could be linked to the time scale in next creep test. Also, the total extrapolation of the recovery data into the next creep test period was no more than 16% of the total recovery period. The subtraction of the recovery voltages also eliminated any accumulated drift in the strain gages by effectively zeroing the voltages before each creep test segment.

The next adjustment, applied to each strain gage reading, corrected the 2.0 gage factor used during data collection to the quoted manufacturers gage factor adjusted to the actual

test temperature using the procedures recommended by Micro Measurements [42]. Finally, the strain gage data was corrected for transverse sensitivity effects using the procedures recommended by Micro Measurements [43]. The transverse sensitivity correction was not required for the 90 degree specimen since the ratio of transverse to axial strain was very small. The predicted error in the strain measurements without the transverse sensitivity was less than 1% for the S_{22} direction and approximately 150% for the S_{21} direction. Since the fiber/transverse coupling compliance, S_{21}, is highly susceptible to transverse sensitivity error in the 90 degree specimen, the preferred method to determine the coupling compliance is to use a 0 degree specimen. The 0 degree specimen produces larger strains in the transverse direction and permits a more accurate determination of the fiber/transverse coupling compliance, S_{12} term.

Ideally, the load is applied instantaneously as a step function at the start of a creep test. In practice, the load is actually applied over a certain period of time. During this study, the load was applied by lowering the table supporting the weight by manually turning the loading handle counterclockwise. Typically, the loading process was accomplished in about 4 seconds. The creep response resulting from the ramp loading will obviously be different from that of a step loading. The difference in creep responses will become neg-

ligible after a certain time, usually referred to as the initial transient period. Lou and Schapery [36] recommended waiting a period equal to five times the initial loading period to allow the compliance response from a ramp load to converge to the step loading response. During this study, the calculation of the compliance response was started 20 seconds after the load was applied. The sensitivity of the aging rate to the 20 second transient period was checked by recalculating the aging rates using a 60 second transient period. The variation in aging rate between the 20 and 60 second transient periods ranged from -0.3% to +3.3% for the five test temperatures used with the 90 degree specimen. Since the variation was small, the start of the creep compliance data was computed after the 20 second transient period.

4 CHARACTERIZATION RESULTS AND DISCUSSION

This chapter contains the results and discussion of the momentary creep tests conducted to characterize the effect of physical aging on the Radel X/IM7 composite. The physical aging theory developed by Struik [59] was successfully applied to the orthotropic composite material. The compliance response of the composite was characterized in each of the principal material directions.

4.1 Room Temperature Material Response

Room temperature tensile tests were conducted to determine the basic material properties of the "as received" composite material. The results were used to estimate the linear elastic range for the 90 and 0 degree orientations. The tests were conducted using an Instron 4204 test machine with a MTS model 632.13B-20 extensometer. The specimens were held using wedge action friction grips. The active specimen length was 5 in. (12.7 cm) with the strain measured over a 0.5 in. (1.27 cm) gage length. The ultimate strength and stress-strain behavior were recorded while the specimen was loaded at a high rate.

The resulting stress-strain curve for the 90 degree specimen is shown in figure 4.1. A linear regression routine was used to calculate a modulus value of 1.07 Msi (7.38 GPa). The stress in the gage section at failure was 4.04 Ksi (27.8 MPa).

The specimen failed near the grip where the thickness was slightly reduced, yielding an ultimate failure stress of 4.46 Ksi (30.8 MPa). A comparison of the test results to commercially available data is given in table 4.1. The commercial data in table 4.1 was determined for a composite with T650-42 fiber instead of IM7. The two graphite fiber materials have similar material properties. Table 4.2 provides a list of the properties of T650-42 and IM7 fiber materials for comparison. The tensile modulus obtained during the room temperature testing was within 8.5% of the published value, but the tensile strength was about 35% low. The low tensile strength may be attributed to a slight misalignment of the specimen or the absence of specimen end tabs which help lower the load concentration effect near the grips. After analyzing the results of Gramoll et al [25], a stress level equal to approximately 10% of the ultimate room temperature strength was chosen as a starting stress level for linear viscoelastic testing. Verification tests were used to show that the material remained in the linear viscoelastic range at this stress level.

The 0 degree stress-strain curve is shown in figure 4.2. A linear response was obtained up to a stress level of about 185 Ksi (1275 MPa). At this stress level, the extensometer began slipping and noticeable cracking of the fibers was heard. The curve was linearly extrapolated, dashed line in figure 4.2, to the ultimate failure stress of 261 Ksi (1800 MPa).

Again, a linear regression routine was used to determine a fiber direction tensile modulus of 23.1 Msi (159.3 GPa). The tensile modulus was within 2.5% of the published value, but similar to the 90 degree specimen, the ultimate tensile strength in the 0 degree specimen was low by about 21%. The stress level used for creep testing of the 0 degree specimen was selected at a value equal to 20% of the failure stress in order to produce measurable strains in the transverse direction.

Room temperature testing also included ultimate tensile tests of both 45 and 30 degree specimen orientations. The specimens were held using the friction grips that were utilized during creep testing. This insured that the same end rotation constraint was used on the unbalanced off-angle laminates for both ultimate tension and creep testing. The ultimate specimen stress of the 45 and 30 degree orientations were 6.32 Ksi (43.6 MPa) and 13.2 Ksi (90.9 MPa) respectively. Both specimens failed in shear parallel to the fibers with the fracture originating at the grip.

4.2 90 Degree Specimen Tests, S_{22} Determination

The 90 degree specimen orientation was used to determine the transverse direction compliance, S_{22}, in the linear viscoelastic range using the methods explained in section 2.3. The 90 degree specimen orientation was tested first to

demonstrate that the composite physically ages. This orientation is resin dominated and was expected to age similarly to a neat polymer.

4.2.1 Linearity and Sequencing Effects

Initial tests of the 90 degree specimen were used to verify that the proposed 400 psi (2.76 MPa) applied stress level would produce a linear viscoelastic response. A series of creep tests were conducted at different stress levels, at an aging time of 3 hours, with the temperature held constant at 392°F (200°C). Between each test, the specimen was heated above T_g and air quenched back to the aging temperature. The compliance response of the material at the four stress levels tested is shown in figure 4.3. The compliance curves have the same shape with a slight offset in the initial compliance values. The slightly increased curvature of the 490 psi (3.38 MPa) curve was attributed to a slight increase, ≈1-2°F (1°C), in temperature during this test. The consistency of the compliance curves over the stress range tested indicated that the material remained in the linear viscoelastic range at the test temperature. The 400 psi (2.76 MPa) stress level was, therefore, used for all the aging tests of the 90 degree specimens.

The validity of the creep test sequencing procedure was checked using the procedure described in section 2.2.5.1. Both compliance curves shown in figure 4.4 were obtained at 338°F (170°C) with an aging time of 9 hours. The compliance curve

with asterisk symbols was the third creep test in an aging sequence test. The compliance curve with circle symbols was from an unsequenced test where the initial two creep tests of the sequence were omitted. The compliance curves have the same shape with a 1.2% offset in the initial compliance magnitude. This slight offset can be attributed to the error introduced during the fitting and subtraction of the recovery response from the previous creep test in the aging sequence. The overall agreement between the two compliance curves demonstrates the applicability of using the aging test sequence to characterize the aging effect in the linear stress range.

4.2.2 Aging Shift Rate Determination

The effect of physical aging on the transverse direction compliance, S_{22}, was determined using a sequence of short-term momentary creep tests. The tests were conducted at five temperature levels using the procedures described in section 3.6. The compliance curves resulting from the short-term tests are shown in figures 4.5-4.9. The symbols in these figures depict the actual test data with the solid line representing the numerical fit of Struik's equation (eqn. 2.19) to the data. An average m value of 0.4167 was used in the fitting program. This value was calculated by averaging the individual m values from the 338, 365, and 195^{0}F (170, 185 and 195^{0}C) aging sequences. The m value from the individual creep curves showed considerable scatter varying from a low of 0.2921 to a high of 0.4894.

The scatter is most likely attributed to the variability of the shape of the compliance curve during the short time span of the momentary creep tests.

The momentary creep compliance curves were shifted to form master momentary compliance curves. The master curve data, referenced to the 81 hour aging time, is shown in figure 4.10. The shifting process was accomplished using the procedures described in section 2.2.5.2. The amount of horizontal shift $-\log a$ and the vertical shift $\log B$ for each creep curve are given in table 4.3.

The aging shift rate, μ, was determined for each aging test sequence using a linear regression routine. A plot of the aging data, $-\log a$ versus $\log t_e$, and the calculated aging shift rate, slope of the curve, for each test sequence are shown in figure 4.11. The aging shift rate increased as the temperature decreased, until a temperature of 365°F (185°C) was reached. At this point, the aging shift rate started to decrease as the temperature decreased. The effect of temperature of the aging shift rate is discussed further in section 4.5.

4.2.3 TTSP Master Momentary Compliance Curve

TTSP master momentary compliance curves were formed by shifting momentary compliance curves, obtained at various temperatures with the same aging time, using the time-

temperature superposition principle. The 90 degree long-term test was started at an aging time of 9 hours with the temperature at 338°F (170°C). Several methods were examined for obtaining the TTSP master momentary compliance curve at this reference state.

The first method numerically fit the test data from various temperatures at an aging time of 9 hours to Struik's equation (eqn. 2.19) using the average m value of 0.4167. The horizontal shift factors were calculated using equation 2.47. The resulting transverse direction master momentary compliance curve, referenced to 338°F (170°C) and t_e = 9 hours, is shown in figure 4.12.

The second method utilized a graphical procedure, described in section 2.2.5.3, to determine the shift factors required to form the master curve. The resulting curve, again referenced to 338°F (170°C) and t_e = 9 hours, is shown in figure 4.13. An examination of the shift factor summaries, given in figures 4.12 and 4.13, shows that first and second methods give essentiality the same shift factors.

The final shift method utilized the graphical procedure to obtain the master curve referenced to 338°F (170°C) at an aging time of 81 hours instead of 9 hours. The resulting curve, referenced to 338°F (170°C) and t_e = 81 hours, is shown in figure 4.14. The aging shift rate, μ, at a temperature of 338°F (170°C), was 0.77. Using this aging rate and equation

2.48, the shift factor required to shift the t_e = 81 hours curve to t_e = 9 hours was determined. An additional small vertical shift was also included during shifting procedure. The resulting TTSP master momentary curve is shown along with the curves resulting from the first two methods in figure 4.15. The curves show essentially the same shape with a small variation between 10^4 to 10^6 seconds. The effect of the small variation in the compliance curves on long-term predictions is discussed in section 5.0.

4.3 45 Degree Specimen Tests, S_{66} Determination

The 45 degree specimen orientation was used to determine the shear direction compliance, S_{66}, in the linear viscoelastic range using the methods explained in section 2.3. Experimentally obtaining the shear direction compliance data provided the unique challenge of getting twelve strain gages working at the same time in a high temperature environment.

4.3.1 Linearity and Sequencing Effects

The 45 degree specimens were tested at an applied stress level of 800 psi (5.52 MPa). Using equation 2.60, the applied stress was found to produce a normal stress component of 400 psi (2.76 MPa) in the matrix material. This was the same matrix normal stress used during testing of the 90 degree specimens. A series of creep tests were conducted to determine if the material remained in the linear viscoelastic range at

the applied stress level. The compliance curves from tests at different stress levels, at an aging time of 3 hours with the temperature held constant at 365°F (185°C), are shown in figure 4.16. The excellent overlap of the compliance curves shows that the material remained in the linear viscoelastic range up to the 800 psi (5.52 MPa) stress level. The 800 psi (5.52 MPa) test was repeated and with the results also shown in figure 4.16 as triangular symbols. The excellent overlap with the previous 800 psi (5.52 MPa) test demonstrates the repeatability of the creep test results.

The effect of sequencing creep tests and using Boltzmann's superposition principle to subtract the recovery strain from previous creep tests was also checked for the 45 degree specimen orientation. Compliance curves from tests conducted with and without sequencing at two different temperatures and aging times are shown in figure 4.17. The sequenced and unsequenced compliance curves, from both test conditions, have the same shape with a 1.8% maximum offset between them. The agreement between sequenced and unsequenced test results verifies the applicability of using the aging test sequencing procedure.

4.3.2 Aging Shift Rate Determination

The effect of physical aging on the shear direction compliance, S_{66}, was determined at three temperature levels. The upper two temperature levels, 399 and 392°F (204 and 200°C), that were used with the 90 degree specimen orientation, were

not tested. They were eliminated in view of time constraints and the desire to reduce the risk of failing the specimen. The compliance curves resulting from the aging sequence tests are shown in figures 4.18-4.20. Again, the symbols depict the test data with the solid line representing the numerical fit of Struik's equation to the data. The individual m values from the three aging sequences were averaged resulting in an average m value of 0.4564. This value was used in the computer fitting program. The m values from the individual creep curves varied from a low of 0.3518 to a high of 0.5082.

The momentary creep compliance curves were shifted to form master momentary compliance curves. The master curve data, referenced to the 81 hour aging time, is shown in figure 4.21. The amount of horizontal shift $-\log a$ and the vertical shift $\log B$ for each creep curve are given in table 4.4.

A plot of the aging data, $-\log a$ versus $\log t_e$, used to calculate the aging shift rate, μ, for each test sequence are shown in figure 4.22. The aging shift rate, i.e., slope of the curve, increased as the test temperature decreased. A comparison of the aging shift rates determined from the 90 and 45 degree specimen tests is presented in section 4.5.

4.3.3 TTSP Master Momentary Compliance Curve

TTSP master momentary compliance curves were formed using the same methods described in section 4.2.3 for the 90^0

specimens. Again, the goal was to obtain the compliance curve at the long-term test reference aging time of 9 hours with the temperature at 338°F (170°C).

The first method numerically fit the test data from various temperatures at an aging time of 9 hours to Struik's equation (eqn. 2.19) using the average m value of 0.4564. The horizontal shift factors were calculated using equation 2.47. The resulting transverse direction TTSP master momentary compliance curve, referenced to 338°F (170°C) and t_e = 9 hours, is shown in figure 4.23. Note that fitted curve is extrapolated beyond the test data at times greater than $10^{4.5}$ seconds.

The TTSP master momentary compliance curve resulting from graphical shifting of the t_e = 9 hours compliance curves is shown in figure 4.24, along with the required shift factors. Similar to the 90 degree test results, the numerical and graphical methods produce equivalent shift factors for the same referenced aging time.

Finally, the graphical shift procedure was used to obtain the master curve referenced to 338°F (170°C) at an aging time of 81 hours instead of 9 hours. The resulting curve, referenced to 338°F (170°C) and t_e = 81 hours, is shown in figure 4.25. The aging shift rate, μ, of 0.92 was used in the calculations to determine the horizontal shift required to move the t_e = 81 hours curve to a t_e = 9 hours reference time. The shifted curve is shown in figure 4.26 along with the curves that were

determined by the two other methods. Initially, the three curves are nearly identical initially. However, as the time increases beyond $10^{4.5}$ seconds, the curves start to separate. This time was observed to correspond to the end of the shifted compliance data shown in figures 4.23-4.24. The separation of the curves beyond $10^{4.5}$ seconds results from the extrapolation of the curves beyond the test data. Obtaining a better compliance representation beyond $10^{4.5}$ seconds would require testing at higher temperatures. Unfortunately, nonlinear effects, aging to equilibrium, and possible specimen rupture may occur as the test temperature approaches T_g.

4.4 0 Degree Specimen Tests

The 0 degree specimen orientation was used to determine the fiber direction compliance, S_{11}, and the fiber/transverse coupling compliance, S_{12}. The 0 degree orientation is dominated by the properties of the elastic graphite fiber. Previous testing of graphite fiber composites [26,50,68,74] revealed little time-dependent behavior in the 0 degree fiber orientation. As expected, neither S_{11} or S_{12} showed appreciable time-dependent behavior at temperatures from 338°F (170°C) to 399.2°F (204°C). Thus, both S_{11} and S_{12} were considered temperature and aging independent.

4.4.1 S_{11} Determination

The 0 degree specimen orientation was tested at 338°F (170°C) for linear behavior at stress levels of 5000 psi (34.5 MPa) and 7500 psi (51.7 MPa). The resulting S_{11} compliance curves were nearly identical and are shown in figure 4.27. The compliance data from an aging sequence test conducted at 338°F (170°C) is shown in figure 4.28. No physical aging effects were evident from the test results. The data points from the 338°F (170°C) aging tests were averaged yielding a fiber compliance value of S_{11} = 40.230 (1/Gsi) (0.005835 (1/GPa)). The average compliance value is shown as a solid line in figure 4.28.

The compliance data from a second aging sequence test, conducted at 399.2°F (204°C), is shown in figure 4.29. A slight negative time dependence (contraction under tension) of 8 με over a 10^4 second creep test was noticed at the higher temperature. Griffith et al [26] also noticed a slight negative time dependence during his testing of 0 degree specimens of T300/934 graphite/epoxy composite material. He attributed the phenomena to the viscoelastic nature of the strain gage adhesive. The small magnitude of the strain change, only 8 με, could also be attributed to normal experimental error associated with the strain measurement.

4.4.2 S_{12} Determination

The fiber/transverse coupling compliance term, S_{12}, was obtained by measuring the strain in the transverse direction on the 0 degree specimen, as explained in section 2.3. The S_{12} compliance curves from the linearity check on the 0 degree specimen are shown in figure 4.30. A linear response was obtained between the 5000 psi (34.5 MPa) and 7500 psi (51.7 MPa) applied stress levels. Since the S_{12} compliance value is negative, the log of the absolute value of the S_{12} compliance term was plotted.

The compliance data from an aging sequence test, conducted at 338°F (170°C), is shown in figure 4.31. Similar to S_{11}, the S_{12} compliance term showed no aging effects or time-dependent behavior at 338°F (170°C). An average compliance value, S_{12} = -13.991 (1/Gsi) (-0.002029 (1/GPa)), was calculated and is shown as a solid line in figure 4.31. The compliance data shown in figure 4.32 was from an aging sequence test conducted at 399.2°F (204°C). The apparent time-dependence of the S_{12} term results from a small change in strain, 9 με over the 10^4 second creep test, at the higher test temperature. It was impossible to determine if this small strain change was a viscoelastic material response or a strain measurement anomaly at the higher test temperature.

4.5 Temperature Dependence of Aging Shift Rate

The aging shift rate, μ, of the composite material was found to have a temperature dependence similar to that of polymer materials. The aging shift rate values calculated at various test temperatures with specimen fiber orientations of 90, 45, and 30 degrees are shown in figure 4.33. Although some scatter exists between specimen orientations, a general trend in the data appears and is represented by the solid curve in figure 4.33. The aging shift rate appears to increase from aging equilibrium (zero aging shift rate) at T_g to a plateau region where the aging shift rate is about unity. Tests at temperatures below 338°F (170°C) were not conducted because of difficulties in measuring the small creep response. It is expected that the aging shift rate would decrease with lower test temperatures as the material approaches the secondary β transition temperature. Below this temperature physical aging ceases because the free volume can no longer change as explained in section 2.2.1. Sullivan [66] noticed a slight decrease in the aging shift rate of a composite material, made of Dow Derakane 470-36 resin with glass fibers, at temperatures of Tg - 126°F (T_g - 70°C). The β transition temperature is usually determined using Dynamic Mechanical Analysis (DMA). The test is conducted over a wide temperature range obtained by heating

the specimen in an oven and cooling it with a liquid nitrogen injection system. The β transition temperature was not determined during this study.

The decrease in μ observed at 338°F (170°C) in the 90 degree specimen was not found in the 45 or 30 degree specimen orientations. A more extensive characterization program with multiple specimen tests for each fiber orientation would be required to determine if the decrease in the 90 degree μ value at 338°F (170°C) was a point anomaly or a material trend for the 90 degree specimen orientation.

4.6 Temperature Dependence of Shift Factors

The horizontal shift factors required to form a TTSP master momentary compliance curve are functions of both the test temperature and the referenced aging time. Both the Arrhenius and WLF models, which are usually used to represent temperature shift factor data, are based on polymer viscoelasticity behavior without physical aging. Any future models developed must also include the aging state of the material as a variable. The shift factors computed for compliance curves obtained at different temperatures with the same aging time have contributions due to temperature and contributions due to aging. The aging contribution is not the same for each compliance curve because the aging shift rate, μ, has a temperature dependence.

The horizontal shift factors, $-\log a_T$, that are used to form the TTSP master momentary compliance curves shown in figures 4.13-4.14 and 4.24-4.25 are plotted versus test temperature in figures 4.34 and 4.35 respectively. An observation from these figures is that the shift factors for the 81 hour referenced aging time appear to be larger in magnitude than for the 9 hour referenced aging time. This may be due to the decrease in the aging rate at temperatures greater than the referenced temperature of 338°F (170°C). Continued investigation of the aging dependence of the horizontal shift factors offers an excellent opportunity for follow on work to this study.

4.7 Quench Rate Effect

The effect of physical aging has been shown to significantly change the compliance properties of a specimen that is quenched from above T_g to an aging temperature below T_g. The high pressure air quenching procedure used in this study yielded a quench rate of 9.5°F/sec (5.3°C/sec). This rate was determined using the procedures described in section 3.2.2. However, normal composite processing procedures would use a slower rate to cool the material. An obvious question is: How is physical aging process affected by a slower cooling rate?

An effort to study the cooling rate effect on physical aging was made by testing the 90 and 45 degree specimens at

a slower cooling rate. A slower cooling rate was obtained by shutting the oven controller off and allowing the closed oven to cool to the aging temperature. This procedure yielded an oven cooling rate of 0.056°F/sec (0.031°C/sec), or about 170 times slower than the air quench. Aging sequence tests were conducted on both the 90 and 45 degree specimens after they were oven cooled to 383°F (195°C). The shifted master compliance curves, referenced to t_e = 81 hours, are shown in figures 4.36 and 4.37 for the 90 and 45 degree specimens respectively. The compliance curves are essentially the same shape with the oven cooled data shifted slightly to longer times. The aging shift rate, μ, for the S_{22} compliance direction decreased from 0.66 for the air quench to 0.59 for the oven cool. Similarly, μ, for the S_{66} compliance direction decreased from 0.78 for the air quench to 0.73 for the oven cool. The decrease in aging shift rate with decreasing cooling rate is consistent with the observations of Booij and Palmen [6] during their study of the effects of thermal history on the viscoelasticity of ABS samples.

Clearly the effect of physical aging continues at the slower oven cooling rate. Theoretically an infinitely slow cooling rate would produce a state of free volume equilibrium where physical aging would not be possible. However, time constraints associated with the manufacture of composite parts

require removal of the part from the oven as soon as the curing or consolidation process is complete. Physical aging effects should therefore be expected in actual composite structures.

5 LONG-TERM CREEP RESULTS AND DISCUSSION

In the previous chapter, the short-term testing used to characterize the effect of physical aging on the compliance response of the composite material in each of four material principal directions was described. In this chapter, the results of long-term tests, conducted to verify the influence of physical aging on the Radel X/IM7 composite material, are presented. Long-term compliance results are compared with theoretical predictions determined using Struik's effective time theory and the short-term characterization data.

5.1 90 Degree Specimen Test, S_{22} Comparison

A comparison of the transverse direction long-term compliance predictions with the observed test data is shown in figure 5.1. The long-term test was conducted at a temperature of 338^{0}F (170^{0}C) with a starting age time of 9 hours. The test data is depicted with asterisk symbols, while the predictions obtained using each of the TTSP master momentary compliance curves from figure 4.15, along with the effective time theory, are shown as various line types. All of the long-term predictions with aging show the same shape as the test data. The predictions consistently under-predicted the compliance test data. The same under-prediction trend was noticed in long-term

compliance data presented by Sullivan [65]. The cause of the under-prediction is believed to be related to drift of the strain gage voltages during long-term tests. The effect of strain gage drift was effectively canceled out during short-term tests by the subtraction of the recovery voltages from the previous test. The accumulation of the drift of the strain gage voltages could be responsible for the increased strain readings during long-term tests. Small changes in the bridge balance and excitation voltages were noticed at the end of long-term tests. Unfortunately, numerous factors can effect the drift of strain gage voltages over long time durations. The factors include the initial balance of the specimen, quality of the solder connections, supply voltage variations, and specimen thermal history. Measurement of the specimen strain using optical techniques along with strain gages offers a possible future means to determine the strain gage drift effect.

The sensitivity of the long-term compliance predictions to the short-term data fitting procedure is apparent in figure 5.1. The variation of the long-term predictions from the experimental data range from 7.3% for the m_{avg} = 0.41671 curve to 3.5% for the TTSP curve which was obtained at an aging time of 81 hours and shifted to the referenced aging time of 9 hours. The closeness of the predictions makes it difficult to determine if one data reduction technique is more reliable than another.

Also included in figure 5.1 is the compliance prediction calculated using the real time instead of effective time for the TTSP = 9 hr. data reduction technique. The prediction without aging effects included over-predicts the compliance data by 50%. The corresponding prediction with aging effects under-predicts the compliance data by 5.7%. Clearly, the effect of physical aging must be included in order to use short-term momentary compliance data to predict the long-term compliance response.

5.2 45 Degree Specimen Tests, S_{66} Comparison

Long-term shear direction compliance tests were conducted at a temperature of 338°F (170°C) at starting age times of 9 and 3 hours. As in figure 5.1, the test data is again depicted with asterisk symbols, while the compliance predictions are shown with various line types in figures 5.2 and 5.3 for the 9 and 3 hour starting age times respectively. Noted with respect to both figures is the region where the predictions were made using the extrapolation of the characterization data. The sensitivity of the long-term prediction to the short-term fitting procedure becomes more apparent in the extrapolated region. The best fit to the test data was the prediction obtained by graphically shifting the TTSP data to the aging time of the test. The predictions from this method were only 6.3% and 7.3% from the test data at starting age times of 9

and 3 hours respectively.

The effect of physical aging on the long-term compliance prediction becomes evident at smaller starting aging times. The compliance prediction without aging for the 9 hour starting age time, shown in figure 5.2, is 65% from the actual test data at the end of the test. The prediction without aging for a test at a 3 hour starting age time, shown in figure 5.3, is greater than 165% from the actual test data at the time corresponding to the end of the 9 hour aging time test. As the aging time before the start of the creep test was increased, the apparent effect of physical aging was shifted to longer test times. Significant variation between "with aging" and "without aging" predictions starts at about $10^{3.5}$ and 10^{4} seconds respectively for 3 and 9 hours aging start times. Clearly, the aging time at the start of the creep test and the test duration determine if physical aging significantly changes the creep response of the material during the test.

The ambiguous thermal history of the specimens used in previous test programs [13,25,26,68] makes it impossible to determine if physical aging effects were significant. Typically, specimens from other test programs were tested in succession at increasing stress levels at a constant temperature or at a constant stress level with the temperature increased

between tests. Since the tests were usually conducted in succession, the physical aging effects were most likely blended in with temperature and stress effects.

5.3 30 Degree Specimen Test, S_{xx} Comparison

The load direction compliance, referred to as S_{xx}, was determined using equation 2.68a and the four principal compliance terms S_{11}, S_{12}, S_{22}, and S_{66}. The TTSP momentary compliance curves used in the computations were determined using the graphical procedure at an aging time of 9 hours and referenced to a temperature of 338°F (170°C). Aging shift rate, μ, values of 0.77 and 0.93 were substituted, respectively for the S_{22} and S_{66} principal compliance directions, into equation 2.55 during the calculation of the effective time for long-term predictions. The test data and predictions for the load direction long-term compliance at a temperature of 338°F (170°C) and a starting age time of 9 hours is shown in figure 5.4. Predictions are shown for fiber angles of 29.5, 30 and 30.5 degrees to demonstrate the sensitivity of the compliance predictions to the possible misalignment of the fiber orientation during specimen fabrication or the misalignment of the strain gage. The 29.5 degree prediction matches the initial compliance value the best, but under-predicts the compliance at 10^6 seconds by 9.1%. This under-prediction of the compliance was also seen in the

S_{22} and S_{66} long-term predictions. The compliance prediction obtained without physical aging effects over-predicted the test compliance value at 10^6 seconds by 137%.

5.4 Overall S_{xx} Comparison

Predictions of the load direction compliance, S_{xx}, for fiber orientation angles ranging from 0 to 90 degrees at a temperature of 338°F (170°C) and an aging start time of 9 hours are shown in figure 5.5. The 90, 45, 30 and 0 degree fiber angle long-term load direction compliance test data is also shown in figure 5.5 with asterisk symbols. The gradual stiffening of the material from physical aging is apparent in both the predictions and the test data. The predictions and test data compare quite well considering the possible sources of experimental error and specimen to specimen material property variations. Ideally, multiple specimens of each fiber orientation would be tested so a statistical distribution of the compliance response could be determined.

The shape of the compliance curve beyond the end of the test data at 10^6 seconds can be estimated by determining the double-logarithmic slope of the long-term creep curves. The shape of the double-logarithmic slope primarily depends on the aging shift rate μ. A μ value of 0.85 yields a nearly constant double-logarithmic slope value producing a straight line on the double-logarithmic plot of compliance versus time. Values

of μ greater than 0.85 produce a slope that slightly decreases with time. When the value of μ is less than 0.85 the slope slightly increases with time. The proximity of the μ values for both the S_{22} and S_{66} compliance directions to 0.85 explains the nearly straight line prediction of the compliance at longer test times.

6 SUMMARY, RECOMMENDATIONS, AND CONCLUSIONS

6.1 Summary

The goal of this study was to determine the effect of physical aging on the creep response of Radel X/IM7 composite material in the linear viscoelastic region. Three program objectives were defined to meet this goal. The first objective was to develop the experimental procedures to conduct physical aging experiments. The second objective was to apply the experimental procedures to characterize the influence of sub T_g physical aging on the creep response of the thermoplastic composite material in each of the material principal directions. The third objective was to use short-term momentary compliance test results and the effective time theory to predict the long-term compliance response of unidirectional laminates.

All three objectives were accomplished. Experimental problems were encountered and solved during the study. Momentary compliance results were used to characterize the aging effect by determining the aging shift rate of the material. Momentary creep tests revealed significant changes in the compliance response of the composite as it physically aged. Finally, long-term predictions using the effective time theory varied from the test data by less than 10% at the end of the long-term test period.

The Radel X/IM7 thermoplastic composite material characterization process was completed by conducting momentary creep tests of 90, 45, and 0 degree unidirectional laminates. The effect of physical aging on the compliance response was determined in each of the four principal material directions. The resin dominated transverse direction compliance, S_{22}, and shear direction compliance, S_{66}, were found to be time and aging dependent. The fiber direction compliance, S_{11}, and the fiber/transverse coupling compliance, S_{12}, were found to be virtually independent of time and aging effects.

The aging shift rate, μ, of the composite was found to have a temperature dependence. The aging shift rate appeared to increase from a predicted zero value at the glass transition temperature to a plateau region starting at a temperature about $63^{0}F$ ($35^{0}C$) below T_g. It was not possible during this study to determine if the variation between the aging shift rate of the various specimen orientations was experimental scatter or a function of the fiber angle of the specimen.

The Time-Temperature Superposition Principle was successfully used to determine TTSP master momentary compliance curves at a specific referenced aging time. The horizontal shift factors, $-\log a_T$, were found to depend on temperature and the referenced aging time of the master curve. Long-term predictions using the TTSP master momentary compliance curves,

without including effective time theory to account for the physical aging process, significantly overestimated the compliance response.

The rate the specimen was cooled from above T_g to the aging temperature was found to slightly affect the aging shift rate. The aging shift rate was found to decrease when the specimen cooling procedure was changed from an air quench to an oven cool method. Continually decreasing the cooling rate to an infinitely slow rate should theoretically produce a state of equilibrium free volume that would eliminate physical aging effects in the material. Although, achieving the equilibrium free volume may require a cooling rate that is impractical for industrial composite manufacturing applications

Momentary compliance data and the effective time theory were used to accurately predict long-term S_{22} and S_{66} compliance responses of the 90 and 45 degree specimens. Additionally, the four principal compliance terms were substituted into a laminate transformation equation to predict the load direction compliance for a 30 degree specimen. The long-term load direction compliance prediction matched the test data within normal error ranges associated with slight misalignments in the fiber orientation or strain gage direction.

6.2 Recommendations

This research project successfully addressed some of the questions concerning the effect of physical on composite

materials and subsequently created a few new ones. Many of the uncertainties in this study came from using test results from one specimen. Ideally, each creep test would be repeated with multiple specimens so that a reliable statistical distribution of the compliance properties could be determined. Obviously, testing more specimens would require a much longer time period and/or the use of multiple test fixtures. Future studies should concentrate on one fiber angle orientation and examine numerous test variables in more detail.

During this study, the effect of moisture was minimized by drying the material and keeping it in an environment with desiccant to maintain constant humidity. The absorption and desorption of moisture will affect the compliance response of the composite in a manner similar to temperature. Both the moisture and temperature environment will experience cyclic variation during the design life of the composite structure. The effect of physical aging on the properties of the material after complex moisture, thermal, and stress histories needs further investigation.

The physical aging theory should be extended so that nonlinear stress effects in composite materials are included. Sequencing of creep tests is no longer possible in the nonlinear stress range. Thus, the specimen must be reheated above T_g and quenched back to the aging temperature between each creep

test. The study of nonlinear effects will significantly increase the amount of test time required to characterize the material.

Development of improved strain measuring methods which do not require elaborate time-consuming specimen preparation are needed in order to conduct a larger quantity of tests in a short-time frame. Strain measurement procedures utilizing laser interferometry may provide required long-term stability and ease of use required to measure the strains in a high temperature environment. Another alternative is to use dynamic mechanical analyzer (DMA) equipment to measure the creep response. The strain or displacement is measured using a built-in sensor in the equipment. This alleviates problems associated with strain gages. DMA equipment usually includes a liquid-nitrogen cooling attachment to the oven. This feature can be used to produce various cooling rates in the oven. This would facilitate the study of cooling rate effects on physical aging. Unfortunately, DMA equipment is quite expensive and is rarely devoted to long-term aging studies.

Finally, the prediction capability needs to be extended from unidirectional laminates to general laminates and verified with experimental testing. This could be accomplished by modifying incremental numerical procedures developed by Dillard et al [13] or Gramoll et al [25] to include physical aging effects.

6.3 Conclusions

The creep response of Radel X/IM7 composite material has been found to be significantly affected by physical aging in the temperature range between 338°F (170°C) and 399.2°F (204°C). Physical aging effects become more predominant during long-term tests where the test duration is much longer than the aging time at the start of the test. Prediction methods based solely on the time-temperature superposition principle will significantly over-predict the creep response of the material if the effect of physical aging is ignored.

REFERENCES

1. Aklonis, J.J. and W.J. MacKnight, *Introduction to Polymer Viscoelasticity*, Second Edition, John Wiley and Sons, New York, NY, 1983.

2. Augl, J.M. and D.J. Land, "A Numerical Approach for Obtaining Nonlinear Viscoelasticity Parameters of Polymeric Materials and Composites," *Journal of Applied Polymer Science*, Vol. 30, 1985, pp. 4203-4233.

3. Augl, J.M., "Nonlinear Creep Effects of Physical Aging, Temperature and Moisture of an Epoxy Resin," *Journal of Rheology*, Vol. 31, No. 1, 1987, pp. 1-36.

4. Bertolotti, A., "A Computer-Based Solution for Evaluating the Parameters in Schapery's Nonlinear Viscoelastic Model," Senior Project, Department of Engineering Mechanics and Science, VPI & SU, Blacksburg, VA, Spring Quarter, 1982.

5. Boller, K.H., "Tensile Stress-Rupture and Creep Characteristics of Two Glass-Fabric-Base Plastic Laminates," Forest Products Laboratory, Report No. 1863, June 1957.

6. Booij, H.C. and J.H.M. Palmen, "Viscoelasticity of ABS Samples Differing in Thermal History," *Polymer Engineering and Science*, Vol. 18, No. 10, Mid-August, 1978, pp. 781-787.

7. Caplan, E.S. and H.F. Brinson, "Nonlinear Viscoelastic Characterization of Polycarbonate," Virginia Polytechnic Institute and State University, VPI-E-82-7, Blacksburg, VA, March 1982.

8. Chai, C.K. and N.G. McCrum, "Mechanism of Physical Aging in Crystalline *Polymers*," Polymer, Vol. 21, June 1980, pp. 706-712.

9. Chamis. C.C. and J.H. Sinclair, "Ten-deg Off-axis Test for Shear Properties in Fiber Composites," *Experimental Mechanics*, Vol. 17, No. 9, Sept., 1977, pp. 339-346.

10. Chang, T.D. and J.O. Brittain, "Studies of Epoxy Resin Systems: Part C: Effect of Sub-T_g Aging on the Physical Properties of a Fully Cured Epoxy Resin," *Polymer Engineering and Science*, Vol. 22, No. 18, Dec. 1982, pp. 1221-1227.

11. Christensen R.M., *Mechanics of Composite Materials*, John Wiley & Sons, Inc., New York, NY, 1979.

12. Dally, J.W. and W.F. Riley, *Experimental Stress Analysis*, 2nd Edition, McGraw-Hill, New York, NY, 1978.

13. Dillard, D.A., D.H. Morris and H.F. Brinson, "Creep and Creep Rupture of Laminated Graphite-Epoxy Composites," Virginia Polytechnic Institute and State University, VPI-E-81-3, Blacksburg, VA, March 1981.

14. Dillard, D.A., M.R. Straight and H.F. Brinson, "The Nonlinear Viscoelastic Characterization of Graphite/Epoxy Composites," *Polymer Engineering and Science*, Vol. 27, No. 2, Jan. 1987, pp. 116-123.

15. DuPont Instruments DSC Standard Data Analysis Program Manual, Version 2.0, DuPont, March 1987.

16. Ferry, J.D., *Viscoelastic Properties of Polymers*, Third Edition, Wiley, New York, NY, 1980.

17. Findley, W.N. and D.B. Peterson, "Prediction of Long-Term Creep with Ten-Year Creep Data of Four Plastic Laminates," *American Society for Testing Materials, Proceedings*, Vol. 58, 1958, pp. 841-855.

18. Findley, W.N. and G. Khosla, "Application of the Superposition Principle and Theories of Mechanical Equation of State, Strain, and Time Hardening to Creep of Plastics under Changing Loads," *Journal of Applied Physics*, Vol. 26, No. 7, July 1955, pp. 821-832.

19. Findley, W.N. and J.F. Tracy, "16-Year Creep of Polyethylene and PVC," *Polymer Engineering and Science*, Vol. 14, No. 8, Aug. 1974, pp. 577-580.

20. Findley, W.N., "26-Year Creep and Recovery of Poly(Vinyl Chloride) and Polyethylene," *Polymer Engineering and Science*, Vol. 27, No. 8, April 1987, pp. 582-585.

21. Findley, W.N., C.H. Adams, and W.J. Worley, "The Effect of Temperature on the Creep of Two Laminated Plastics as Interpreted by the Hyperbolic-Sine Law and Activation Energy Theory," *American Society for Testing Materials, Proceedings*, Vol. 48, 1948, pp. 1217-1239.

22. Findley, W.N., J.S. Lai, and K. Onaran, *Creep and Relaxation of Nonlinear Viscoelastic Materials*, North-Holland Publishing Company, Amsterdam, New York, 1972.

23. Flugge, W., *Viscoelasticity*, Blaisdell Publishing Co., Waltham, Massachusetts, 1967.

24. Freelance Plus, 3.01 Reference Manual, Lotus Development Corporation, 55 Cambridge Parkway, Cambridge, MA 02142, 1989.

25. Gramoll, K.C., D.A. Dillard, and H.F. Brinson, "Thermo-viscoelastic Characterization and Predictions of Kevlar/Epoxy Composite Laminates," Virginia Polytechnic Institute and State University, VPI-E-88-12, Blacksburg, VA, May 1988.

26. Griffith, W.I., D.H. Morris, and H.F. Brinson, "The Accelerated Characterization of Viscoelastic Composite Materials," Virginia Polytechnic Institute and State University, VPI-E-80-15, Blacksburg, VA, April 1980.

27. Hiel, C., A.H. Cardon, and H.F. Brinson, "The Nonlinear Viscoelastic Response of Resin Matrix Composite Laminates," Virginia Polytechnic Institute and State University, VPI-E-83-6, Blacksburg, VA, March 1983.

28. IMSL FORTRAN Math/Library, Vol. 3, Chapters 8-10, Houston, TX.

29. Jones, R.M., *Mechanics of Composite Materials*, McGraw-Hill, New York, NY, 1975.

30. Kong, E.S.W., "Sub-T_g annealing studies of advanced epoxy-matrix graphite-fiber-reinforced composites," *Journal of Applied Physics*, Vol. 52, No. 10, October 1981, pp. 5921-5925.

31. Kovacs, A.J., La contraction isotherme Du volume des polymeres amorphes, *Journal of Polymer Science*, Vol. 30, 1958, pp. 131-147.

32. Kovacs, A.J., R.A. Stratton, and J.D. Ferry, "Dynamic Mechanical Properties of Polyvinyl Acetate in Shear in the Glass Transition Temperature Range," *Journal of Phys. Chem.*, Vol. 67, No. 1, Jan. 1963, pp. 152-161.

33. Lai, J.S.Y. and W.N. Findley, "Creep of Polyurethane under Varying Temperature for Nonlinear Uniaxial Stress," *Transactions of the Society of Rheology*, Vol. 17, No. 1, 1973, pp. 63-87.

34. Lai, J.S.Y. and W.N. Findley, "Elevated Temperature Creep of Polyurethane under Nonlinear Torsional Stress with Step Changes in Torque," *Transactions of the Society of Rheology*, Vol. 17, No. 1, 1973, pp. 129-150.

35. Leaderman, H., "Elastic and Creep Properties of Filamentous Materials and Other High Polymers," The Textile Foundation, Washington, 1943, p. 175.

36. Lou, Y.C. and R.A. Schapery, "Viscoelastic Behavior of a Nonlinear Fiber-Reinforced Plastic," Purdue University and Texas A&M University, Technical Report AFML-TR-70-113, May 1970.

37. Lou, Y.C. and R.A. Schapery, "Viscoelastic Characterization of a Nonlinear Fiber-Reinforced Plastic," *Journal of Composite Materials*, Vol. 5, April 1971, pp. 208-234.

38. Mark, J.E., A. Eisenberg, W.W. Graessley, L. Mandelkern, and J.L. Koenig , *Physical Properties of Polymers*, American Chemical Society, Washington, D.C., 1984.

39. MM Bulletin B-130-12, "Strain Gage Installations with M-Bond 43-B, 600, and 619 Adhesive Systems," Micro-Measurements Division, Measurements Group, Inc., P.O. Box 27777, Raleigh, NC, 27611.

40. MM Catalog 500, Part B, "Strain Gage Data," Micro-Measurements Division, Measurements Group, Inc., P.O. Box 27777, Raleigh, NC, 27611.

41. MM Tech Note TN-502, "Strain Gage Excitation Levels," Micro-Measurements Division, Measurements Group, Inc., P.O. Box 27777, Raleigh, NC, 27611.

42. MM Tech Note TN-504, "Strain Gage Temperature Effects," Micro-Measurements Division, Measurements Group, Inc., P.O. Box 27777, Raleigh, NC, 27611.

43. MM Tech Note TN-509, "Transverse Sensitivity Errors," Micro-Measurements Division, Measurements Group, Inc., P.O. Box 27777, Raleigh, NC, 27611.

44. MM Tech Note TN-514, "Shunt Calibration," Micro-Measurements Division, Measurements Group, Inc., P.O. Box 27777, Raleigh, NC, 27611.

45. Mohan, R. and D.F. Adams, "Nonlinear Creep-Recovery Response of a Polymer Matrix and its Composites," *Experimental Mechanics*, Vol. 25, No. 3, Sept. 1985, pp. 262-271.

46. Moore, R.H., "AP1, Acquisition Program One," VPI & SU Data Acquisition Program, July 1987.

47. Morris, D.H., H.F. Brinson, and Y.T. Yeow, "The Viscoelastic Behavior of the Principal Compliance Matrix of a Unidirectional Graphite/Epoxy Composite," *Polymer Composites*, Vol. 1, No. 1, Sept. 1980, pp. 32-36.

48. Ogale, A.A. and R.L. McCullough, "Influence of Microstructure on Elastic and Viscoelastic Properties of Polyether Ether Ketone," *Composite Science and Technology*, Vol. 30, 1987, pp. 185-201.

49. Ophir, Z.H., J.A. Emerson, and G.L. Wilkes, "Sub-T_g Annealing Studies of Rubber-Modified and Unmodified Epoxy Systems," *Journal of Applied Physics*, Vol. 49, No. 10, Oct. 1978, pp. 5032-5038.

50. Osiroff, R., "Damorheology Creep-Fatigue Interaction in Composite Materials," Ph.D Dissertation, Department of Materials Engineering Science, VPI & SU, Blacksburg, VA, June 1990.

51. Owens, G.R., "An Experimental Investigation of the Material Response of Graphite/Polyphenylene Sulfide," M.S. Thesis, Department of Engineering Science and Mechanics, VPI & SU, Blacksburg, VA, 1986.

52. Pindera, M.J. and C.T. Herakovich, "Shear Characterization of Unidirectional Composites with the Off-Axis Tension Test," *Experimental Mechanics*, Vol. 26, No. 1, March 1986, pp. 103-112.

53. Rabinowicz, E., *An Introduction to Experimentation*, Addison-Wesley Publishing Co., Reading, MA, 1970.

54. Schapery, R.A., "An Engineering Theory of Nonlinear Viscoelasticity with Applications," *Int. Journal of Solids and Structures*, Vol. 2, 1966, pp. 407-425.

55. Schapery, R.A., "On the Characterization of Nonlinear Viscoelastic Material," *Polymer Engineering and Science*, Vol. 9, No. 4, July 1969, pp. 295-310.

56. Schapery, R.A., "Stress Analysis of Viscoelastic Composite Materials," *Journal of Composite Materials*, Vol. 1, 1967, pp. 228-267.

57. Schapery, R.A., "Viscoelastic Behavior and Analysis of Composite Materials," *Mechanics of Composite Materials*, G.P. Sendeckyj (Ed.), Chapter 4, Vol. 2, Academic Press, New York, NY, 1974, pp. 85-162.

58. Smith, T.L., "Nonlinear Viscoelastic Response of Amorphous Elastomers to Constant Strain Rates," *Transactions of the Society of Rheology*, VI, 1962, pp. 61-80.

59. Struik, L.C.E., *Physical Aging in Amorphous Polymers and Other Materials*, Elsevier North-Holland Inc., New York, N.Y., 1978

60. Struik, L.C.E., "Mechanical Behavior and Physical Ageing of Semi-Crystalline Polymers: 3. Prediction of Long Term Creep from Short Time Tests," *Polymer*, Vol. 30, No. 5, May 1989, pp. 799-814.

61. Struik, L.C.E., "Mechanical Behavior and Physical Ageing of Semi-Crystalline Polymers: 4," *Polymer*, Vol. 30, No. 5, May 1989, pp. 815-830.

62. Struik, L.C.E., "Physical Aging in Plastics and Other Glassy Materials," *Polymer Engineering and Science*, Vol. 17, No. 3, March 1977, pp. 165-173.

63. Struik, L.C.E., "Physical Aging: Influence on the Deformation Behavior of Amorphous Polymers," *Failure of Plastics*, W. Brostow and R.D. Corneliussen (Eds), Hanser Publishers, New York, NY, 1986, pp. 209-234.

64. Struik, L.C.E., "The Mechanical and Physical Ageing of Semicrystalline Polymers: 1," *Polymer*, Vol. 28, August 1987, pp. 1521-1533.

65. Struik, L.C.E., "The Mechanical behavior and Physical Ageing of Semicrystalline Polymers : 2," *Polymer*, Vol. 28, August 1987, pp. 1534-1542.

66. Sullivan, J.L., "Creep and Physical Aging of Composites," *Composite Science and Technology*, Vol. 39, 1990, pp. 207-232.

67. Tant, M.R. and G.L. Wilkes, "An Overview of the Non-equilibrium Behavior of Polymer Glasses," *Polymer Engineering and Science*, Vol. 21, No. 14, Mid-October, 1981, pp. 874-895.

68. Tuttle, M.E. and H.F. Brinson, "Accelerated Viscoelastic Characterization of T300/5208 Graphite/Epoxy Laminates," Virginia Polytechnic Institute and State University, VPI-E-84-9, Blacksburg, VA, March 1984.

69. Tuttle, M.E. and H.F. Brinson, "Resistance-foil Strain-gage Technology as Applied to Composite Materials," *Experimental Mechanics*, Vol. 24, No. 1, March 1984, pp. 54-65.

70. Vleeshouwers, S., A.M. Jamieson, and R. Simha, "Effect of Physical Aging on Tensile Stress Relaxation and Tensile Creep of Cured EPON 828/Epoxy Adhesives in the Linear Viscoelastic Region," *Polymer Engineering and Science*, Vol. 29, No. 10, May 1989, pp. 662-670.

71. Wang, S.F. and A.A. Ogale, "Influence of Aging on Transient and Dynamic Mechanical Properties of Carbon Fiber/Epoxy Composites," *Sampe Quarterly*, Vol. 20, No. 2, January 1989, pp. 9-13.

72. Williams, M.L., R.F. Landel, and J.D. Ferry, "The Temperature Dependence of Relaxation Mechanisms in Amorphous Polymers and Other Glass-forming Liquids," *Journal of the American Chemical Society*, Vol. 77, No. 14, July 20, 1955, pp. 3701-3707.

73. Yen, S.C., "The Creep and Creep Rupture of SMC-R50 Under Different Thermomechanical Conditions," Ph.D Dissertation, Department of Engineering Science and Mechanics, VPI & SU, Blacksburg, VA, March 1984.

74. Yeow, Y.T., D.H. Morris, and H.F. Brinson, "Time-Temperature Behavior of a Unidirectional Graphite/Epoxy Composite," *Composite Materials: Testing and Design (Fifth Conference)*, ASTM STP 674, S.W. Tsai, Ed., American Society for Testing and Materials, 1979, pp. 263-281.

75. Zallen,R., *The Physics of Amorphous Solids*, John Wiley & Sons, New York, NY, 1983.

TABLES

Table 4.1 Comparison of Commercial Data of Radel X/T650-42 and Radel X/IM7 Composite Materials.

Property	Radel X/T650-42[a] (62% fiber volume)	Radel X/IM7 (test data)
Tensile Strength 90^0	6.91 Ksi (47.6 MPa)	4.46 Ksi (30.8 MPa)
Tensile Modulus 90^0	1.17 Msi (8.07 GPa)	1.07 Msi (7.38 GPa)
Tensile Strength 0^0	330 Ksi (2275 MPa)	261 Ksi (1800 MPa)
Tensile Modulus 0^0	23.7 Msi (163.4 GPa)	23.1 Msi (159.3 GPa)

[a] Amoco Performance Products

Table 4.2 Comparison of Commercial T650-42 and IM7 Fiber Properties.

Property	T650-42[a] Fiber	IM7[b] Fiber
Tensile Strength	730 Ksi (5037 MPa)	683 Ksi (4713 MPa)
Tensile Modulus	42 Msi (290 GPa)	41 Msi (283 GPa)
Density	0.064 lb/in^3 (1.78 g/cm^3)	0.064 lb/in^3 (1.78 g/cm^3)
Ultimate Elongation	1.7%	1.6%

[a] Thornel, Advance Composite Systems

[b] Hercules, Graphite Materials & Composite Structures Marketing

Table 4.3 Shift Factors Required for S_{22} Master Momentary Compliance Curves Referenced to t_e = 81 hours.

Temperature	t_e (hour)	−log a	log B
399°F (204°C)	1	-0.7914	0.0168
	3	-0.5713	0.0095
	9	-0.3584	-0.0016
	27	-0.1306	-0.0106
	81	0.0000	0.0000
392°F (200°C)	1	-0.9535	-0.0015
	3	-0.6805	0.0000
	9	-0.4183	0.0009
	27	-0.1968	0.0024
	81	0.0000	0.0000
383°F (195°C)	1	-1.2458	-0.0124
	3	-0.9400	-0.0090
	9	-0.6105	-0.0067
	27	-0.3043	-0.0066
	81	0.0000	0.0000
365°F (185°C)	1	-1.5795	-0.0071
	3	-1.1668	-0.0065
	9	-0.8030	-0.0051
	27	-0.3647	-0.0036
	81	0.0000	0.0000
338°F (170°C)	1	-1.4950	-0.0142
	3	-0.9979	-0.0121
	9	-0.7098	-0.0074
	27	-0.3158	-0.0037
	81	0.0000	0.0000

Table 4.4 Shift Factors Required for S_{66} Master Momentary Compliance Curves Referenced to t_e = 81 hours.

Temperature	t_e (hour)	−loga	logB
383°F (195°C)	1	-1.4755	-0.0041
	3	-1.0519	-0.0119
	9	-0.6838	-0.0083
	27	-0.2987	-0.0038
	81	0.0000	0.0000
365°F (185°C)	1	-1.6068	-0.0243
	3	-1.1803	-0.0200
	9	-0.7435	-0.0181
	27	-0.3220	-0.0129
	81	0.0000	0.0000
338°F (170°C)	1	-1.7643	0.0021
	3	-1.2829	-0.0052
	9	-0.8979	-0.0021
	27	-0.4168	0.0013
	81	0.0000	0.0000

FIGURES

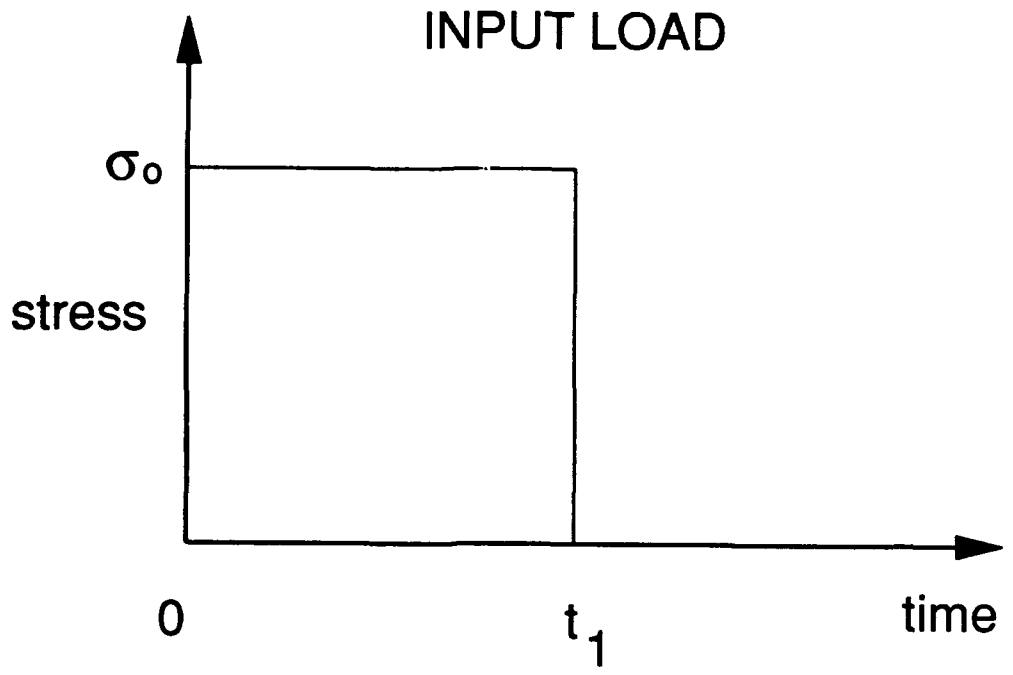

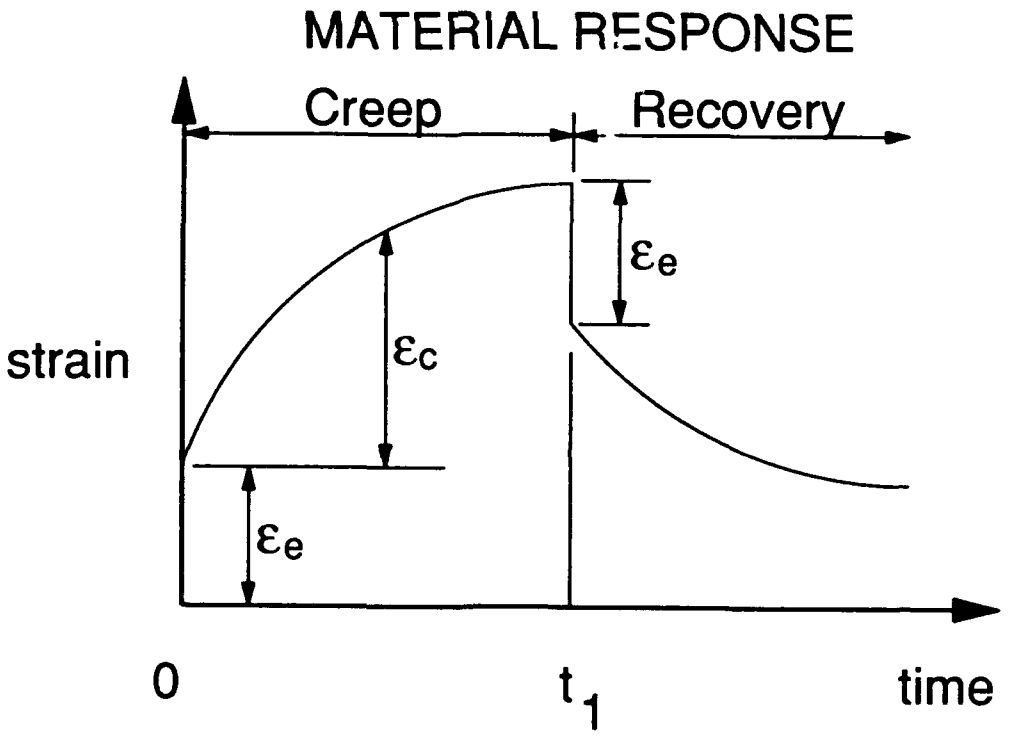

Figure 2.1 Stress and Strain Response for a Creep/Recovery Test.

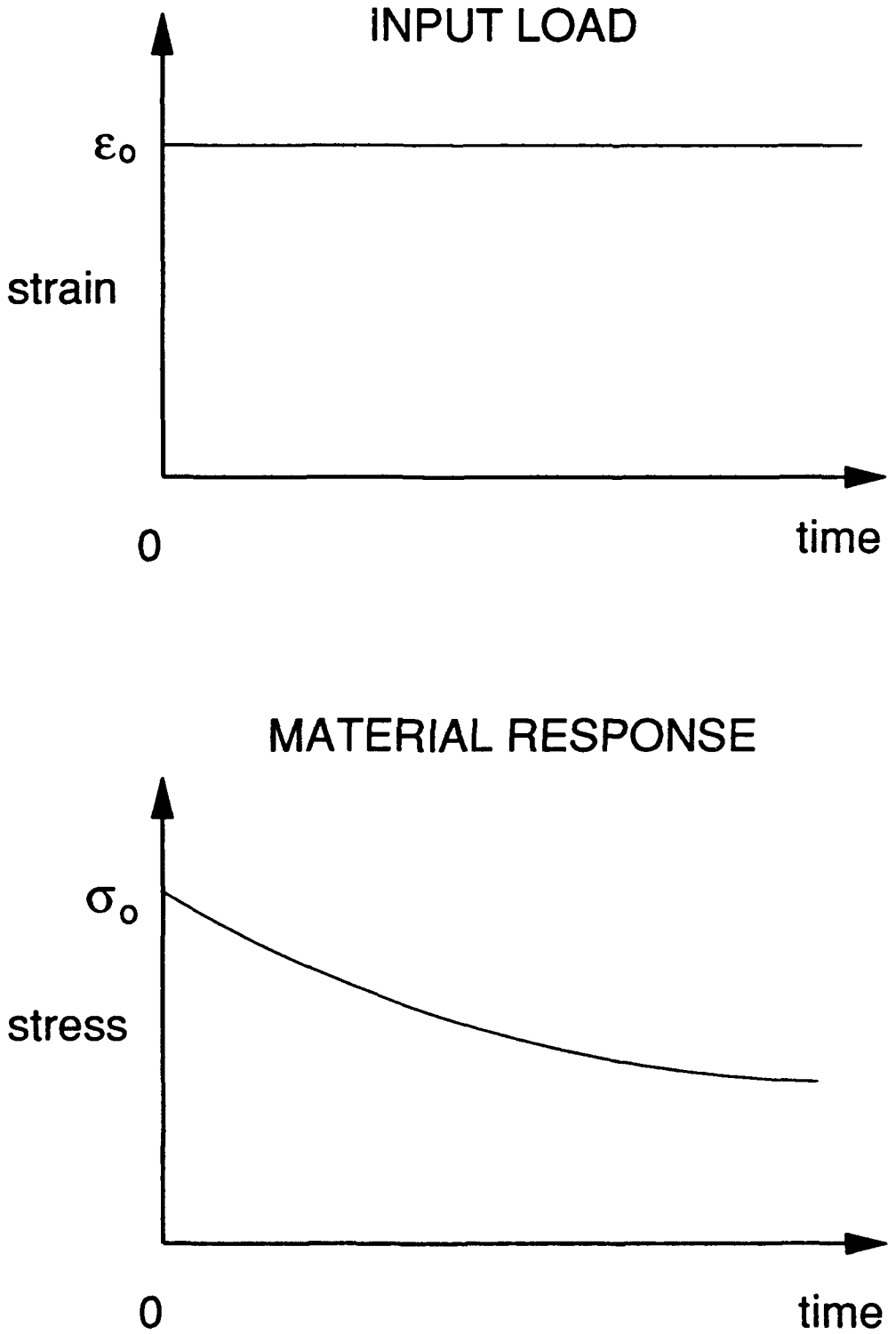

Figure 2.2 Stress and Strain Response for a Stress Relaxation Test.

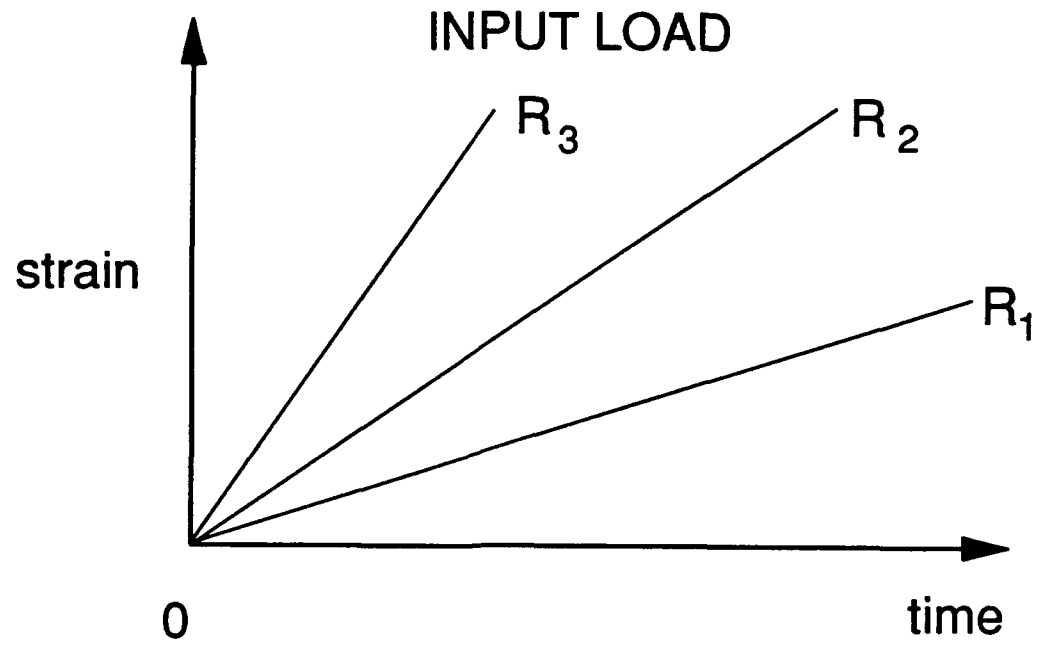

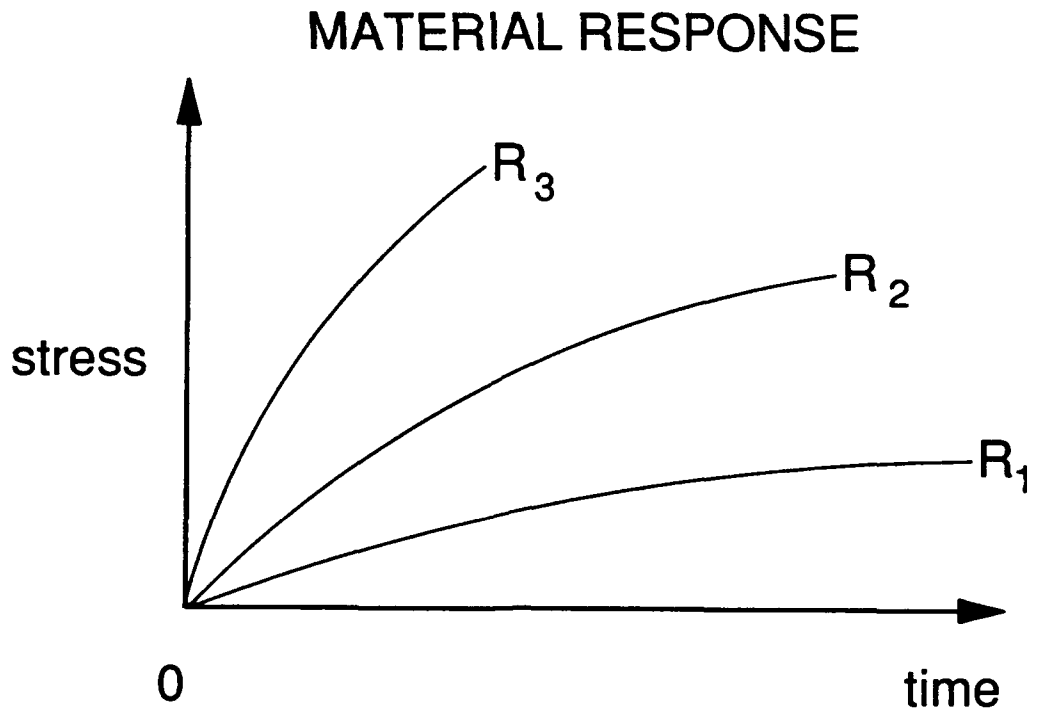

Figure 2.3 Stress and Strain Response for a Constant Strain Rate Test.

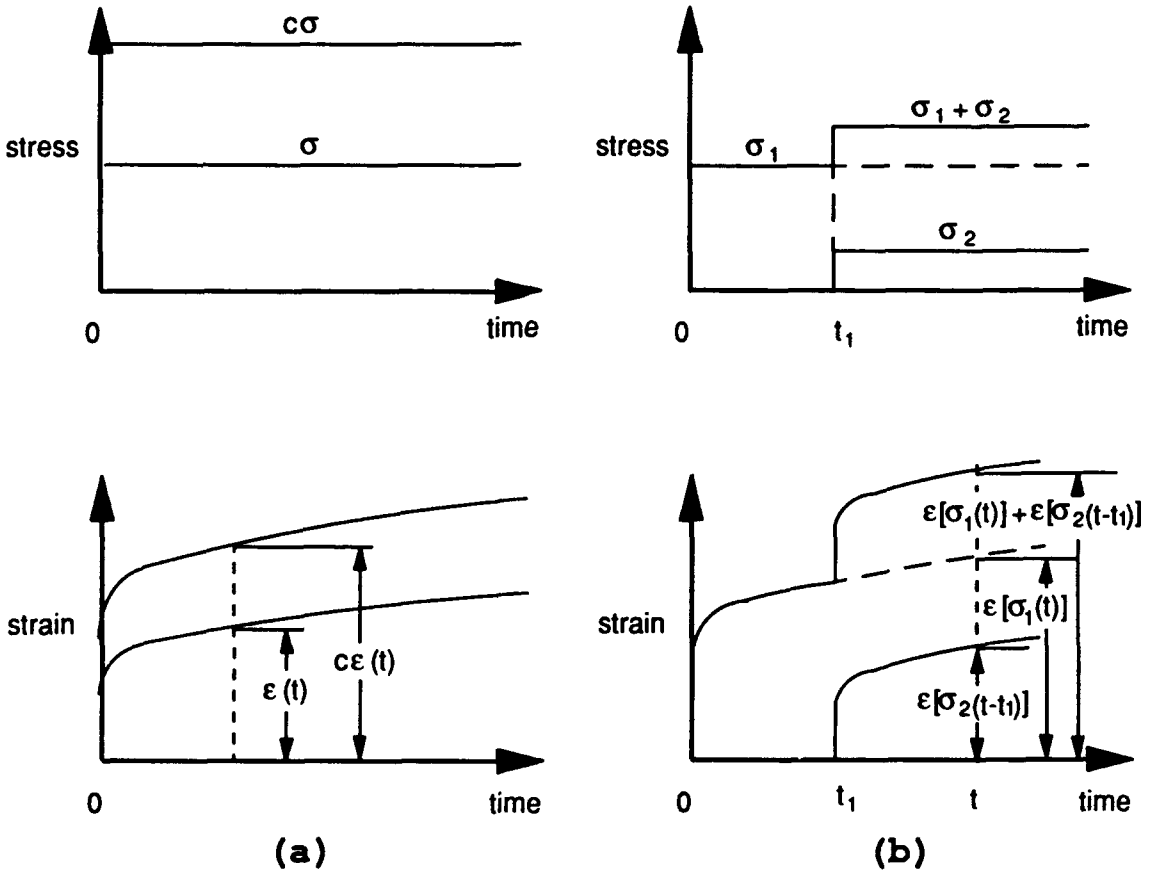

Figure 2.4 Graphical Representation of the Requirements for a Linear Viscoelastic Material.

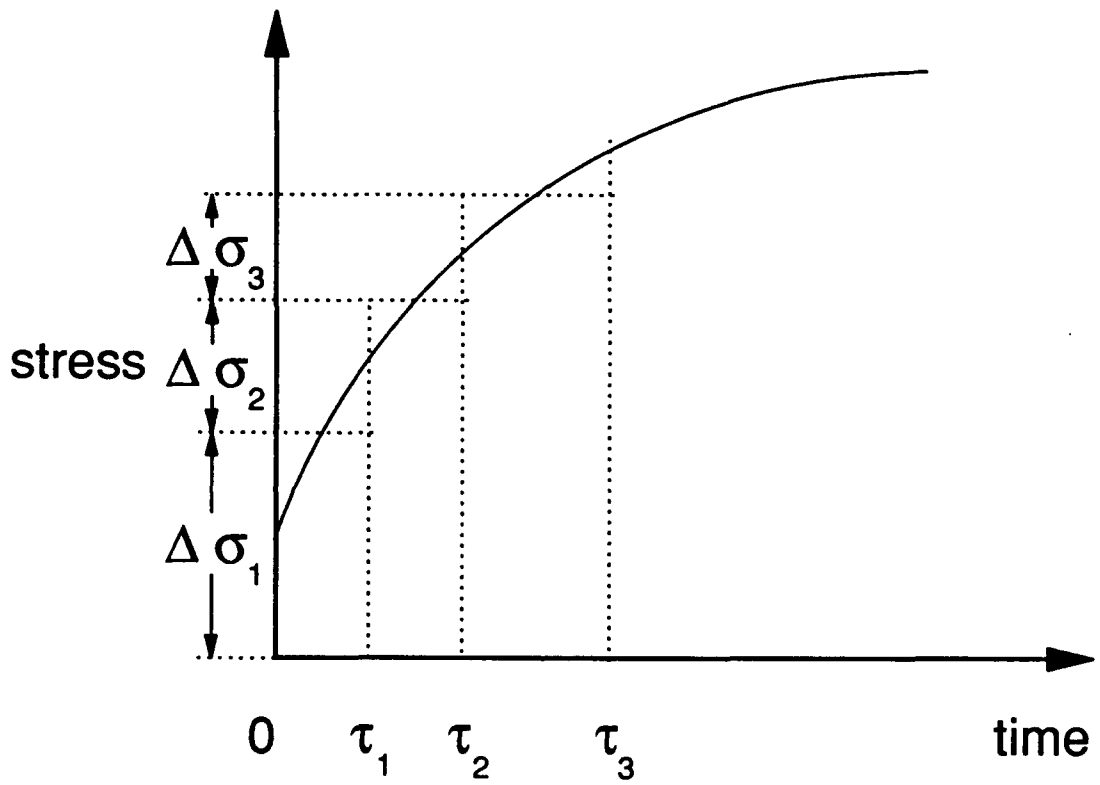

Figure 2.5 Stress History Approximation Using a Series of Step Stress Inputs.

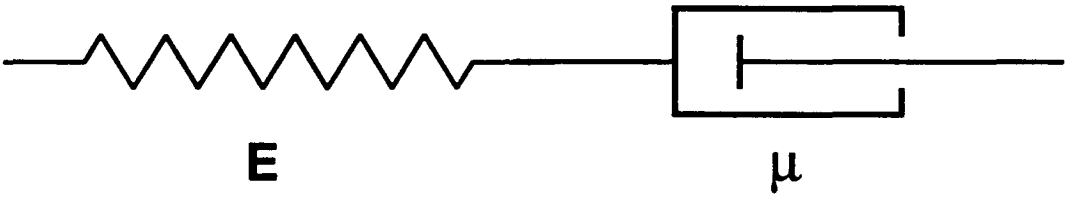

Maxwell Model

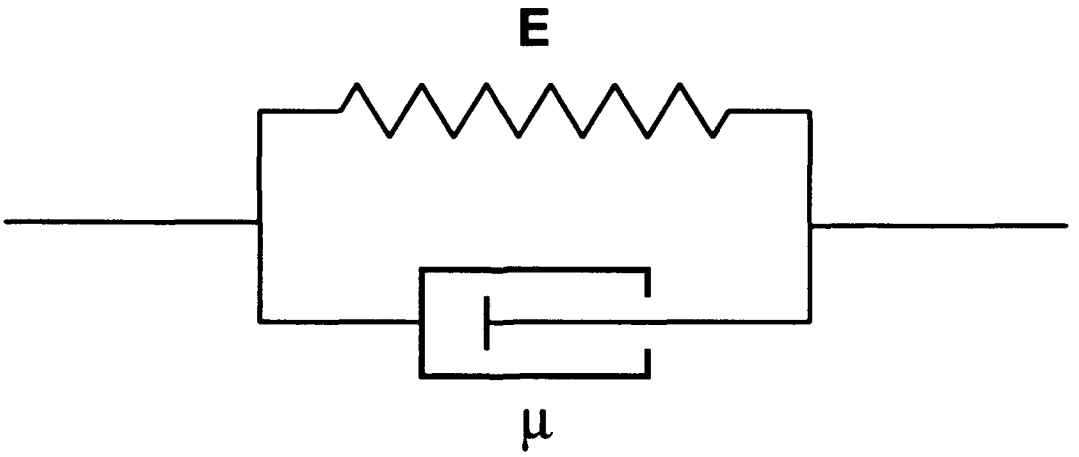

Kelvin Model

Figure 2.6 Representation of Maxwell and Kelvin Mechanical Analog Models.

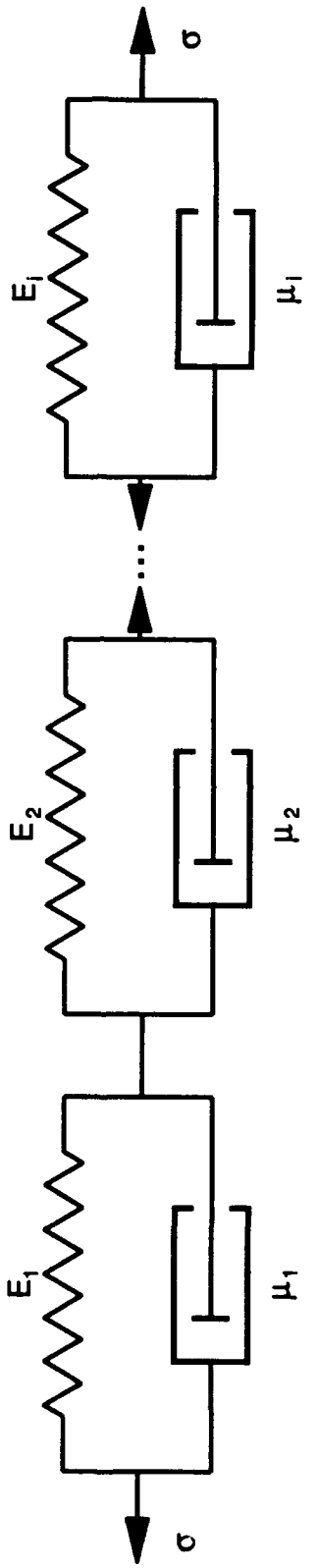

Figure 2.7 Representation of Generalized Kelvin Model.

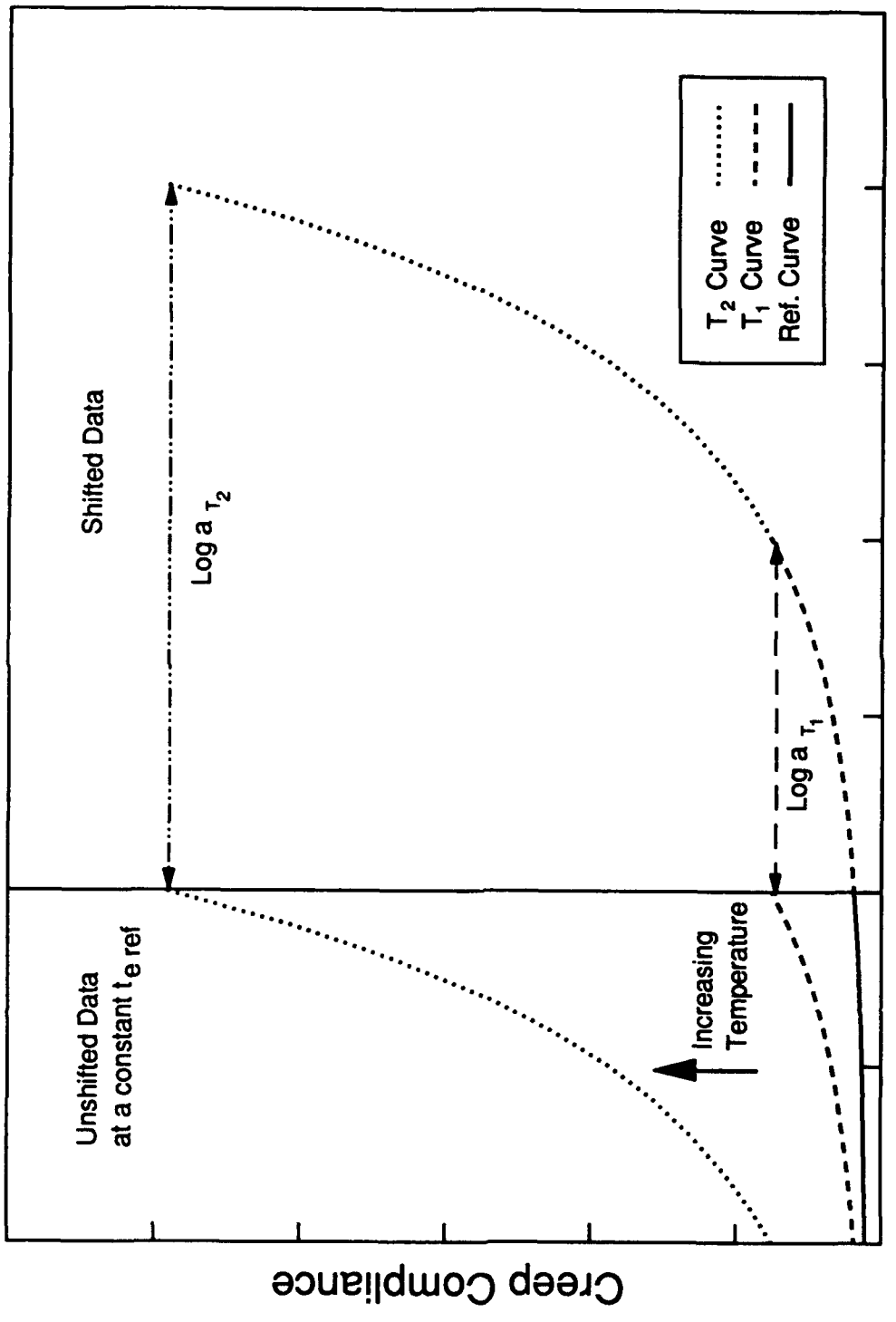

Figure 2.8 Time-Temperature Superposition Principle Illustration.

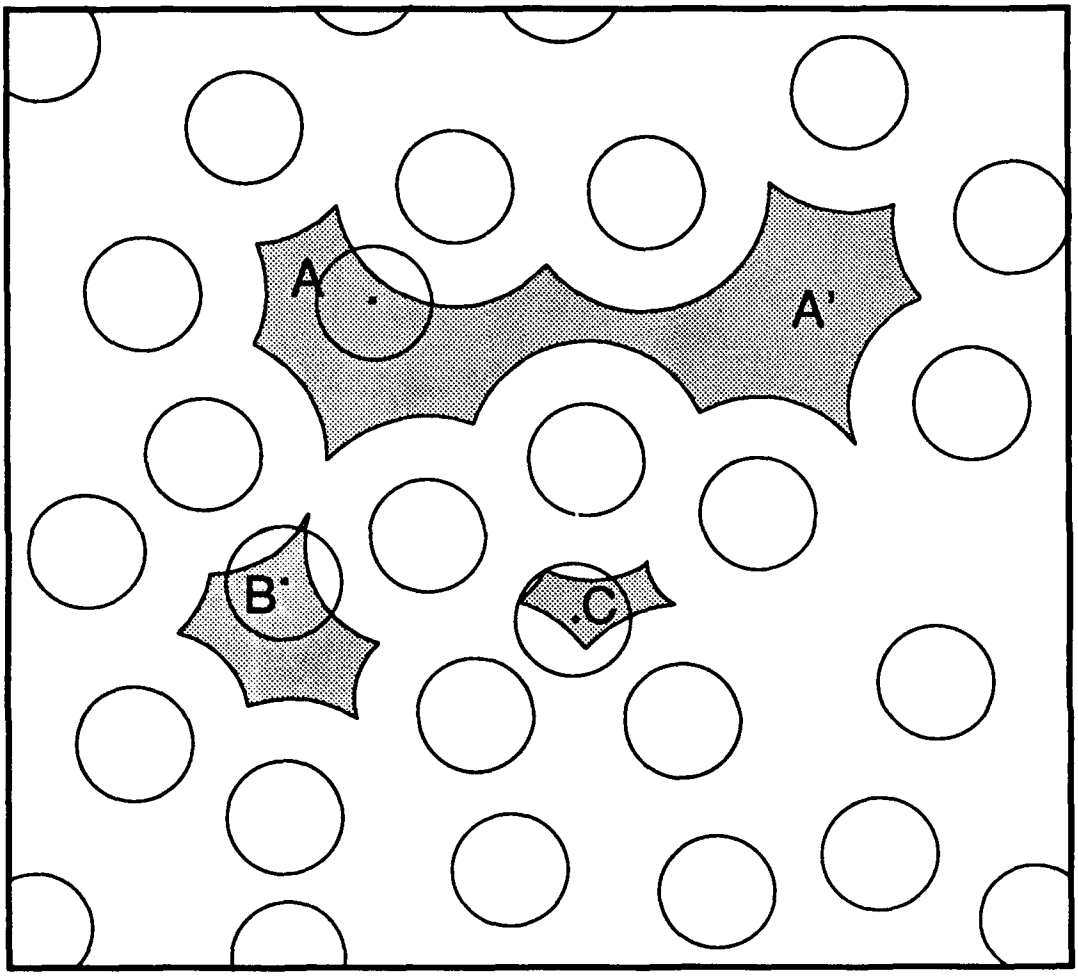

Figure 2.9 Visualization of Two-Dimensional Hard-Sphere Model of Free Volume [75].

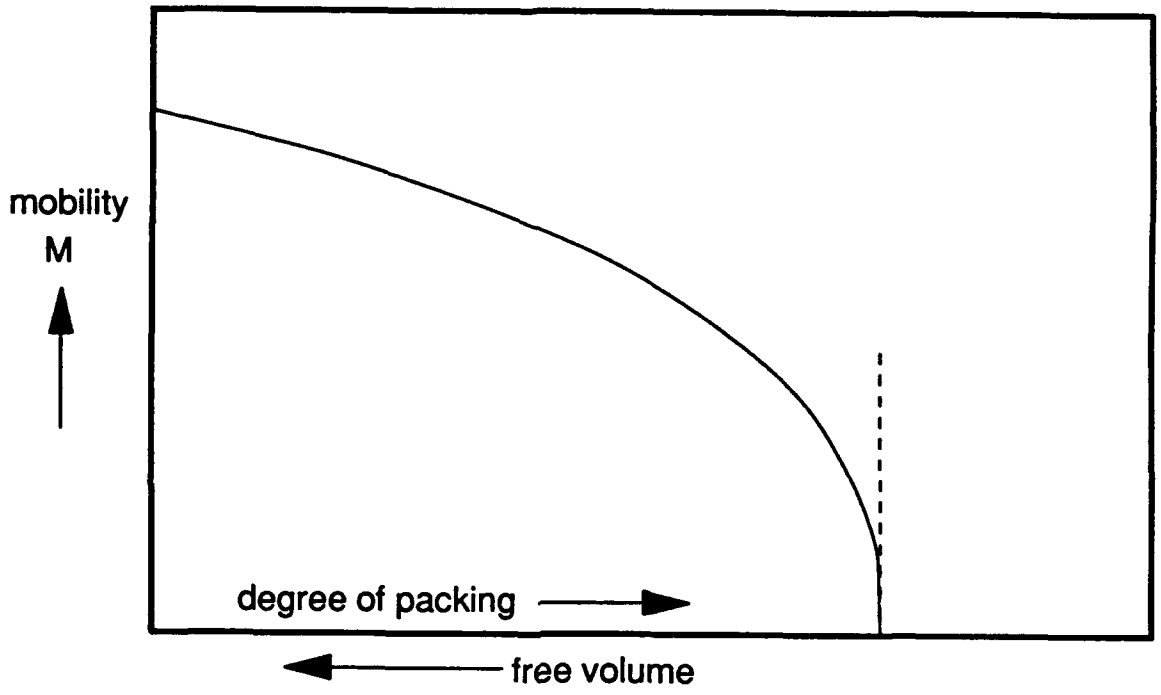

Figure 2.10 Illustration of the Qualitative Free Volume Concept [41].

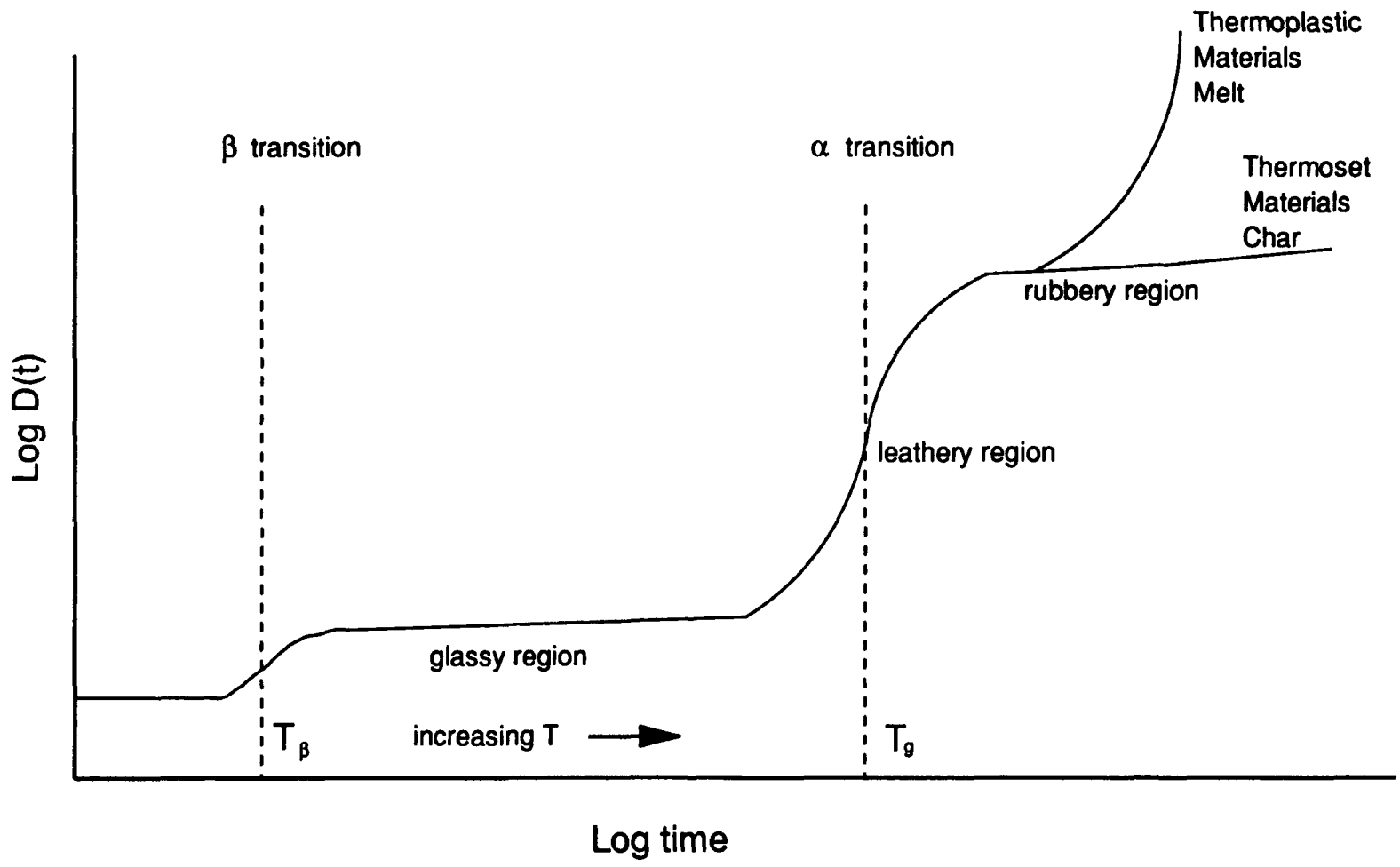

Figure 2.11 Typical Compliance Response of Thermoplastic and Thermoset Materials.

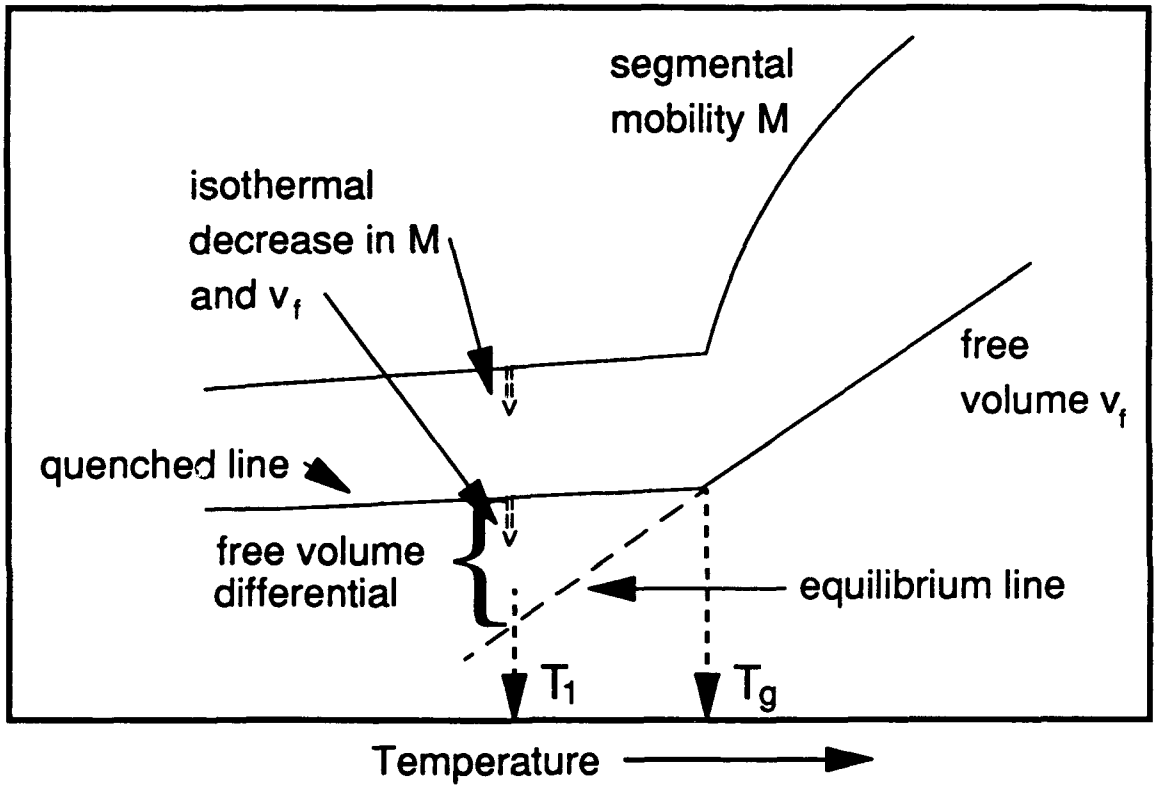

Figure 2.12 The Origin of Aging Explained from Free Volume Concepts [59].

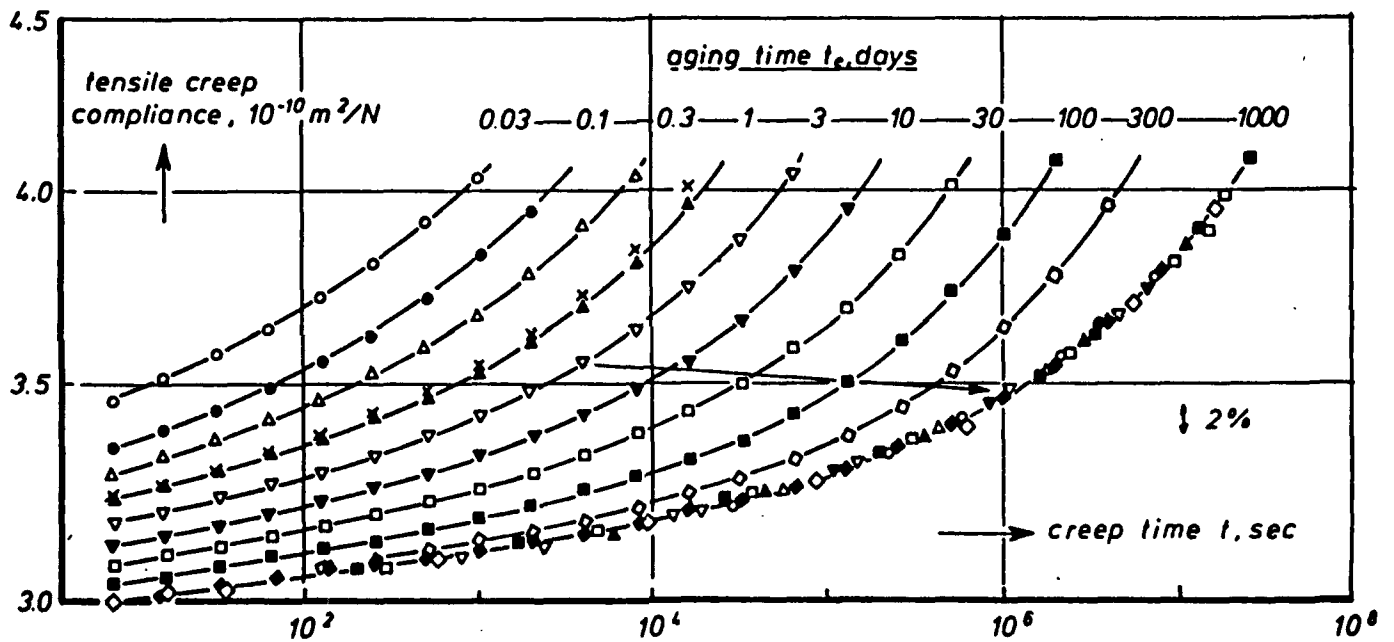

Figure 2.13 Tensile Creep Compliance Curves for PVC Quenched from 90 to 20 °C [59].

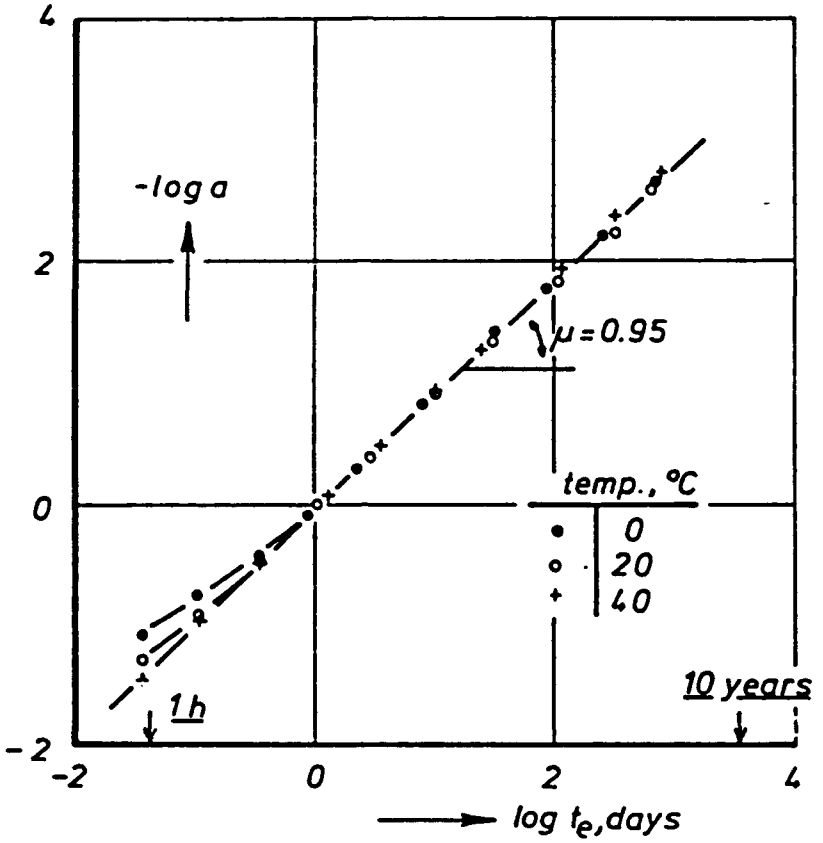

NOTE: Log a is the shift relative to the creep curve measured at a t_e of 1 day.

Figure 2.14 Calculation of μ from the Shifting of the Creep Curves of Rigid PVC Quenched from 90 °C to 0, 20, and 40 °C [59].

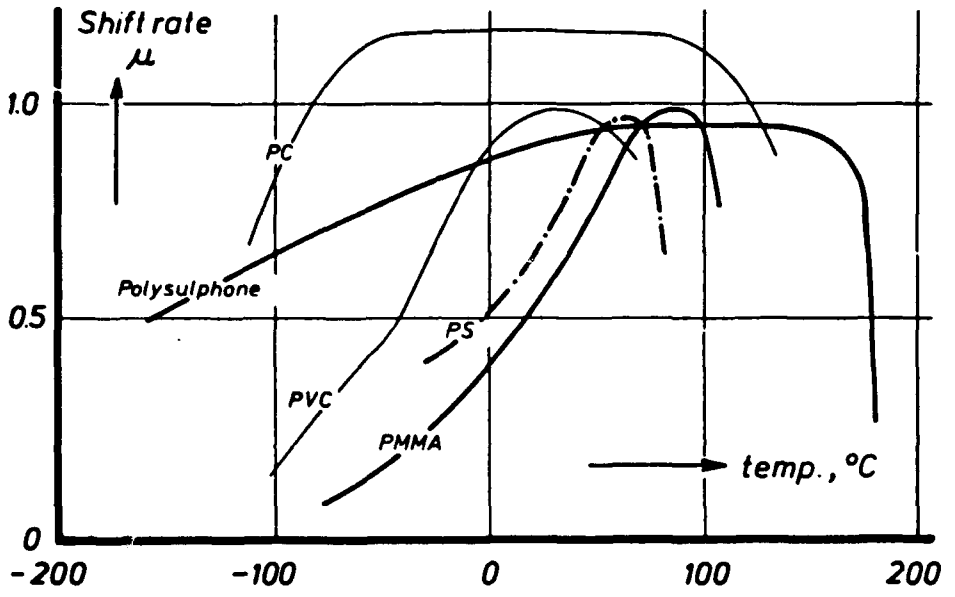

Figure 2.15 The Aging Shift Rate, μ , vs. Temperature for Various Polymers [59].

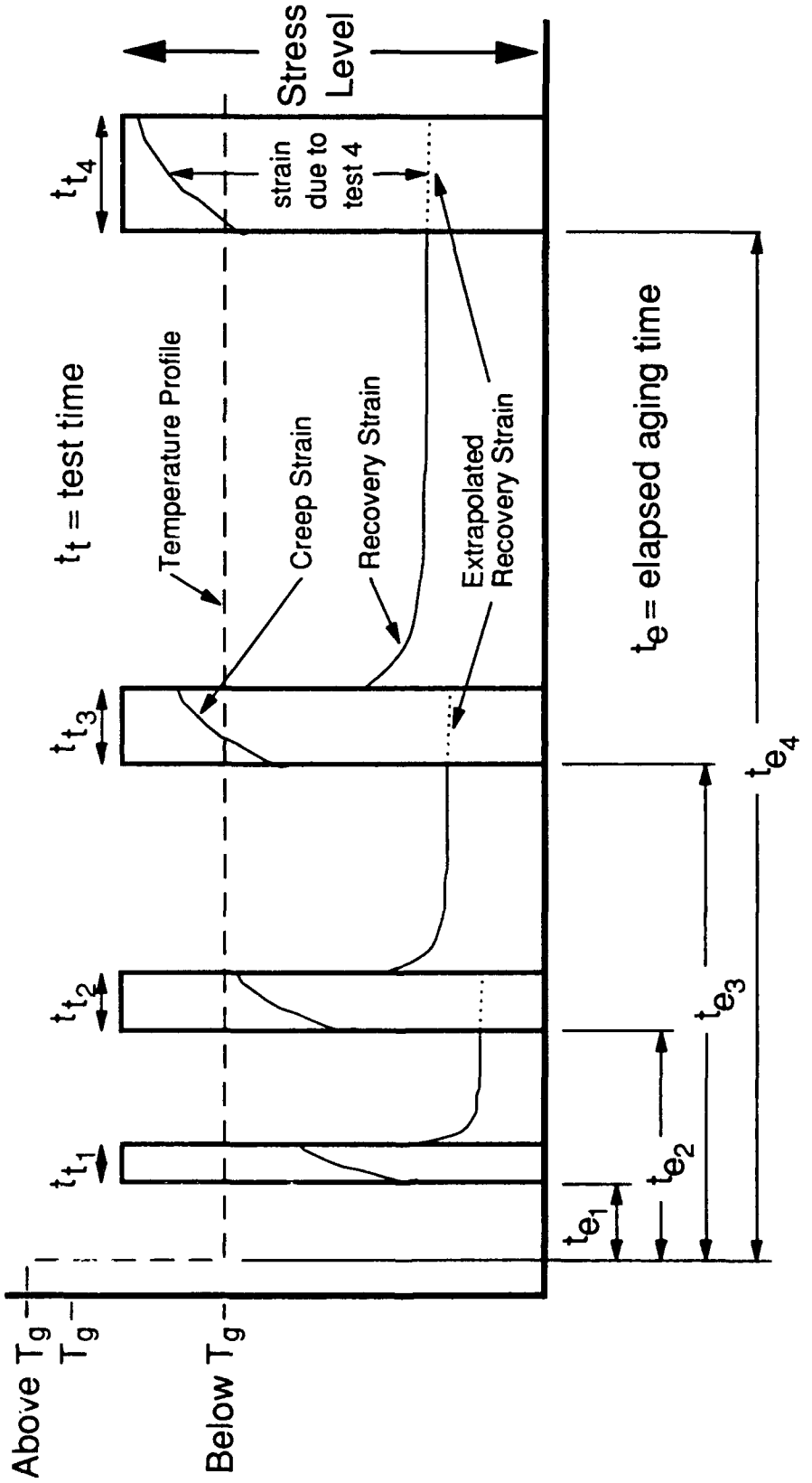

Figure 2.16 Illustration of the Sequence of Creep and Recovery Tests for Determining Aging Effects [59].

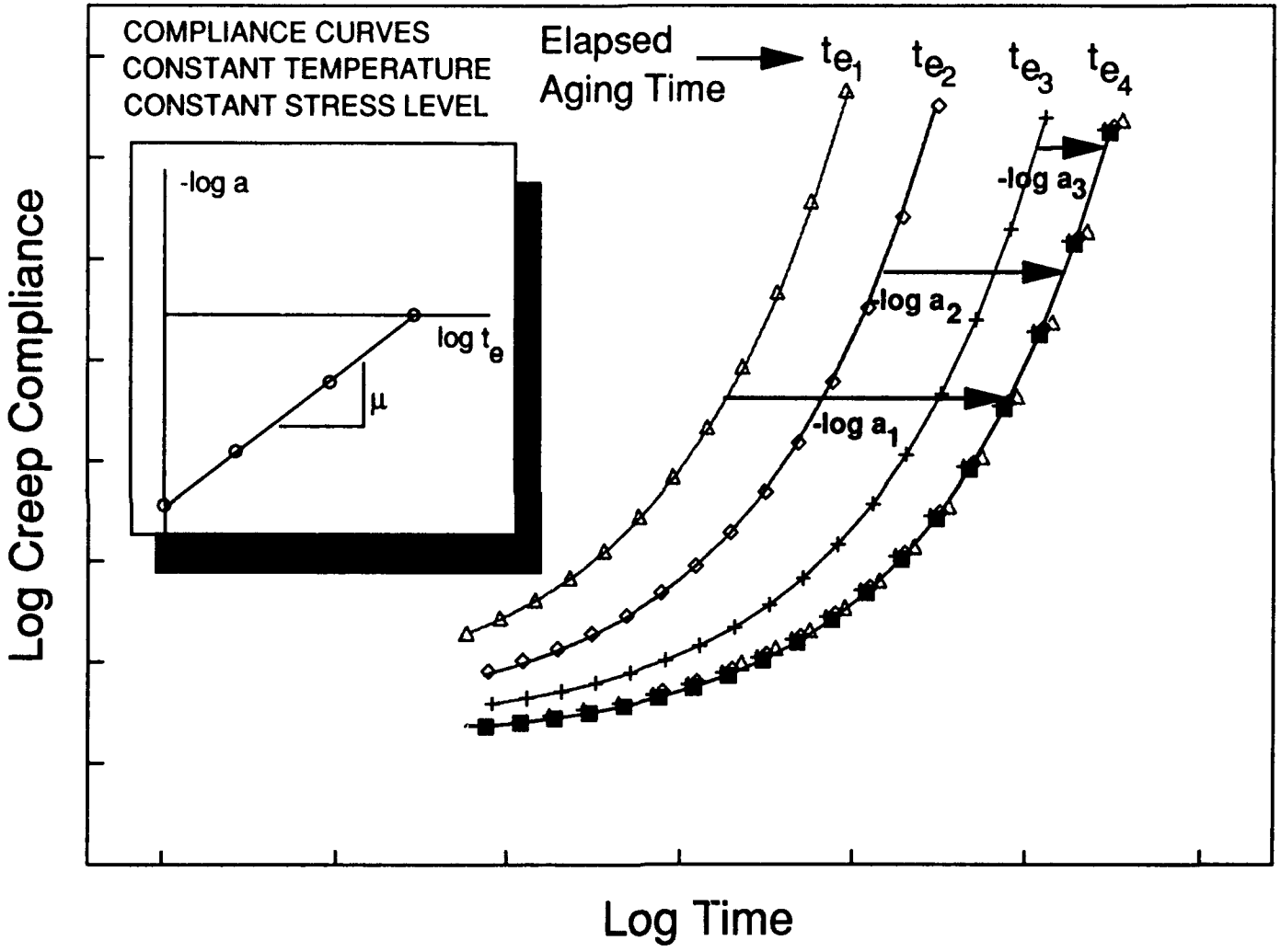

Figure 2.17 Illustration of Aging Shift Rate Determination by Shifting Momentary Creep Compliance Curves.

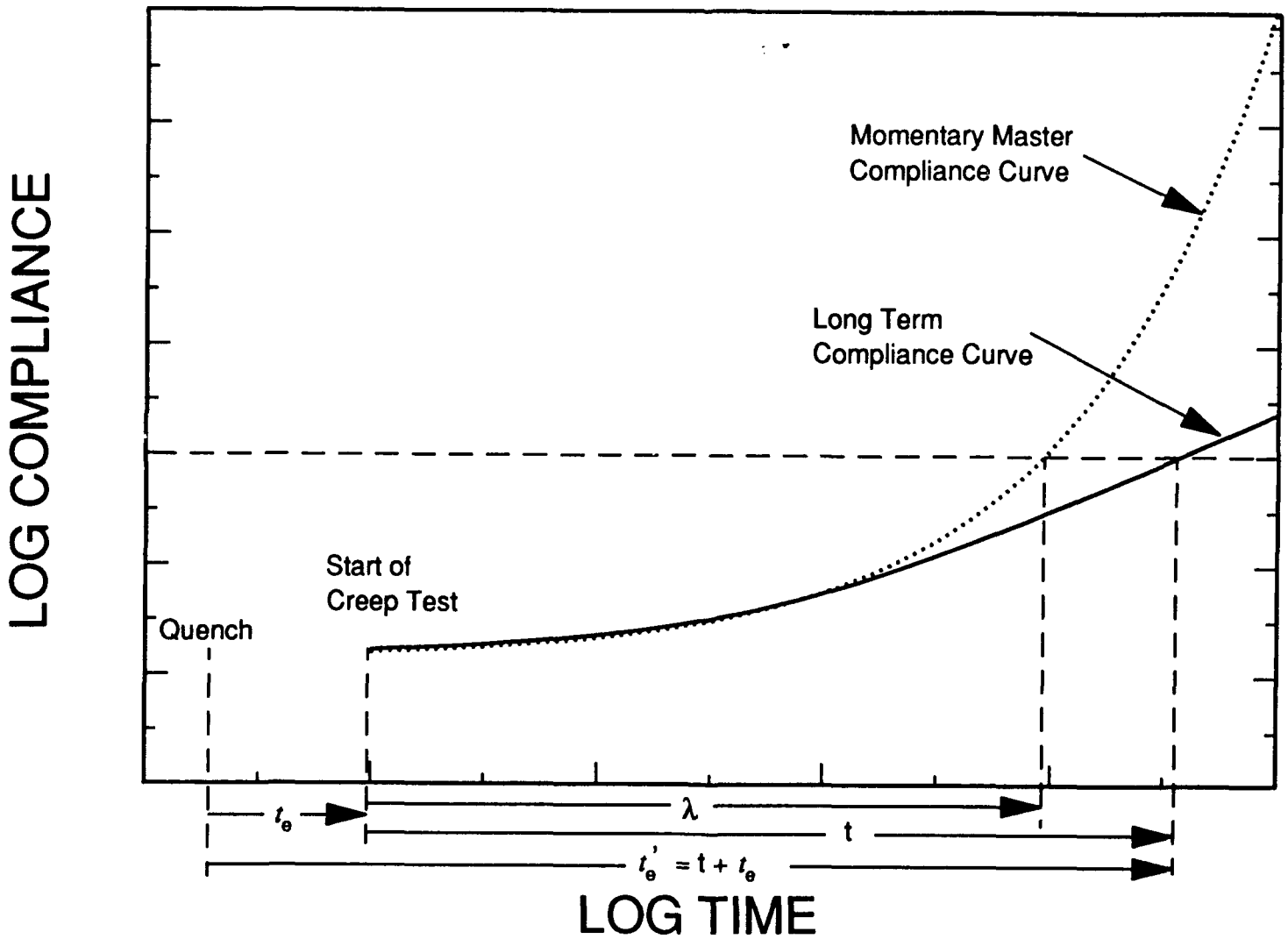

Figure 2.18 Illustration of Effective Time Variables.

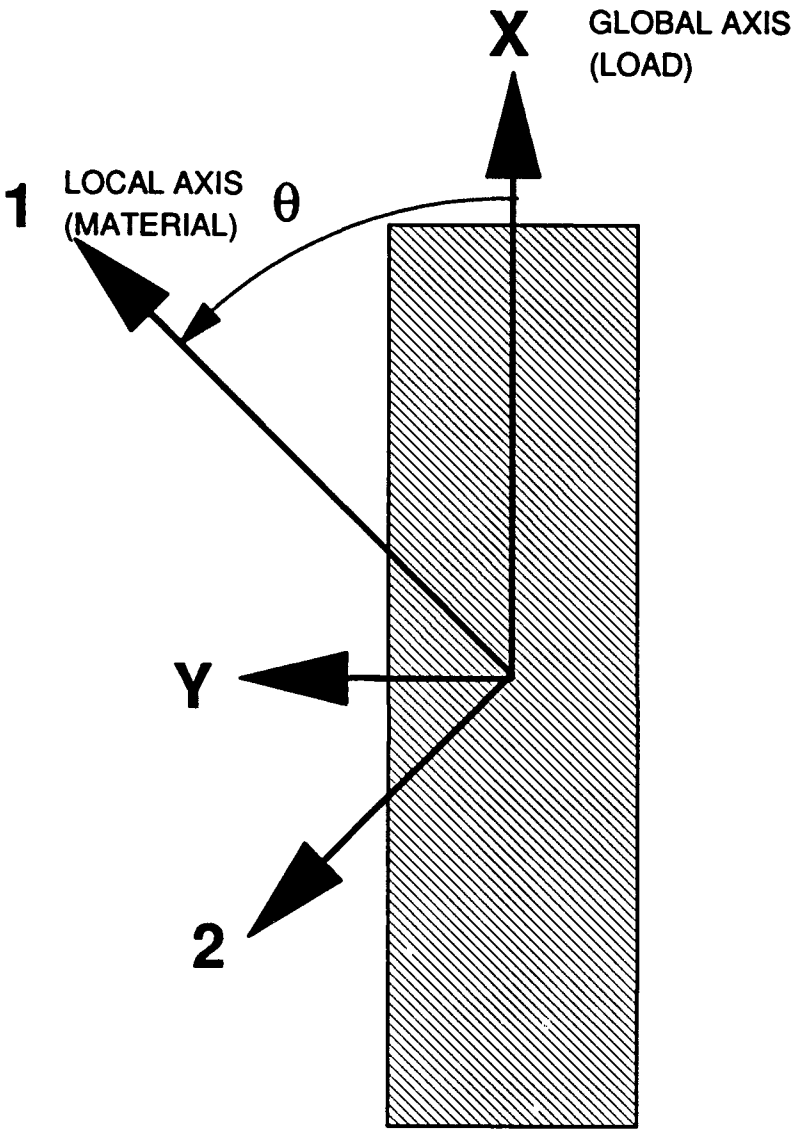

Figure 2.19 Coordinate Systems Used to Define Material Properties.

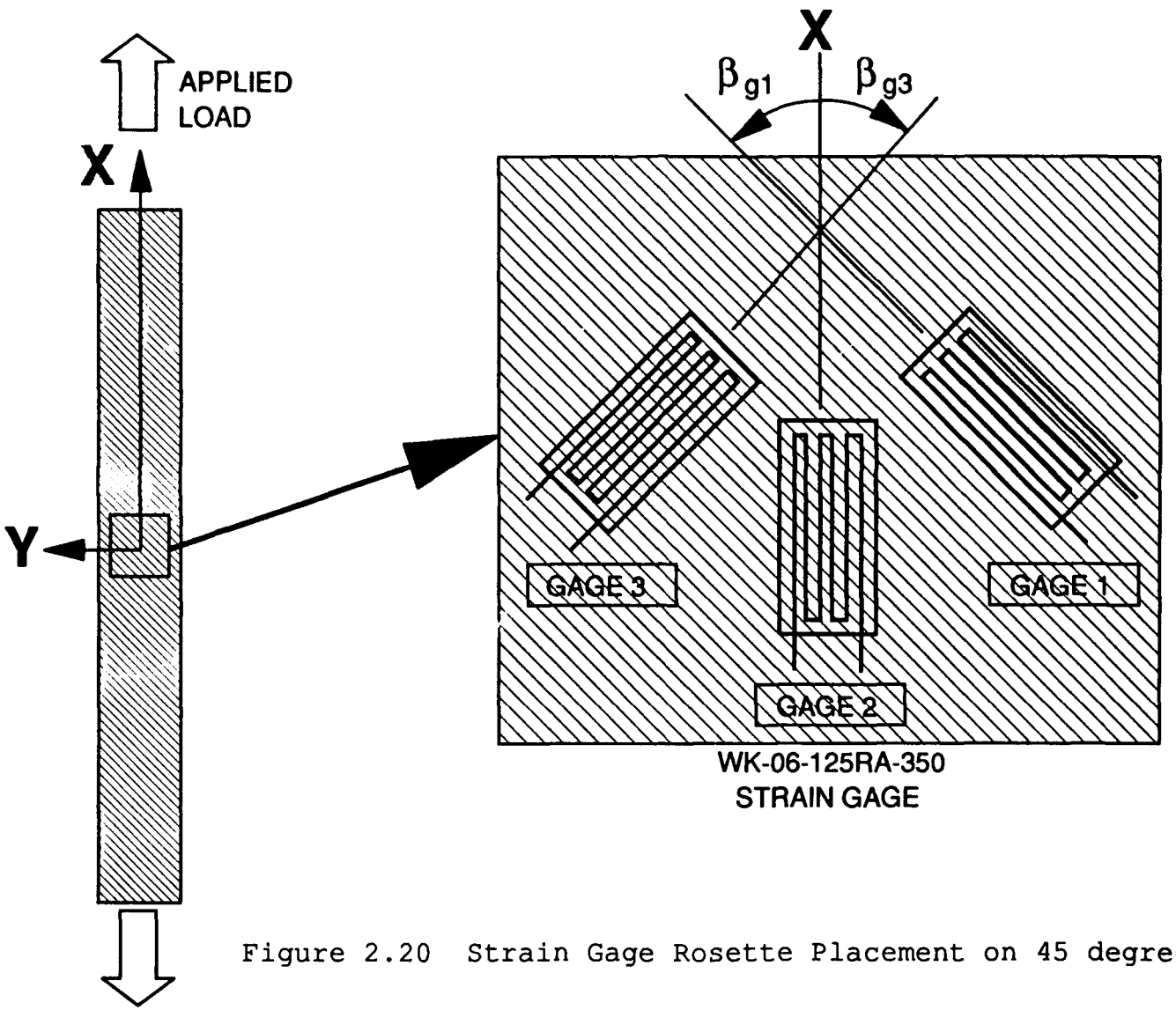

Figure 2.20 Strain Gage Rosette Placement on 45 degree Specimen.

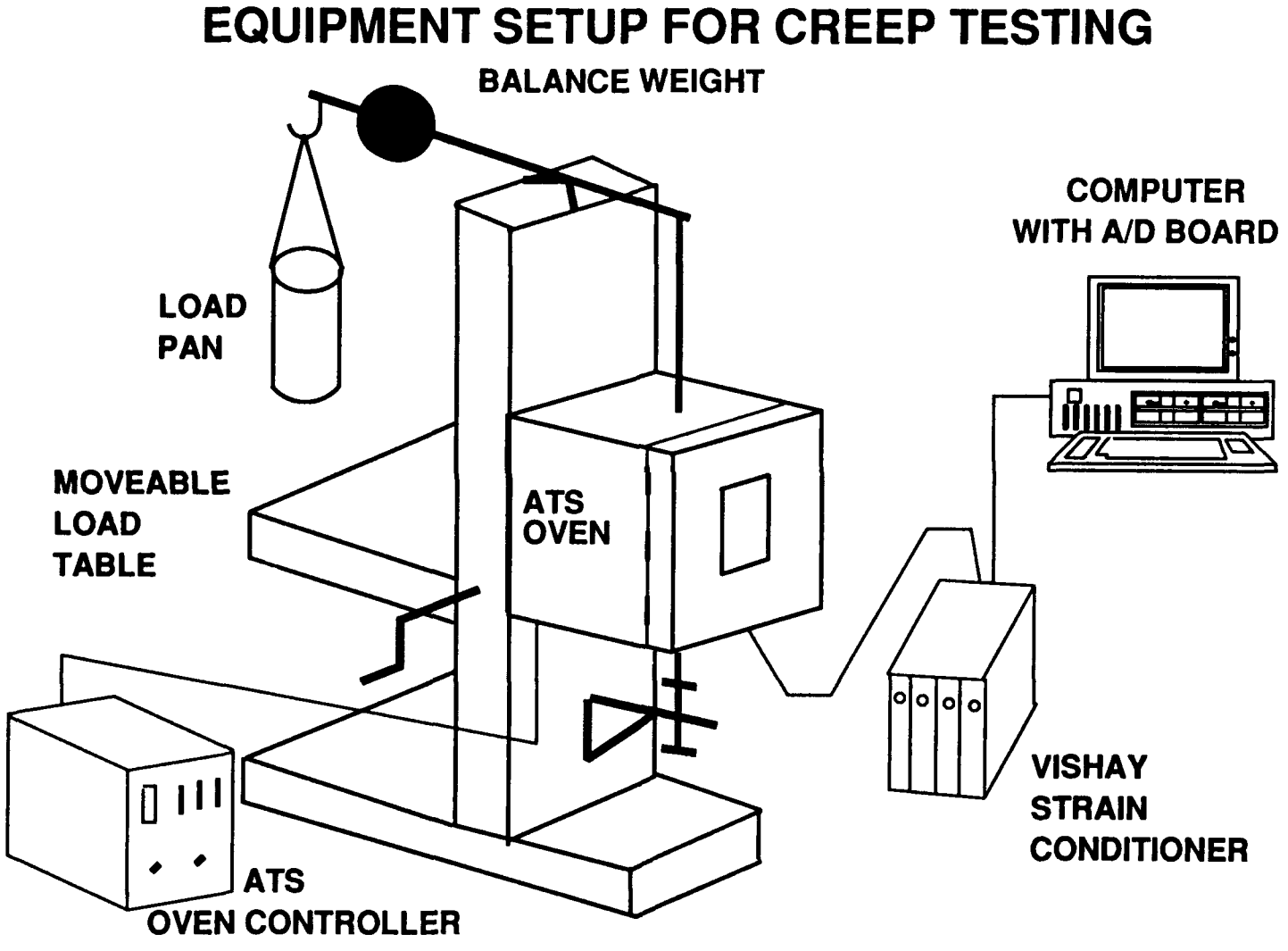

Figure 3.1 Illustration of Equipment Used for Creep Testing.

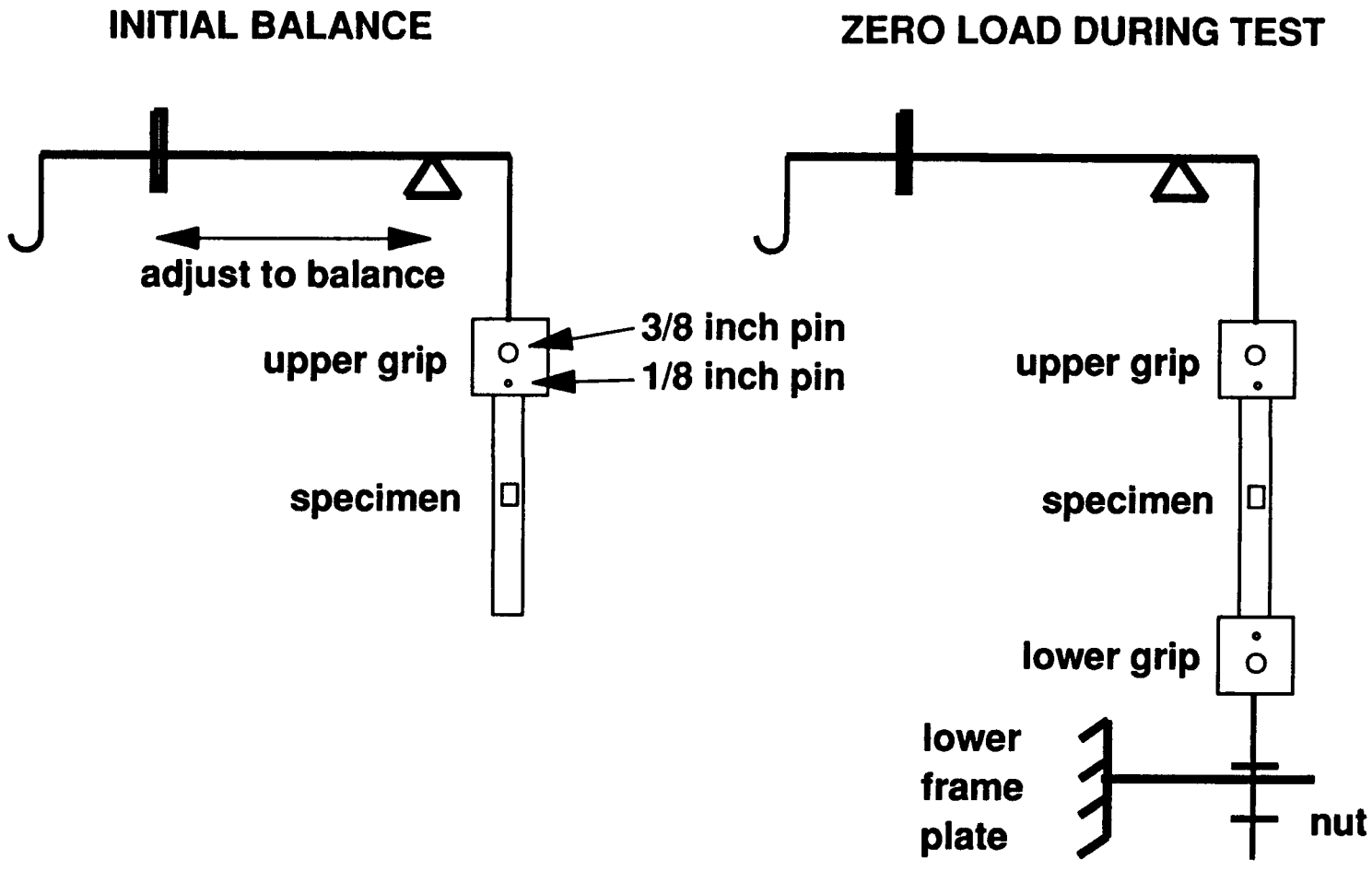

Figure 3.2 Illustration of Specimen Attachment to Load Frame.

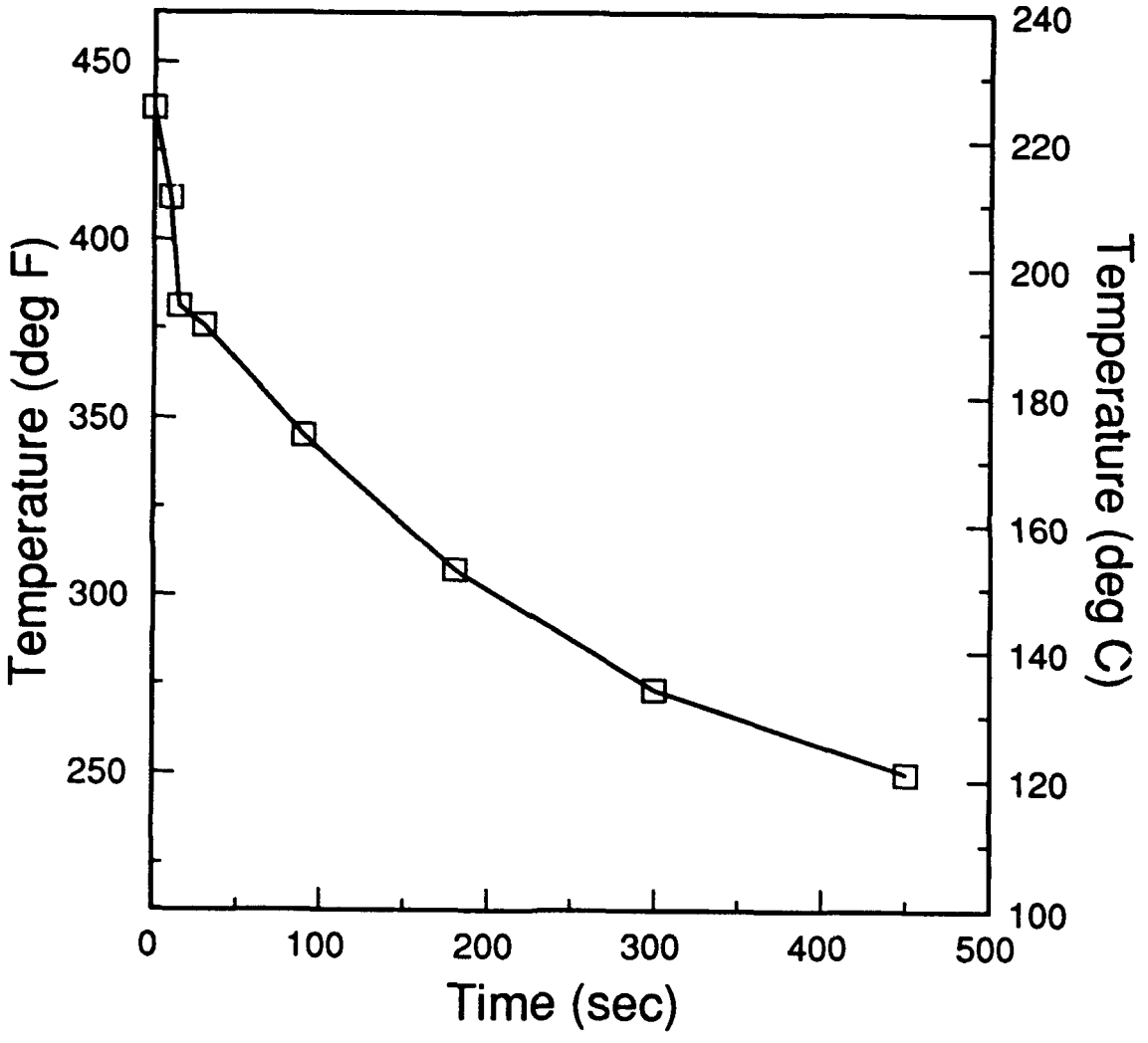

Figure 3.2 Stabilization Temperature vs. Quench Time.

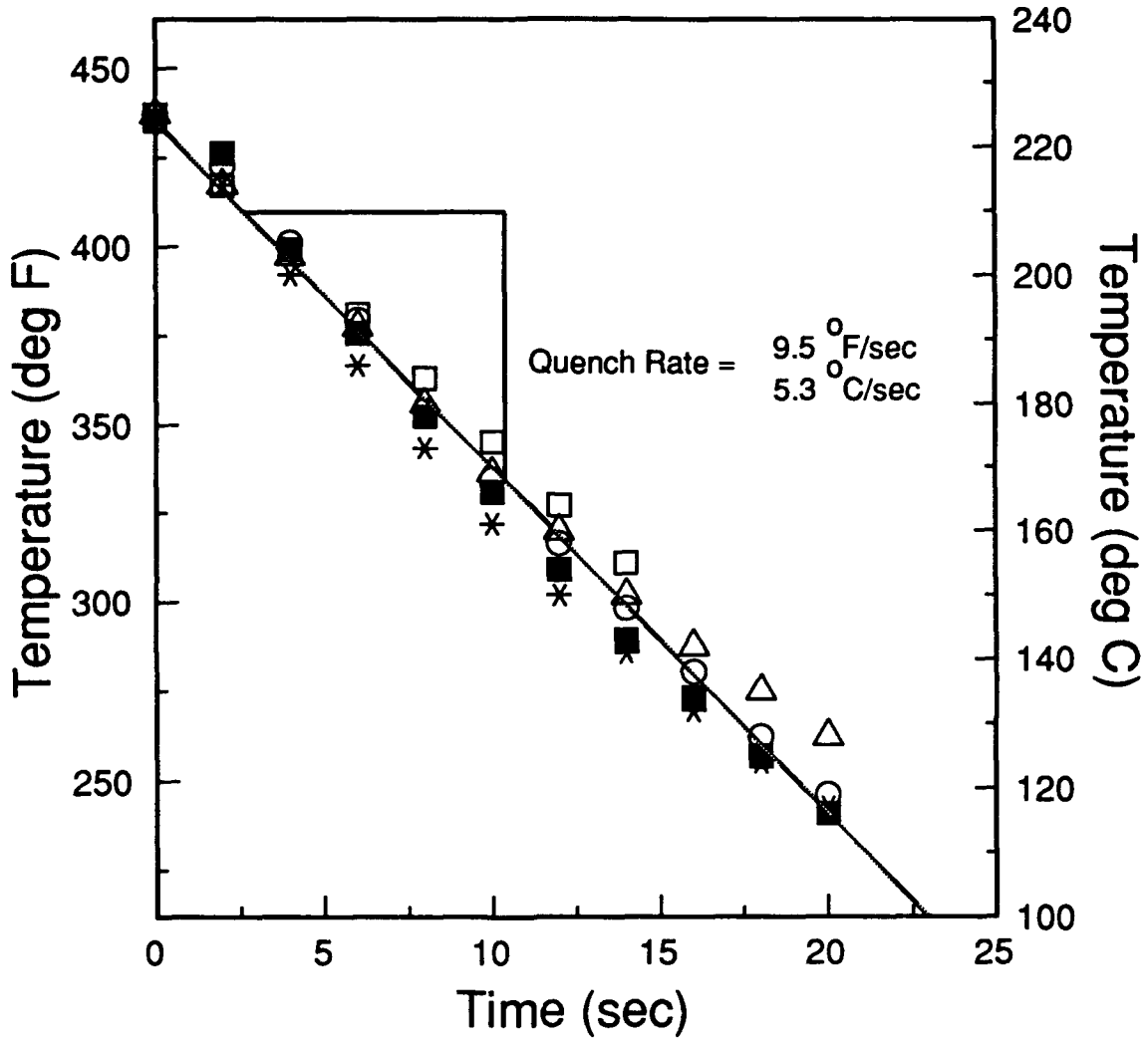

Figure 3.4 Specimen Temperature vs. Time Data Used for Quench Rate Calculation.

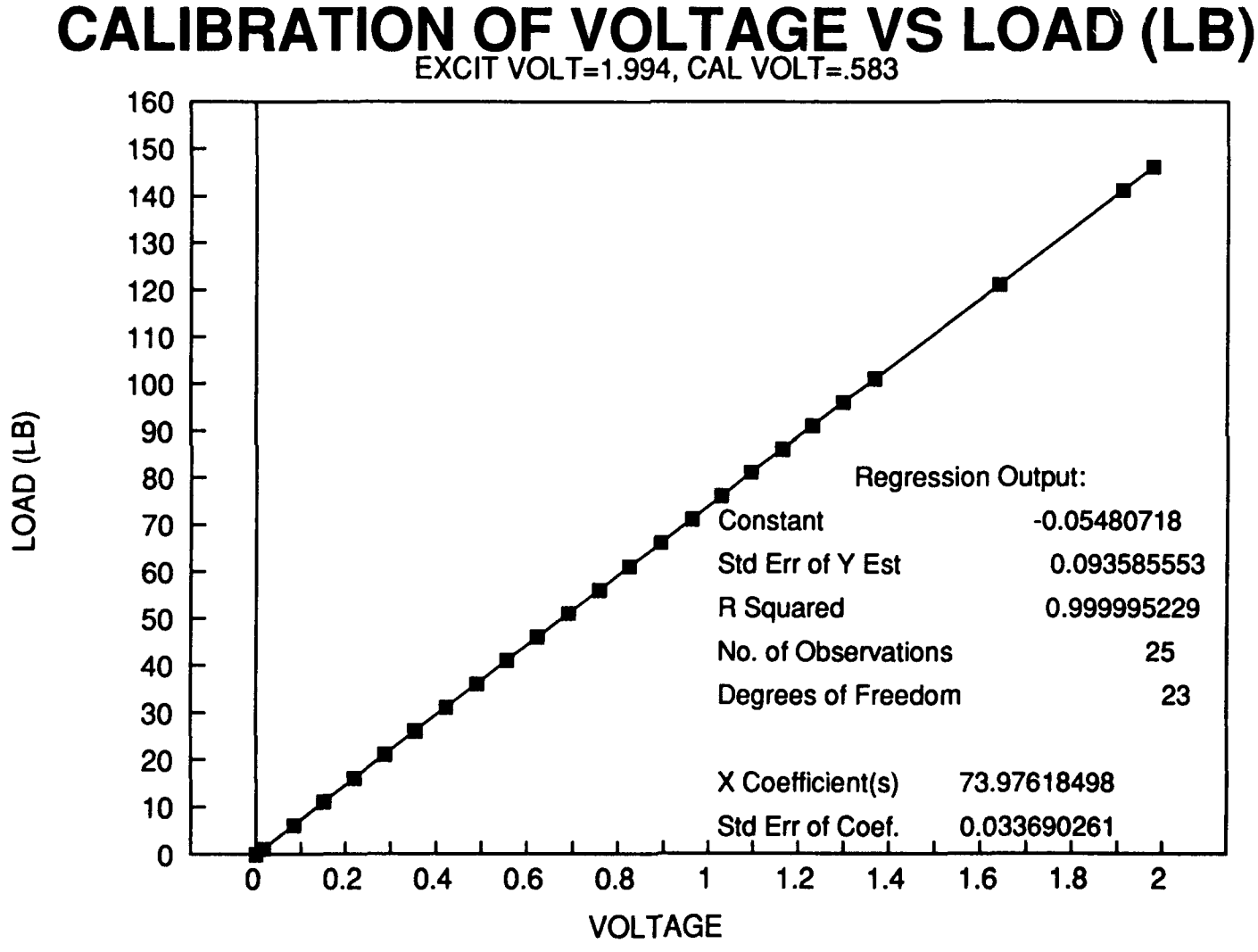

Figure 3.5 Calibration of Output Voltage vs. Specimen Load.

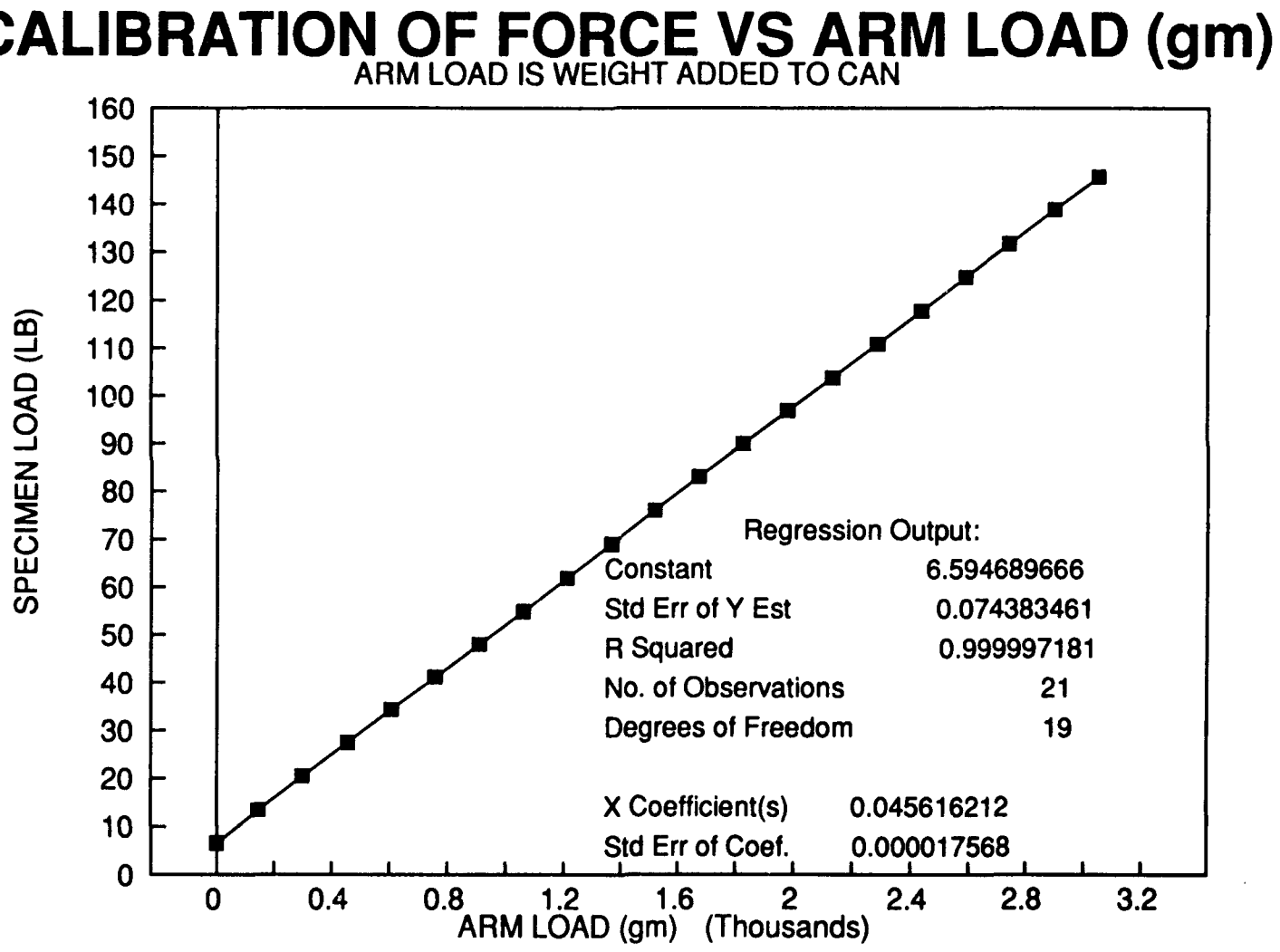

Figure 3.6 Calibration of Specimen Load vs. Applied Load on Arm.

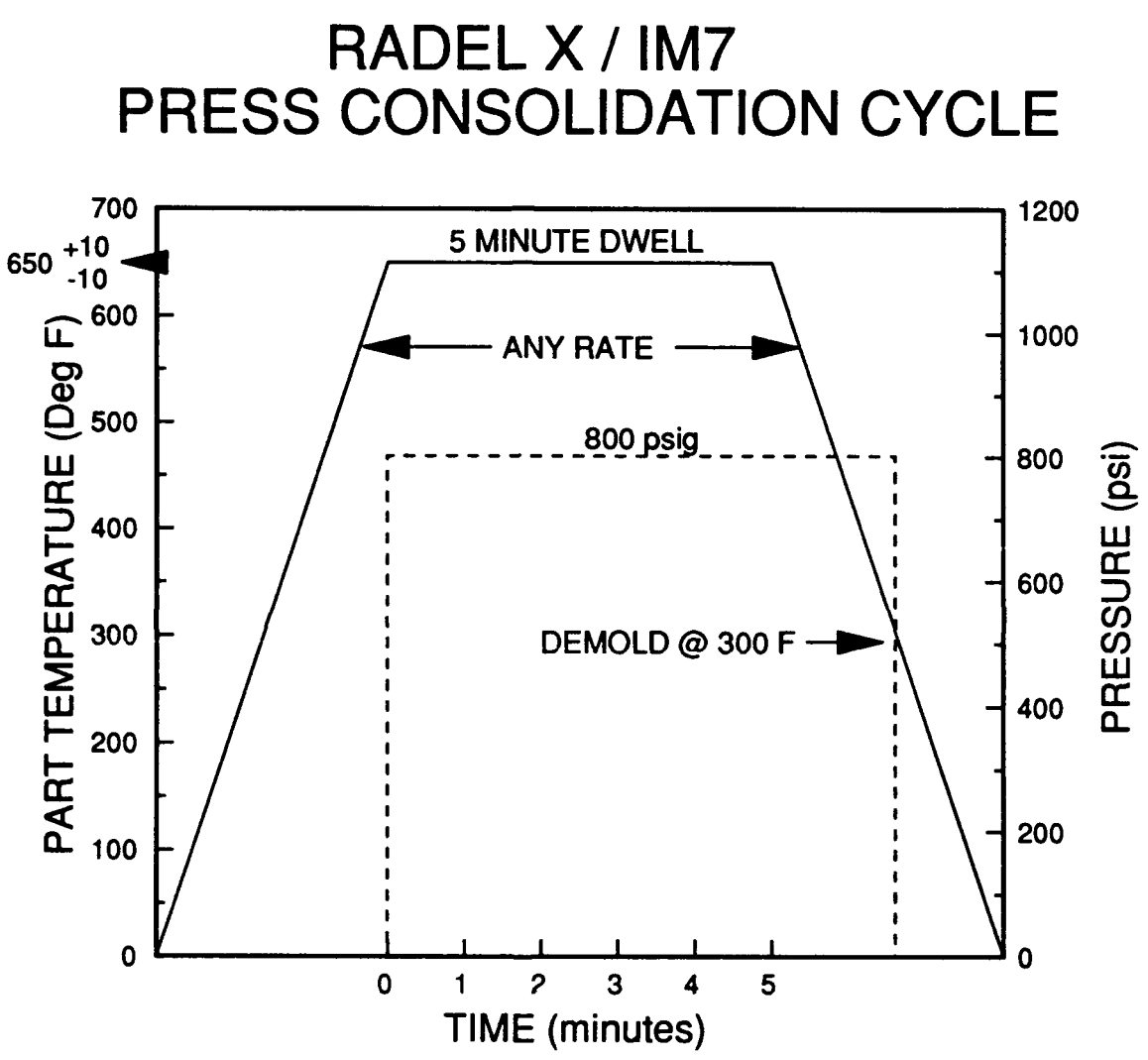

Figure 3.7 Hot Press Cure Cycle.

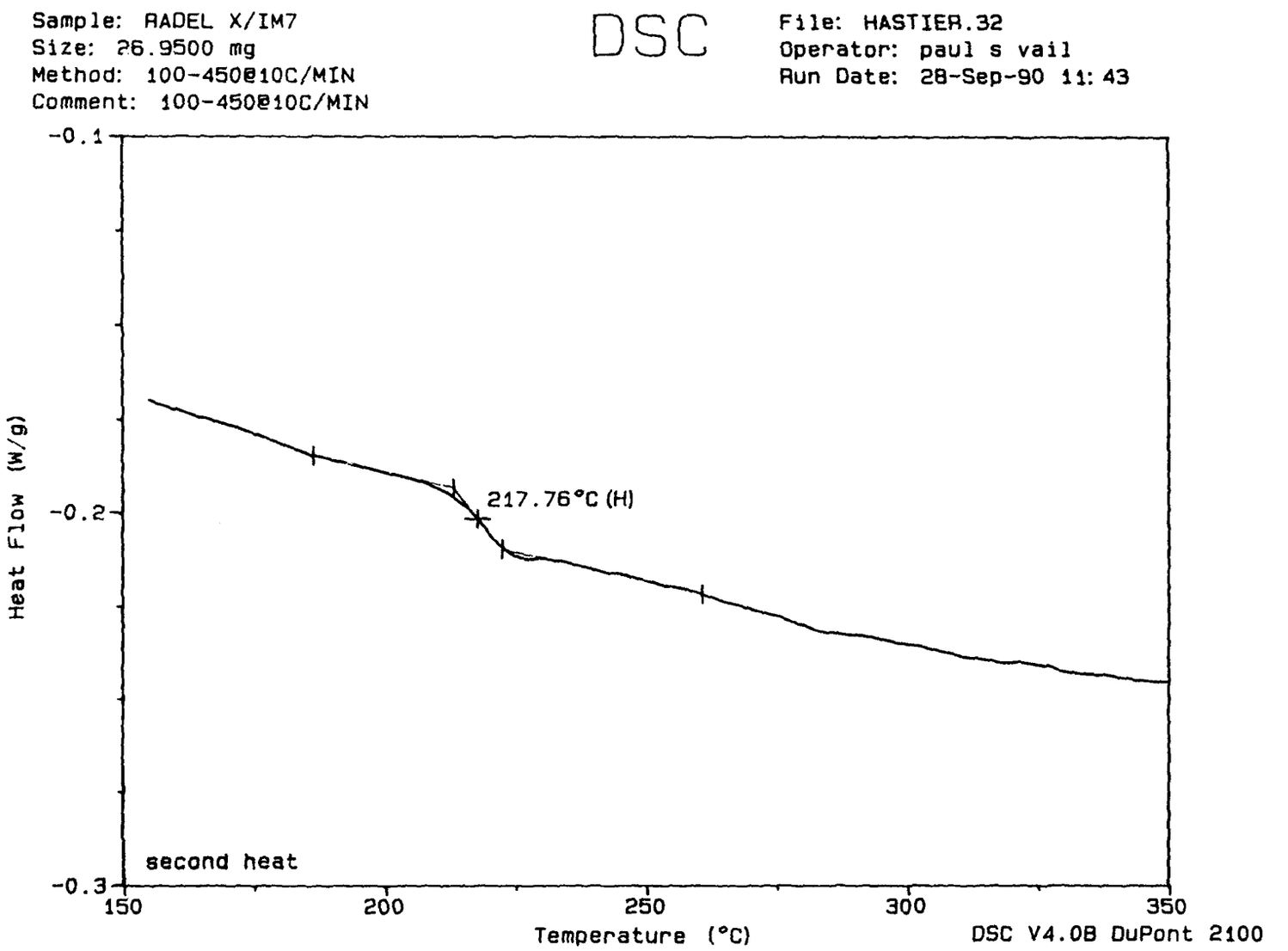

Figure 3.8 DSC Trace of the Radel X/IM7 Composite.

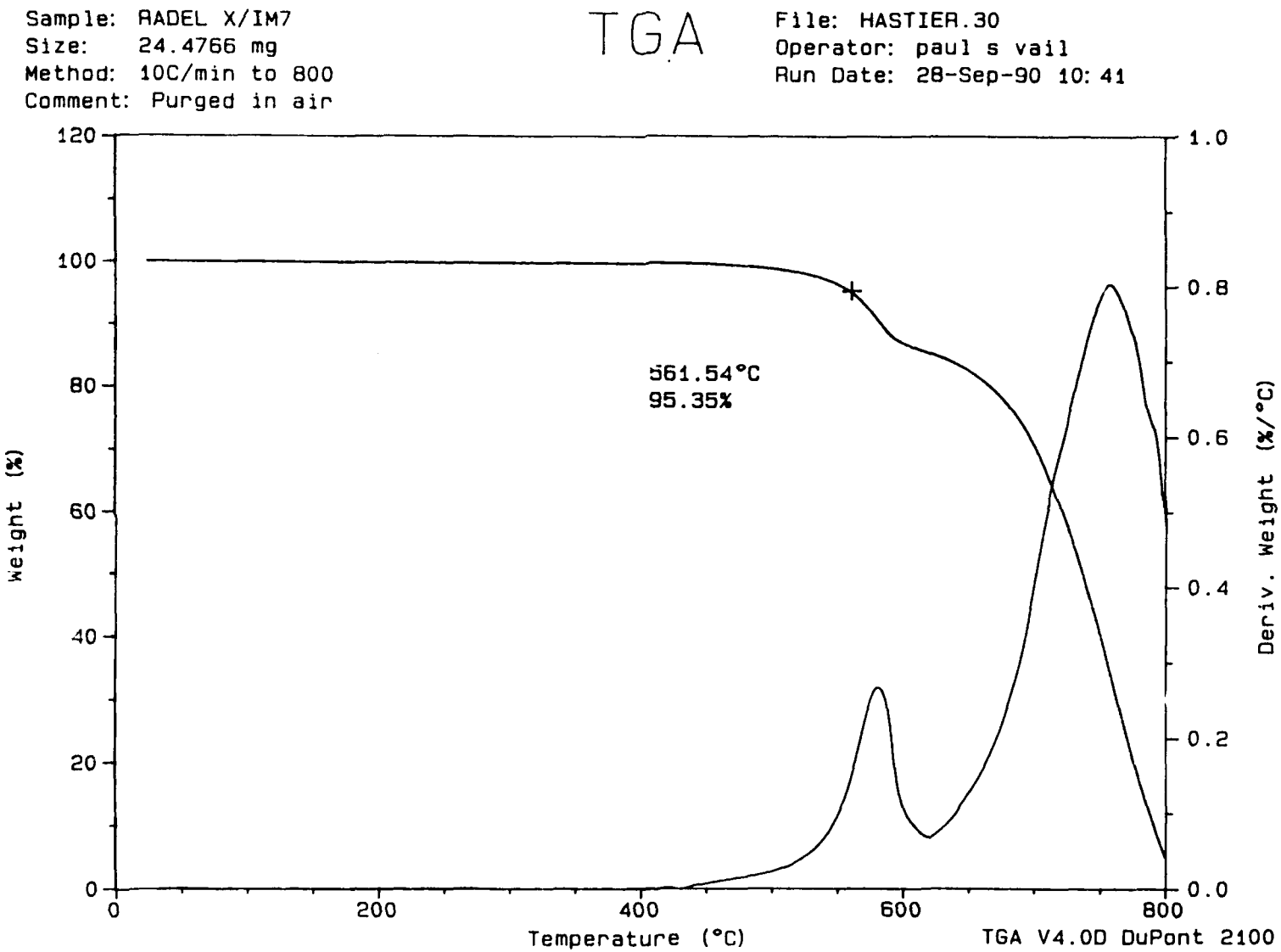

Figure 3.9 TGA Trace of the Radel X/IM7 Composite.

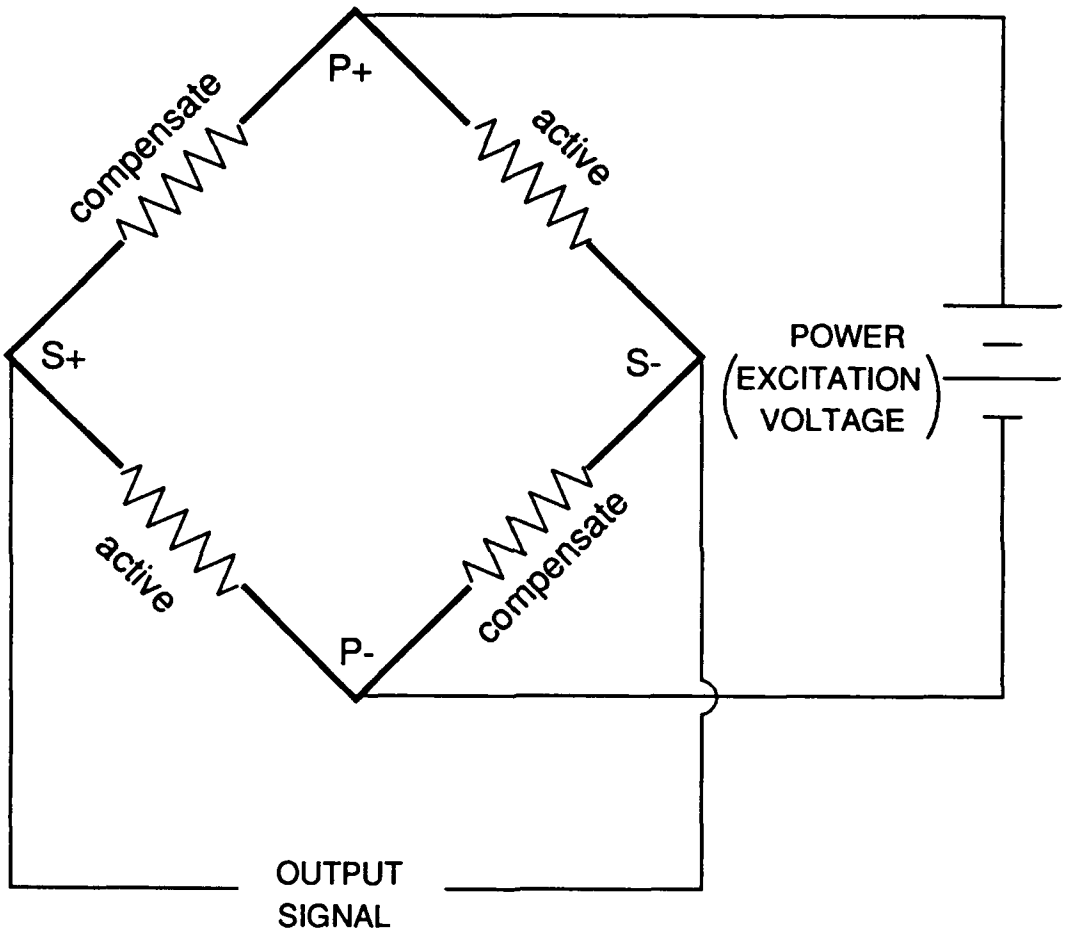

Figure 3.10 Illustration of Full Bridge Wheastone Circuit.

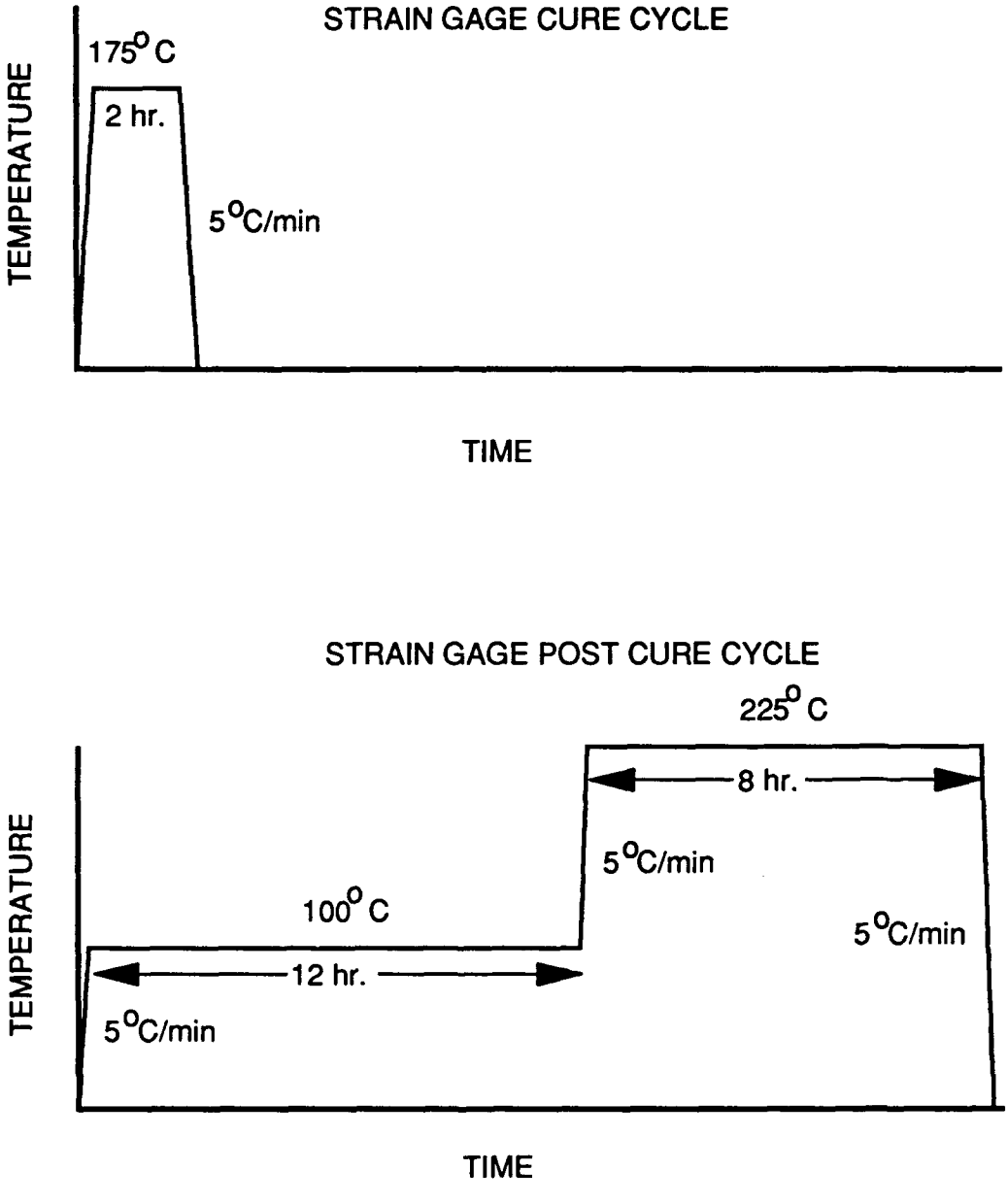

Figure 3.11 Strain Gage Curing Cycles.

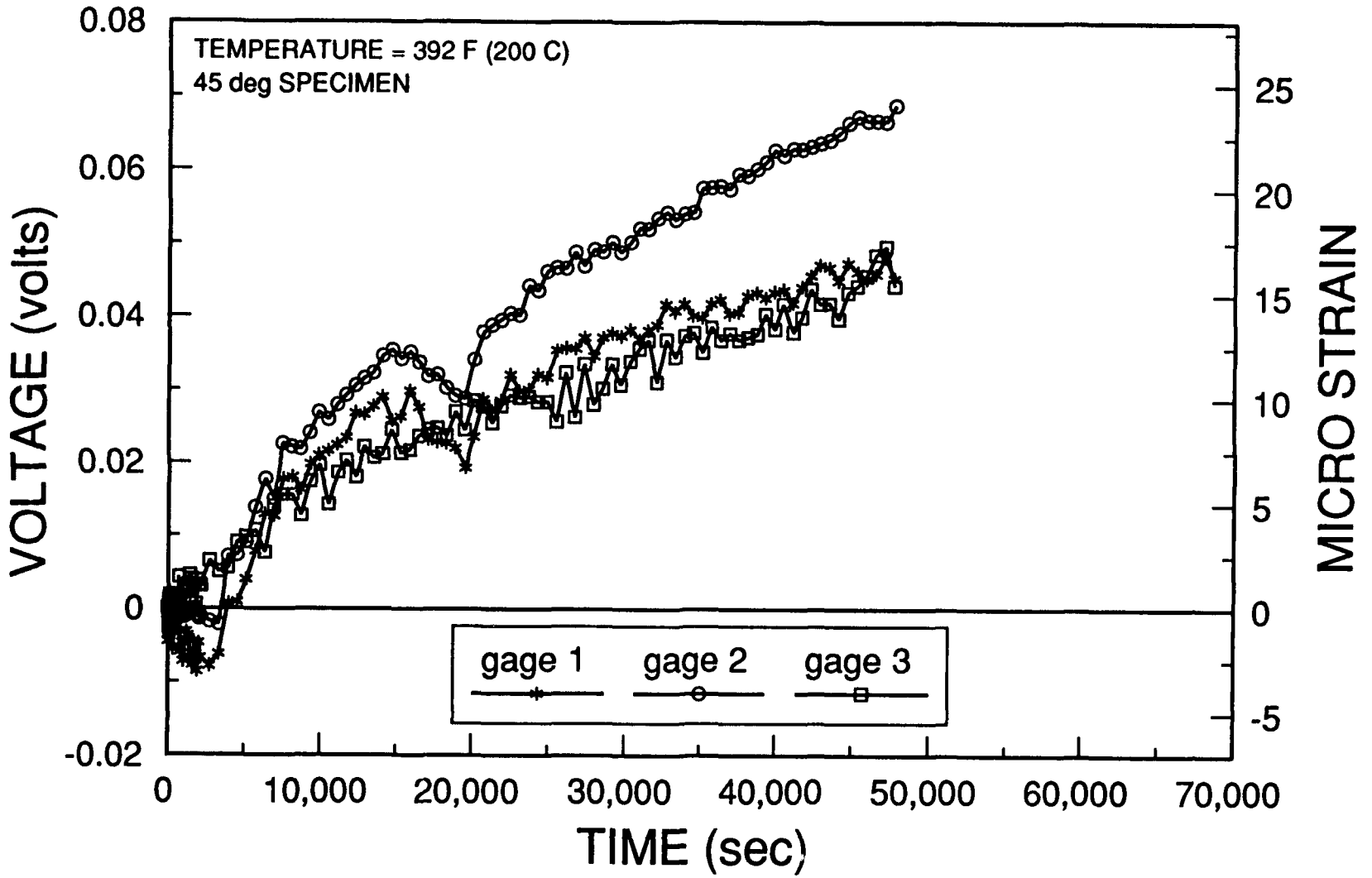

Figure 3.12 Initial Zero Drift Measurements.

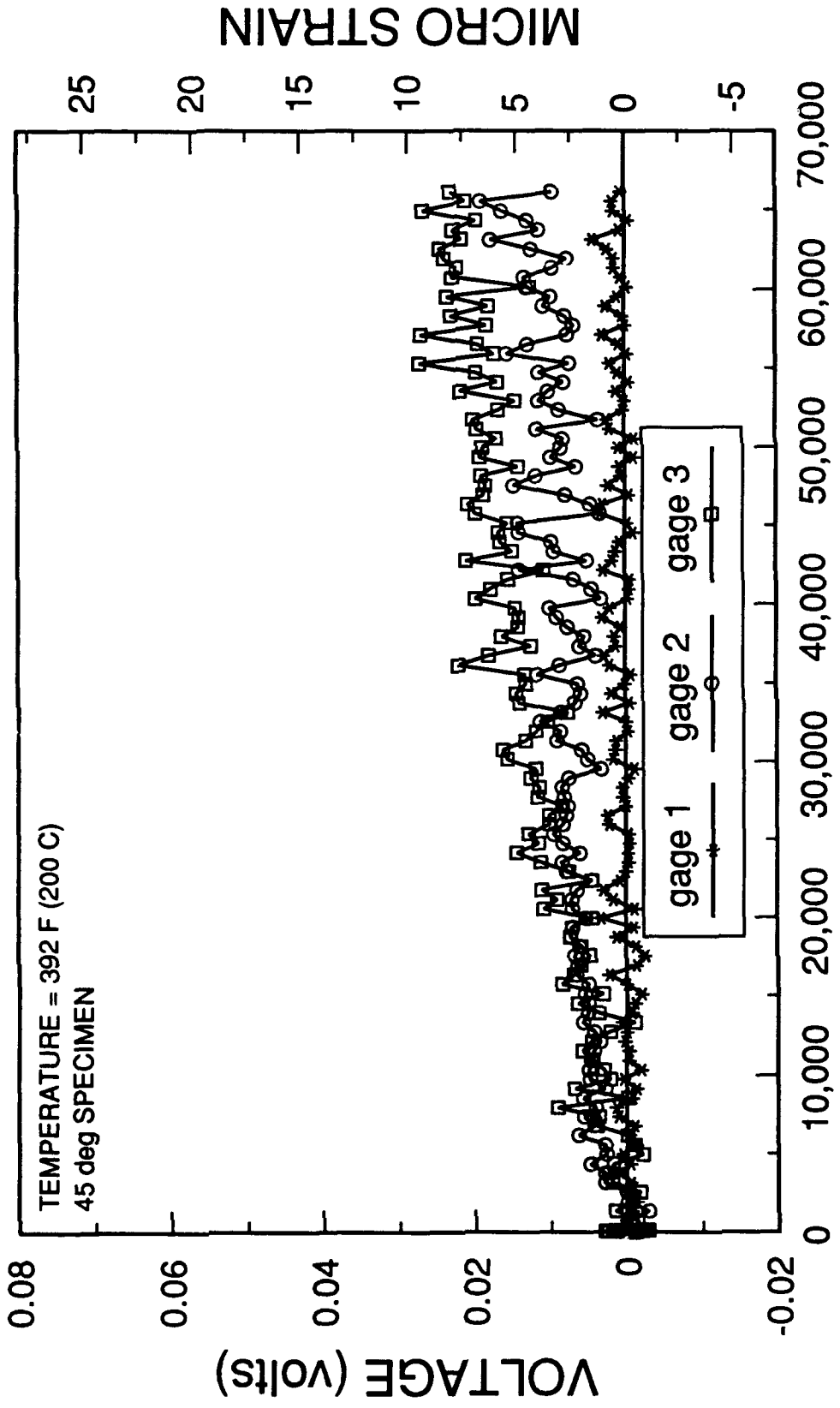

Figure 3.13 Zero Drift Measurements after Resoldering.

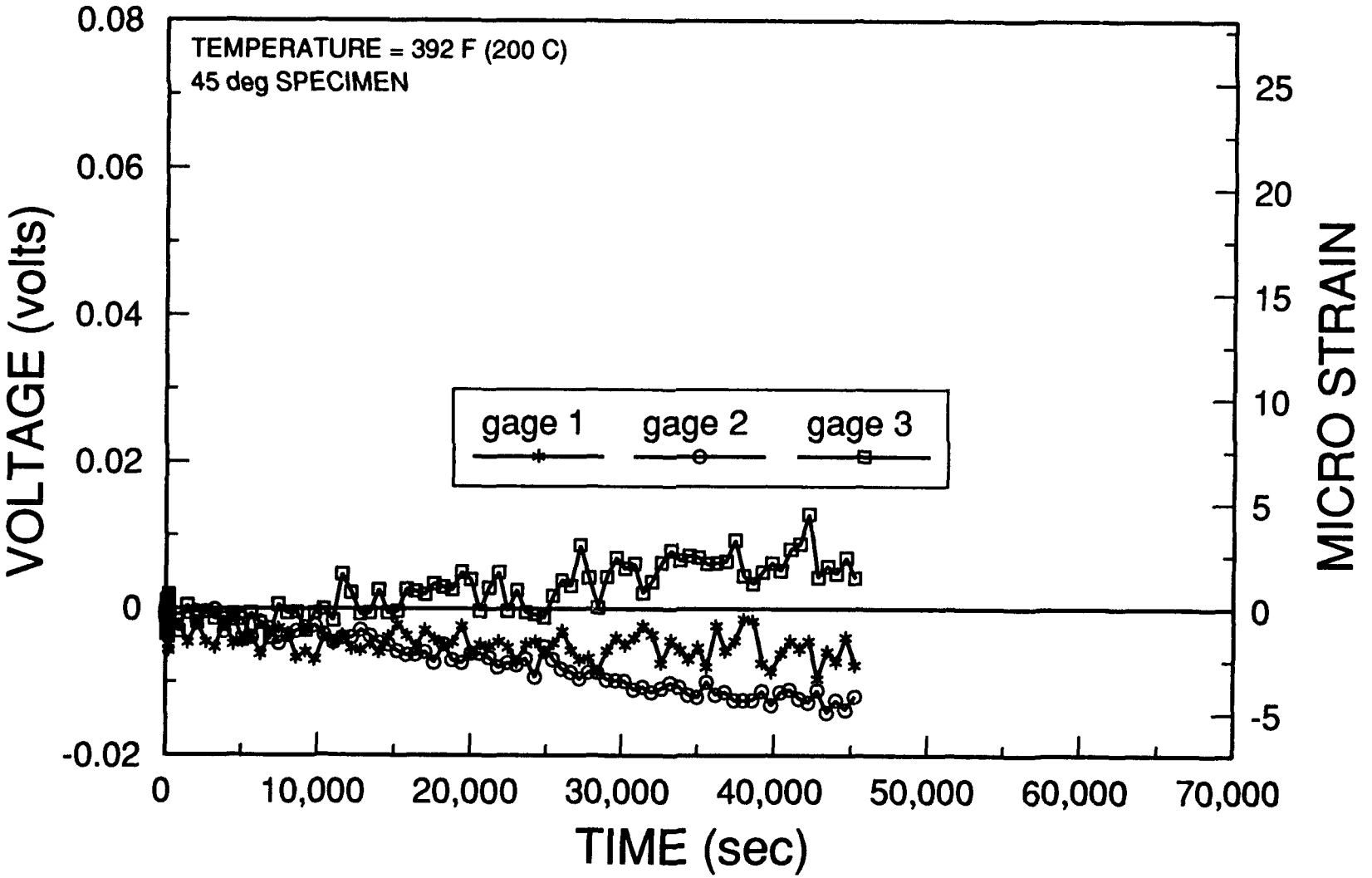

Figure 3.14 Zero Drift Measurements after Remounting Dummy Specimen.

STRAIN GAGE LINE NOISE REDUCTION

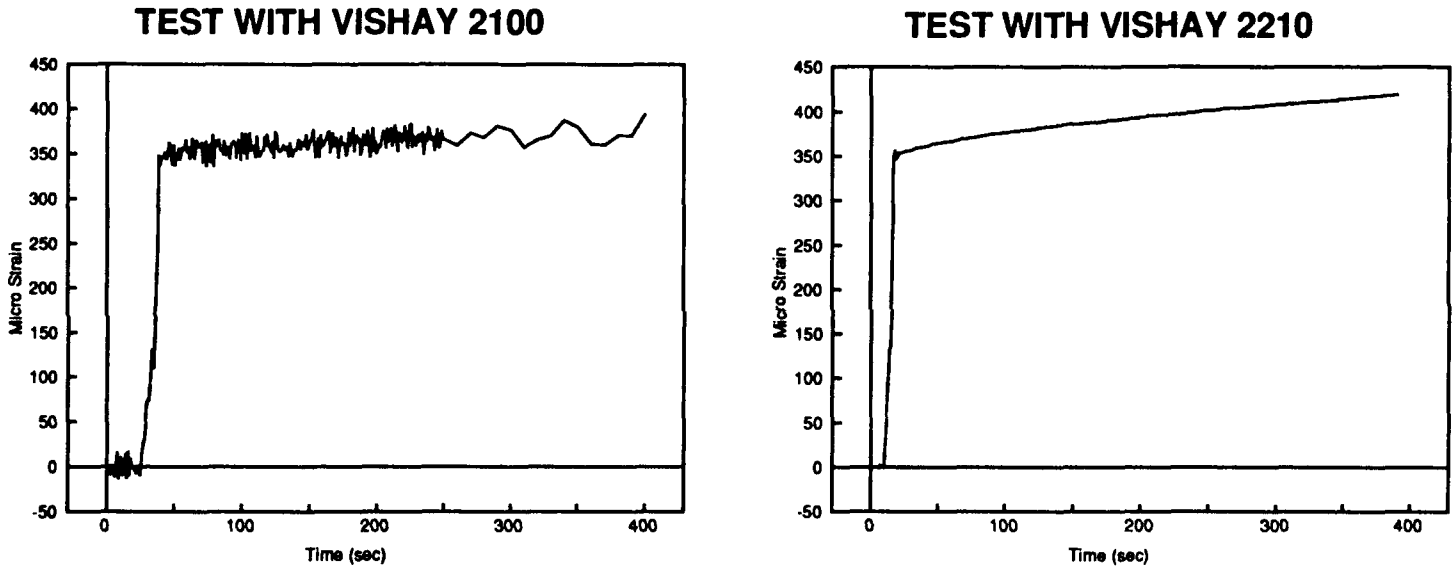

Figure 3.15 Comparison of Line Noise Between the Vishay 2100 and 2210 Signal Conditioner Amplifiers.

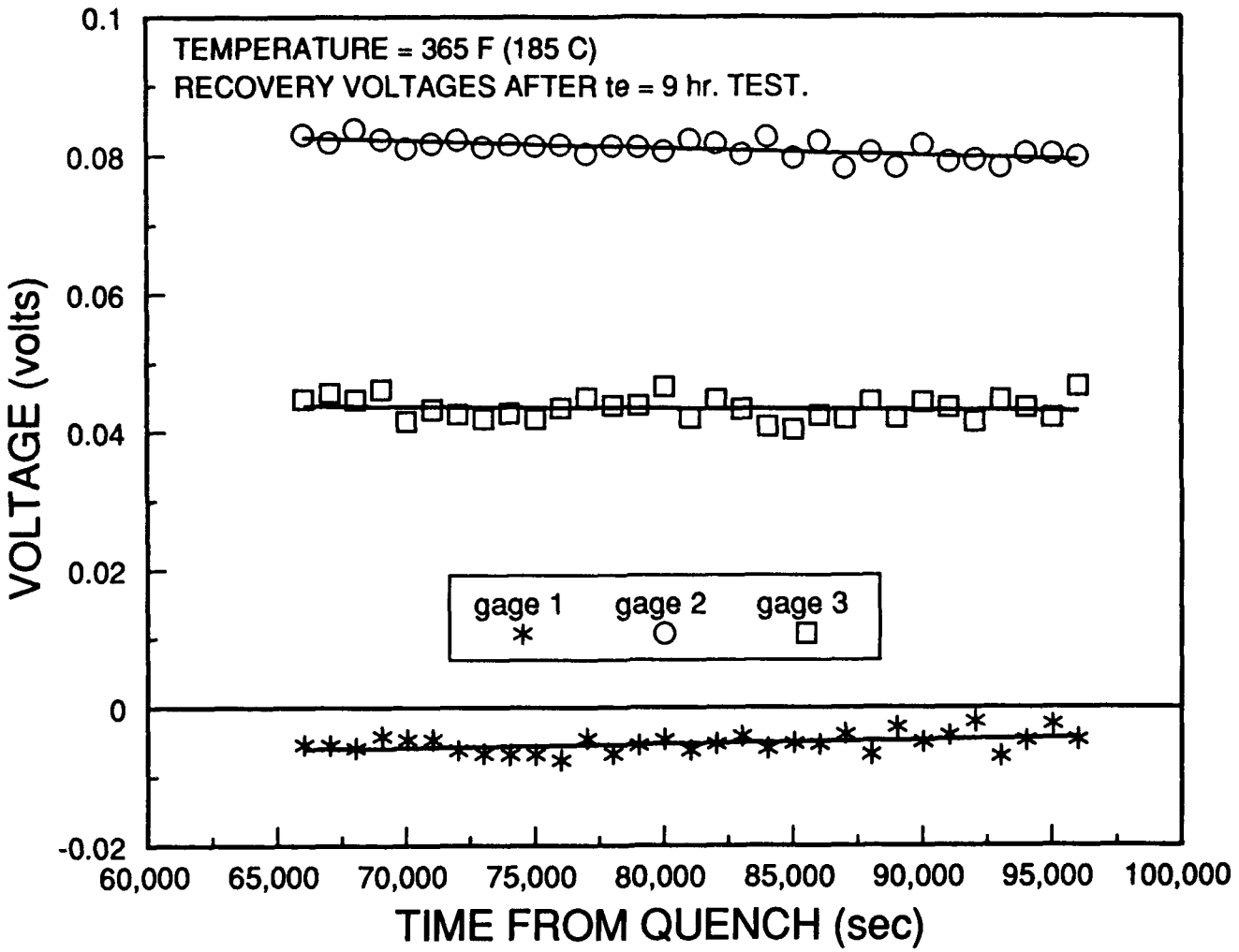

Figure 3.16 Linear Fit to Recovery Voltages.

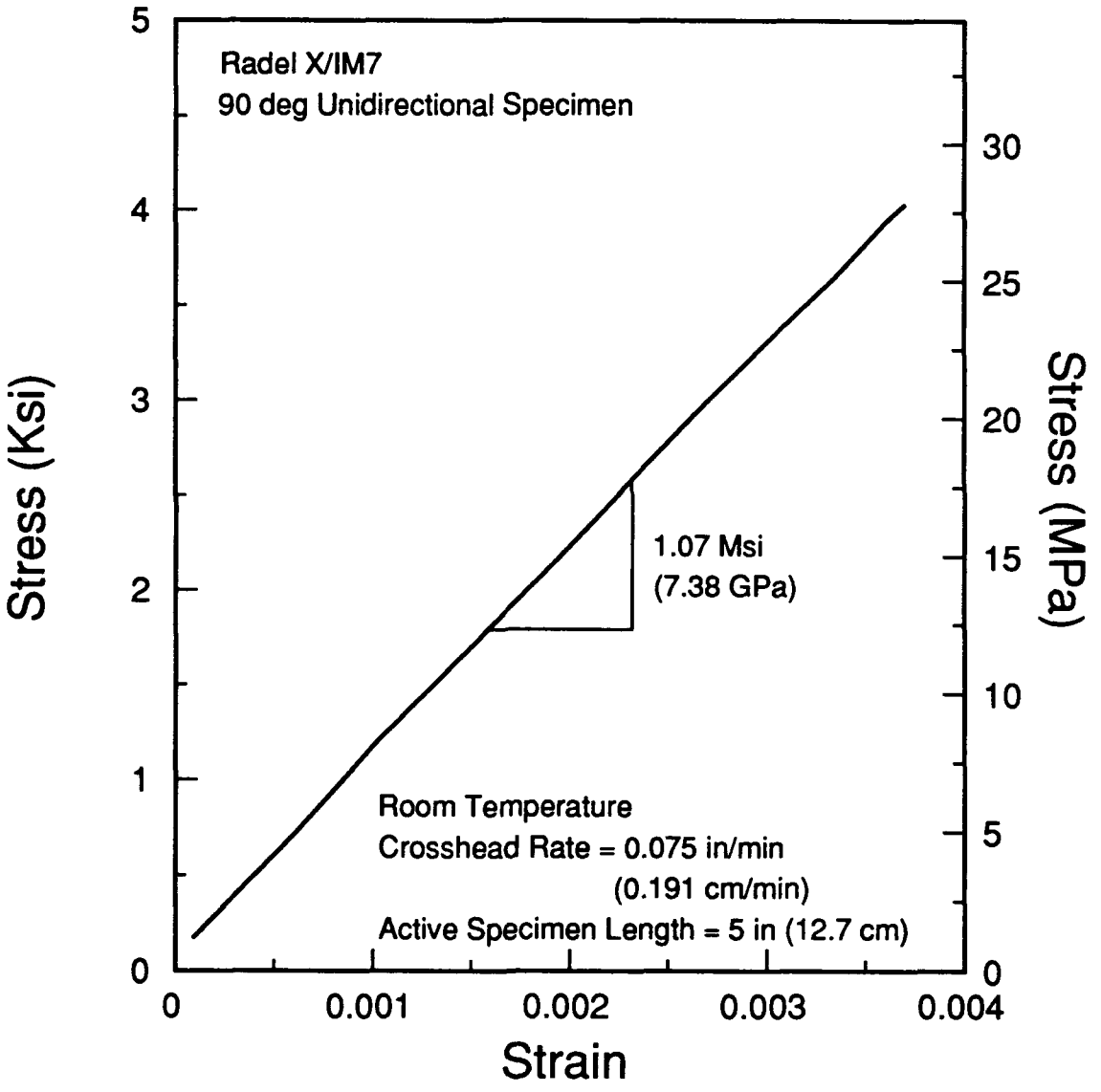

Figure 4.1 Stress Strain Curve for Transverse Direction.

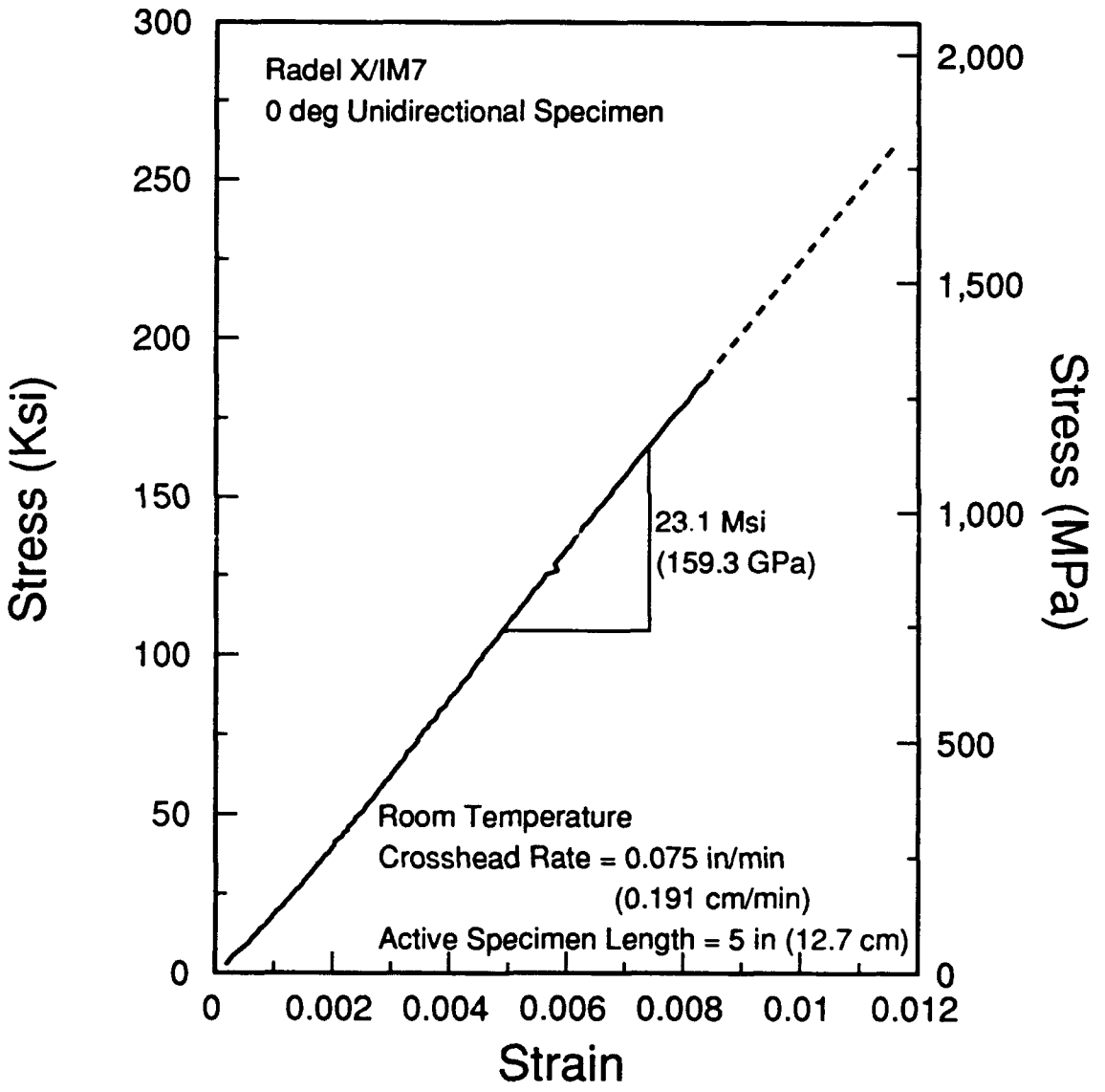

Figure 4.2 Stress Strain Curve for Fiber Direction.

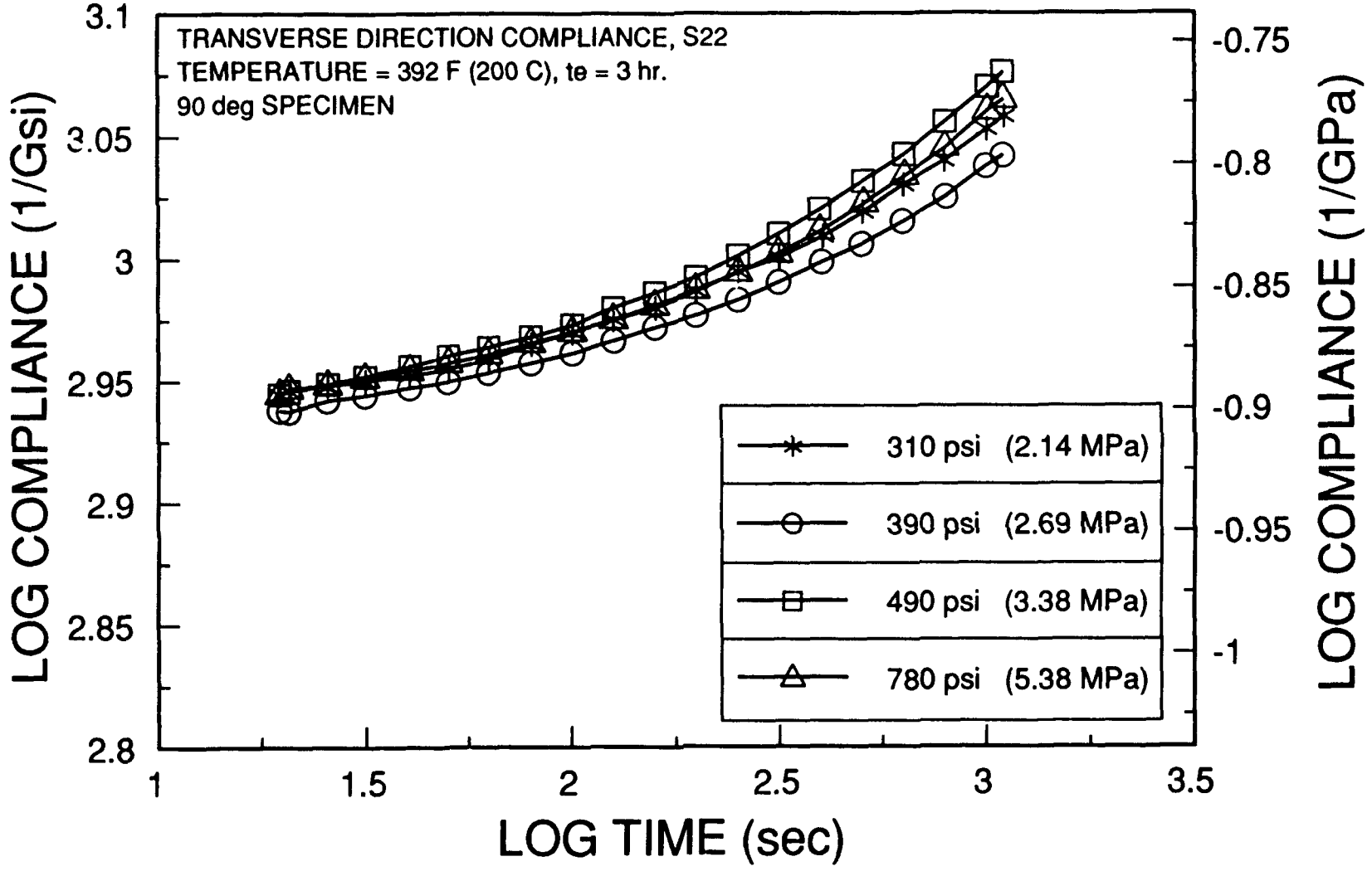

Figure 4.3 Linearity Check of Transverse Direction Compliance at a Constant Temperature of 392 F (200 C) and te = 3 hours.

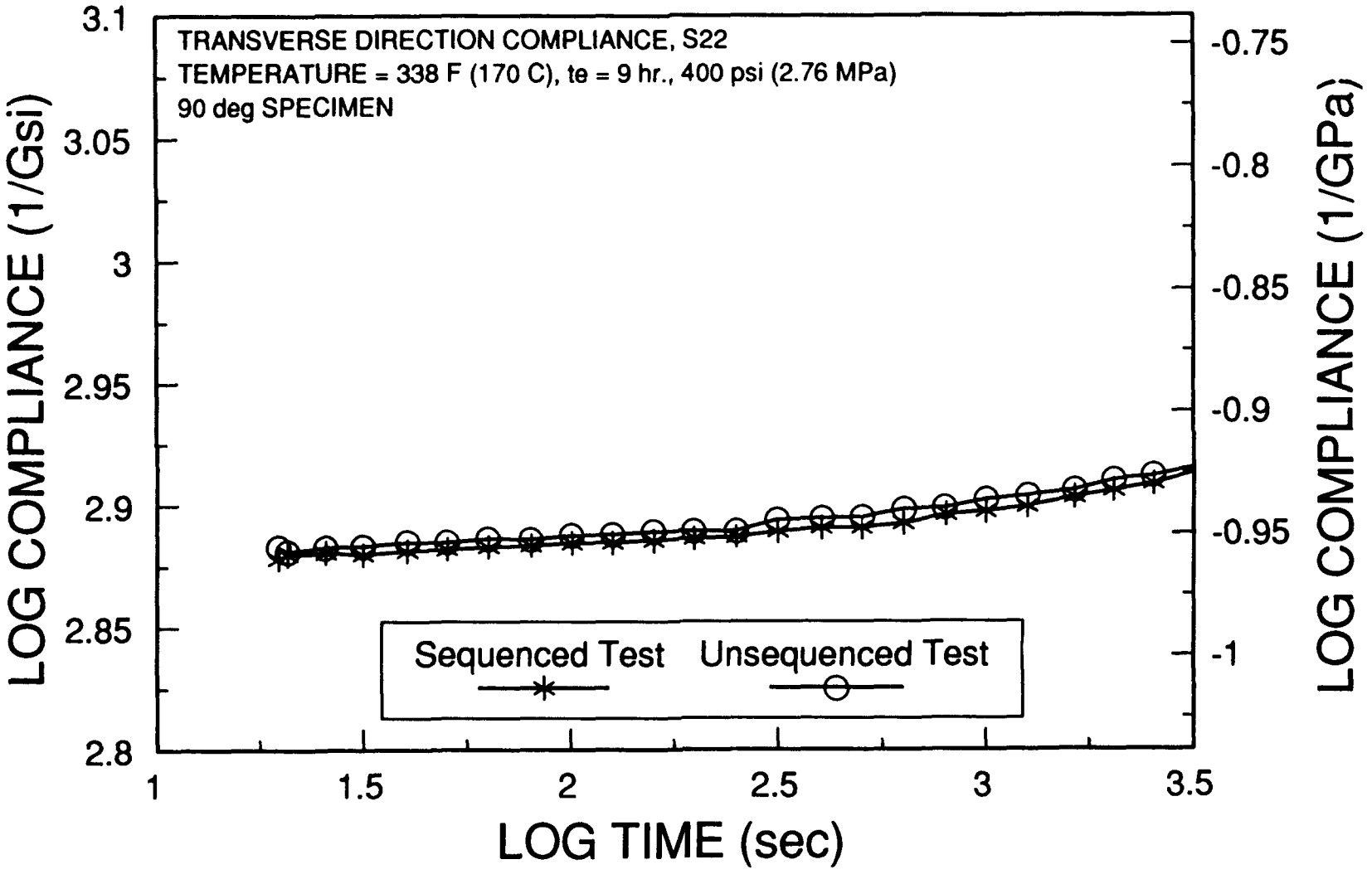

Figure 4.4 Check of Test Sequencing Effect on Transverse Direction Compliance at a Temperature of 338 F (170 C) and te = 9 hours.

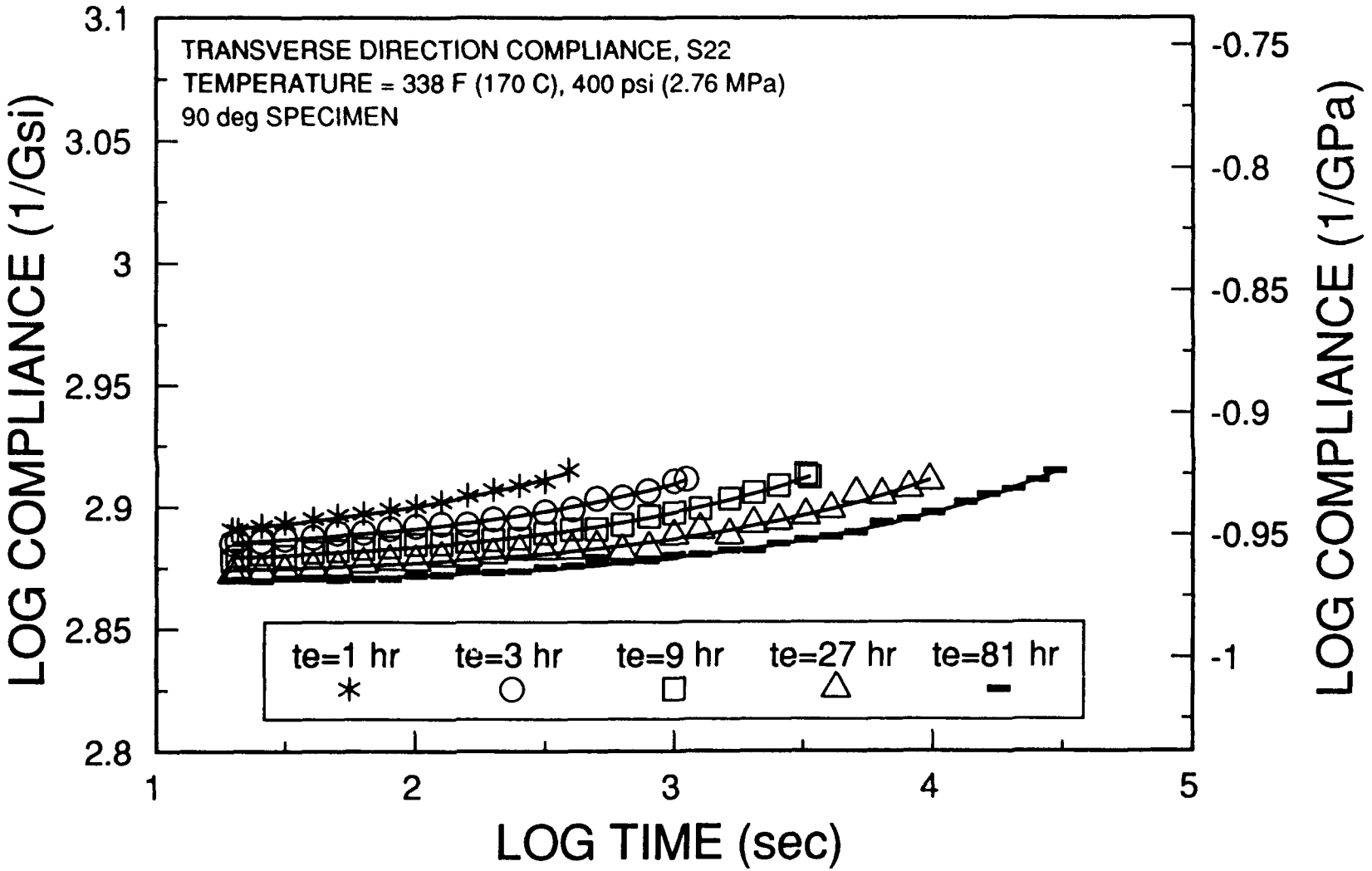

Figure 4.5 Transverse Direction Compliance for a Constant Temperature of 338 F (170 C) at Various Aging Times.

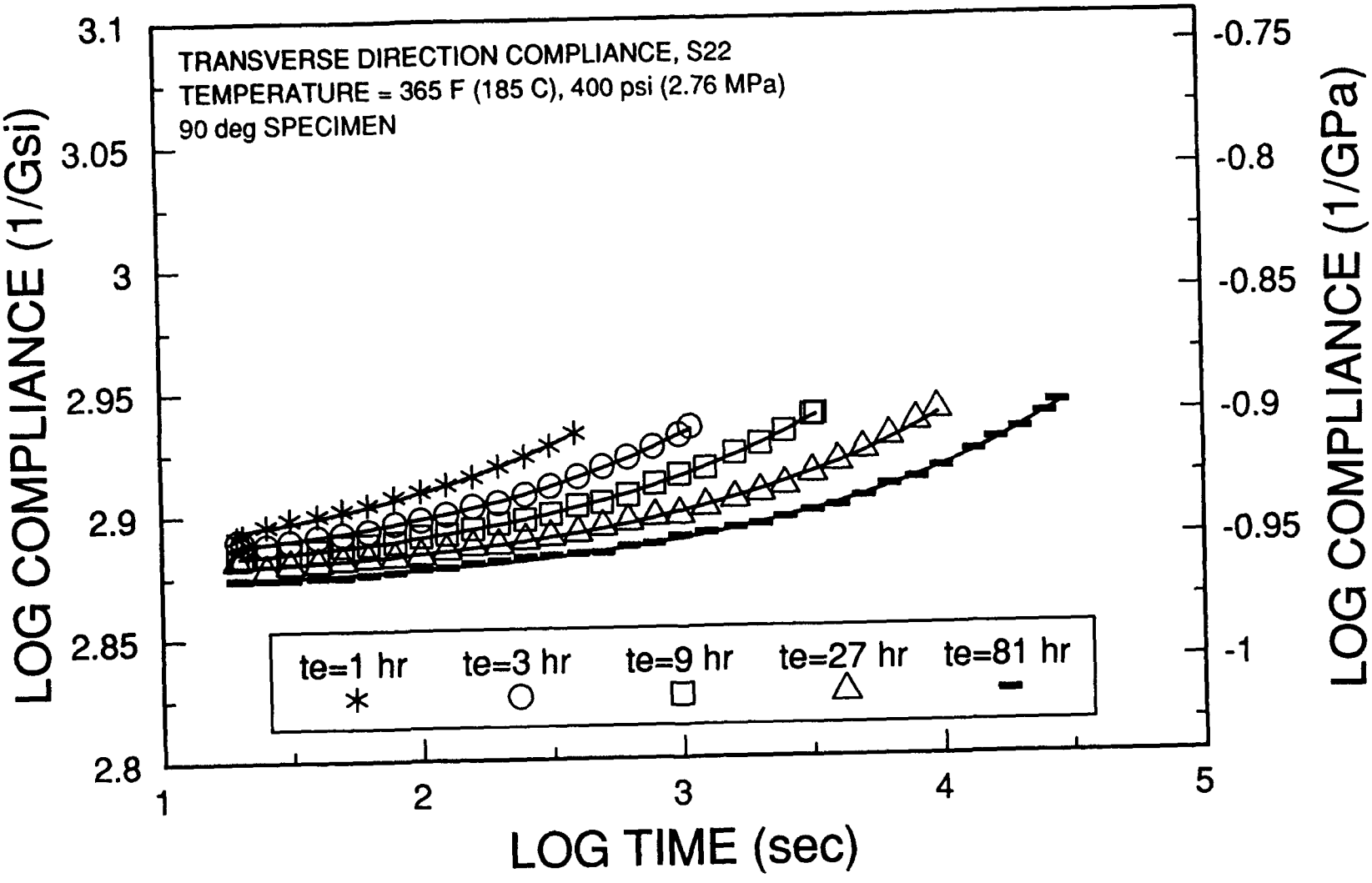

Figure 4.6 Transverse Direction Compliance for a Constant Temperature of 365 F (185 C) at Various Aging Times.

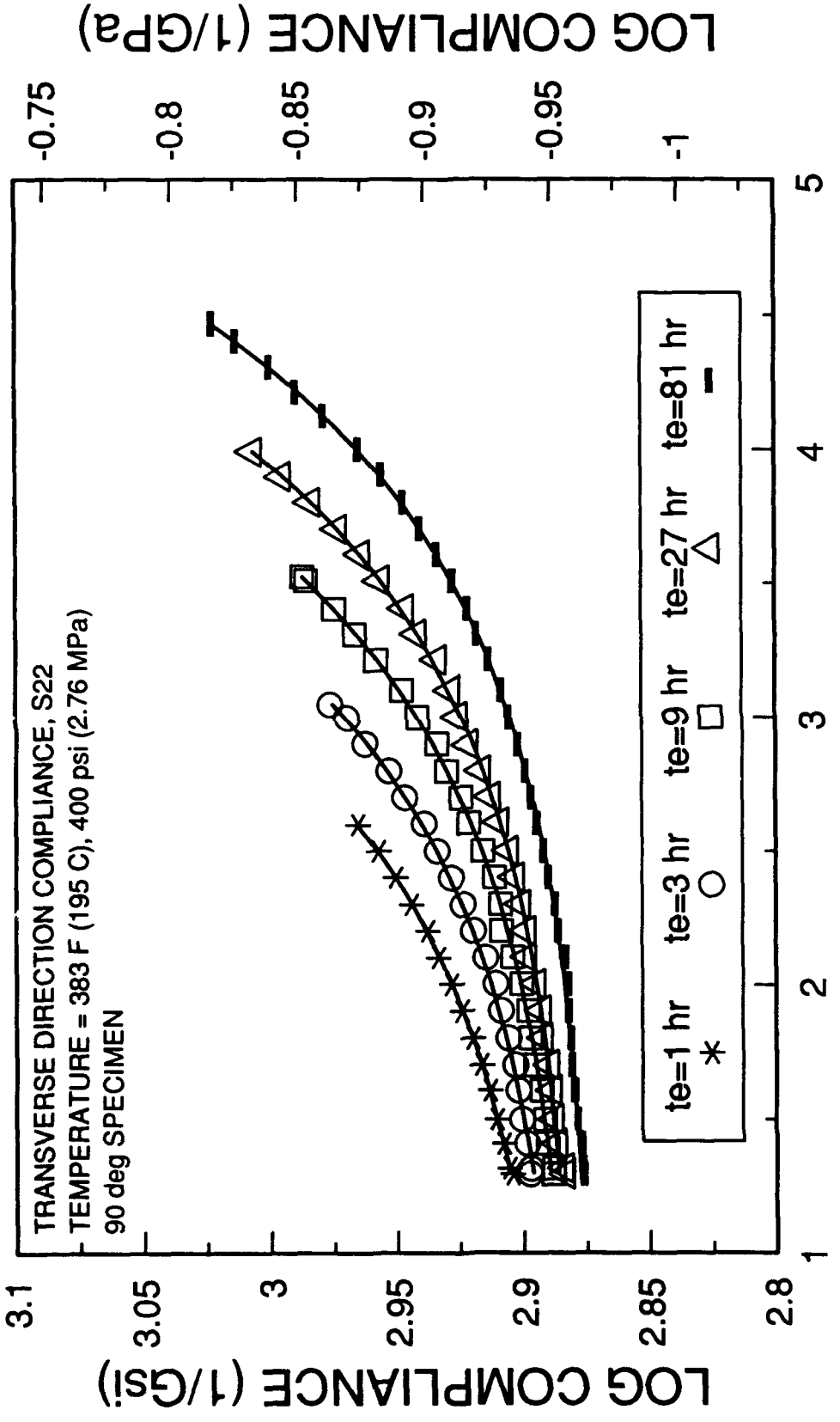

Figure 4.7 Transverse Direction Compliance for a Constant Temperature of 383 F (195 C) at Various Aging Times.

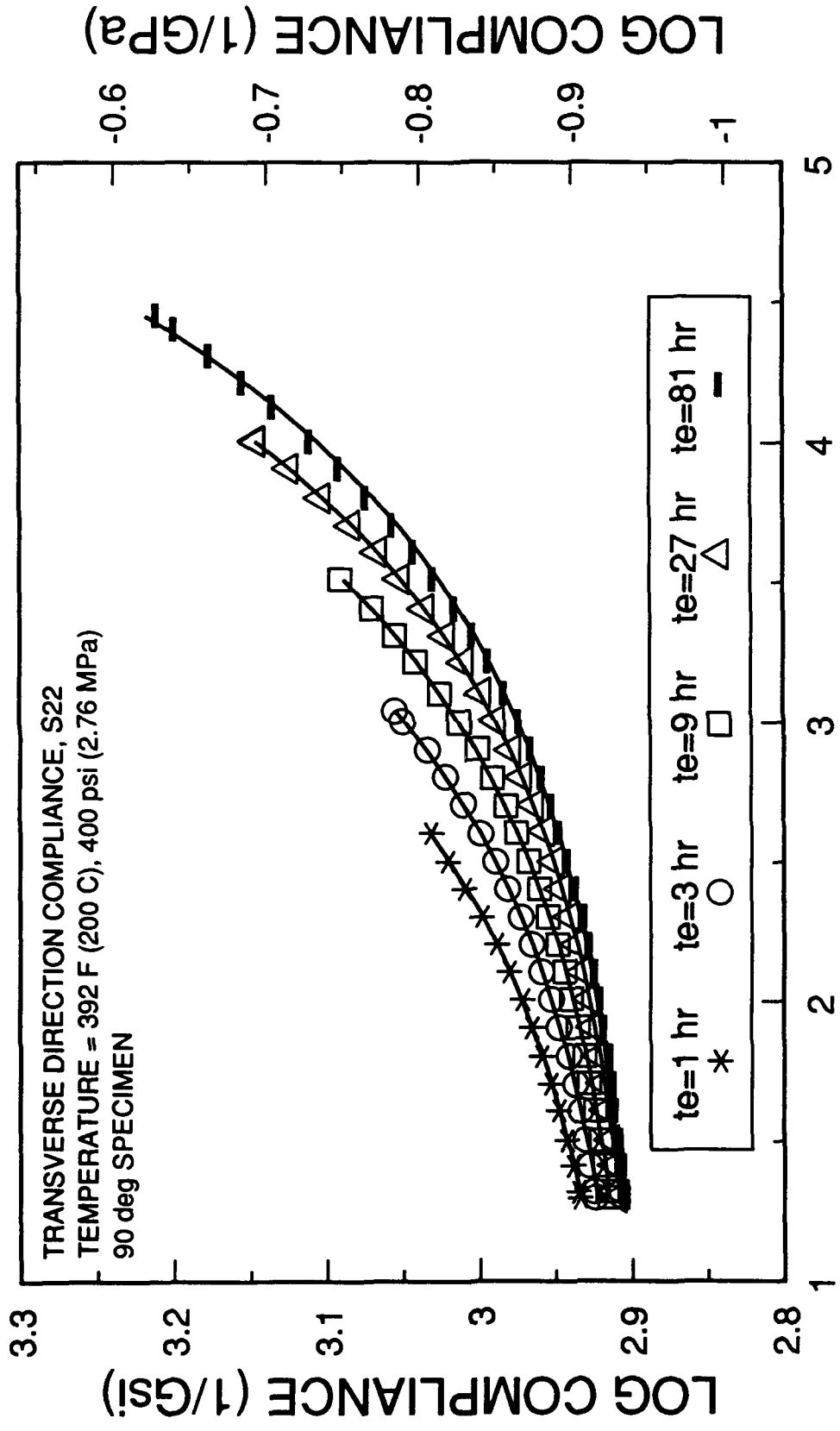

Figure 4.8 Transverse Direction Compliance for a Constant Temperature of 392 F (200 C) at Various Aging Times.

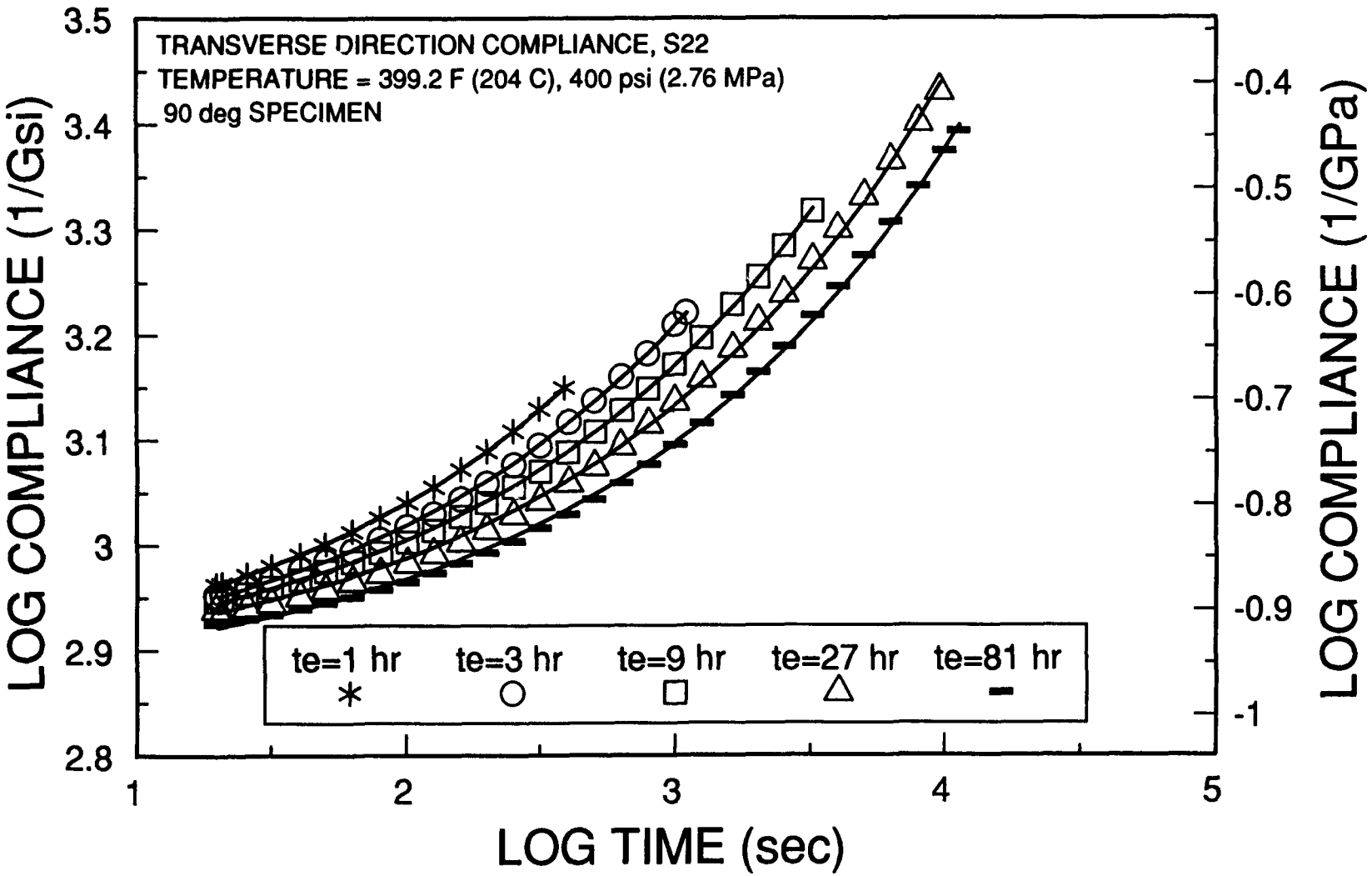

Figure 4.9 Transverse Direction Compliance for a Constant Temperature of 399.2 F (204 C) at Various Aging Times.

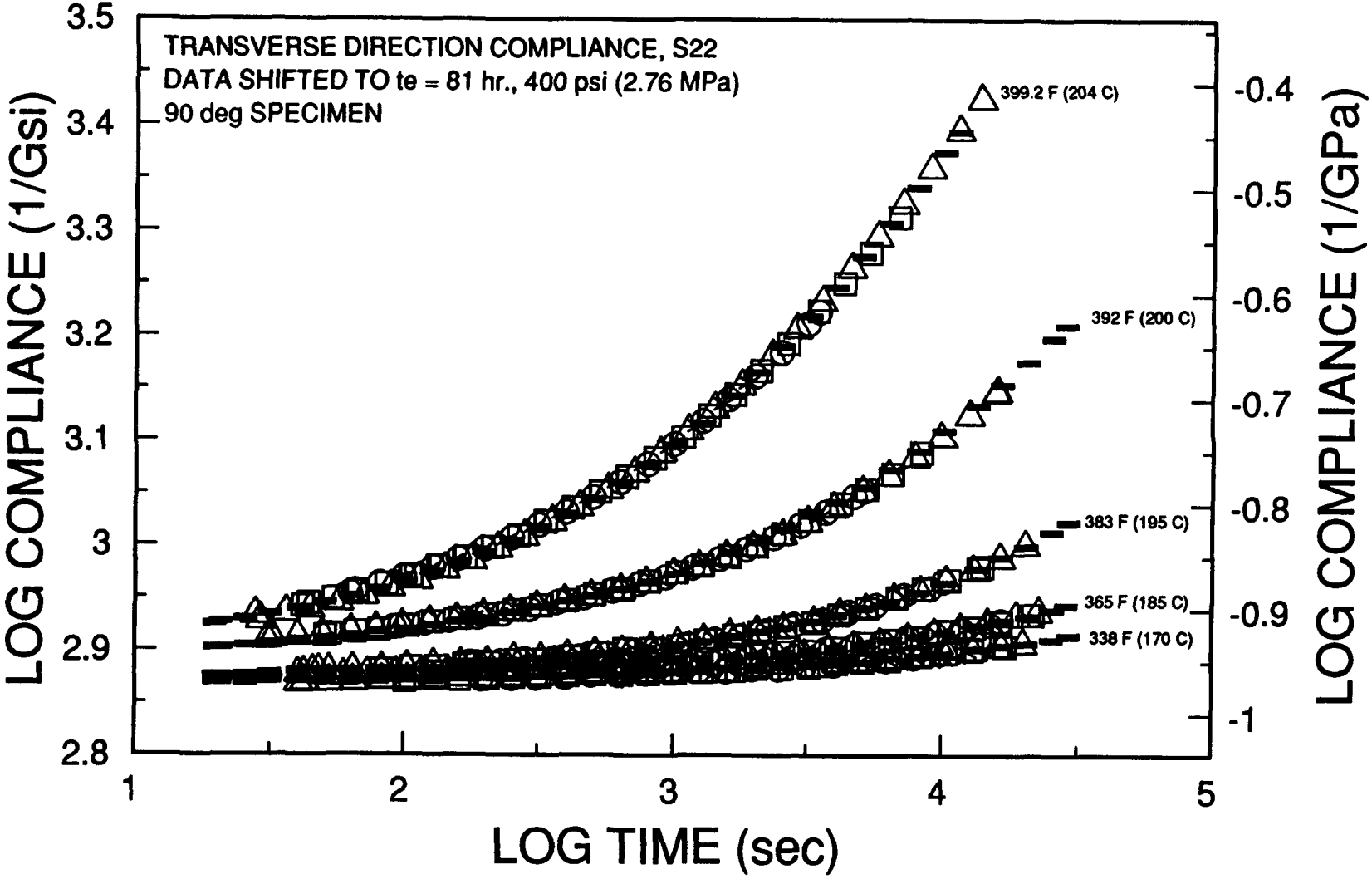

Figure 4.10 Transverse Direction Master Momentary Compliance Curves at Various Temperatures Shifted to the 81 hour Aging Time.

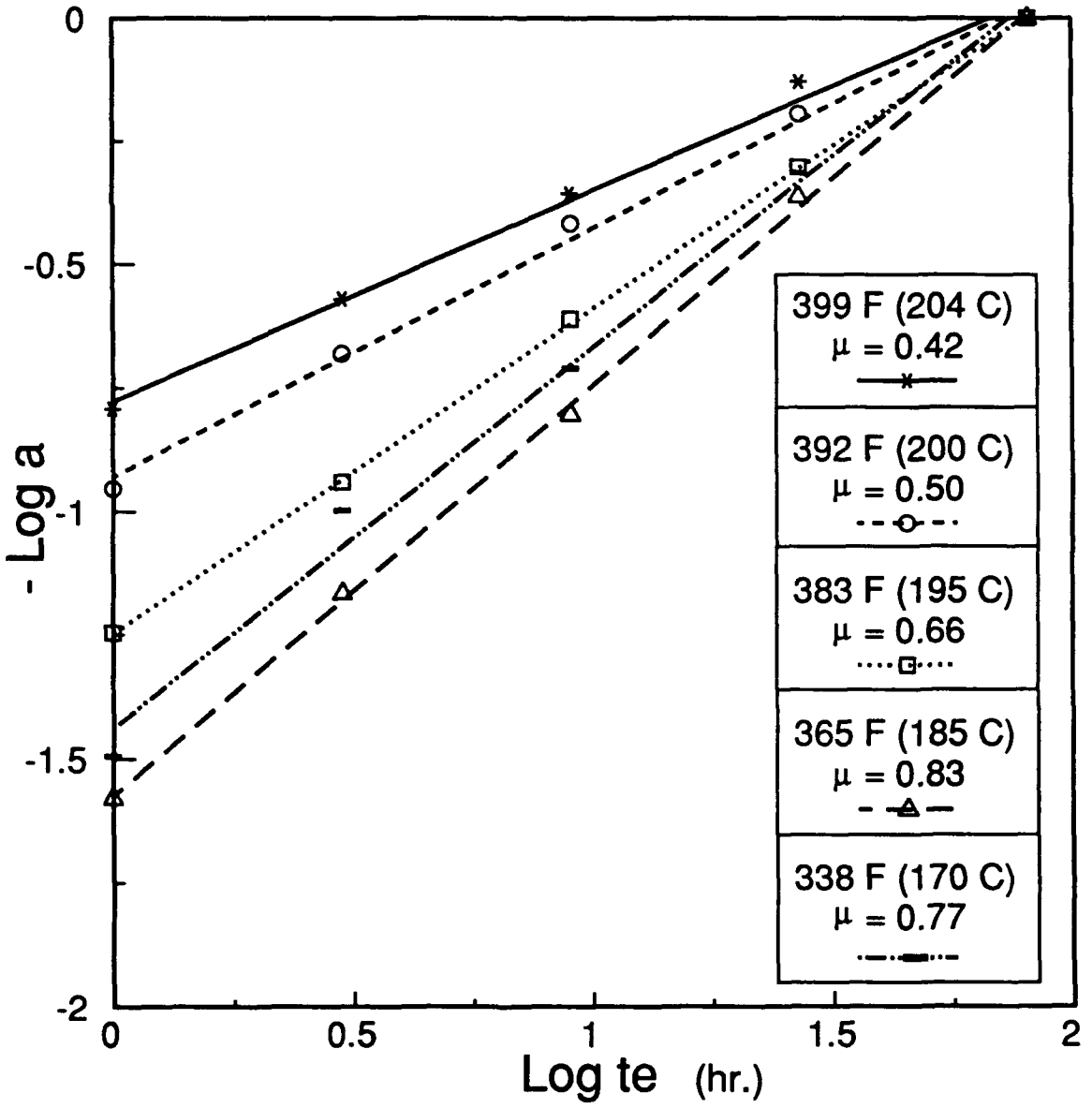

Figure 4.11 Aging Shift Rate for the 90 degree Test Sequence at Various Temperatures.

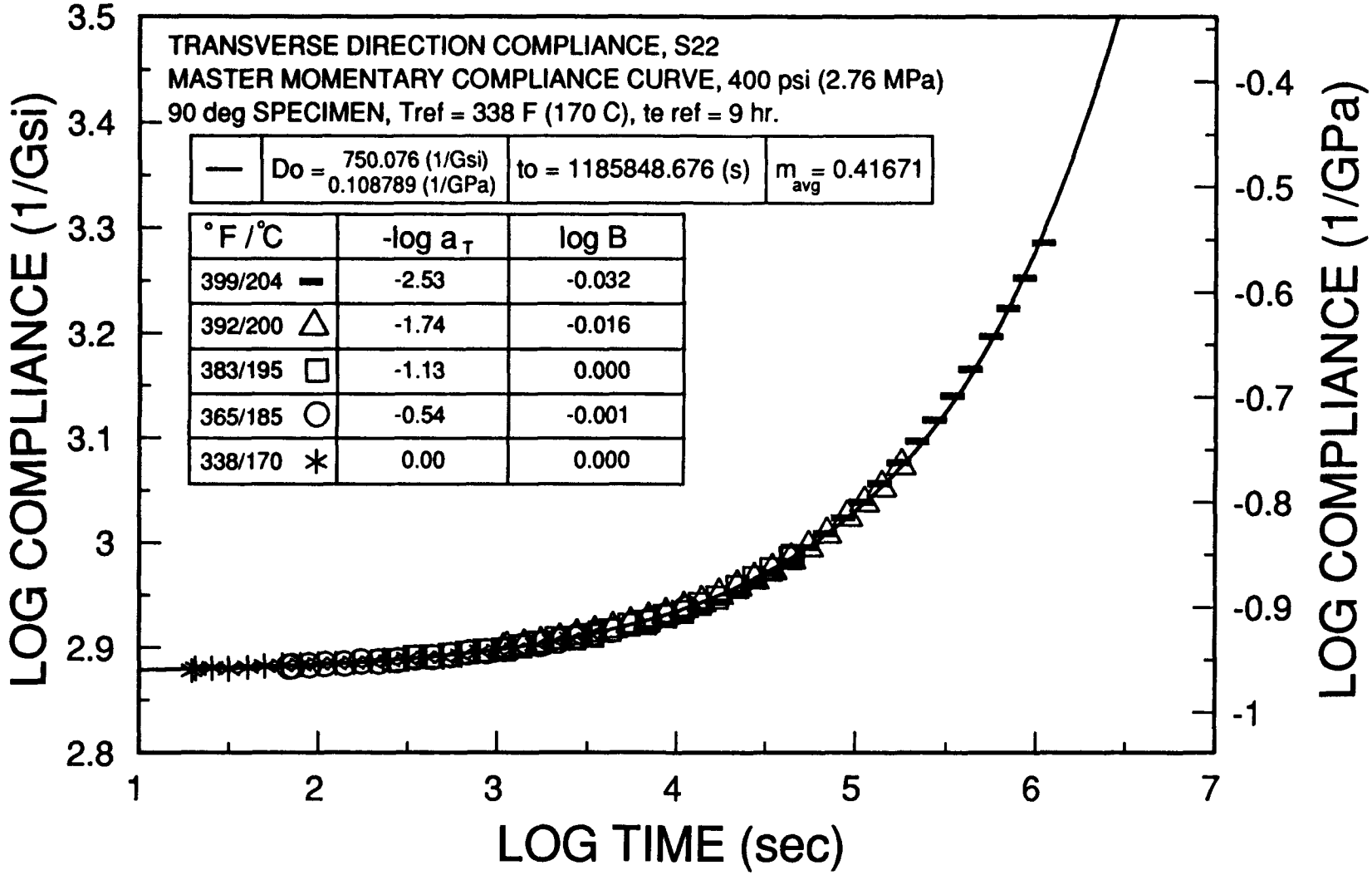

Figure 4.12 Transverse Direction TTSP Master Momentary Compliance Curve Computer Fit with m avg = 0.4167 and Referenced to T=338F (170C), te=9 hours.

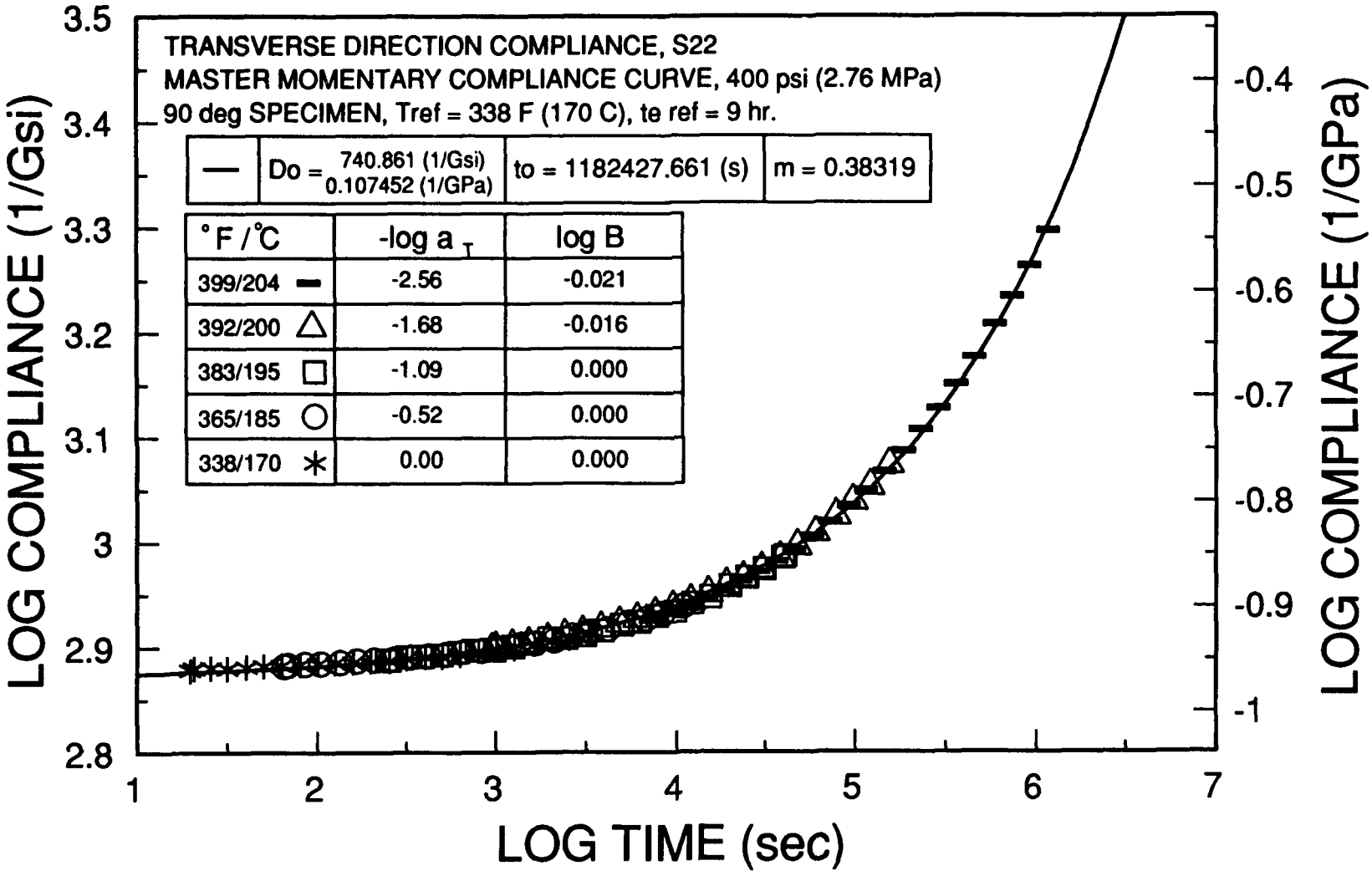

Figure 4.13 Transverse Direction TTSP Master Momentary Compliance Curve Graphically Fit and Referenced to T=338F (170C), te=9 hours.

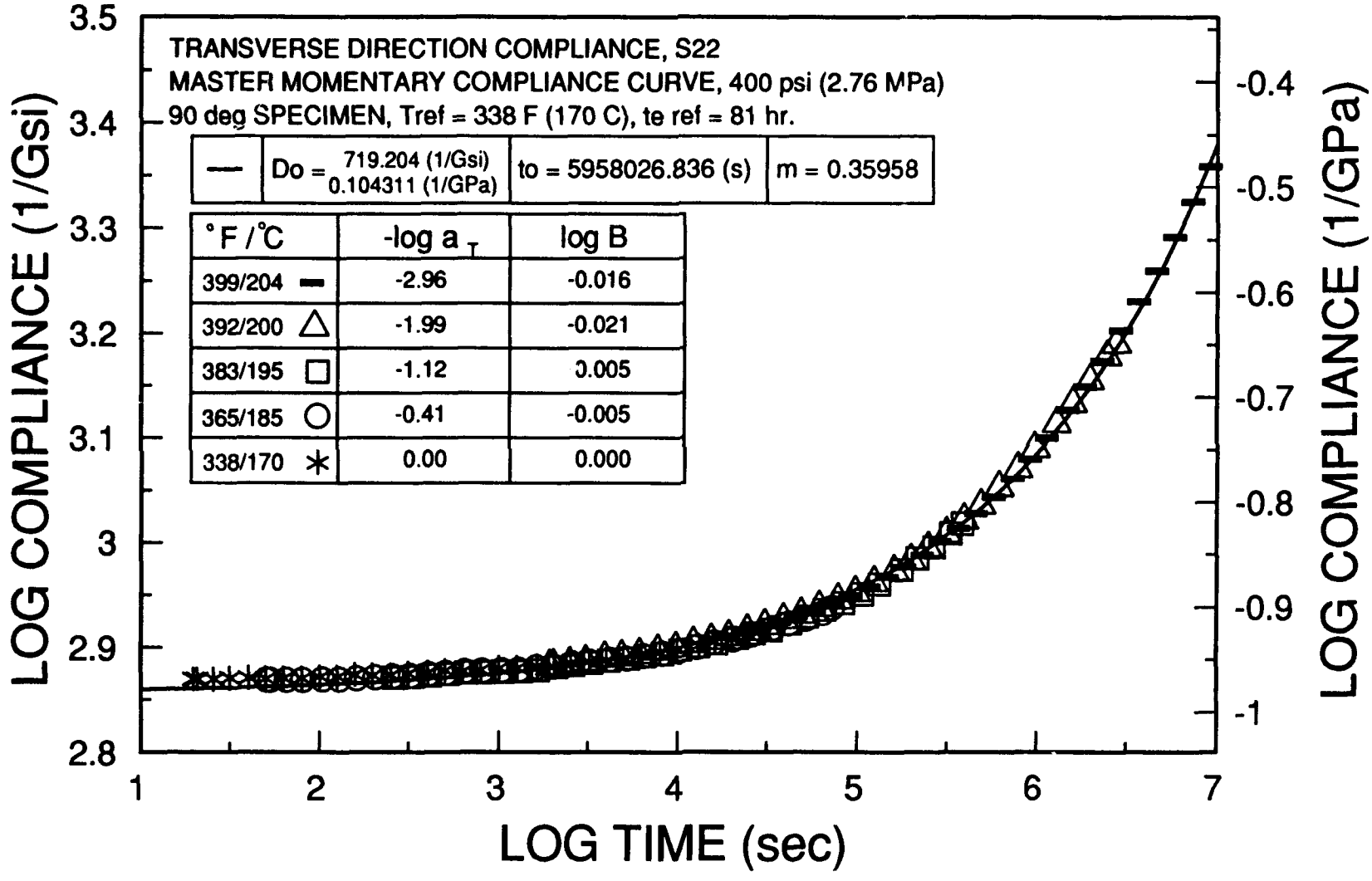

Figure 4.14 Transverse Direction TTSP Master Momentary Compliance Curve Graphically Fit and Referenced to T=338F (170C), te=81 hours.

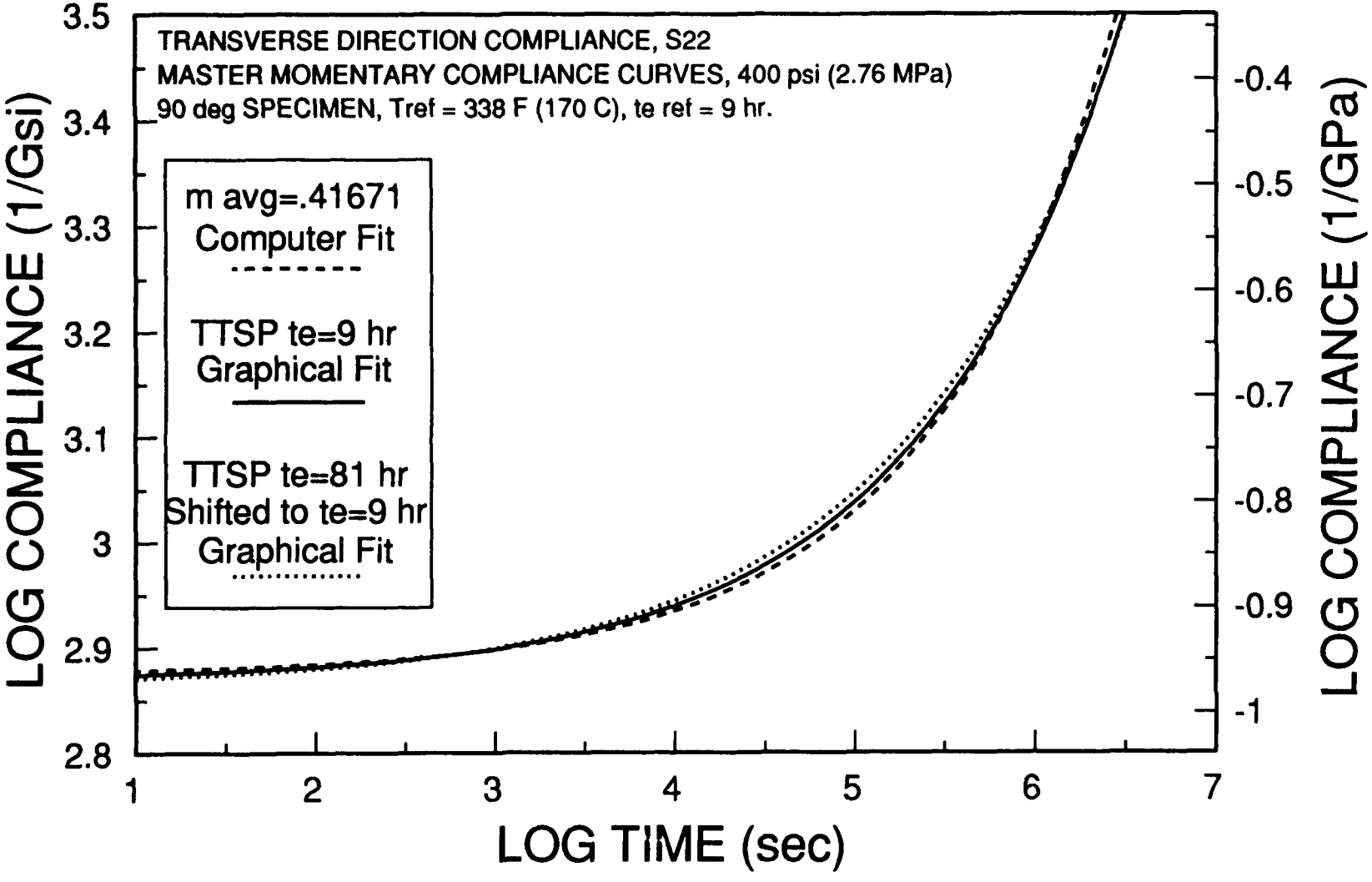

Figure 4.15 Comparison of Transverse Direction TTSP Master Momentary Compliance Curves Referenced to T=338F (170C), te=9 hours.

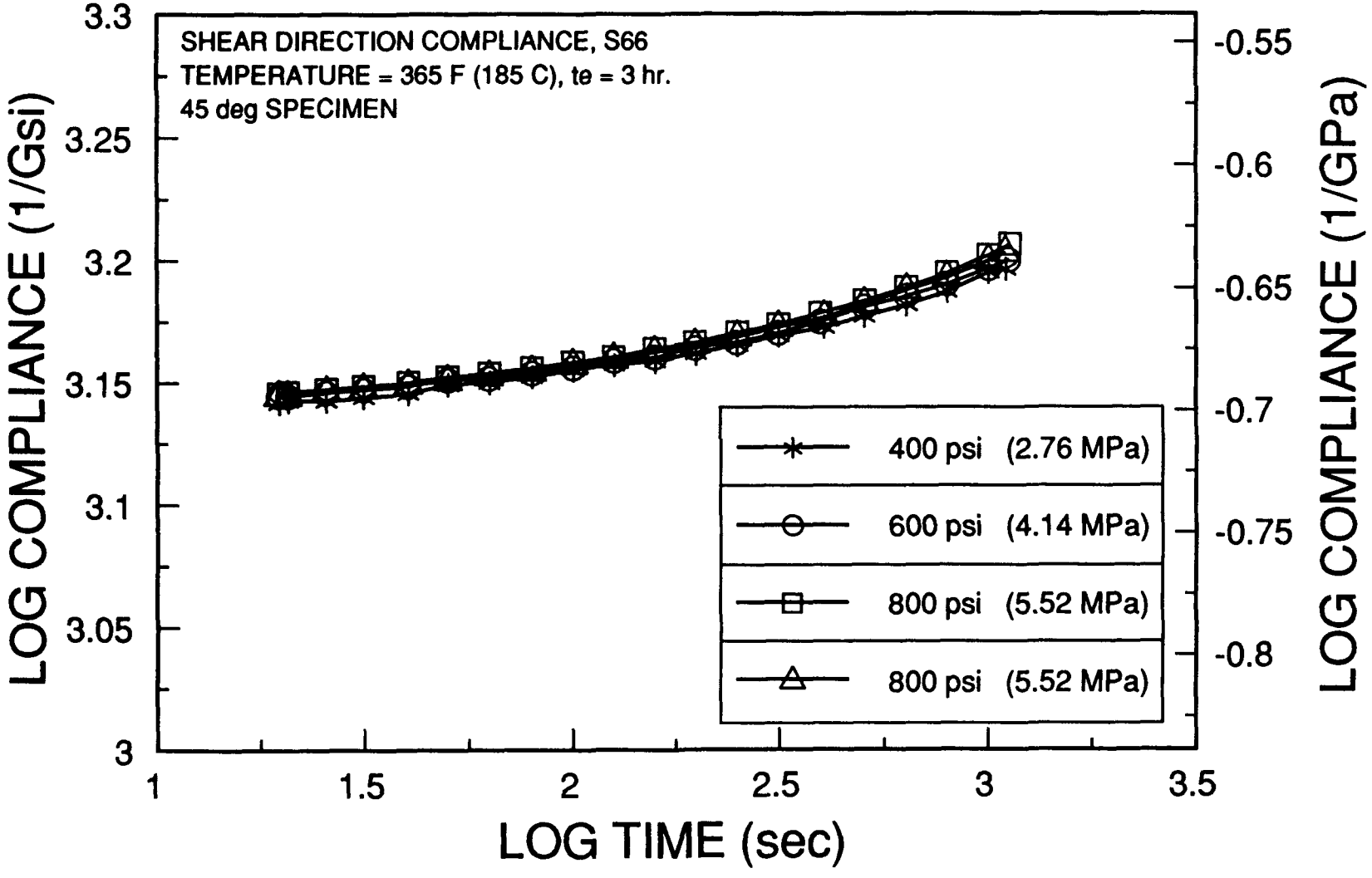

Figure 4.16 Linearity Check of Shear Direction Compliance at a Constant Temperature of 365 F (185 C) and te = 3 hours.

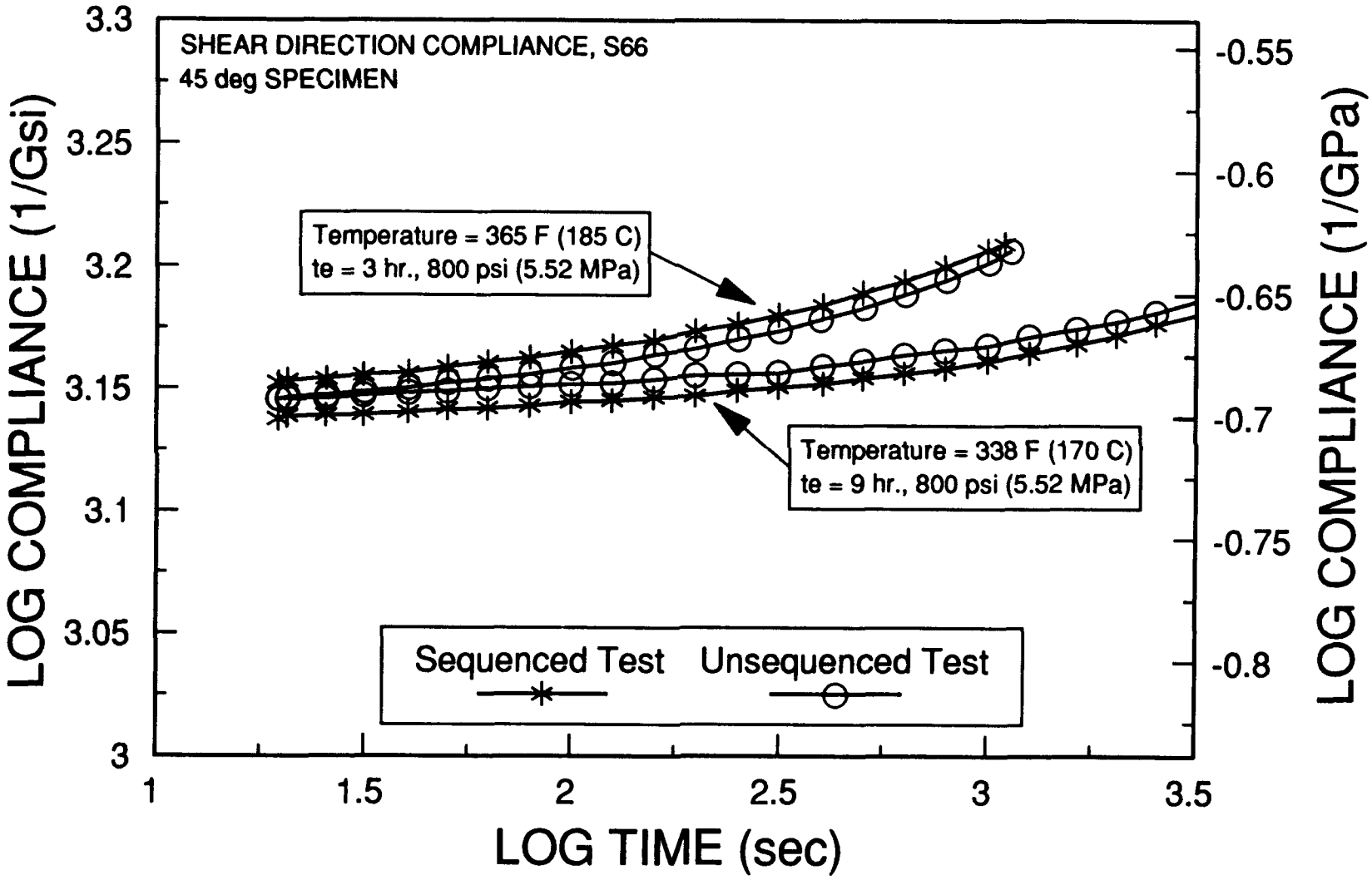

Figure 4.17 Check of Test Sequencing Effect on Shear Direction Compliance.

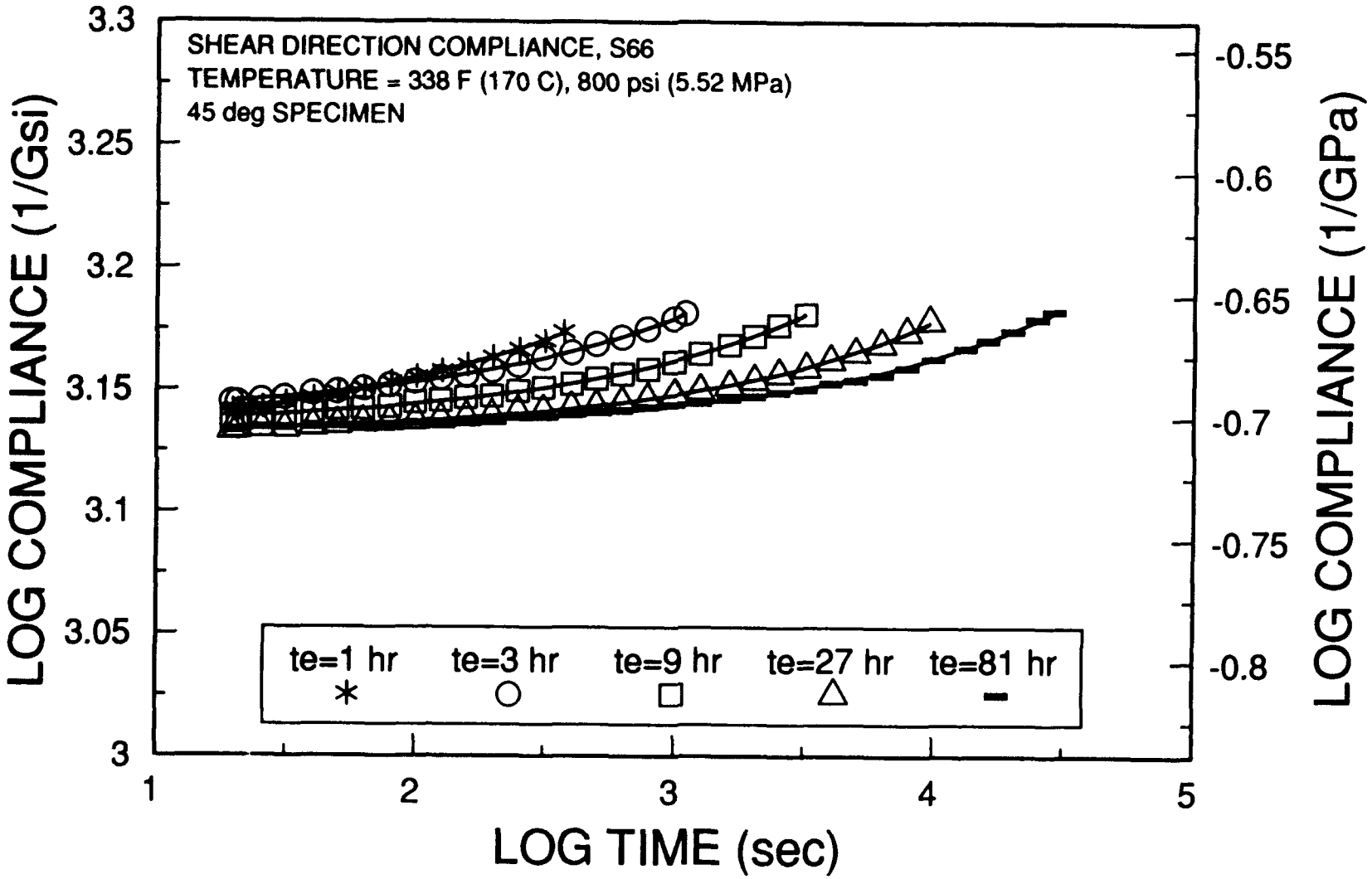

Figure 4.18 Shear Direction Compliance for a Constant Temperature of 338 F (170 C) at Various Aging Times.

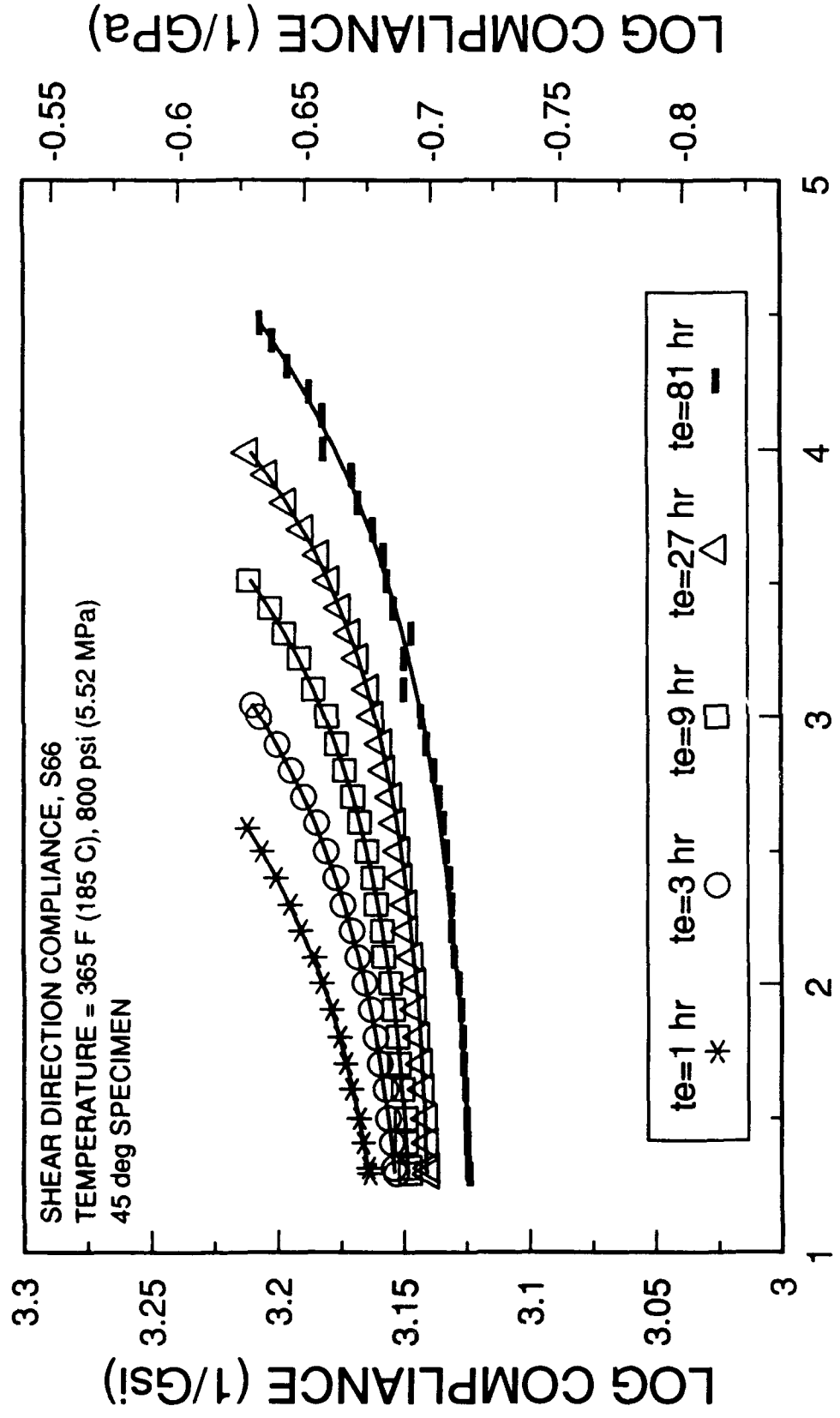

Figure 4.19 Shear Direction Compliance for a Constant Temperature of 365 F (185 C) at Various Aging Times.

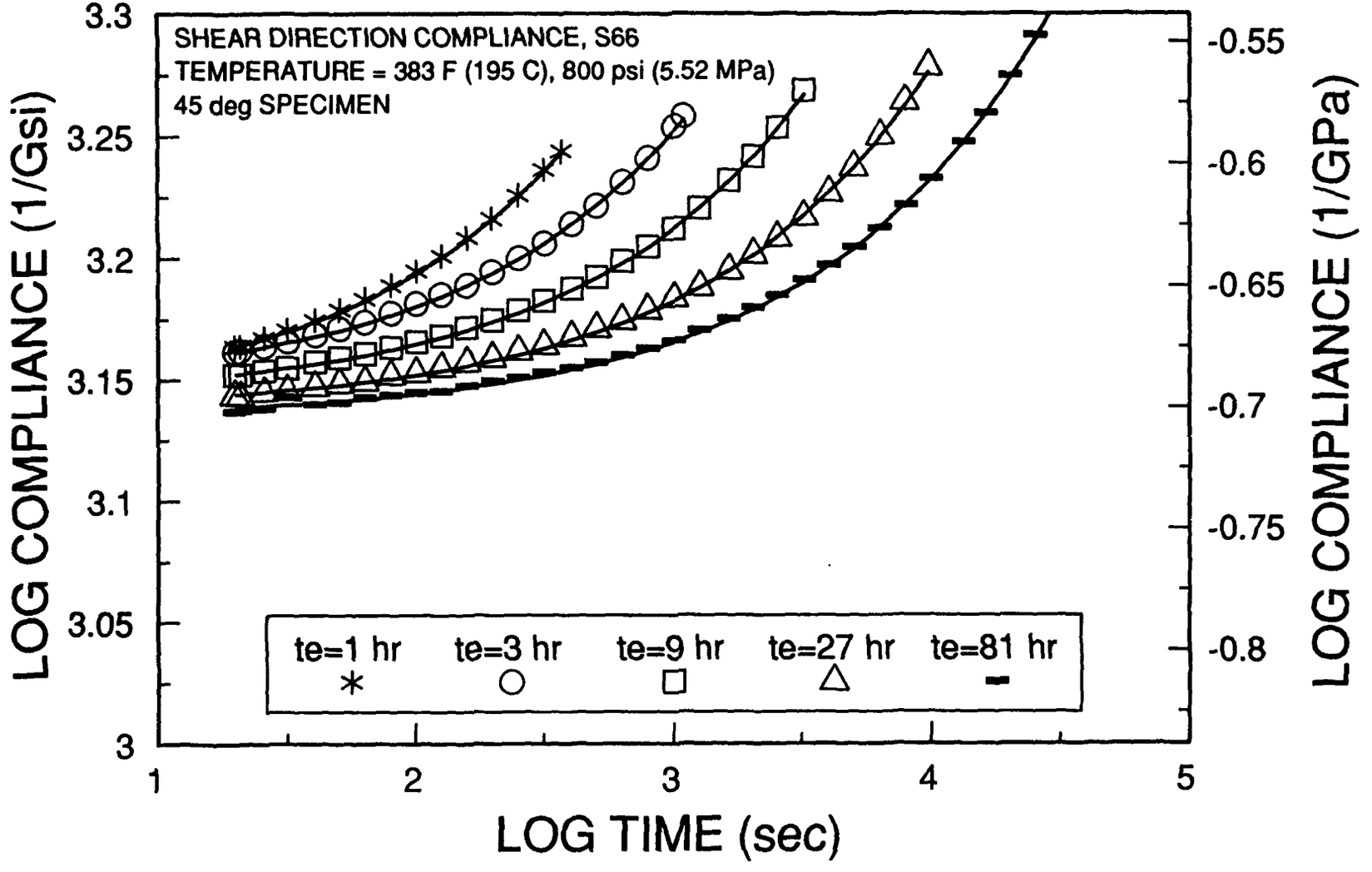

Figure 4.20 Shear Direction Compliance for a Constant Temperature of 383 F (195 C) at Various Aging Times.

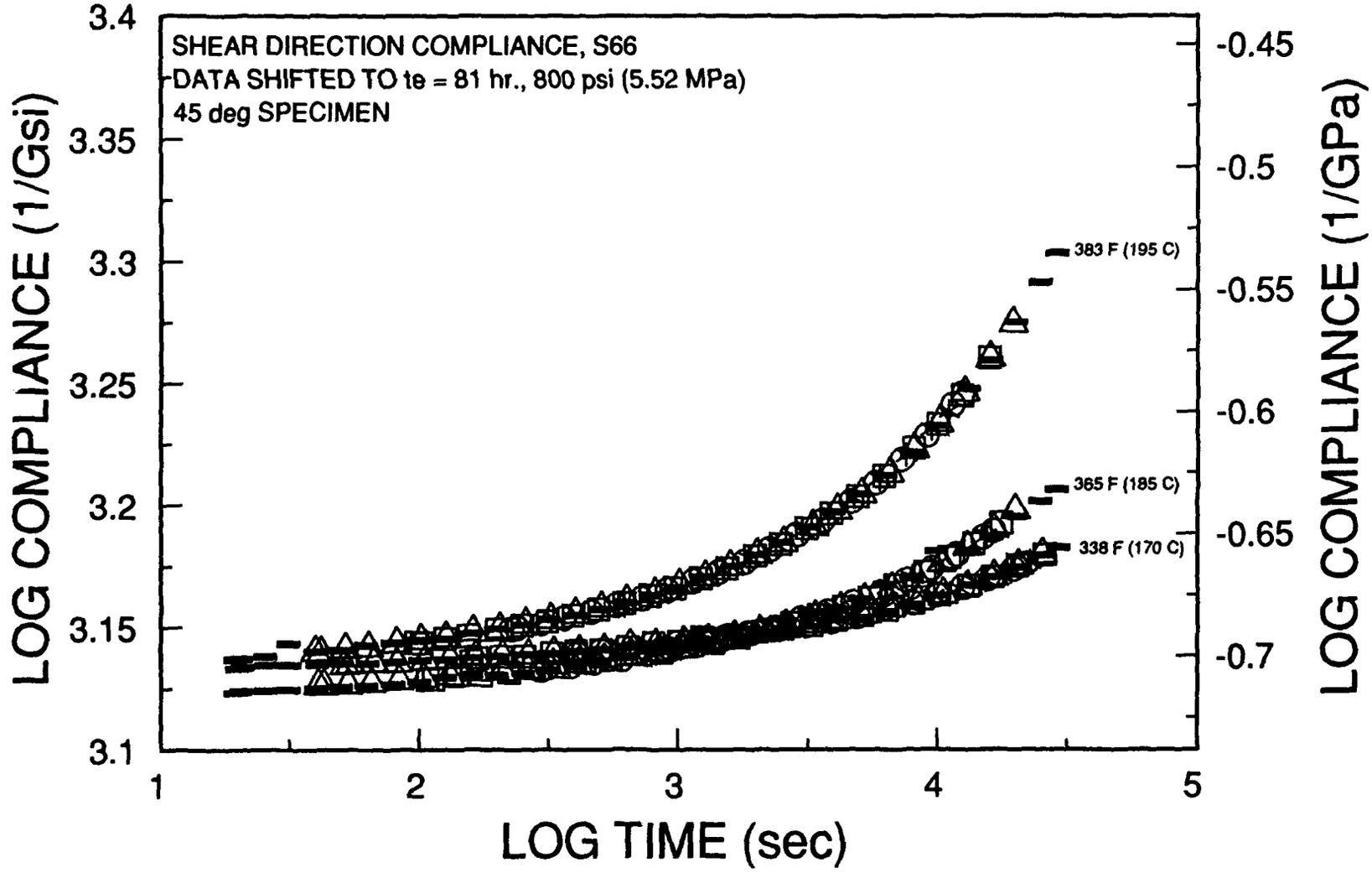

Figure 4.21 Shear Direction Master Momentary Compliance Curves at Various Temperatures Shifted to the 81 hour Aging Time.

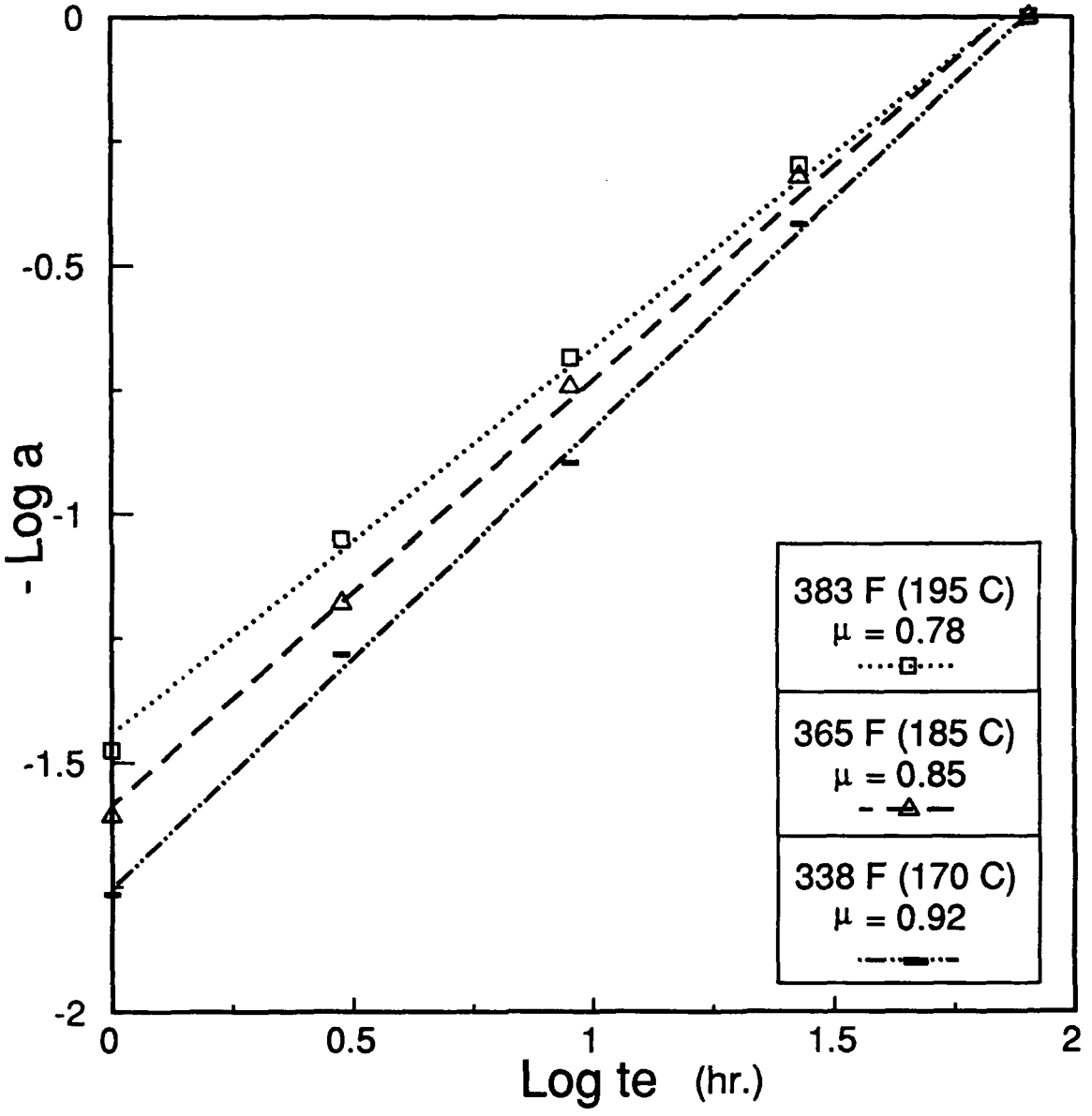

Figure 4.22 Aging Shift Rate for the 45 degree Test Sequence at Various Temperatures.

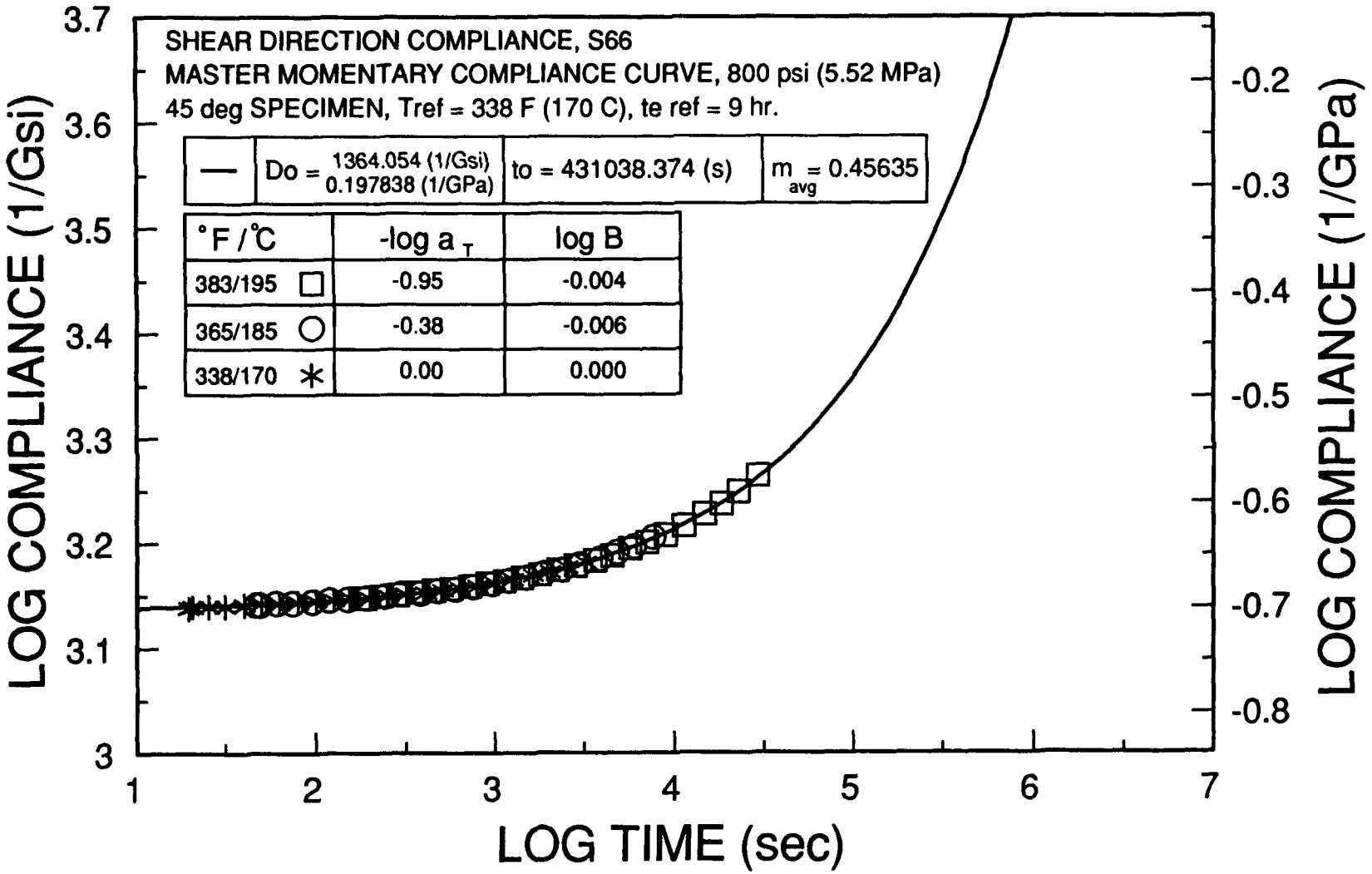

Figure 4.23 Shear Direction TTSP Master Momentary Compliance Curve Computer Fit with m avg = 0.4564 and Referenced to T=338F (170C), te=9 hours.

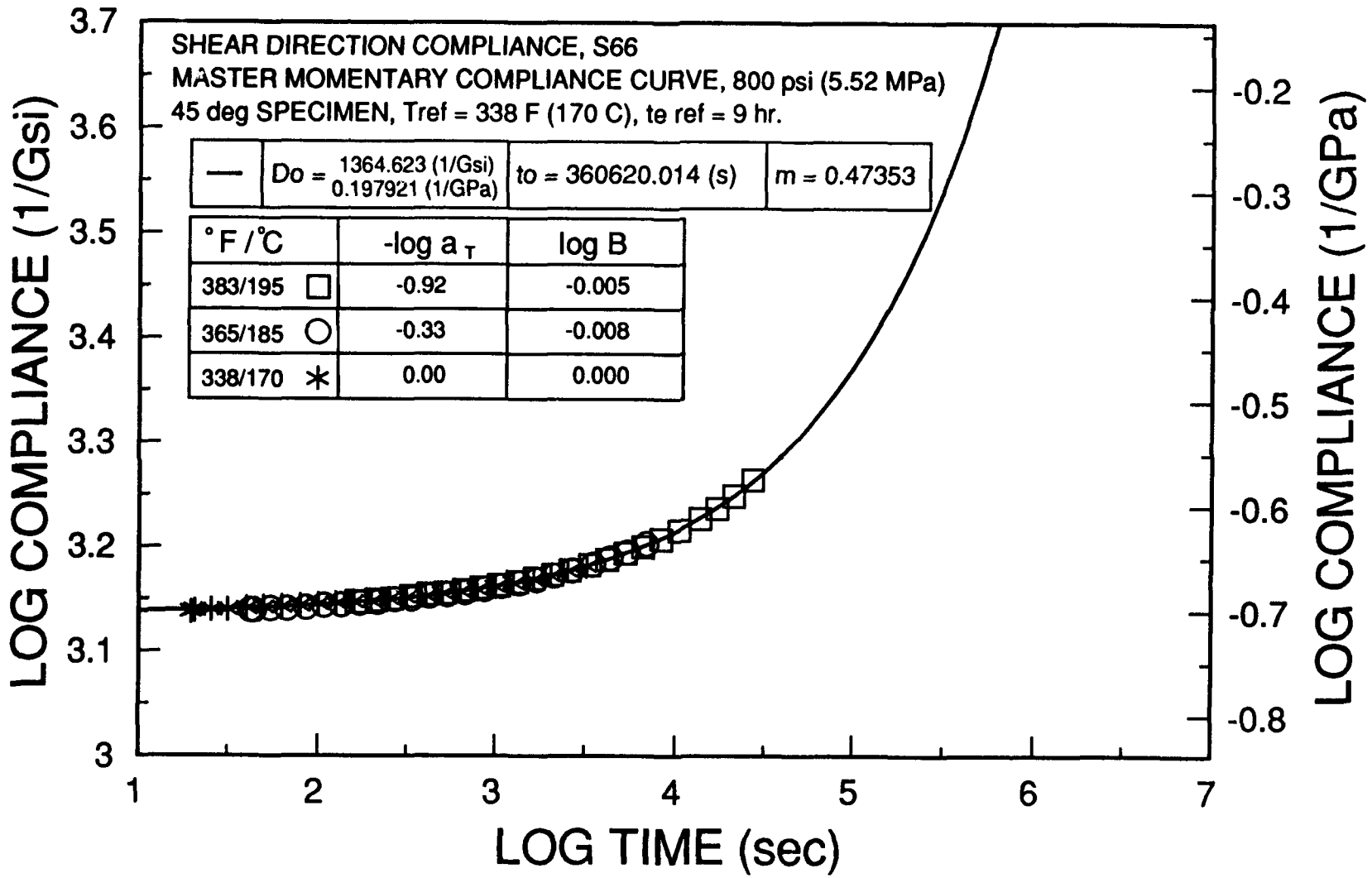

Figure 4.24 Shear Direction TTSP Master Momentary Compliance Curve Graphically Fit and Referenced to T=338F (170C), te=9 hours.

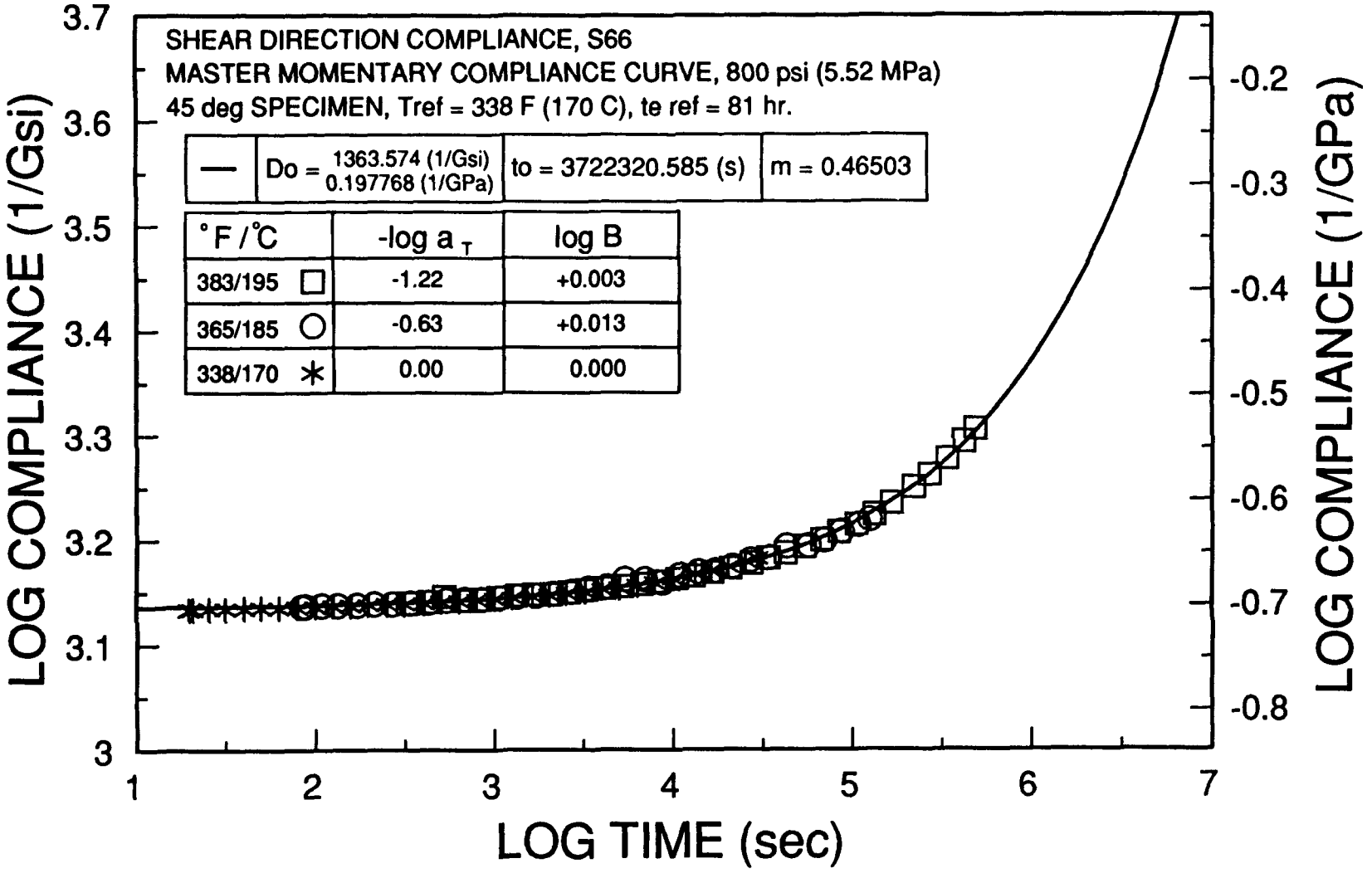

Figure 4.25 Shear Direction TTSP Master Momentary Compliance Curve Graphically Fit and Referenced to T=338F (170C), te=81 hours.

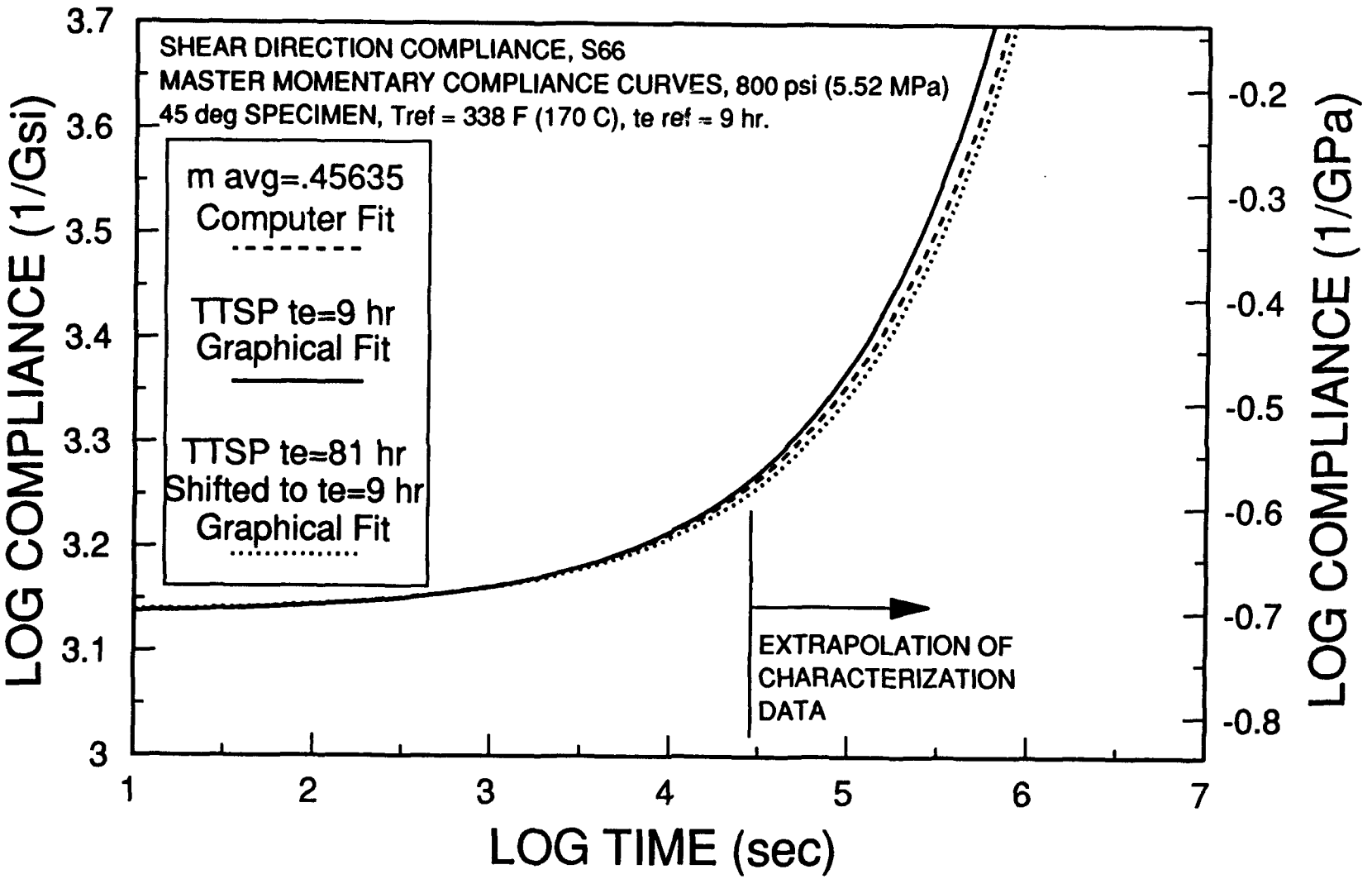

Figure 4.26 Comparison of Shear Direction TTSP Master Momentary Compliance Curves Referenced to T=338F (170C), te=9 hours.

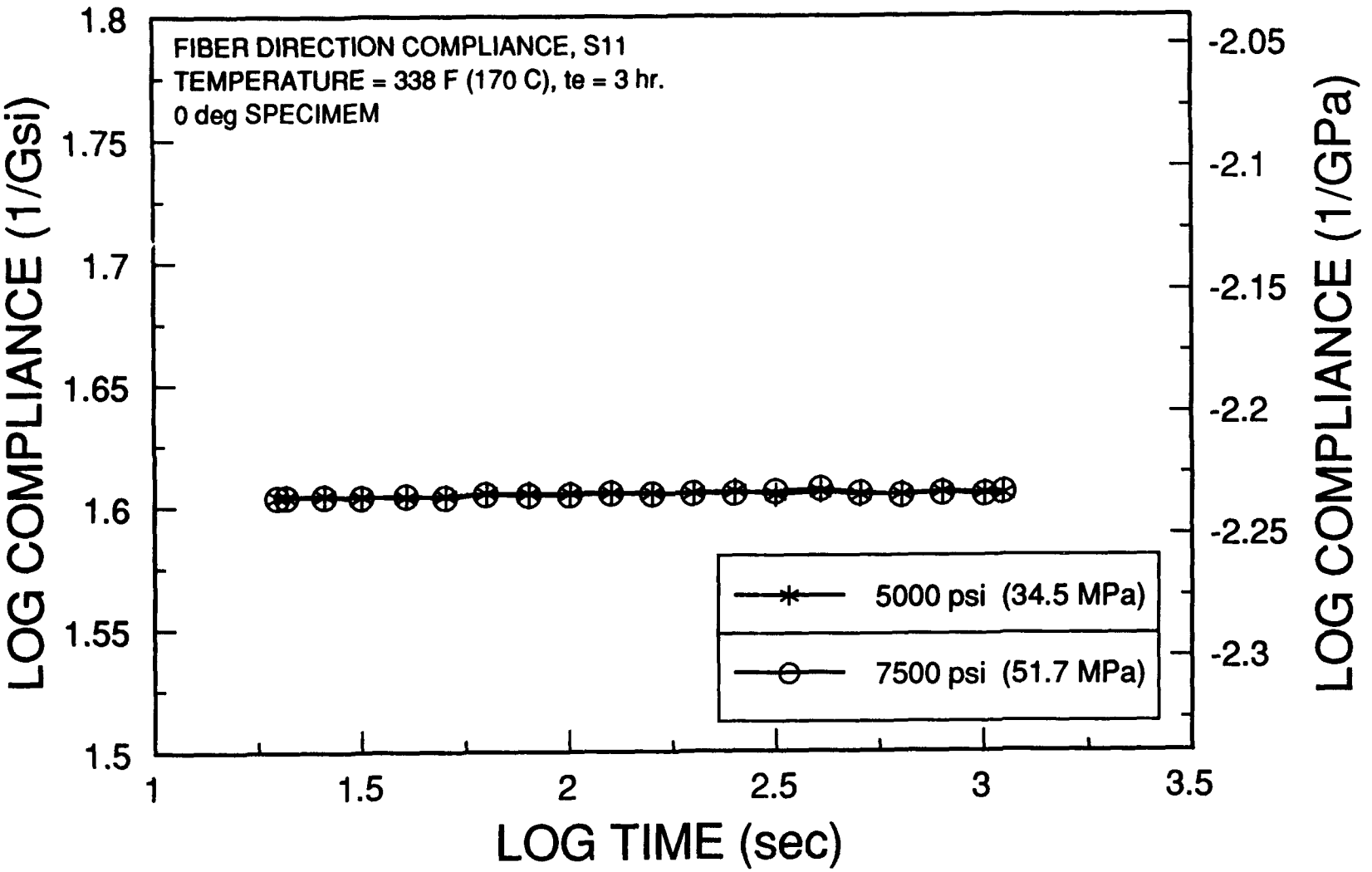

Figure 4.27 Linearity Check of Fiber Direction Compliance at a Constant Temperature of 338 F (170 C) and te = 3 hours.

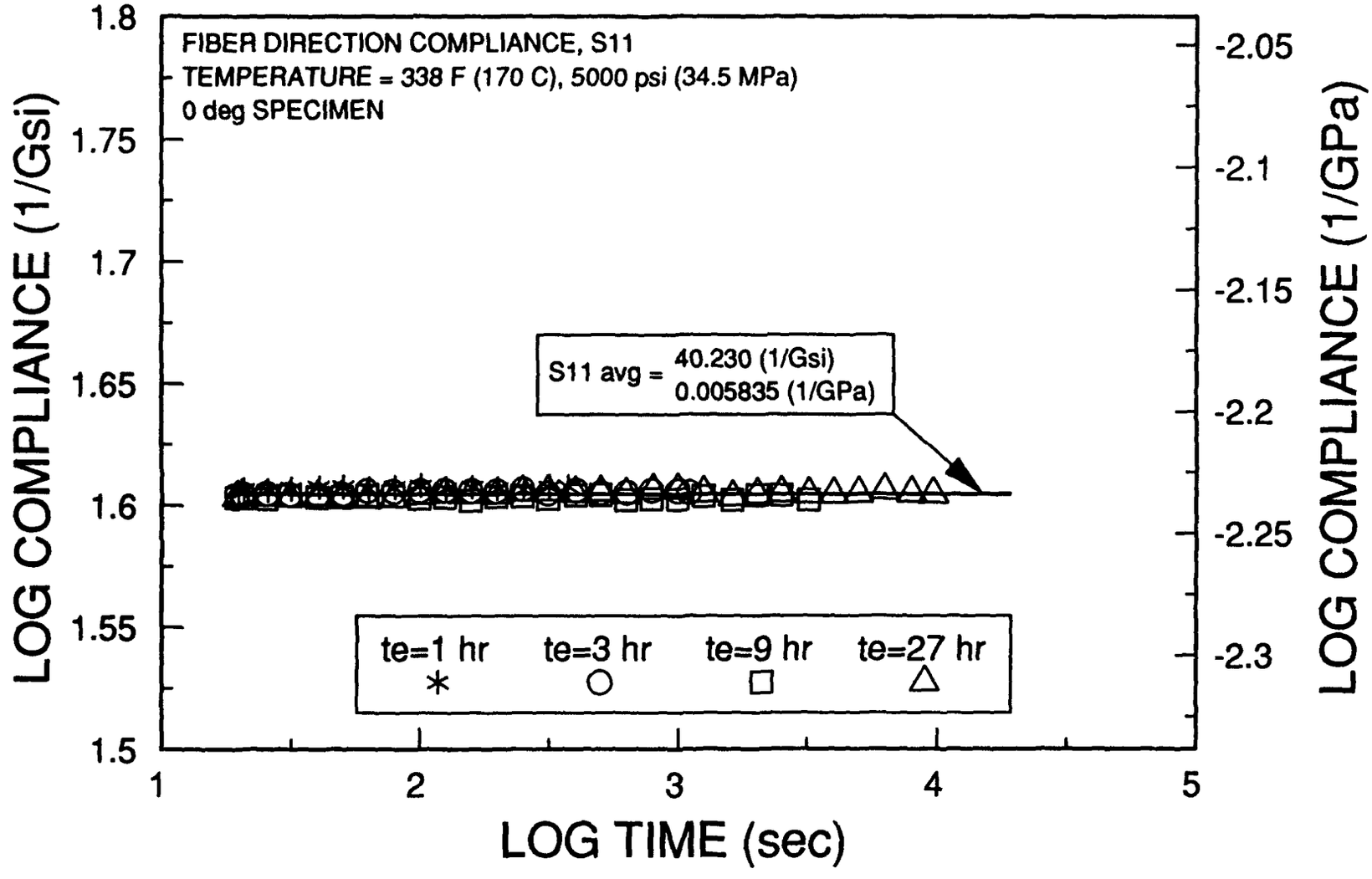

Figure 4.28 Fiber Direction Compliance for a Constant Temperature of 338 F (170 C) at Various Aging Times.

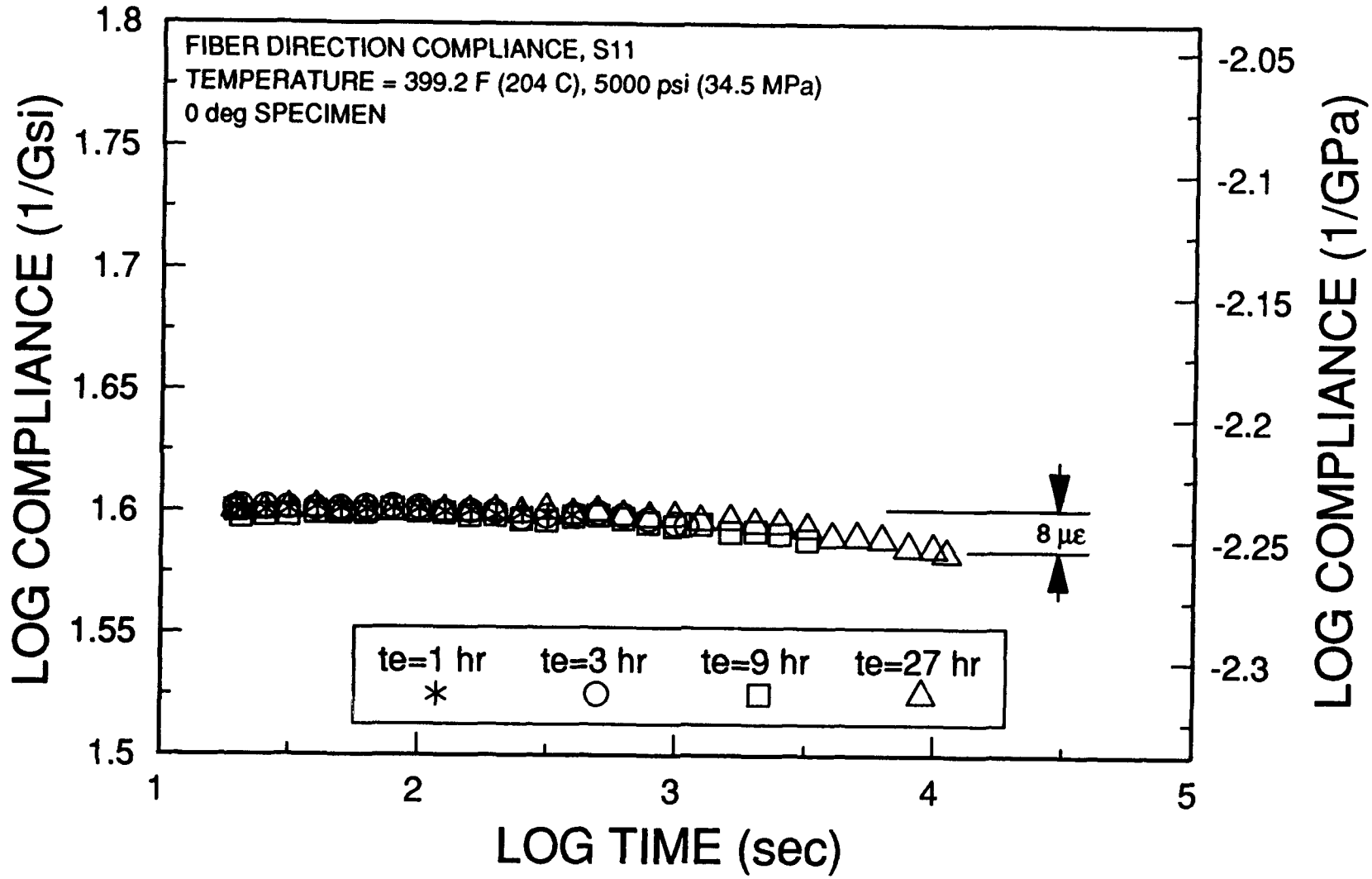

Figure 4.29 Fiber Direction Compliance for a Constant Temperature of 399.2 F (204 C) at Various Aging Times.

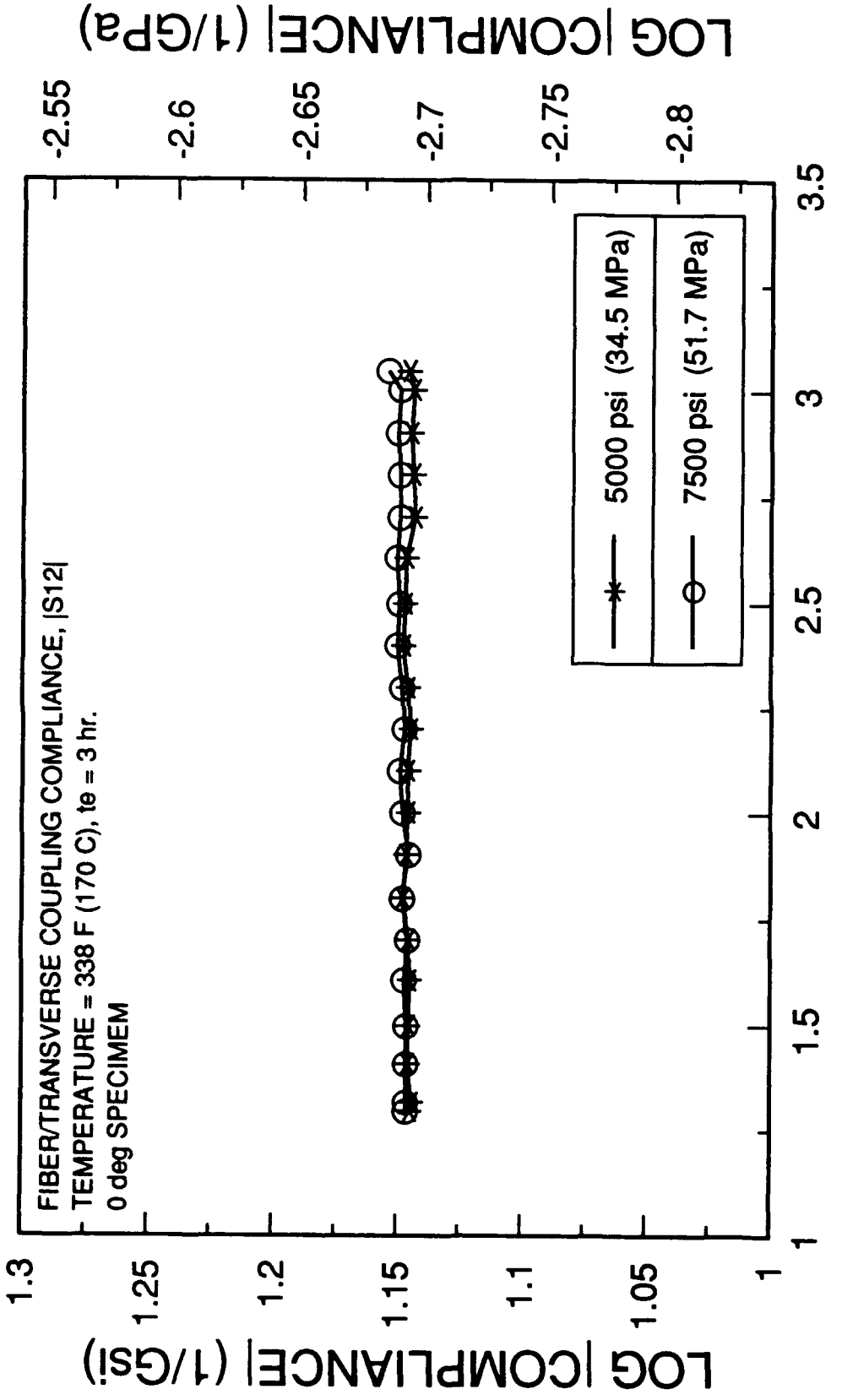

Figure 4.30 Linearity Check of Fiber/Transverse Coupling Compliance at a Constant Temperature of 338 F (170 C) and te = 3 hours.

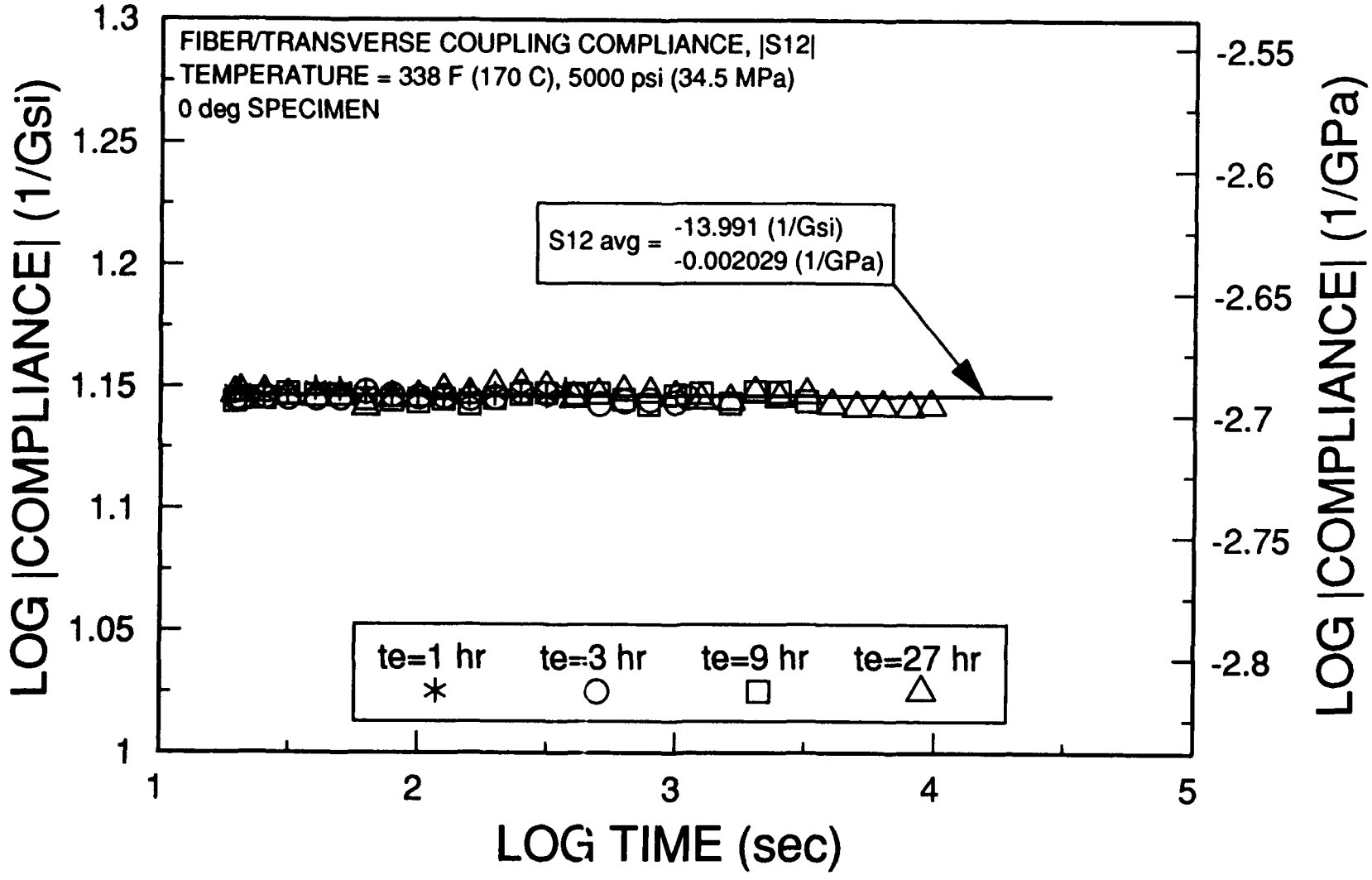

Figure 4.31 Fiber/Transverse Coupling Compliance for a Constant Temperature of 338 F (170 C) at Various Aging Times.

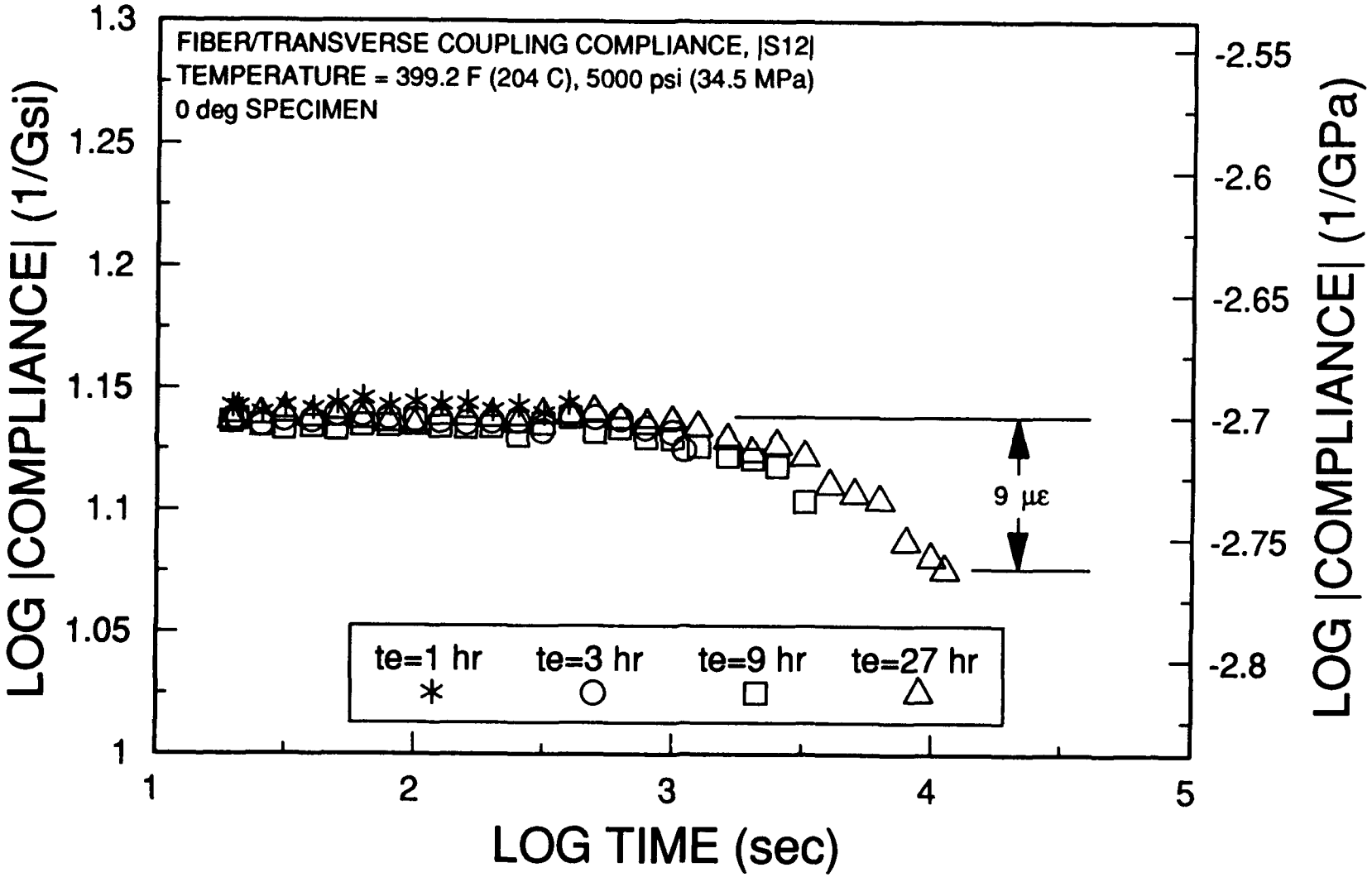

Figure 4.32 Fiber/Transverse Direction Compliance for a Constant Temperature of 399.2 F (204 C) at Various Aging Times.

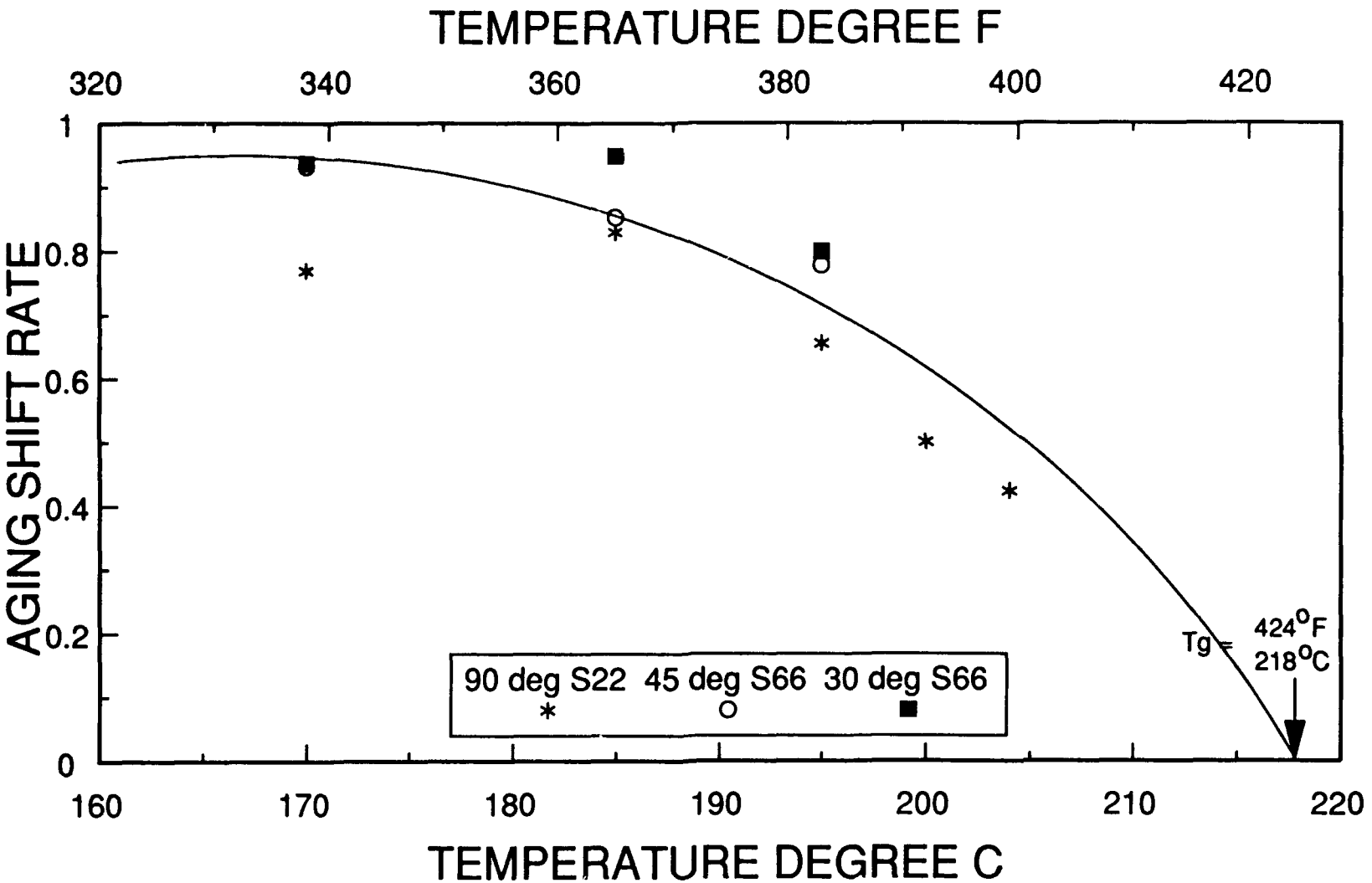

Figure 4.33 Temperature Dependence of the Aging Shift Rate.

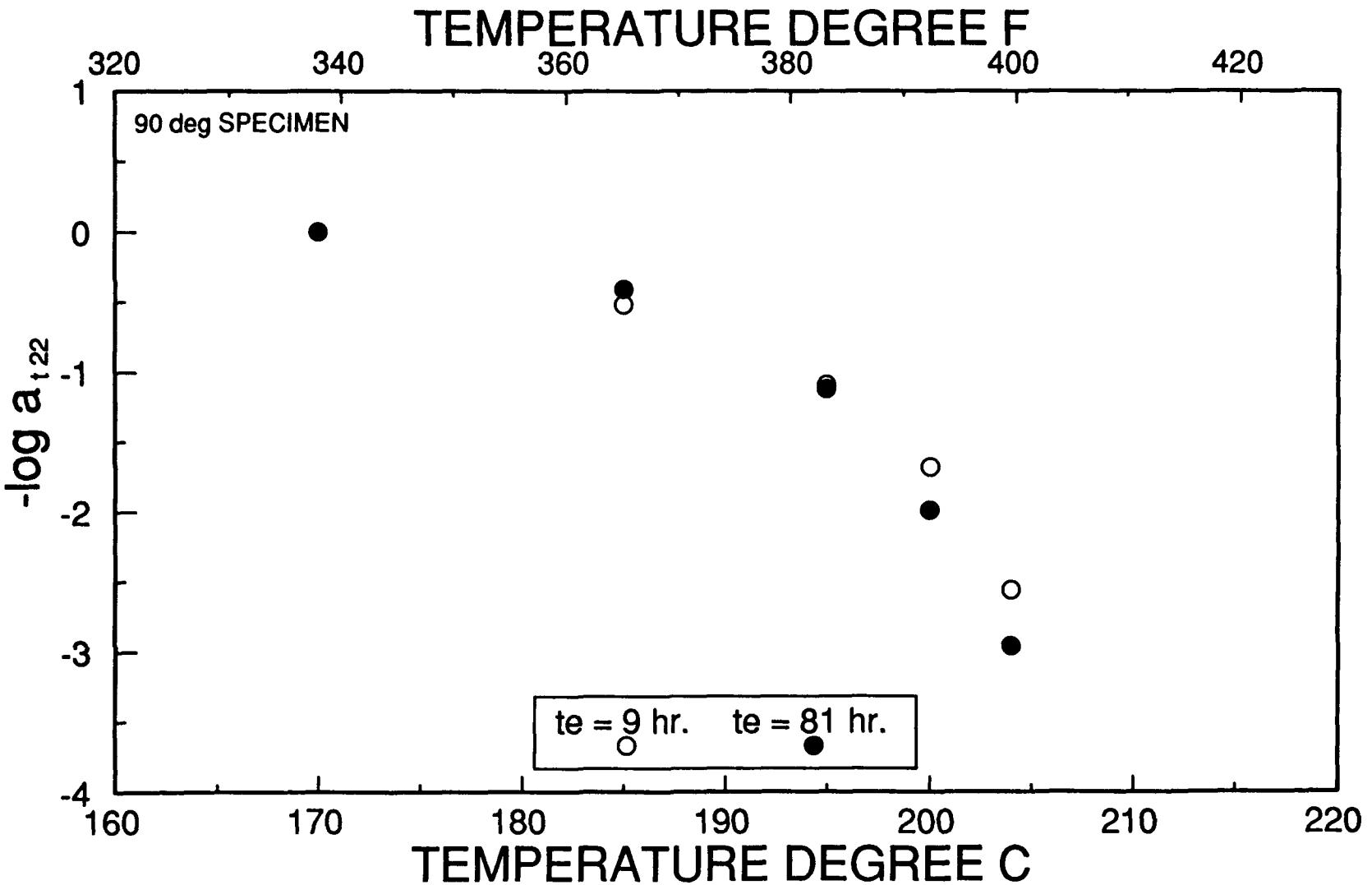

Figure 4.34 Temperature Dependence of the Transverse Direction TTSP Horizontal Shift Factors.

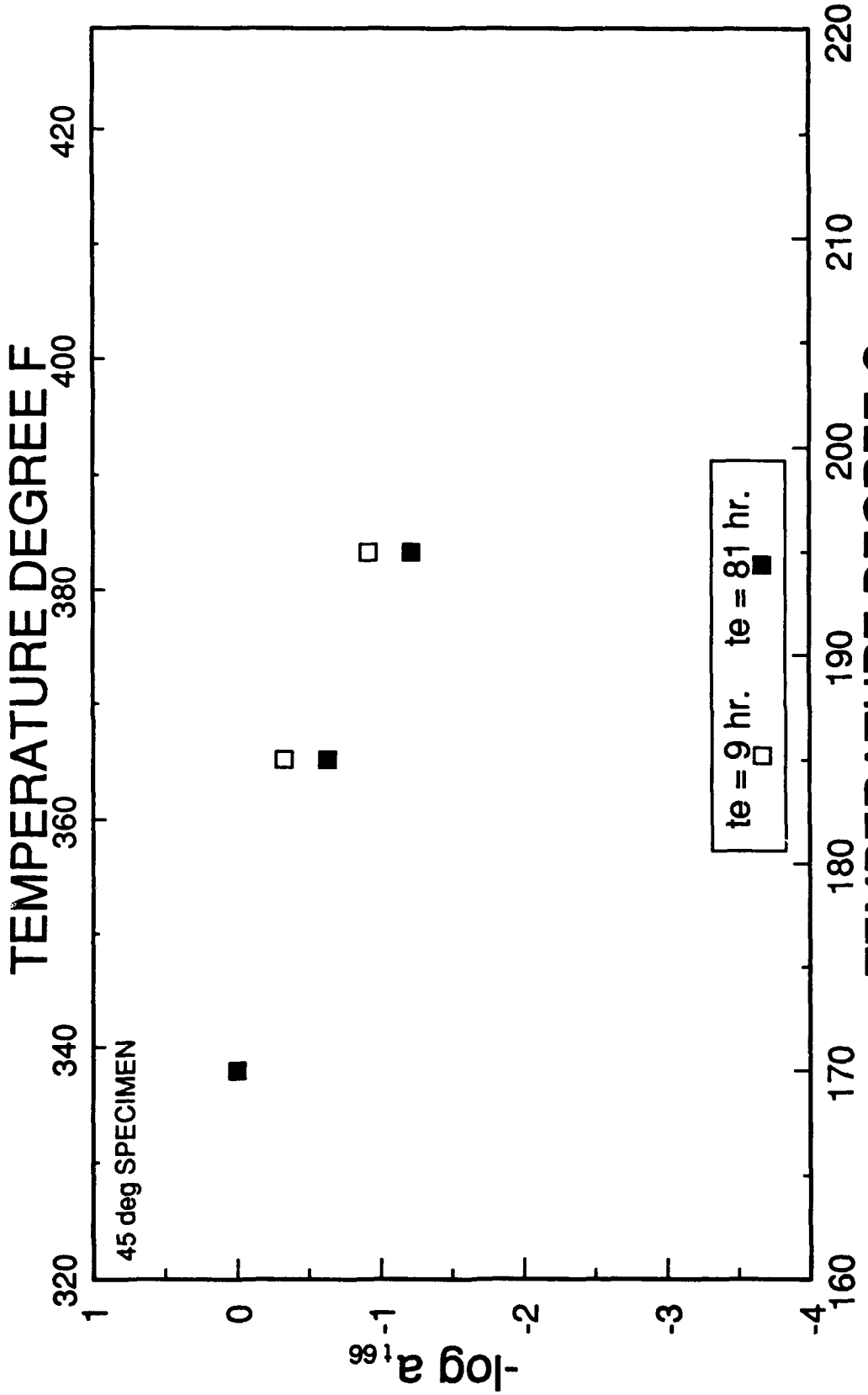

Figure 4.35 Temperature Dependence of the Shear Direction TTSP Horizontal Shift Factors.

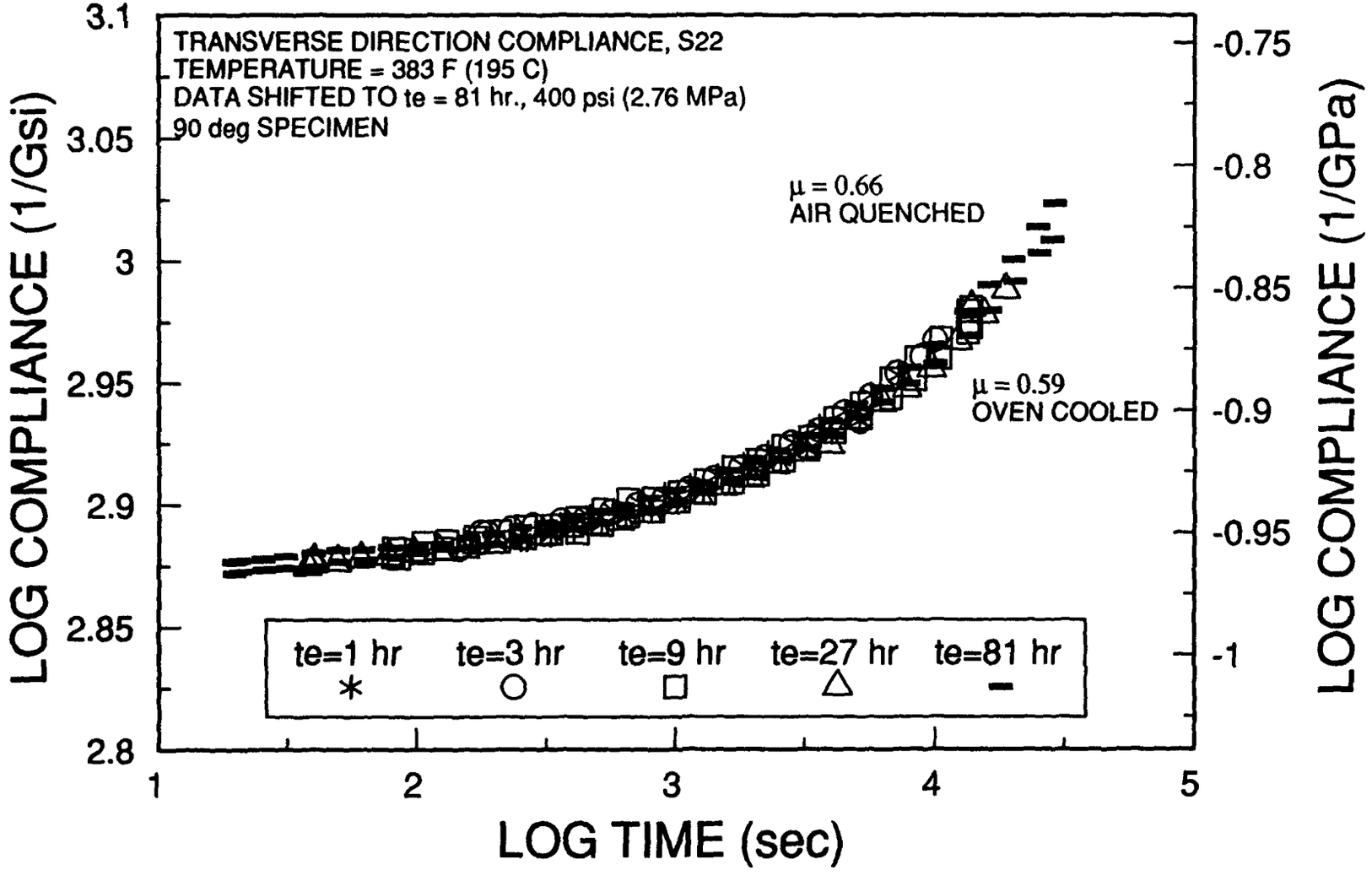

Figure 4.36 Comparison of Air Quenched and Oven Cooled Transverse Direction Master Momentary Compliance Curves at 383 F (195 C) with te=81 hours.

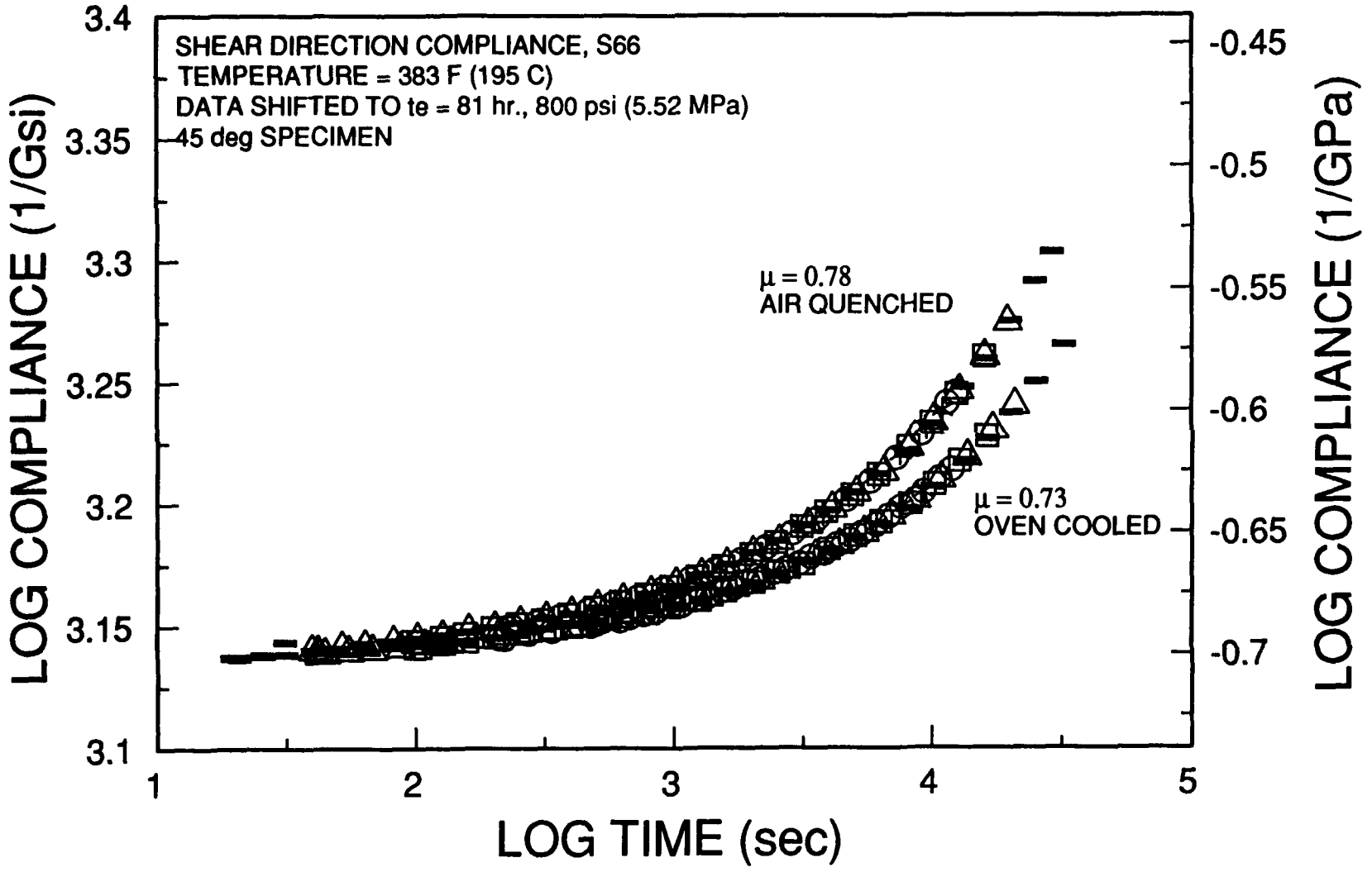

Figure 4.37 Comparison of Air Quenched and Oven Cooled Shear Direction Master Momentary Compliance Curves at 383 F (195 C) with te=81 hours.

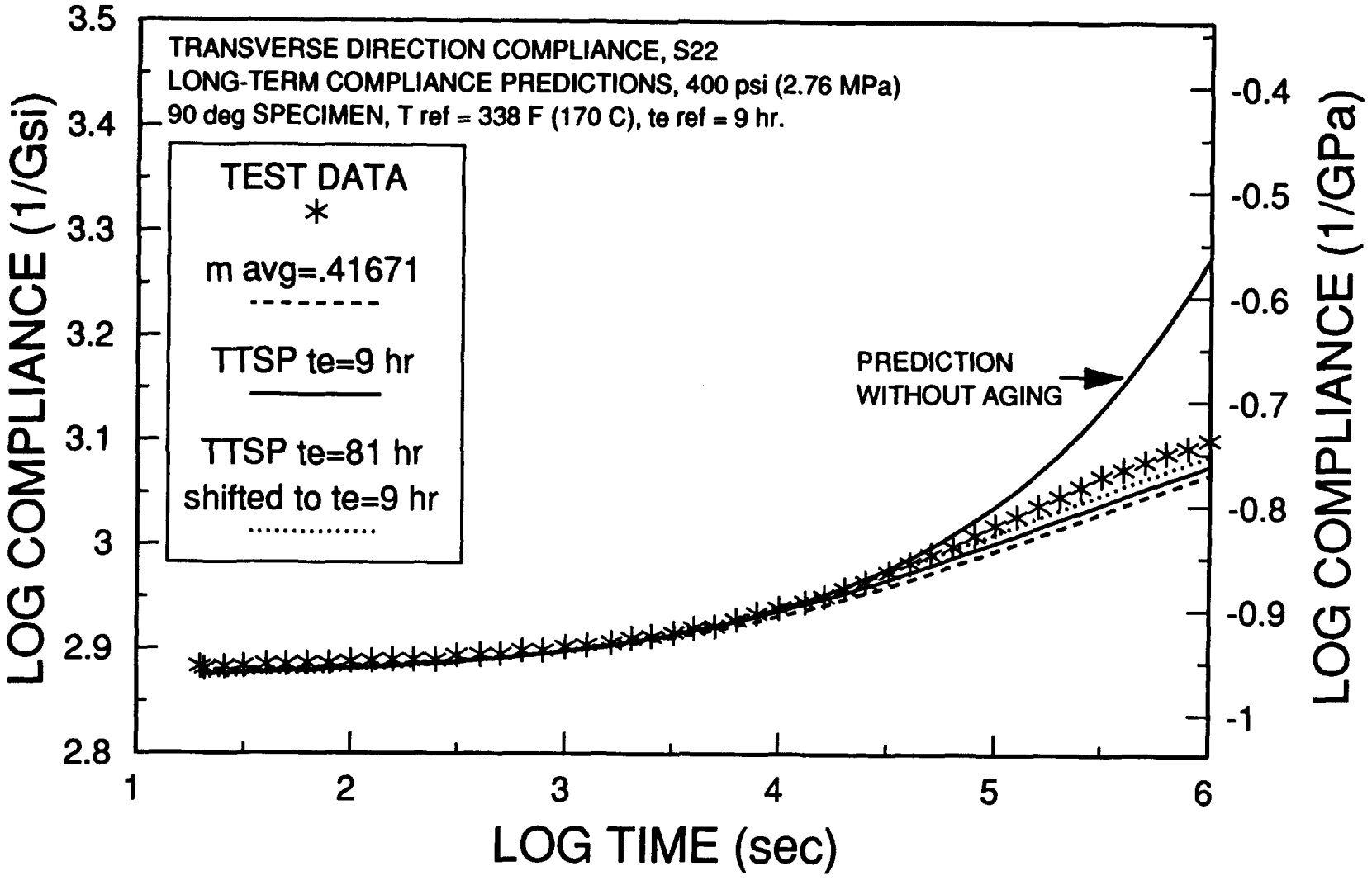

Figure 5.1 Transverse Direction Long-Term Compliance Predictions and Test Data at 338 F (170 C) and te = 9 hours.

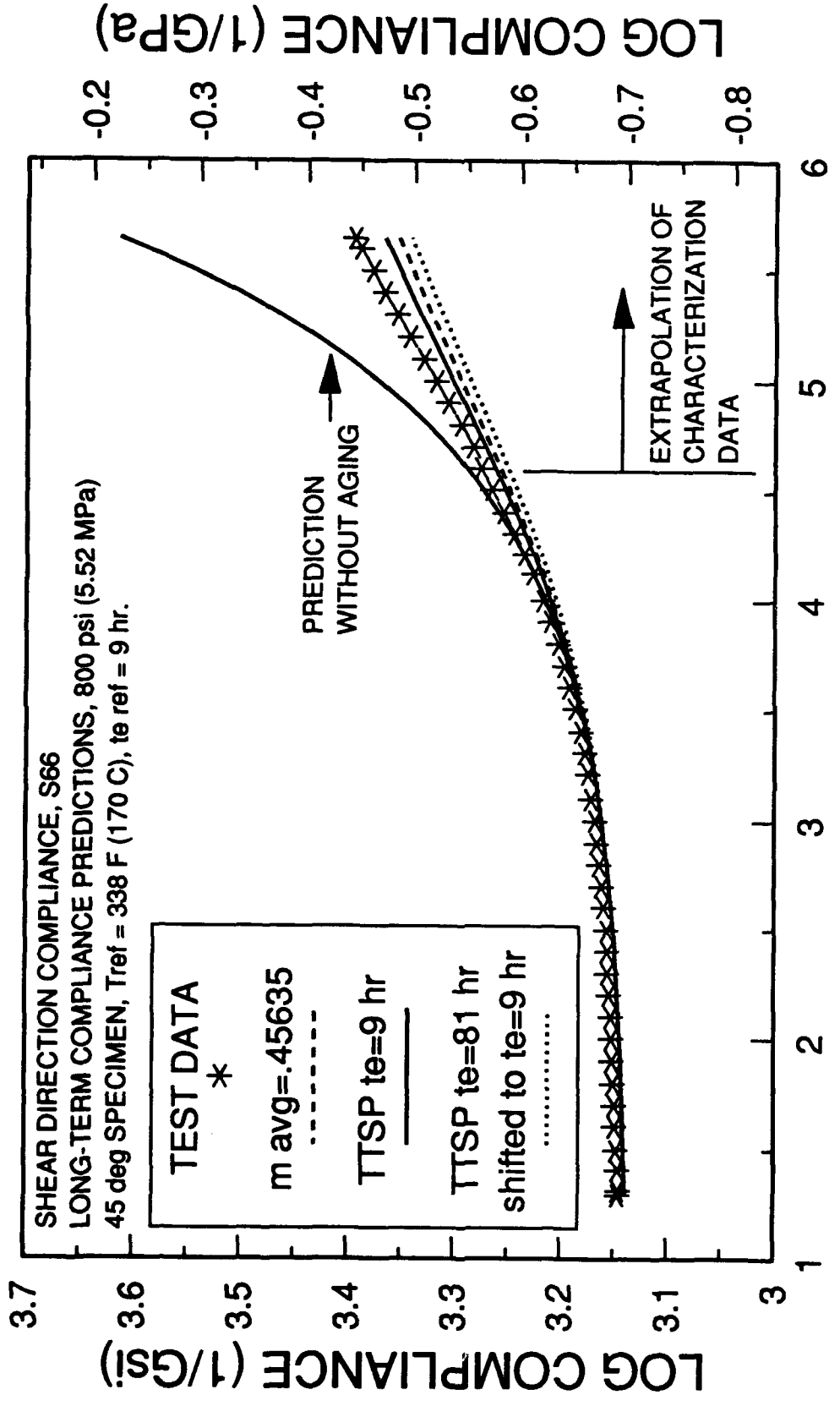

Figure 5.2 Shear Direction Long-Term Compliance Predictions and Test Data at 338 F (170 C) and te = 9 hours.

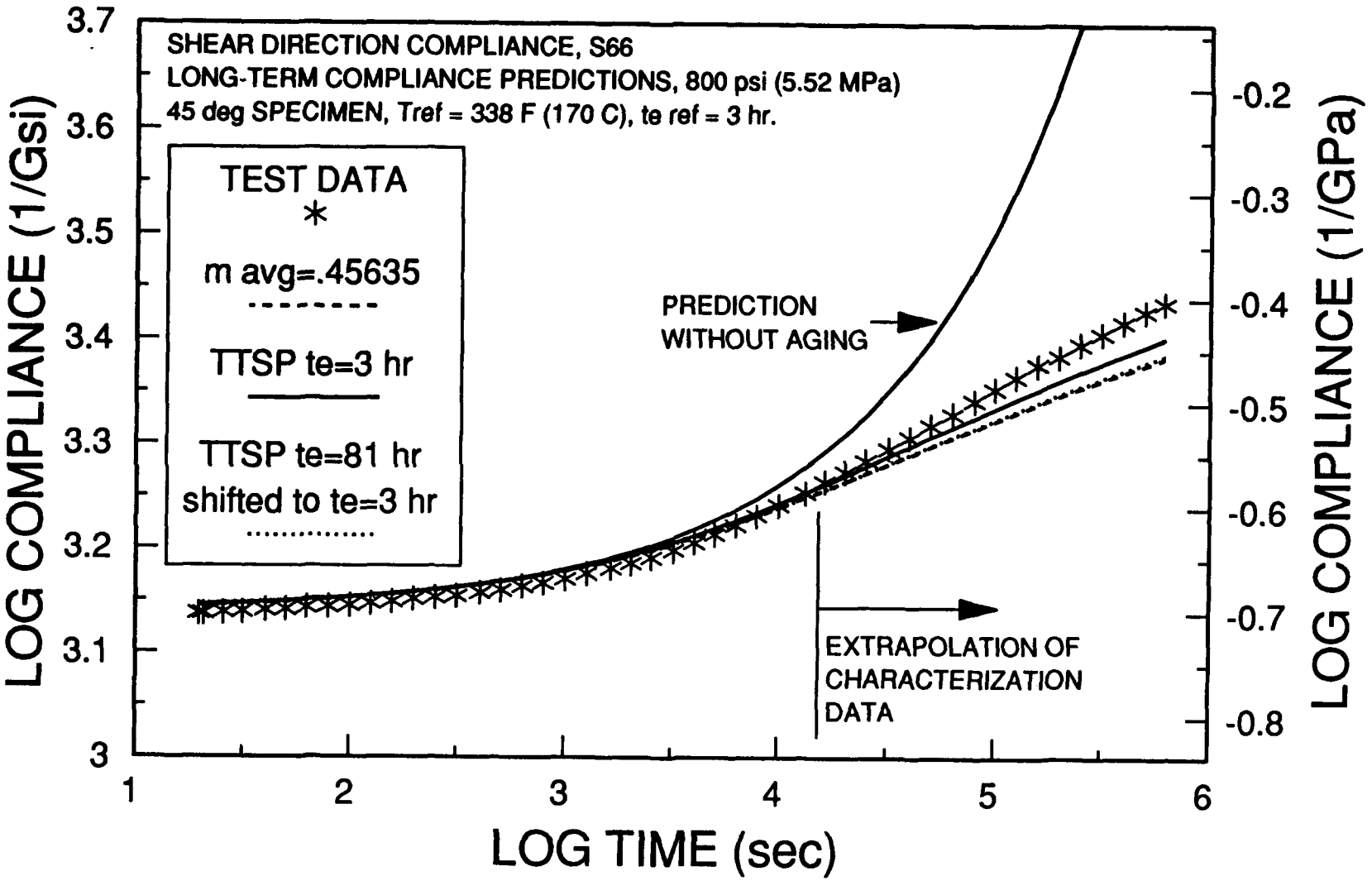

Figure 5.3 Shear Direction Long-Term Compliance Predictions and Test Data at 338 F (170 C) and te = 3 hours.

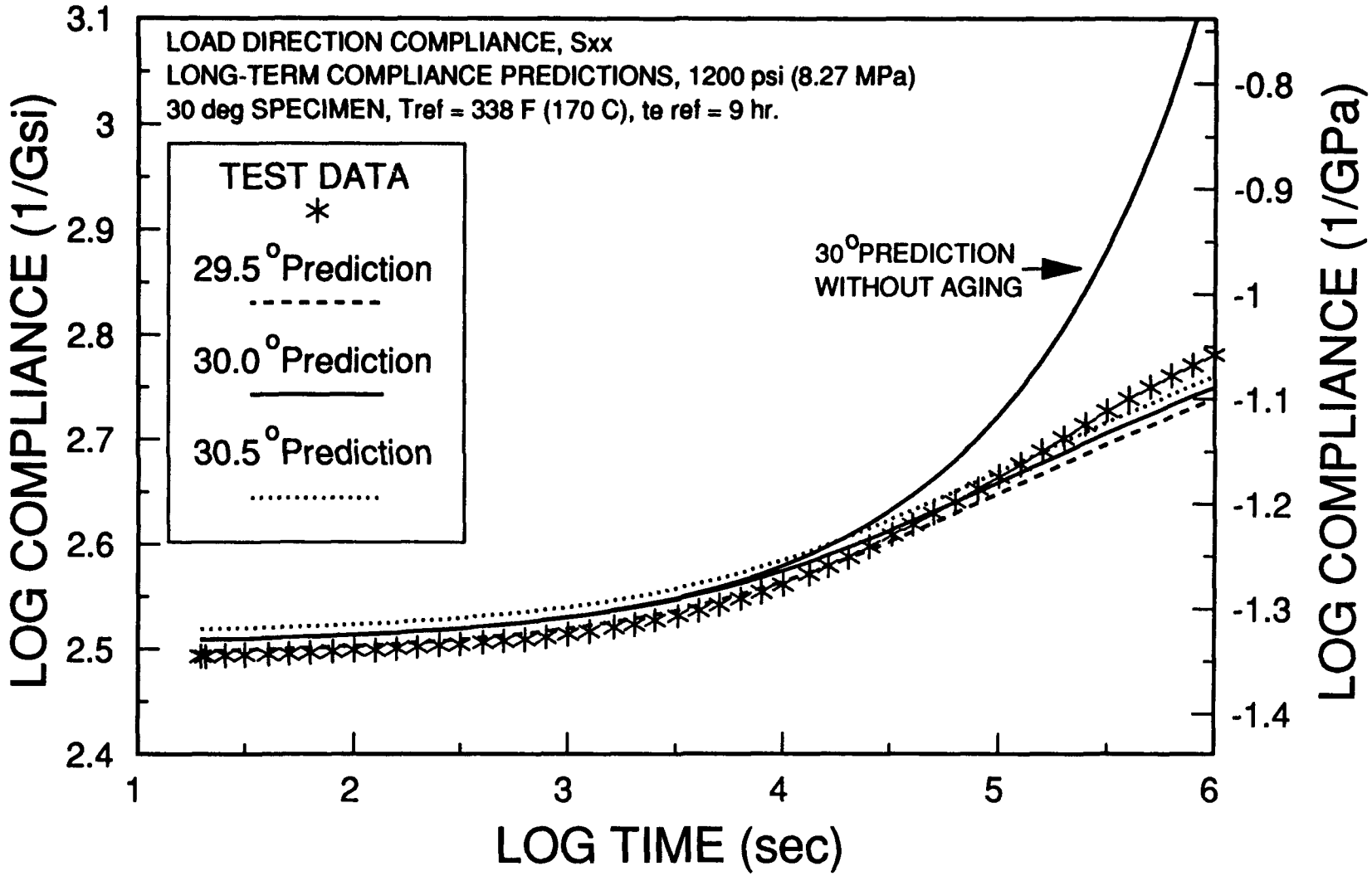

Figure 5.4 Load Direction Long-Term Compliance Predictions for the 30 degree Specimen at 338 F (170 C) and te = 9 hours.

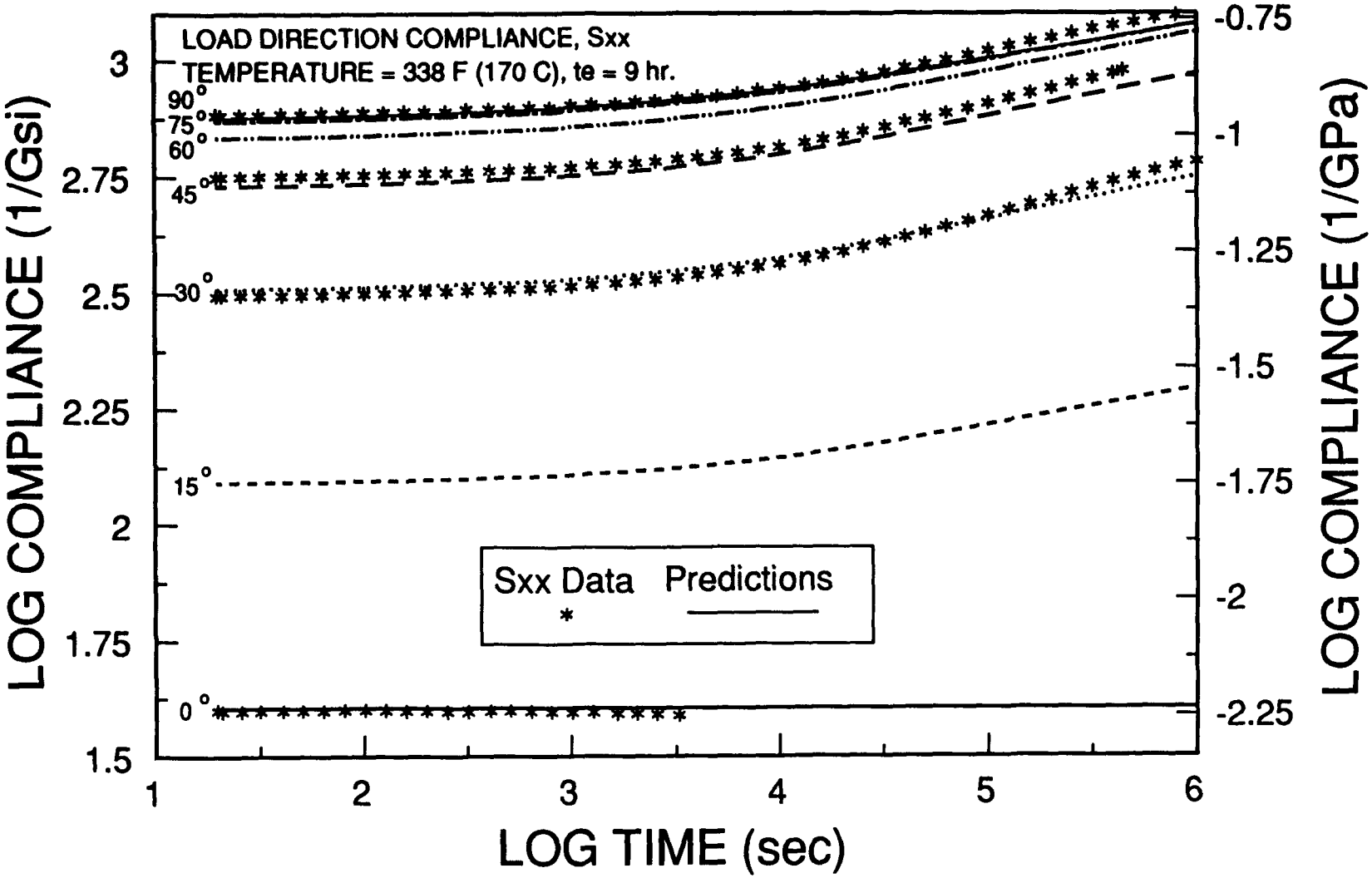

Figure 5.5 Load Direction Long-Term Compliance Predictions and Test Data at 338 F (170 C) and te = 9 hours.

VITA

Robert Leroy Hastie Jr. was born 18 Nov. 1957 in Harrison, Pennsylvania. He graduated from Kiski Area Senior High in 1975. He continued his education at Grove City College, Grove City, PA where he was awarded an Air Force ROTC scholarship. After graduating in 1979, with a B.S. in Mechanical Engineering, he was commissioned as a Second Lieutenant, USAF. He initially served as a structural durability engineer for the F100 engine in the Deputy for Propulsion, WPAFB, OH. Next, he was selected to work on the TF-34 Durability and Damage Tolerance Assessment at General Electric, Lynn, MA. This was followed by an assignment as the lead structural engineer for the F100 engine back at WPAFB, OH. He then attended the Air Force Institute of Technology, WPAFB, OH, receiving a Master of Science degree in Astronautical Engineering in Dec., 1985. He then served as an assistance professor in the Engineering Science and Mechanics Department at the USAF Academy. While at the USAF Academy, he was selected to pursue a Doctor of Philosophy degree under USAF sponsorship. He enrolled in the Engineering Science and Mechanics Department at VPI & SU in August, 1988. Upon completion of his degree, he will return to teaching at the USAF Academy. He is married to the former Victoria Ann Manikas of Haverhill, Massachusetts and has a daughter Jessica, age 3.